DEVELOPMENT OF BISPECIFIC ANTIBODY MIMETICS

MATTHEW COLLINS

A thesis submitted in partial fulfilment of the requirements of the University of East London for the degree of Doctor of Philosophy

September 2023

Abstract

Chronic neovascular retinal diseases can be treated by antibody-based medicines which are administered by intravitreal injection Ongoing efforts are focused on improving treatment outcomes for patients taking these medicines. One strategy to improve treatments is the development of bispecific antibodies which are capable of binding to 2 intraocular therapeutic targets simultaneously. Bispecific antibodies are suggested as an alternative to the use of combination therapies within the eye.

Many different bispecific antibody motifs have been prepared including motifs derived from antibody fragments such as Fabs and single chain variable fragments. Previously our research group developed a monospecific antibody motif called a Fab-PEG-Fab (FpF) in which 2 identical Fabs are conjugated to either end of a PEG di *bis*-sulfone protein dimerisation reagent **5** mimicking an IgG antibody. It was thought to try and develop the FpF platform further by preparing bispecific FpFs (BsFpF).

The aim of this PhD thesis was to synthesise BsFpFs capable of binding to two therapeutic targets within the eye. To prepare BsFpFs, it is required to digest IgGs using the proteolytic enzyme papain to obtain Fabs. Previously an immobilised form of papain was used to digest IgGs with the methodology being laborious and slow. A new method using a soluble form of papain was developed, which allows the digestion of up to 100 mg of IgG within 30 minutes and with a yield in excess of 50%. Purification of the digestion mixtures to obtain highly purified Fabs was achieved using Protein L chromatography. The developed digestion method using soluble papain was published in literature during this PhD –

Collins M, Khalili H. Soluble Papain to Digest Monoclonal Antibodies; Time and Cost-Effective Method to Obtain Fab Fragment. Bioengineering (Basel). 2022 May 12;9(5):209. doi: 10.3390/bioengineering9050209. PMID: 35621487; PMCID: PMC9137653.

To synthesise BsFpFs, different chemistry methods were used. A conjugation-ligation strategy in which two different Fabs are conjugated to di-functional reagents was explored. Two di-functional reagents PEG *bis*-sulfone transcyclooctene (TCO) and PEG *bis*-sulfone tetrazine (Tz) were prepared by our research group. The *bis*-sulfone group enabled conjugation to Fabs to proceed, forming TCO and Tz functionalised intermediates. The free TCO and Tz moieties ligate, allowing the TCO and Tz functionalised intermediates to combine into a single molecule, a BsFpF. Key

to the preparation of BsFpFs via conjugation-ligation was the removal of any free PEG *bis*-sulfone TCO and PEG *bis*-sulfone Tz reagents prior to ligation of the TCO and Tz functionalised intermediates.

14 different BsFpFs were prepared via conjugation-ligation. It was possible to obtain highly purified BsFpFs using ion exchange (IEX) and size exclusion chromatographies (SEC) with purity being confirmed via silver staining. Isolated yields of BsFpFs were between 10-15% with yield being limited by the purity of reagents **26** and **27**. BsFpFs were stored at their intended storage temperature of 5°C for 6 months with no evidence of deconjugation or aggregation being observed.

Ligand binding studies performed using enzyme linked immunosorbent assays (ELISA) and surface plasmon resonance (SPR) were able to confirm that BsFpFs were capable of binding to both of their intended targets, with SPR confirming binding in a concentration dependent manner. ELISA demonstrated that an anti-VEGF/IL-6R BsFpF had a similar affinity towards vascular endothelial growth factor (VEGF) and the interleukin-6 receptor (IL-6R) as anti-VEGF and anti-IL-6R TCO and Tz functionalised Fab conjugates. This indicated that the VEGF binding arm of the anti-VEGF/IL-6R BsFpF did not interfere during binding of the BsFpF to IL-6R and vice versa. During SPR binding experiments the same finding was found during VEGF binding assays, however the same was not found when binding to IL-6R.

The data presented in this thesis demonstrates that it is possible to reproducibly prepare and purify BsFpFs targeting two intraocular targets simultaneously. Future work would focus on the assessment of the functional activity of BsFpFs using *in-vitro* cell-based assays. Preliminary work showed that human umbilical vascular endothelial cells (HUVECs) may be a suitable choice of cell model for these assays.

Declaration

I declare that this thesis has been composed solely by myself and that it has not been submitted, in whole or in part, in any previous application for a degree. Except where stated otherwise by reference or acknowledgment, the work presented is entirely my own.

Name: Matthew Collins

Signed:

Date: 02 SEP 23

Table of Contents

Lists of figures, tables and schemes

Figures

Tables

Schemes

Abbreviations

µL	Microliter
ADA	Anti-drug antibody
ADC	Antibody-drug conjugate
ADCC	Antibody-dependent cell mediated cytotoxicity
ALL	Acute lymphoblastic leukaemia
ANG-2	Angiopioetin-2
APC	Allophycocyanin
BCA	Bicinchoninic acid assay
BCMA	B-cell maturation antigen
BiTE	Bispecific T-cell engager
BLA	Biologics license application
BRB	Blood-retinal barrier
BSA	Bovine serum albumin
BsFab2	Bispecific Fab2
BsFpF	Bispecific Fab-PEG-Fab
CAR-T	Chimeric antigen receptor T-cell
CD13	Aminopeptidase N
CD19	B-lymphocyte antigen CD19
CD20	B-lymphocyte antigen CD20
CD3	Cluster of differentiation 3
CDR	Complimentary determining region
CEA	Carcinoembryonic antigen
CH1	Constant heavy region 1
CH2	Constant heavy region 2
CH3	Constant heavy region 3
CL	Constant light region
CNV	Choroidal neovascularisation
CRS	Cytokine release syndrome
CuAAC	Copper catalysed azide-alkyne cycloaddition
DARPin	Designed ankyrin repeat unit
DART	Dual-affinity re-targeting
DBCO	Dibenzocyclooctyne
DLS	Dynamic light scattering
DME	Diabetic macular edema
DMSO	Dimethyl sulfoxide

DOL	Degree of labelling
DR	Diabetic retinopathy
DTT	Dithiothreitol
DVD-Ig	Dual-variable-domain IgG antibody
E. coli	Escherichia coli
ECM	Extracellular matrix
EDC	1-Ethyl-3-(3-dimethylaminopropyl)carbodiimide
EDTA	Ethylenediaminetetraacetic acid
EGF	Epidermal growth factor
EGFR	Epidermal growth factor receptor
ELISA	Enzyme linked immunosorbent assay
EMA	European Medicines Agency
EpCAM	Epithelial cellular adhesion molecule
ErbB3	Receptor tyrosine-protein kinase erbB-3
Fab	Fragment antigen binding
Fab'	Fab prime
Fc	Fragment crystallisable
FDA	Food and Drug Administration
FITC	Fluorescein isothiocyanate
FpF	Fab-PEG-Fab
GCSF	Granulocyte colony-stimulating factor
GLP-1	Glucagon like peptide
Gp100	Glycoprotein 100
HCl	Hydrochloric Acid
HER2	Receptor tyrosine-protein kinase erbB-2
HMW	High molecular weight
HSA	Human serum albumin
HSA	Human serum albumin
HUVEC	Human umbilical vascular endothelial cells
ICAM-1	Intercellular adhesion molecule 1
iEDDA	Inverse-electron-demand Diels-Alder
IEX	Ion exchange chromatography
IFN	Interferon
IGFR-1	Insulin-like growth factor receptor 1
IgG	Immunoglobulin G
IL-17A	Interleukin-17A

IL-1α	Interleukin-1 alpha
IL-1β	Interleukin-1 beta
IL-6R	Interleukin-6 receptor
ILM	Internal limiting membrane
K_a	Association rate constant
K_d	Dissociation rate constant
K_D	Affinity
kDa	Kilodalton
LAG-3	Lymphocyte-activation gene 3
ME	Macular edema
mg	Milligram
mL	Milliliter
mRNA	Messenger ribonucleic acid
MST	Microscale thermophoresis
MW	Molecular weight
MWCO	Molecular weight cut off
NaOH	Sodium Hydroxide
ng	Nanogram
NHS	N-Hydroxysuccinimide
nM	Nanomole
nm	Nanometer
NVG	Neovascular glaucoma
PBS	Phosphate buffered saline
PD-1	Programmed cell death protein 1
PDGF-B	Platelet-derived growth factor-B
PDGFR-B	Platelet-derived growth factor-B receptor
PDI	Polydispersity index
PEG	Poly(ethylene glycol)
PIGF	Placental growth factor
RPE	Retinal pigment epithelium
RpR	Receptor binding region-PEG-receptor binding region
RU	Response units
S1P	Sphingosine-1-phosphate
ScFv	Single chain variable fragment
sdAbs	Single domain antibodies
SDS PAGE	Sodium dodecyl sulfate–polyacrylamide gel electrophoresis

SEC	Size exclusion chromatography
SPAAC	Strain-promoted azide-alkyne cycloaddition
SPR	Surface plasmon resonance
TCO	Trans-cyclooctene
TF	Tissue factor
TNFR2	Tumour necrosis factor alpha receptor 2
TNF-α	Tumour necrosis factor alpha
Tz	Tetrazine
VCAM-1	Vascular cell adhesion molecule 1
VEGF	Vascular endothelial growth factor
VEGFR-1	VEGF receptor 1
VEGFR-2	VEGF receptor 2
VH	Variable heavy region
VL	Variable light region
w-AMD	Wet age-related macular degeneration

Acknowledgements

Firstly, I would like to say a massive thank you to my supervisory team, Dr. Hanieh Khalili, Professor Steve Brocchini and Dr. Lesley Smyth. Without their constant support and guidance completing my PhD would not have been possible. I have become a better and more rounded scientist due to your guidance.

Without the funding kindly provided by the University of East London, School of Health, Sport and Bioscience this PhD would not have been possible. I would like to thank UCL School of Pharmacy for allowing me to work in their laboratories, I was always made to feel very welcome whenever I worked at SoP.

Finally, I want to give a special thanks to my wife Christina and my family for having been by my side and giving me constant encouragement throughout my PhD.

This PhD is dedicated to our son Edward, the light of our lives.

Chapter 1 – Introduction

Introduction to antibody therapeutics

There is an ever-increasing clinical interest in the development of antibody-based medicines with the FDA approving about 4 new antibody medicines per year [1] with the 100th antibody therapeutic being approved in May 2021 [2] . Antibody based medicines include IgG antibodies, Fc-fusion proteins and peptides, antibody-drug conjugates and multiple antibody fragment-based structures which are in development or have been approved. IgG antibodies are endogenous molecules with a structure comprising of light and heavy amino acid chains. An IgG is made up of two Fabs containing both light and heavy chains and a Fc region containing solely heavy chains that are stabilised by 2 disulfide bonds at the hinge. The two Fabs are also stabilised by a single disulfide bond found at their terminus.

Figure 1 shows representative structures of antibody-based motifs that have been developed into therapies. The different colours that make up the structures in Figure 1 relate to different parts of the antibody-based motifs. The light blue parts are light chains and the dark blue heavy chains, the same colouring is used throughout this thesis for antibody-based molecules. The light red and dark red chains (Figure 1C) are again light and heavy chains respectively but are differentiated to distinguish them as coming from another antibody. They are not the same light and heavy chains as the light and dark blue parts of the same molecule showing that it is bispecific in nature. The smaller light blue and dark regions at the top of Figure 1D denote the receptor binding regions present in a Fc-fusion protein.
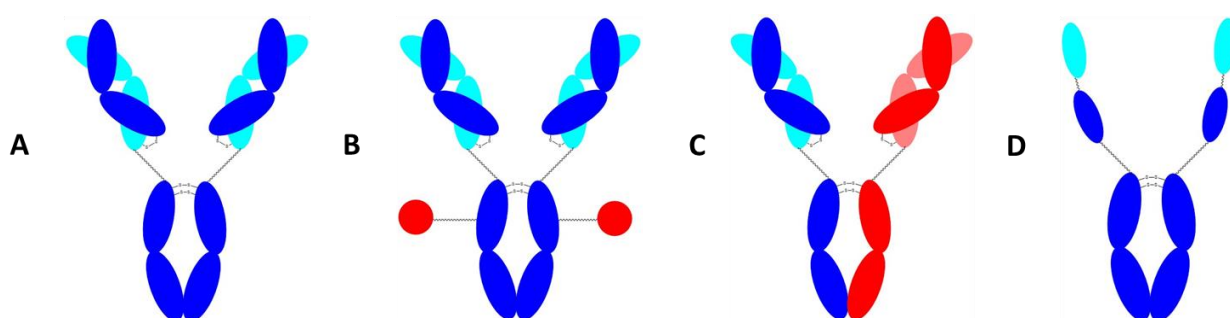
Figure 1: Structures of three antibody derived motifs used to develop therapies. **(A)** Monospecific immunoglobulin G (IgG) antibody – A monospecific IgG antibody has two identical fragment antigen binding (Fab) and fragment crystallisable (Fc) regions stabilised by inter and intra-chain disulfide bonds, it is a bivalent molecule. The molecule can only interact with one target at a time. **(B)** Antibody-drug conjugate – An antibody-drug conjugate is a monospecific IgG antibody linked to an anti-cancer drug. The antibody attaches itself to antigens present on cancerous cells which ensures delivery of the cytotoxic anti-cancer drug. **(C)** Bispecific IgG antibody – A bispecific IgG antibody has two different Fab and Fc regions stabilised by inter and intra-chain disulfide bonds, it is a monovalent molecule. The molecule can interact with two different targets at a time. **(D)** Fc-fusion protein – Two binding regions (examples include soluble receptors and peptides) are bound to an IgG Fc region.

Examples of marketed monospecific protein therapies are adalimumab (Humira®), aflibercept (Eylea®) and bevacizumab (Avastin®). These three antibodies had a combined revenue in excess of $20 billion in 2015 [3]. The global combined revenue for monoclonal antibody therapies may be as high as $380 billion by 2027 [4] with further growth expected.

Adalimumab (Humira®) is a monoclonal IgG commercialised by AbbVie to treat rheumatoid arthritis; it was the first fully human antibody approved by the FDA. It specifically interacts and blocks a ligand called Tumour Necrosis Factor Alpha (TNF-α) which is involved in inflammatory response. Rheumatoid arthritis is a heterogeneous and complex condition in which multiple proinflammatory cytokines including TNF-α contribute to progressing the condition [5]. Adalimumab only contains a variable region that binds to a single epitope in TNF-α, so it is monospecific [6]. Ranibizumab (Lucentis) which is an antibody fragment (Fab), aflibercept (Eylea®) which is a Fc-fusion, and the IgG bevacizumab (Avastin®) each bind to a ligand called Vascular Endothelial Growth Factor (VEGF). VEGF drives angiogenesis and its inhibition is important to slow the progression of wet age-related macular degeneration (w-AMD) which is the main cause of blindness in elderly people. Although these three medicines bind to VEGF and are monospecific, they each bind to different regions or epitopes on the VEGF ligand.

Monoclonal antibodies have a total molecular weight of about 150 kilodaltons (kDa) and comprise of two equivalent heavy chains and two equivalent light chains that yield two binding regions known as the complementary determining region (CDR). Each can bind to the same epitope, or antigenic site on a target molecule or pathogen. Monoclonal IgG antibodies are thus mono-specific as they bind to one epitope but are bivalent in that they bind to two copies of the epitope. Antibodies which contain two different CDRs are termed bispecific antibodies.

Bispecific antibodies is an umbrella term for a variety of protein molecules that are capable of interacting with two target epitopes [7]. Many of these protein molecules do not have CDRs, and may bind to the target epitopes by other means, e.g. utilisation of the extracellular region of a target receptor as is seen with Fc-fusion molecules. A key advantage of a bispecific antibody-based medicine is that such molecules offer the chance to exploit spatial-temporal effects. For example, a bispecific molecule capable of binding to a receptor on one cell and another receptor on a different cell have the potential for bringing the two cells together. Analogously, if a bispecific

molecule binds to two different proteins, then it is possible to bring these two proteins into close contact with each other. Bispecific antibody formats are non-endogenous and are products of genetic engineering.

Bispecific antibody design is not limited to the traditional IgG format. Many formats have been described including single chain variable fragments (scFv), bi-specific T-cell engagers (BiTE) and nanobodies[8]. These formats are discussed in more detail later in this chapter. An interesting example is a bispecific Fc fusion protein called "Valpha" which binds to VEGF-A and TNF-a. Valpha is a Fc-fusion protein that is comprised of the extracellular VEGF-A binding domain from the VEGF receptor 1 (VEGF-R1) and the extracellular binding domain for TNF-α from the TNF-α receptor 2 (TNFR2)[9].

In total there are in excess of 100 bispecific formats at different stages of development [10]. To date there have been nine approved bispecific protein therapies; Catumaxomab (now withdrawn), blinatumomab, bimekizumab, emicizumab, amivantamab, faricimab, tebentafusp (a bispecific fusion protein), mosunetuzumab and teclistamab. Five of the eight bispecifics have been approved since December 2021 [11,12] indicating the unmet medical need that has been identified and the progression of technologies needed to manufacture bispecifics. Details of approved bispecifics are shown below in Table 1.

Name	Trade name	Company	Format	Therapeutic Area	Targets	Year of Approval
Catumaxomab	Removab	Fresenius Biotech	Bispecific IgG	Oncology	CD3	2009 (since removed from market)
					EpCAM	
Blinatumomab	Blincyto	Amgen	BiTE	Oncology	CD3	2014
					CD19	
Emicizumab	Hemlibra	Genentech	Bispecific IgG	Haemophilia	Factor IX	2018
					Factor X	
Amivantamab	Rybrevant	Jannsen-Cilag	Bispecific IgG	Oncology	EGF	2021
					MET	
Bimekizumab	BimZelx	UCB	Bispecific IgG	Dermatology	IL-17A	2021
					IL-17F	
Faricimab	Vabysmo	Roche	Bispecific Cross MAb	Ophthalmology	VEGF	2022
					ANG-2	
Tebentafusp	Kimmtrak	Immunocore	Bispecific Fc-fusion protein	Oncology	CD3	2022
					Gp100	
Teclistamab	Tecvayli	Jannsen-Cilag	Bispecific IgG	Oncology	CD3	2022
					BCMA	
Mosunetuzumab	Lunsumio	Roche	Bispecific IgG	Oncology	CD3	2022
					CD20	

Table 1: Approved bispecific antibody therapeutics.

As shown in Table 1, most of the approved bispecifics are for oncology indications. Blinatumomab was developed to improve treatment of relapsed B-cell malignancies [13]. Blinatumomab has a novel mechanism of action in which it binds to the CD19 receptors present on malignant B-cells and the CD3 receptor present on T-cells. By bringing the malignant B-cell into closer contact with a T-cell, it was found possible to trigger a T-cell signal cascade against the malignant B-cells [14].

There is clear rationale for the development of bispecific immune modulatory protein therapies to treat cancer which has included T cell redirection, natural-killer cell redirection, tumour-targeted immunomodulators or dual immunomodulators, these are all possible to create with bispecific therapies but not monospecific therapies [15]. Most bispecific antibodies currently in clinical development are intended for oncology

indications. The mechanism of action for the majority of these molecules involves binding and activation of T cells via CD3 receptors and subsequent direction of the activated T cells to a tumour [15]. Blinatumomab is an approved example of a T-cell redirecting bispecific.

Bispecific antibodies also have application for the treatment of rheumatoid arthritis along with other inflammatory conditions (e.g. atopic dermatitis and psoriasis). Cytokine mRNA and protein analysis of rheumatoid arthritis tissue has revealed that proinflammatory cytokines and chemokines are present within inflamed tissue [16]. MT-6194 is a bispecific antibody targeting two proinflammatory cytokines; IL-6R and IL-17A. These two targets were selected as they act in a positive feedback loop together [17]. Surface plasmon resonance showed that MT-6194 had similar affinity for IL-6R compared to the control drug (tocilizumab) and higher affinity for IL-17 than another control drug (secukinumab). *In vivo* mouse inflammation models showed that MT-6194 is capable of simultaneous inhibition of both IL-6R and IL17A with the potential to enhance efficacy and synergistic effects when compared to each of the control monospecific therapies. The current development stage of MT-6194 is not known.

Two important bispecific antibodies not in the areas of oncology or inflammation are (i) emicizumab and (ii) faricimab. Emicizumab, approved in 2018 is a bispecific, humanised antibody which has been approved to treat haemophilia-A [18]. Emicizumab is known as a non-factor-VIII treatment for haemophilia-A. Prior to the introduction of emicizumab, factor-VIII protein-based drugs were used exclusively to replace the factor VIII missing in patients suffering from haemophilia A. Factor-VIII based drugs have relatively short half-lives of between 8-12 hours with the production of anti-FVIII antibodies observed in 20-30% of patients[19]. Emicizumab address both of these issues, its half-life is longer up to 28 days [20] and there are less anti-drug antibodies generated (e.g. 2 of 39 patients in a clinical trial) [19]. Emicizumab functions by creating a bridge between two proteins; factors IXa and X mimicking the behaviour of factor VIII which is critical for the coagulation cascade.

Faricimab, a bispecific antibody developed by Roche to treat retinal disease was approved by the FDA in 2022 [21]. Faricimab targets VEGF and angiopoietin-2 (ANG-2) in the vitreous cavity of the eye and is used in the treatment of wAMD. Chronic angiogenesis diseases in the back of the eye have become one of the leading blinding conditions over the world, mainly including w-AMD, diabetic retinopathy (DR), and

choroidal neovascularization (CNV). The introduction of intravitreally injected antibody-based anti-VEGF biologics have revolutionised the therapy of neovascular diseases in the back of the eye.

Developing formulations for intravitreal injection must meet stringent interocular criteria based on the need to maintain ocular tolerability and to use very small injection volumes of 50 μL, precluding the use of combination formulations. Due to the chronic nature of many retinal diseases, frequent intravitreal injection is required to deliver sufficient biotherapeutics to the back of the eye. Much effort has focused on drug and formulation development to reduce the frequency of administration because intravitreal injections are of considerable burden on patients and health care providers. The burden of intravitreal injections also precludes the use of multiple medicines being injected to provide combination therapies to treat retinal disease. Faricimab succeeded where combination therapies targeting VEGF and ANG-2 did not [22].

Bispecific antibody-based formats

Many different bispecific formats have been described from preclinical research settings, and some of these formats now exist in the clinic and in clinical development. A dual-variable-domain IgG antibody (DVD-Ig) is one example (Figure 2). The structure of a DVD-Ig differs from an endogenous IgG antibody by the arrangement of their heavy and light chains. In a traditional endogenous IgG antibody, the heavy and light chains are organised with (1) the heavy comprised of a variable region (VH) and three constant regions (CH1, CH2, and CH3). The VH region is responsible for antigen binding, while the constant regions provide stability and effector functions, while (2) the light chain comprises a variable region (VL) and a constant region (CL). The VL region pairs with the VH region of the heavy chain to form the antigen-binding site (i.e. the CDR).

In contrast, a DVD-Ig incorporates two different antigen-binding domains within a single IgG molecule[23]. Overall, the key structural difference between a DVD-Ig antibody and an endogenous IgG antibody lies in the arrangement of their heavy and light chains to enable dual antigen binding in the former. This is achieved by modifying the heavy and light chain structures. The heavy chain of a DVD-Ig is typically engineered to accommodate two VH regions, each derived from different antibodies. These VH regions retain their antigen-binding capabilities and are connected to the corresponding CH1, CH2, and CH3 regions. The combination of two different heavy

and light chain pairs in a DVD-Ig allows for dual-target recognition and binding. It enables the antibody to simultaneously engage with two distinct antigens, providing potential advantages in targeting multiple disease pathways or antigens with a single therapeutic molecule.
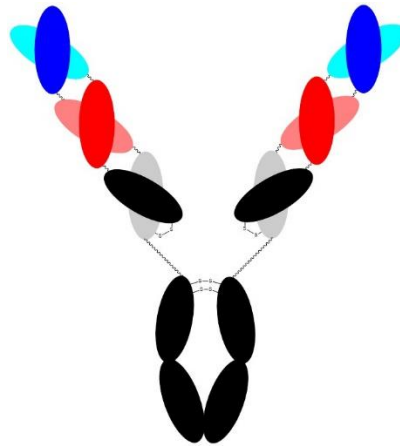
Figure 2: Structure of a DVD-Ig. A DVD-Ig comprises of an IgG antibody to which additional variable regions are linked via peptide linkages. It is an example of a bivalent bispecific molecule. The light blue and dark blue regions and light red and dark red regions correspond to light and heavy chains from 2 different antibodies. The grey and black regions correspond to light and heavy chains from a 3rd antibody source.

DVD-Ig molecules were described in 2007 [24] with a molecular weight in excess of 200KDa. A DVD-Ig can be produced from mammalian cell lines and from human sequences which can potentially reduce the immunogenicity of the DVD-Ig molecule [23], as it is not an endogenous molecule. The structure of the peptide linkers between the variable domains on each arm are critical to the functionality and stability of a DVD-Ig [24],[25] which adds additional complexity to the preparation of DVD-Ig bispecifics.

Two examples of DVD-Igs in clinical development are both manufactured by Abbvie. The first ABT-122 simultaneously targets TNF-α and IL-17A for the treatment of psoriatic arthritis. ABT-122 completed a Phase II clinical trial (NCT02349451) in 2018. Results of the trial indicated that ABT-122 had safety and efficacy comparable to Adalimumab over the course of the 12 week trial [26]. Because it only achieved comparable efficacy with Adalimumab, development of ABT-122 was discontinued. The second molecule Lutikuzumab (ABT-948) simultaneously targets IL-1α and IL-β to treat patients with knee osteoarthritis with evidence of synovitis. Lutikuzumab completed a Phase II clinical trial (NCT02087904) in 2018. Results showed that dual inhibition of IL-1α and IL-β was not effective in reducing inflammation or pain associated with the condition [27].

It is possible to create a "two-in-one" antibody by introducing mutations into the light chain CDR regions of a monospecific IgG antibody. These mutations give the molecule the ability to bind to a second target epitope simultaneously. Therefore, each Fab arm of a "two-in-one" antibody can bind to two different epitopes in contrast to a traditional bispecific IgG antibody in which each arm binds independently. The structure of a "two-in-one" antibody is shown in Figure 3.
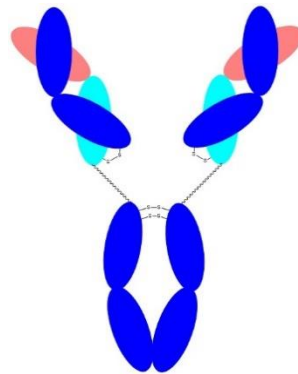
Figure 3: Structure of a two-in-one antibody. A two in one antibody comprises of an IgG antibody with mutations present in the light chain of the Fab variable regions (pink region). This mutation allows the light and heavy chains of the Fab variable regions to bind independently to different targets.

An example of a two-in-one antibody was described by Bostrom *et al.* [28] where using trastuzumab (Herceptin®), which targets HER2 they generated variants with mutations in the light chain CDR to produce a two-in-one antibody capable of binding to HER2 and VEGF simultaneously. A combination of Colo 205 (human colorectal cancer cell line) and BT474M1 (human breast cancer cell line) *in vitro* cell growth assays demonstrated that the VEGF and HER2 binding components were active.

Another example of a two-in-one antibody in clinical development is Duligotuzumab. Duligotuzumab targets EGFR and HER2 for the treatment of metastatic colorectal cancer. Results of its Phase II clinical trial (NCT01652482) [29] found there was no clinical benefit of the dual inhibition of EGFR and HER2 over inhibition of EGFR alone resulting in the cessation of clinical development. The epitopes of this two-in-one antibody were found to be close to each other, so it is possible a steric hinderance effect may be limiting the effectiveness of the molecule. It is also possible that there may have been clinical factors with patient selection or the lack of target synergism that would yield a clinical benefit.

Antibody fragments fused to Fc regions or whole IgG antibodies

Antibody fragments that can bind with affinity have been described. Many antibody fragments display reduced circulation times and thus have been fused to the Fc region of an IgG (Figure 4). The Fc region can also be engineered to facilitate effector function, for example, antibody-dependent cell-mediated cytotoxicity (ADCC) which can result in immune mediated killing of tumour cells [30].
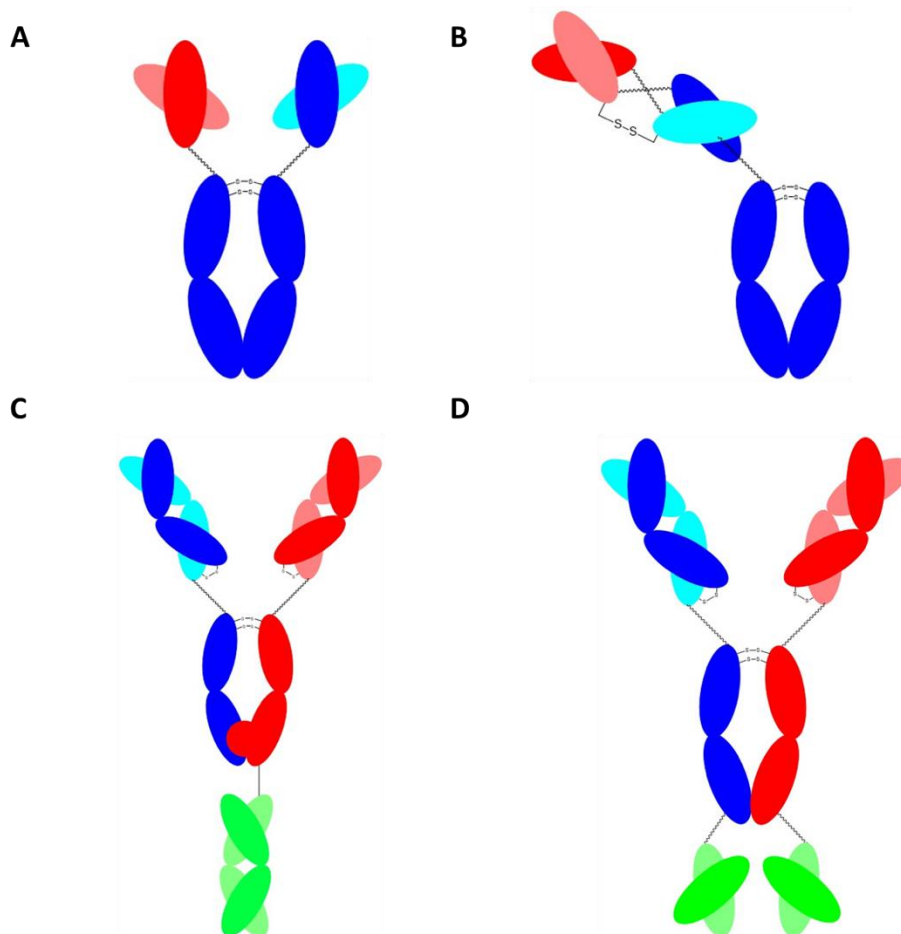
Figure 4: Examples of antibody fragments fused to Fc regions or whole antibodies. **(A)**. Bispecific tandem ScFv Fc in which two heterogenous ScFvs are fused to a IgG Fc region **(B)**.DART Fc molecule in which a DART antibody fragment is fused to a IgG Fc region. **(C)**. Trivalent, trispecific tandem-Fab antibody in which a 3rd Fab (light green and dark green regions) is fused to a bispecific CrossMAb. **(D)** Trispecific IgG ScFv fusion in which two ScFvs from a 3rd antibody (light green and dark green regions) are fused to a bispecific IgG to form a trispecific molecule.

A single-chain variable fragment (ScFv) is comprised of the VH and VL peptide chains connected into a single chain by a short linker peptide. This linker is flexible, allowing the two chains to come together and form an antigen-binding site similar to a natural IgG antibody. An ScFv can maintain the specificity of a full-length antibody, but the ScFv is a much smaller molecular weight and size than a full IgG antibody. The smaller size of ScFv antibodies can result in a greater potential to penetrate tissues more effectively than a full IgG molecule, making them useful in cancer treatment. ScFvs can also be easily produced in bacteria, making them more cost-effective to manufacture than full-length antibodies.

Fusion of two different ScFvs to an Fc region creates a bispecific ScFv-Fc as shown in Figure 5. The ScFv-Fc format retains the binding properties of the ScFv

fragment, and the introduction of the Fc region increases the systemic half-life of the molecule by Fc receptor recycling. Antibody fragments in general have short systemic half-lives, and ScFv fragments have been shown to display systemic half-lives of approximately ten minutes [31], which can be increased by fusion of the ScFv to an Fc region

ScFvs can also be fused to the C-terminus of IgG antibodies, creating ScFv-IgG molecules which can be bispecific and trispecific [32]. The structure of a trispecific ScFv-IgG is shown above in Figure 4. An ScFv-IgG molecule in clinical development is Istiratumab. Istiratumab simultaneously targets IGFR-1 and ErbB3, it is being developed by Merimack and as of 2020 is in a phase II clinical trial (NCT02399137).
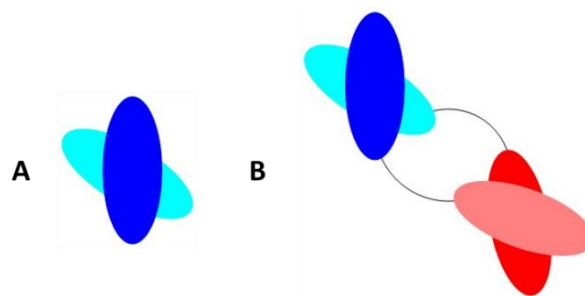
Figure 5: Structure of an ScFv and a bispecific diabody. **(A)** A ScFv is made from variable heavy and variable light chains expressed in E coli. **(B)** The variable regions that can bind to two different targets are linked by a short amino acid sequence of no more than 25 amino acid sequences.

Bispecific antibody-based motifs

Diabodies are recombinantly manufactured bispecific antibody fragments that can be expressed in E. *coli*. To construct a diabody, two single-chain variable fragments (ScFvs) are engineered such that they do not have the linker sequence that would usually connect the variable heavy (VH) and variable light (VL) chains into a single unit. Instead, the VH and VL domains are able to associate freely, which leads them to pair with the complementary domains of a second ScFv to form a bivalent molecule – a diabody [33].

As with most antibody fragments that have been described, bispecific diabodies are smaller in size than bispecific IgG molecules. Diabodies are approximately 60 kDa molecular weight. The small size of diabodies results in faster clearance compared to IgGs, but can also result in better tumour penetration for solid cancer applications and lower immunogenicity compared to IgGs [34]. Anti-CEA diabodies have demonstrated substantial and persistent tumour uptake alongside rapid clearance from blood and normal tissues, this resulted in favourable tumour: blood ratios [35]. Despite this only one diabody is in preclinical development and none in clinical development as of 2019.

The bispecific diabody in preclinical development is aiming to redirect T cells to CEA-positive tumour cells [36]. Figure 5 shows the structure of a ScFv and a bispecific diabody.

A Bi-specific T-cell engager (BiTE) is constructed from two ScFvs and has a molecular weight of approximately 50kDa (Figure 6). Each ScFv is made of a variable light chain (VL) and a variable heavy chain (VH) from an antibody, connected by a short linker peptide [37].
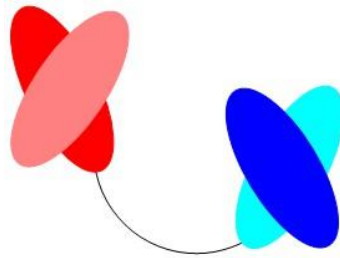
Figure 6: Structure of a BiTE molecule. A BiTE molecule consists of two different ScFv regions linked together by a freely rotatable peptide chain. BiTEs form a link between tumour and T cells.

Key to the functionality of BiTE molecules is the freely rotatable peptide linkage. The freely rotatable linkage enables the ScFvs to interact with targets on different cell surfaces or while in solution. Blinatumomab (Blincyto®) is a marketed BiTE molecule to treat acute lymphoblastic leukaemia (ALL). One of the targets of blinatumomab is CD19, a protein that is typically found on the surface of B cells, including B cell leukemias and lymphomas. The other target of blinatumomab is CD3, a protein that is present on the surface of T cells. By binding to both CD19 and CD3, blinatumomab brings the T cells into close proximity with the malignant B cells, enhancing the T cells ability to attack and kill the cancerous B cells.

The small size of blinatumomab makes it an effective molecule but it does have its disadvantages, these disadvantages are likely to be true for all BiTE molecules not just blinatumomab. Blinatumomab is rapidly excreted from the body with a short half-life of approximately 1.5 hours, which means blinatumomab must be continuously infused for a period of 4 weeks [38]. A 4-week continuous infusion requires vast quantities of blinatumomab which comes at significant cost. A significant side effect of blinatumomab is cytokine release syndrome (CRS). CRS is a systemic inflammatory response that activates T cells which release pro-inflammatory cytokines, CRS can be life-threatening. During the phase three trial of blinatumomab 14% of patients

experienced CRS of varying severity. Many immunotherapies are characterised by adverse reactions in the clinic.

A dual-affinity re-targeting (DART) is a type of bispecific antibody in the molecular weight range of approximately 50-55 kDa that is comprised of two different antigen-binding sites derived from the variable domains of different antibodies (Figure 7). These binding sites are connected by a short linker in a DART. The dual-targeting feature of DART proteins has been used to bind to a specific marker on a cancer cell, while the other side is designed to bind to an immune cell. This helps to bring the immune cells into proximity with the cancer cells, enhancing the immune system's ability to attack the cancer. As with other non-endogenous proteins, DART proteins can potentially provoke an immune response (e.g. generation of anti-drug antibodies).
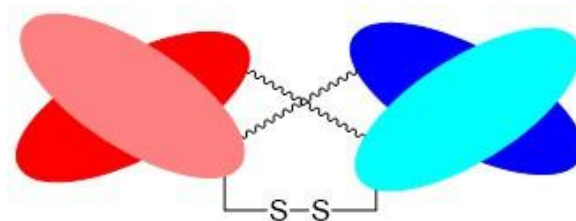
Figure 7: Structure of a DART molecule. A DART molecule is made from two different ScFvs. The heavy and light chains of the ScFvs are linked by short peptide linkages and the light chains are linked via a disulfide stabilised covalent bond.

The less flexible configuration of a DART limits the rotation of the antigen binding domains in contrast to the free rotatable BiTE. The linkage of the heavy chain on the first ScFv to the light chain on the second ScFv reduces the constraint of intervening linker sequences, this helps the molecule achieve association similar to an IgG molecule [39].

An *in vitro* study comparing the ability of DART and BiTE molecules to kill B-cell lymphoma showed that the DART molecule performed better in terms of maximal cell lysis and required a lower concentration than the BiTE molecule for half-cell lysis [40]. The DART and BiTE molecules in this study were derived from the same murine anti-CD3 and anti-CD19 antibodies.

As of 2019 there are two DART molecules in clinical development, both for oncology indications [36]. An issue with DART molecules is possible immunogenicity. A study evaluating the activity of a CD3/CD13 DART in cynomolgus monkeys found that anti-drug antibodies (ADAs) were produced in 23 of the 32 monkeys [41]. The concentrations of ADAs were not homogenous across the animals. An example of a DART molecule in clinical development is Tebotelimab. Tebotelimab targets PD-1 and

LAG-3 and is currently in Phase I clinical trials for the treatment of HER2 positive breast cancer [42], it should be noted however that the molecule is being dosed in combination with another antibody during this trial.

PF-06671008 is an example of a DART-Fc bispecific targeting P-cadherin and CD3. It was developed by Pfizer for a solid tumour indication. The molecule showed promise preclinically demonstrating T-cell mediated regression of solid tumours in mice [43]. Despite this recruitment for a Phase I clinical trial (NCT02659631) was not completed and in 2019 development of the drug was halted.

Single domain antibodies (sdAbs) derived from variable heavy-chains (VHH antibodies), which are also known as nanobodies, are a type of non-endogenous antibody produced by the immune system of camelids, such as camels and llamas. They are unique because, unlike most antibodies, they consist of a single monomeric variable antibody domain. This makes them much smaller than conventional antibodies, hence the name "nanobody", but despite their small size, nanobodies can retain full antigen binding capacity. Nanobodies (Figure 8) can be expressed in E. *coli* and yeast.
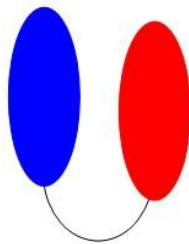
Figure 8: Structure of a bispecific nanobody molecule. A bispecific nanobody is made of two different variable heavy chain regions connected by a short peptide linkage. Nanobodies do not contain light chains.

Nanobodies have advantages including high solubility, small molecular weight, high stability and due to their small size good tissue penetration [44]. Despite their small size, nanobodies which utilise 3 CDRs to form the antigen binding site can retain full antigen binding capacity. Bispecific nanobodies can be linked via peptide linkage (Figure 8), joined to Fc regions or can be conjugated using polymers such as poly(ethylene glycol).

Nanobodies also have advantages during production as they do not bind to light chains, this lack of binding to light chains reduces aggregation tendencies, which can avoid mispairing problems seen with the production of IgG derived bispecific antibodies [44]. The small size of a nanobody molecule does suffer from possessing a short *in vivo* half-life of no more than a few hours [45]. A study looking at tumour

targeting of nanobodies found that the nanobody had an elimination half-life of only 1.5 hours [46]. *In vivo* half-life can be increased by conjugating albumin or a polymer such as poly(ethylene glycol) to the nanobody.

The first bispecific nanobody, Ozoralizumab targeting TNF-α and bovine serum albumin (BSA) was approved in 2022 for the treatment of rheumatoid arthritis in Japan. The molecule was developed by Ablynx and marketed in Japan by Taisho Pharmaceuticals [47]. Ozoralizumab despite having a relatively small molecular weight of 38kDa is dosed subcutaneously every 2 weeks during the induction or loading phase, which is possible because it binds to albumin to increase its circulation time. The frequency of dosing then decreases to maintain a therapeutic concentration in the blood (4-12 weeks).

Three other bispecific nanobodies; ALX00761, ALX0061 and ALX0141 all developed by Ablynx have not progressed past phase two clinical trials [8]. The reasons for the lack of progress are unknown. Modified nanobodies are also being explored with one interesting example being chimeric antigen receptor T-cell (CAR-T) nanobodies. Currently 5 of the approved CAR-T therapies comprise T-lymphocytes which have been engineered to express CAR on their surface with ScFvs being used as the molecular backbone within the T-cell membranes [48]. Using ScFvs for this purpose has limitations including immunogenicity risks and aggregation [48], issues that the use of nanobodies may overcome. A bispecific CAR-T nanobody targeting CD19 and CD20 is currently in phase I clinical trials for the treatment of refractory/relapsed b-cell lymphoma [49], the molecule is being developed by the Henan Hualong Biotechnology company. Monospecific nanobodies have also had success clinically with the FDA approval of caplacizumab for the treatment of thrombotic thrombocytopenic purpura and thrombosis in 2019. Caplacizumab is a bivalent molecule that comprises two peptide linked nanobodies which both bind to von Willebrand factor.

DARPins are antibody mimetics that interact with targets with specificities and affinities similar or surpassing antibodies [50]. DARPins (Figure 9) are adapted from naturally occurring ankyrin repeat units and can be expressed in *E. coli*, they are generally thought to be relatively stable molecules. They are α-helical scaffold proteins with small molecular weights (approx. 15kDa) [51]. An ankyrin repeat is a type of protein motif that consists of a sequence of about 33 amino acids. This motif is named after the protein ankyrin, in which it was first discovered. Structurally, ankyrin repeats

form a helix-loop-helix fold followed by a beta-hairpin. When several ankyrin repeats come together, they form a larger structure known as an ankyrin repeat domain. This domain is capable of mediating protein-protein interactions. Ankyrin repeat domains are one of the most common protein-protein interaction motifs in nature. They are found in a wide variety of proteins and are involved in numerous biological functions, including signal transduction, cell cycle regulation, inflammatory responses, and transcriptional regulation. Ankyrin repeat domains can be engineered to bind to a wide range of target proteins with high specificity and affinity, which is the basis for the development DARPins. The regular packing of the repeat units and conserved networks of hydrogen bonds contribute to the thermodynamic stability of DARPins [52].
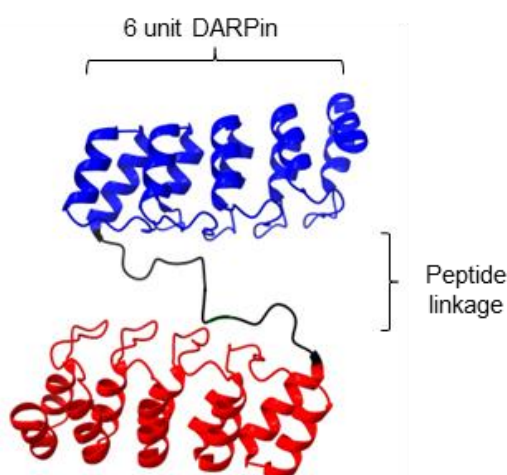
Figure 9: Structure of a bispecific DARPin. A bispecific DARPin comprises of two different α-helical scaffold proteins connected via a flexible peptide linkage.

MP0250 is an example of a tri-specific DARPin that is designed to target VEGF and hepatocyte growth factor (HGF) [53]. MP0250 comprises of four DARPins, one anti-VEGF, one anti-HGF and two anti- Human serum albumin (HSA). The anti-HSA DARPins are included to increase the plasma half-life of the molecule. Each of the DARPins are linked together via a polypeptide linkage. The efficacy of MP0250 was assessed using mouse xenograft and patient derived tumour models. MP0250 was shown to have anti-tumour effect as a monotherapy and the ability to potentiate the effect of paclitaxel. MP0250 which is developed by Molecular Partners is currently in a Phase Ib/II trial (NCT03418532 – ongoing) and a Phase II trial (NCT03136653 – ongoing).

The DutaFab platform was designed and developed by Roche with the molecule being expressed in E. *coli*. DutaFabs are engineered therapeutic Fab fragments that can bind two targets simultaneously [54]. They have been developed as a platform of dual targeting Fab (DutaFab) molecules, which include two spatially separated and independent binding sites within the human antibody CDR loops (Figure 10). These include the H-side paratope (which encompasses HCDR1, HCDR3, and LCDR2) and the L-side paratope (which encompasses LCDR1, LCDR3, and HCDR2). These paratopes can be independently selected and combined into the desired bispecific DutaFabs in a modular manner. Two targets, once bound are extremely close together which could be advantageous when trying to bring a specific molecule close to a specific receptor. Genentech are currently developing a DutaFab molecule targeting VEGF and ANG-2, the molecule RG6120 is currently in Phase I clinical trials [55].
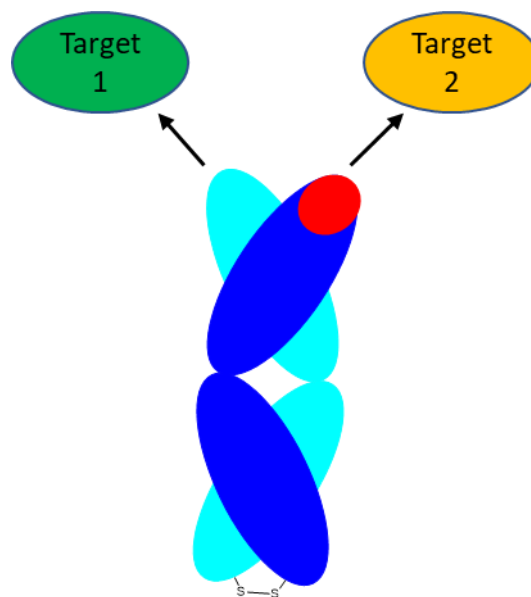
Figure 10: Structure of a DutaFab. A DutaFab is an engineered Fab fragment in which the light and heavy chain CDR regions have affinities towards different targets.

Monoclonal antibodies are produced by hybridoma and recombinant DNA technologies. These well-established methods are capable of producing pure, high-quality products in scales of up to 25,000 litres, with titers ranging from 1-5 g per litre [56]. However, unlike conventional monoclonal antibodies, the development of bispecific antibodies has faced significant production challenges at scale, including maintaining quantity, and achieving quality and stability [37] although these limitations are being solved as evidenced by the increased introduction of bispecific antibody based medicines into the clinic.

The application of sophisticated molecular design and genetic engineering has solved some of the aforementioned technical problems associated with the production of bispecific antibodies [10]. One example is CrossMAb technology. CrossMAb involves modifications to IgG light and heavy chains to allow more efficient production of bispecific antibodies. It is unknown if the use of CrossMAb technology would be practical in a research setting, as it is a proprietary technology that may be costly and technically challenging to replicate.

Bispecific antibodies were first manufactured using a hybrid-hybridoma or quadroma technique (Figure 11), which involves the fusion of two hybridoma cell lines each expressing different antigen binding regions. Once fused the resulting quadroma can express antibodies with the antigen binding capabilities of the two parent cells [37].
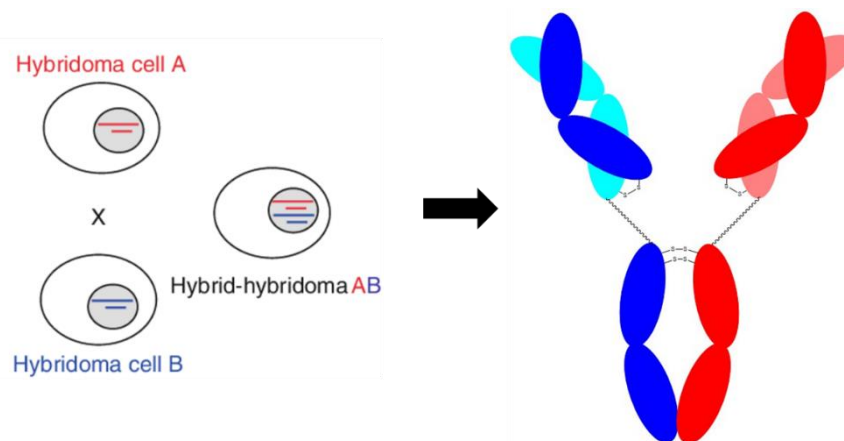
Figure 11: Quadroma technology for producing bispecific antibodies [57]. Quadroma technology is a hybridisation of two different hybridoma cells. A mouse hybridoma cell producing antibodies targeting one epitope and a rat hybridoma cell producing antibodies targeting a second epitope are hybridised to yield a hybrid hybridoma or quadroma cell line. The quadroma cell line produces a bispecific antibody which can bind to both target epitopes simultaneously.

The quadroma technique is regarded as being inefficient because only small quantities of the desired bispecific antibody is being produced. This is because it is theoretically possible to have 16 different combinations of light and heavy chains within the quadroma cell lines and apart from the desired bispecific, the remaining molecules are non-functional or monospecific [10]. Ensuring the correct pairing of heavy and light chains within a quadroma cell line remains a great challenge.

The development of Catumaxomab improved the understanding of the quadroma technique. Catumaxomab is comprised of rat and mouse antibody regions, the differences in these regions allowed established purification techniques such as Protein A chromatography and ion exchange chromatography to be successfully used

[37]. A caveat is the immunogenic effects seen in human subjects because of using murine antibody fragments to create a bispecific antibody.

"Knobs into holes" technology (Figure 12) was developed to ensure the correct heterodimerisation of heavy chains during the production of bispecific antibodies and to improve production efficiency compared to that achieved by quadroma cell lines [58]. Knobs into holes involves engineering antibody heavy chain homodimers leading to a more efficient heterodimerization process. A knob variant is created by the replacement of a small amino acid sequence with a larger sequence in a CH3 domain. The larger, bulkier amino acid literally creates a knob, which is designed to fit into the hole created by the replacement of a larger amino acid chain with a small one in another CH3 domain [59].
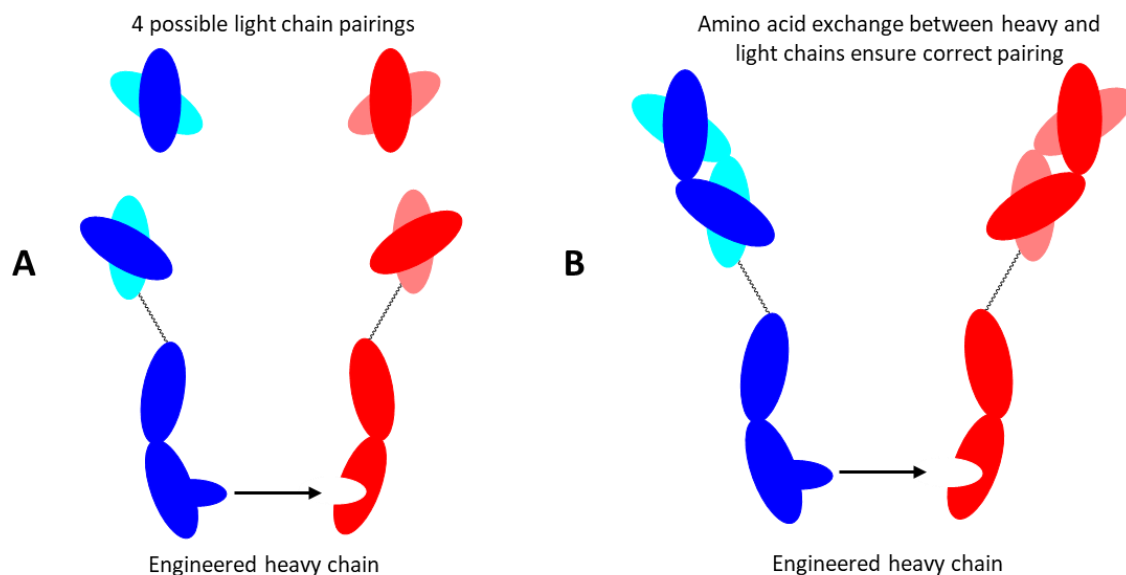
Figure 12: An illustration of **(A)** Knob into hole and **(B)** CrossMAb technologies for producing bispecific antibodies. Knob into hole technology solved the problem of heavy chain mispairing by engineering bulky amino acid sequences into the CH3 domain of the antibody reducing possible combinations to four. CrossMAb technology solves the further problem of light chain mispairing by exchange of amino acid blocks between the heavy and light chains of the antibody creating only the desired antibody.

The use of heavy chain knob into hole engineering reduces the amount of possible combinations to 4, a significant reduction from 16 compared to using quadroma technology [60]. A limitation of knob into hole technology is that light chain mispairing can still occur resulting in undesirable products. To address this limitation Roche developed the CrossMAb technology. CrossMAb involves the exchanging of amino acid blocks between the heavy and light antibody chains, which means that the two different arms bind to a specific light chain [61]. This approach eliminates light chain mispairing and creates only the desired antibody thus reducing purification processes needed to obtain the desired antibody.

As of 2021 a total of 19 CrossMAb bispecifics were in clinical development [62] with one of those molecules faricimab, having since being approved. Quadroma and CrossMAb technologies have been used to produce approved bispecifics based on IgG antibodies, which as a motif, is endogenous. The other bispecific antibody-based motifs that have been described (e.g. BiTE, DART, nanobody, etc) are generally non-endogenous molecular motifs which have been developed to be made recombinantly from bacterial and yeast sources.

Inhibition of VEGF to treat retinal neovascularisation

Visual impairment and blindness have always been a public health issue of great importance. In 2015, more than 253 million people suffered from visual impairment globally, of which 36 million were blind and a further 217 million had moderate to severe visual impairment [63]. Diseases in the back of the eye dominate the causes of blindness, especially for the aging population. The posterior segment of the eye possesses approximately two-thirds of the eyeball and includes the vitreous humour, sclera, choroid, macular, Bruch's membrane, retinal blood vessels, the retinal pigmented epithelium (RPE), and retina [64]. Any pathological factors that may interfere with the structural integrity of the posterior segment and especially the retina and optic nerve, can cause catastrophic vision loss.

The blood-retinal barrier (BRB) is composed of the retinal vascular endothelium and the retinal pigment epithelium. The BRB is a protectant barrier separating the retinal tissue from blood constituents of capillaries. While the breakdown of the BRB caused by multiple pathological processes might make the eye susceptible to inflammation there can also be breakdown of the normal blood supply causing retinal ischemia. Inflammation and hypoxia are generally regarded as the main contributors of the ocular neovascularization that induces new blood vessel growth [65]. Neovascularisation is uncontrolled vessel growth that occurs spontaneously, and angiogenesis is uncontrolled vessel growth from existing vasculature. Both forms of uncontrolled vessel growth are often referred to as neovascularisation. New blood vessels that are present due to uncontrolled growth are usually dysfunctional and unstable resulting in fluid leakage which can cause retinal tissue damage, fibrosis and inflammation.

Age related macular degeneration (AMD) is the leading cause of visual deterioration in developed countries, particularly in people older than 60 years [66] .

There are two broad versions of AMD, known as non-neovascular AMD (dry AMD) and neovascular AMD or wet AMD (w-AMD). The wet form of AMD accounts for 10~15 % of total AMD cases but is still the major cause of visual loss in the elderly population [67]. Diabetic retinopathy (DR) is characterized by retinal neovascularization resulting from retinal ischemia and disruption of the BRB [68]. The fluid leakage of these neovascular vessels can cause other secondary pathological conditions, such as macular edema (ME) and neovascular glaucoma (NVG) all of which can lead to the loss of visual function [69].

Antibody-based medicines have completely revolutionised the treatment of retinal diseases since 2005. These medicines must be administered by intravitreal injection which is the only clinically proven route of administration that can achieve high, reproducible doses of impermeable molecules into the vitreous cavity of the eye. Intravitreal injections are not easy for patients to endure and while the frequency of injections are currently about once every 2-3 months, treating chronic conditions often results in reduced patient compliance. As with most chronic conditions, combination therapies may be most efficacious for reducing disease progression, but the requirements of intravitreal injections and the underlying formulation constraints preclude the possibility for combination therapies either as separate intravitreal injections for each medicine in a combination or as a fixed dosed formulation that can be injected intravitreally.

Dosing antibody-based medicines to the eye topically although far less invasive is not a viable option. Topical administration of drugs to the eye generally results in poor drug bioavailability due to precorneal loss, tear turnover and tear dilution [70]. This coupled with the fact the tight intercellular junctions found within the cornea will not allow a large antibody molecule (150 kDa MW) to diffuse through [71] and have any chance of reaching the back of the eye. These factors are some of the reasons why intravitreal injection is the only clinically proven route to deliver antibodies into the vitreous cavity after which the antibodies diffuse through the vitreous humor with a portion reaching the back of the eye.

Once administered the ocular half-life or residence time of antibody based medicines within the eye is related to the molecular weight of the molecule with larger antibody molecules such as full IgGs (150 kDa MW) having longer residence times than antibody fragments such as Fabs (50 kDa MW) [72]. Elimination of intravitreally administered antibodies occurs via both via anterior or posterior routes. The anterior

elimination route encompasses drug diffusion to the aqueous humor and subsequent elimination via outflow. Posterior elimination occurs via elimination through various cell membranes located at the back of the eye [73].

VEGF is a proven clinical target for several different retinal indications. Since its first discovery as an angiogenic factor in the late 1980s [74], several medicines have been developed as VEGF inhibitors in oncology. Regarding retinal disease, 3 antibody-based therapies targeting VEGF for intravitreal injection have been approved, ranibizumab (Lucentis[®], 2006), aflibercept (Eylea[®], 2011) and brolucizumab (Beovu[®], 2019).

Ranibizumab (Lucentis[®], 2006) was specifically developed and formulated to treat retinal neovascularisation, and is an antibody fragment (Fab) that binds to VEGF-A at its receptor binding region to inhibit VEGF binding to its receptor, VEGFR-2 [75]. Aflibercept (Eylea[®], 2011) also developed and formulated to treat retinal neovascularisation is an Fc-fusion protein that comprises the Fc region of an IgG_1 fused to two copies of the extracellular domain-2 of VEFGR-1 linked to domain 3 of VEGFR-2 [76]. Aflibercept, also called VEGF-trap, has shown a wider binding capacity (VEGF-A, VEGF-B and placental growth factor (PIGF)) and higher VEGF binding affinity compared to ranibizumab[76].

Aflibercept (molecular weight ~ 110 kDa) is formulated at a dose of 2 mg in 50 μL for intravitreal injection while ranibizumab (~ 50 kDa) is formulated at a dose of 0.5 mg in 50 μL. This important difference in dosing amount means that a therapeutic concentration of aflibercept lasts longer in the vitreous cavity than ranibizumab. Aflibercept can be dosed less frequently than ranibizumab. Ranibizumab was initially administered about once monthly which has been extended to longer time points (up to 3 months) following a treat and extend regimen which can be implemented after several monthly injections have been administered. In 2015, the FDA approved (EMA, 2016) the dosing regimen for aflibercept to be administered every 3 months instead of every month. The 3-month dosing regimen for aflibercept is now the standard of care for the treatment of wet AMD and diabetic macular edema (DME). Aflibercept was added to the World Health Organisation (WHO) List of Essential Medicines in 2017.

Brolucizumab (Beovu[®], 2019) is a humanised single chain variable fragment (scFv, molecular weight of ~26 kDa) capable of binding to three isomers of VEGF-A ($VEGF_{110}$ $VEGF_{121}$ and $VEGF_{165}$) to prevent their interaction with both VEGFR-1 and

VEGFR-2 [77]. An intravitreal injection comprises 6 mg of brolucizumab in a single 50 µL dose which is 10 times greater on a molar basis than aflibercept and 20 times greater than ranibizumab. The increased molar dose of brolucizumab is thought to allow administration once every 3 months after completion of a dose loading period comprised of 3 monthly injections [77]. Brolucizumab has only recently been approved [78] and post marketing concerns over safety have been reported to the American Society of Retinal Specialists (ASRS) and case studies [79,80] have subsequently been published [81]. It may be that the higher concentration of brolucizumab in the formulation (compared to ranibizumab and aflibercept) may result in aggregation of brolucizumab.

A PEGylated (branched 2 × 20 kDa PEG) RNA aptamer (28-mer) called pegaptanib (Macugen®, 2004) has also been registered to treat retinal vascularisation. Pegaptanib binds with high affinity to VEGF-A (VEGF$_{165}$) to its heparin-binding site [82]. Binding to the heparin-binding site of VEGF$_{165}$ does not fully prevent the binding of VEGF to VEGFR-2, resulting in poor clinical efficacy compared with the antibody-based anti-VEGF agents.

Bevacizumab is a monoclonal antibody (IgG$_1$) that targets VEGF-A to block new blood vessel growth (angiogenesis) which is used to treat cancer. Bevacizumab is administered by infusion to treat a wide range of malignancies and metastatic disease including, colorectal, kidney, cervical, ovarian, lung and brain cancers. Bevacizumab is formulated at 25 mg/mL in vials that are to be diluted for infusion to treat cancer patients. Bevacizumab has been used off label for intraocular use because it can be fractionated from doses used for cancer to the small volumes used for intravitreal injections reducing the cost by at least 40-fold compared to each intraocular dose of ranibizumab [83]. This unlicensed use of bevacizumab has been supported by the Randomized Comparison of AMD Treatments Trials (CATT) funded by the National Eye Institute and the Inhibition of VEGF in Age-related choroidal Neovascularisation (IVAN) trial funded by UK National Health Institute [84]. Both trials showed the comparable anti- neovascularisation effectiveness of bevacizumab and ranibizumab to treat w-AMD.

Other anti-VEGF biologics currently in late-stage clinical development are abicipar pegol, conbercept, OPT-302 and KSI-301. Abicipar pegol is a designed ankyrin repeat protein (DARPin) targeting VEGF-A which is conjugated to

poly(ethylene glycol) or PEGylated (PEG, 20 kDa) to achieve 3 monthly dosing. DARPins are adapted from naturally occurring ankyrin repeat units, and are α-helical scaffold proteins with small molecular weights [51]. A DARPin with seven binding units has a molar mass of only 26 kDa, which is less than a Fab such as ranibizumab (~50 kDa). Abicipar has an exceptionally high picomolar potency and stability compared to the approved anti-VEGF antibodies in angiogenesis models of the eye [85]. Hence, anti-VEGF DARPin comparably inhibited vascular leakage after dosing at a concentration ten times less than ranibizumab. Phase III results showed that Abicipar has a longer half-life in the eye with quarterly injection compared to a monthly injection of ranibizumab. Intraocular inflammation was reported during the phase II and III trials [86,87] which was thought to be from manufacturing impurities [88]. Although the FDA accepted a Biologics License Application (BLA) it did not approve abicipar due to intraocular inflammation that was observed. However, abicipar appears to still be under development by Alcon for approval at a future date.

Conbercept and OPT-302 are Fc fusion proteins analogous in their structures to aflibercept. Conbercept which has been marketed in China since 2014 and is currently in phase III studies in the US, comprises of 2 copies of domain 2 of VEGFR-1 linked to domains 3 and 4 of VEGFR-2. The Fc region in OPT-302 is fused to two copies of extracellular domains 1-3 of VEFGR-3. OPT-302 inhibits VEGF-C and -D and is currently in Phase IIb trials for the treatment of neovascular AMD in combination with anti-VEGF-A molecules [89,90]. Complete blockade of the VEGF signalling pathway could be achieved through inhibition of VEGF-A along with VEGF-C and -D signalling pathways. This is suggested to have better results in neovascular regression compared to inhibition of single VEGF-A pathway [91].

KSI-301 is another anti-VEGF antibody that has recently entered phase II clinical trials for the treatment of wet-AMD. KSI-301 is designed to block all VEGF-A isomers [92] and comprises of IgG_1 antibody that covalently conjugated to a high molecular weight phosphorycholine biopolymer to have a total molecular weight of 950 kDa. The concept is to increase intraocular duration of action by leveraging hydrodynamic size and molar dose [93].

Other targets to retinal neovascularisation and inflammation

To augment therapies to inhibit uncontrolled retinal vascularisation [94], other potential clinical targets have emerged (Table 2) including neutralising platelet-derived growth

factor-B (PDGF-B), PDGF receptor-B (PDGFR-B) [95] and angiopoietin receptors (Tie-2) [96–98] are also being explored to treat ocular neovascularisation [99]. Targeting vascular pathways such as tyrosine kinase receptor 2 or angiopoietin receptors (Tie-2) and platelet-derived growth factors (PDGF and TGF-B) has shown promising results in neovascularisation regression and vessel stabilisation.

Type of therapeutic target	Therapeutic target	Name of drug	Format	Clinical progress	Company
Neovascular ligand	VEGF	Abicipar Pegol	PEGylated DARPin	Phase III [100,101]	Molecular Partners / Allergan
		KSI-301	IgG1 biopolymer conjugate	Phase II [92]	Kodiak
		OPT-302	Fc-fusion	Phase IIb [89]	Opthea
		Conbercept	Fc-fusion	Phase III [102–109]	Chengdu Kanghong Biotechnology
	PGDF	Rinucumab	IgG4	Phase II in combination with anti-VEGF drug (no benefit over VEGF monotherapy) [110–112]	Regeneron
	ANG-2	Nesvacumab	IgG1	Phase II in combination with anti-VEGF drug (discontinued)[113]	Regeneron
	VEGF/ANG-2	Faricimab	Bispecific CrossMab	Approved for Wet-AMD and DME [114]	Roche
Neovascular receptor	TF	Hl-con1	Fc-fusion protein	Phase II [115,116]	Iconic Therapeutics
	Fibronectin receptor	Volociximab	IgG1	Phase I [117]	Ophthotech
Inflammatory ligand	TNF-α	Adalimumab	IgG1	Approved for non-infectious Uveitis [118,119]	Abbott
	IL6R	Tocilizumab	IgG1	Phase II for non-infectious Uveitis [120]	Roche

Table 2: Possible druggable targets in clinical development for treatment of wet-AMD and non-infectious uveitis.

The Tie-2 receptor, like the VEGF receptor, is expressed in the endothelium and plays an important role in vascular network progression. Angiopoietin-2 (ANG-2) is a ligand that binds to the Tie-2 receptor and acts as a pro-angiogenic factor promoting angiogenesis in conjugation with VEGF. ANG-2 has also been shown to enhance retinal blood vessel sensitivity to the angiogenic effects of VEGF [121].

Nesvacumab, a monoclonal antibody against ANG-2, is in phase II clinical trials in combination with aflibercept for the treatment of DME.

PDGF is another growth factor that stimulates blood vessel formation, proliferation and angiogenesis, and may contribute to neovascularisation in wet-AMD [122]. PDGF binds to PDGFR-A and PDGFR-B which are tyrosine kinase receptors that are expressed in vascular smooth muscle cells and pericytes. Pegleranib (Fovista®, Ophthotech) is a PEGylated aptamer in phase III clinical trials that binds to PDGF-BB to prevent its binding to PDGFR-B [123]. Inhibition of PDGF binding to PDGFR-B causes pericytes to be stripped from vessels that have been abnormally formed, leading to their regression. Several studies demonstrated that when pegleranib was combined with ranibizumab, a strong suppression of retinal neovascularisation was achieved which was greater than monotherapy with ranibizumab [124]. Another example is the development of rinucumab, an IgG4 monoclonal antibody, that targets PDGF-R was and co-formulated with aflibercept for treatment of wet-AMD. These findings suggest that developing biologics inhibiting the PDGF or PDGFR pathway alone or in combination with anti-VEGF biologics could be valid targets for the treatment of ocular neovascularisation.

Drug combinations to target multiple ligands or receptors is successfully widely employed in different areas of medicine. In the case of ocular neovascularisation, great efforts have been made to design and formulate drug combinations with multiple targets with several examples in phase II trials, but so far, these have not been translated into successful phase III trials. For example, targeting PDGF and VEGF has been examined with rinucumab (anti-PDGF IgG4 co-formulated with aflibercept) and E10030/pegleranib (Fovista in combination with ranibizumab) in phase II and III trials respectively [110] but failed to show a benefit over anti-VEGF monotherapies.

Inhibition of ANG-2 in combination with VEGF has also been suggested as a potential combination for treating neovascularisation [22]. Two phase II trials were conducted using nesvacumab (anti-ANG-2 antibody) and aflibercept for the treatment of wet AMD (ONYX, NCT02712008) and DME (RUBY, NCT02712008). Results of these trials showed no statistical difference between best corrected visual acuity and central subfield thickness compared to aflibercept monotherapy [22].

Intraocular inflammation contributes to many disease pathologies including neovascularisation and uveitis. Uveitis is an inflammatory condition in which the uvea, a part of the eye found between the retinal and scleral and corneal layers becomes

inflamed If left uncontrolled uveitis can lead to loss of vision. Several studies in photoreceptor apoptosis have shown that proinflammatory cytokines such as tumour necrosis factor (TNF-α) and several interleukins (IL) [125] could play an important role in the progression of neovascular and inflammatory diseases. Adalimumab, a fully human monoclonal antibody against TNF-α, has been approved by the FDA and European Medicines Agency (EMA) for subcutaneous administration to treat non-infectious, posterior and pan-uveitis in adults and children over 2 years old [118,119]. Treatment of uveitis using adalimumab is, however, through the systemic route using the formulation registered to treat rheumatoid arthritis, rather than by intravitreal injection. High doses (e.g 5 mg/kg) are necessary to achieve adequate therapeutic level within the eye. Local therapy using intravitreal injection is associated with some safety concerns including increased incidence of endophthalmitis. Further studies are needed to explore the safety and efficacy of anti-TNF-α antibodies through intravitreal injection to exploit their rapid onset of action.

While the vitreous is an acellular compartment of the eye, there are cellular targets that are present in the retinal tissue. Protein therapeutics are not generally tissue permeable, so they tend to clear from the front of the eye via aqueous outflow. It is however possible for permeable molecules to interact with retinal tissue. Also in diseased eye, the internal limiting membrane (ILM) which separates the vitreous from the retina can be defective which could allow protein therapeutic more access to cellular membrane targets.

Tissue factor (TF) is a surface receptor target for coagulation factor VII which initiates the extrinsic coagulation pathway, plays an important role in retinal neovascularisation [126]. In a normal healthy eye, TF is not expressed by cells but is expressed in response to inflammation by vascular endothelial cells, monocytes and macrophages [127]. It has been shown that intravitreal injection of anti-TF monoclonal antibody resulted in reduction of CNV in a mouse model. Based on this finding, inhibition of TF was reported as a potential therapeutic target to treat retinal neovascularisation. The ICON-1 molecule completed a Phase II trial with promising results for treatment of choroidal neovascularisation (CNV) [115,116], the molecule is expected to enter the clinic in 2020 [128]. ICON-1 is an Fc-fusion protein comprising of two human factor VII domains, conjugated to a human Fc fragment which selectively binds to TF destroying pathological vessels [129].

Integrins are emerging targets which play an important role in regulating cellular adhesion, kinase signalling pathways, endothelial cell migration, apoptosis and VEGFR-2 activation leading to network formation during vascular development [130]. Inhibition of integrins is of interest because of its potential to have a therapeutic role in inhibiting CNV in AMD patients. In general, integrins are transmembrane proteins that bind to extracellular matrix (ECM) proteins such as laminin, fibronectin and collagen. Integrin a5b1 is a fibronectin receptor involved in endothelial cell migration and proliferation [131]. Volociximab is a monoclonal antibody that binds to fibronectin to inhibit its binding to integrin a5b1. A phase I trial assessing Volociximab's safety profile was completed in 2012 with positive results [117], however, to date no further studies have been undertaken to investigate volociximab for the treatment of AMD.

The bioactive lipid sphingosine-1-phosphate (S1P) was thought to be another potential intraocular target [62] for which an anti-S1P monoclonal antibody (iSONEP or Sphingomab) was developed by Lpath Inc. S1P is a circulating lipid mediator generated from metabolism of cell membranes and involved in multiple mechanisms of action in inflammation and angiogenesis [132,133]. However, iSONEP failed to progress past phase II trials because it did not show any significant improvement in visual acuity of patients with wet AMD.

Dual therapeutic targeting using antibody-based medicines

Faricimab (Vabysmo®, represented in Figure 1A) is a bispecific antibody (bsAb) is produced by CrossMAb technology. Faricimab which is comprised of one Fab with specificity to VEGF and another Fab with specificity to ANG-2 was approved by the FDA and EMA in 2022 after four Phase III trials for the treatment of wAMD and DME. Blocking two soluble targets that drive neovascularisation, this dual acting antibody combines the activities of two pathway-modulating molecules into one for enhanced efficacy.

Faricimab was developed as researchers began to look beyond anti-VEGF monotherapies due to some observed resistance to treatment, variable response and recurrence of disease [134]. Benest et al. [135] found that a reduction in ANG-2 concentration strongly reduced the effect of vascular leakage upon administration of VEGF as ANG-2 upregulates the neovascularisation effects of VEGF.

Faricimab was optimised for use in the eye by abolishing its Fc binding interactions with FcγR and FcRn. This was achieved by exchanging the amino acids

required for Fc related interactions. During the trial, patients had longer intervals between doses compared to ranibizumab, indicating a longer duration of action [22]. Primary assessment during the clinical trials showed non-inferior visual acuity outcomes for faricimab dosed every 16 weeks compared to aflibercept given every 8 weeks, with up to 80% of patients showing favourable outcomes after receiving faricimab every 12 weeks. The results suggested that the dual mechanism of action proposed for faricimab could allow the time between treatments to be extended by physicians without compromising vision outcomes for patients while improving patient acceptability and compliance with less burdensome treatment regimens [136]. The advent of faricimab is now found to extend dosing intervals to up to 4 months where the dose of faricimab (~150 kDa) is 6 mg in 50 mL which is larger than that for the current formulation of aflibercept being used clinically.

Another example of a dual acting antibody with two therapeutic targets is Valpha, which is an Fc-based bispecific molecule that targets VEGF and TNF-α [9]. It comprises of soluble VEGF and TNF-a receptors, which are fused to an Fc IgG region. A study showed that when compared to two control monospecific (anti-VEGF aflibercept and anti-TNFα etanercept) therapies, Valpha has the potential to increase treatment effectiveness due to its dual targeting approach, comparable binding characteristics to TNF-a and VEGF, and a favourable pharmacokinetic profile [9]. Valpha has the potential to be a cost-effective strategy for the treatment of AMD. However, it appears that no further development was carried out on this molecule since 2011. The reasons for the lack of development have not been publicly disclosed but there is no indication of a lack of efficacy. It is possible that the presence of an effector active Fc region in Valpha could lead to ocular cytotoxicity.

Preparation of bispecific proteins by chemical conjugation

Genetic engineering and hybridoma technologies were briefly described as means to make bispecific antibody-based drugs. A third technology strategy is chemical conjugation which has been used for decades to try to make bispecific molecules. The idea here is to use easily produced molecules that are then linked together via chemical conjugation. Utilising chemical conjugation strategies require that conjugation to the protein is efficient and preferably selective. Linking proteins together, must also be efficient and selective.

Much has been done in recent years to develop hybrid protein-based products where chemical conjugation is important for the functionality of the molecule. For example, the covalent conjugation of PEG (PEGylation) to a protein has resulted in at least 12 PEGylated protein products in the clinic [137]. PEGylation was developed to increase the circulation time for proteins that cleared too quickly to be efficacious. Antibody-drug conjugates (ADCs) are another type of hybrid protein where chemical conjugation has been critical for the development of products, not possible by recombinant means alone. There are well over 180 ADCs in clinical trials with at least 14 ADCs having been approved, mostly to treat cancer. ADCs are designed to utilise targeting of an IgG antibody to deliver a toxic drug to malignant tissue. Both ADCs and PEGylated proteins are complex medicines that require significant manufacturing processes to have been developed, but these classes of medicines have shown the potential for utilising chemical conjugation approaches to develop proteins that have enhanced functionality.

Poly(ethylene glycol) (PEG) is a water-soluble polymer which is available at a variety of different molecular weights. The physical state of the polymer is dependent on its molecular weight with high molecular weight variants (>1000MW) being solid at ambient temperature and lower molecular weight variants (<1000MW) being liquid at room temperature. PEG is widely used throughout the pharmaceutical and consumer industries in formulation applications including solubility enhancement and as a plasticiser. The FDA inactive ingredients list [138] lists the concentrations of PEG used within approved pharmaceutical products.

Covalent conjugation of PEG to protein molecules (PEGylation) has shown both pharmacologic and pharmacokinetic benefits. Protein PEGylation was described by Frank Davis and colleagues and involved the conjugation of mono-reactive PEG reagents to amino acid groups on proteins using cyanuric chloride as the coupling agent [139]. The PEG molecule for protein PEGylation had a general structure of MeO-PEG-X where X was a reactive moiety that could result in the formation of a covalent bond with a protein. Davis showed that PEG conjugation could increase the half-life of the protein while also potentially reducing protein immunogenicity. PEGylated catalyse remained detectable in the blood up to a 50 hour timepoint post injection, the non-PEGylated protein was no longer detectable after approximately 25 hours [140].

Many therapeutic proteins are PEGylated using non-specific methods with the amino side chains of lysine or the N-terminus of the protein molecule being the

intended sites for conjugation. This often leads to a heterogenous mixture of proteins each with different activities and characteristics [139]. However, several of these heterogenous products were clinically approved (e.g. interferon-a2, interferon-b, granulocyte colony-stimulating factor, asparaginase). Non-specific PEGylation of interferon-a2a yielded 8 different PEGylated interferon (PEG-IFN) isomers. All the PEG-IFN isomers displayed reduced activity due to the steric shielding of PEG between IFN and its target receptor. Although each isomer demonstrated different and reduced activities compared to unmodified IFN [141], it was the extended circulation time which was important for increasing the efficacy of interferon-a2a as a medicine in the treatment of hepatitis C and cancer.

Many research efforts have focused on the goal of achieving site specific PEGylation to try to make more homogeneous protein conjugates. Site selectivity has also been an object of research focus where it is thought that it should be possible to find sites on a protein for conjugation which will have minimal effect on protein function (e.g. affinity, activity). So, beyond potentially streamlining production and purification, an important feature of site-specific protein PEGylation is if an optimal site exists or can be engineered so that protein activity is not ablated after conjugation [139]. In the case of IFN, it has been possible to combine chemical engineering and site-specific conjugation to give site-selectively PEGylated IFN conjugates that displayed increased activities compared to PEG-IFN obtained by non-selective PEG conjugation [142].

One strategy to achieve site-specific conjugation to protein has been to engineer single, unpaired cysteine residue onto the protein. Most cysteines are paired to form disulfide bonds in therapeutic proteins. The thiol on a free cysteine can undergo reaction in physiological conditions (e.g. pH 6-7) where the amine groups on a protein are protonated and not reactive This means reactions with thiols can proceed without interference from amine based reactions. An example of thiol engineered conjugation is the insertion of cysteine into a glucagon like peptide (GLP-1) [143]. PEG was conjugated to the protein through an inserted C-terminal cysteine using a Michael acceptor, maleimide PEG reagent with a molecular weight of 20 kDa. The cysteine PEGylated peptide was easily purified and displayed decreased blood glucose levels after 120-minutes whereas the unmodified peptide had no effect on blood glucose levels after 120 minutes.

Certolizumab pegol (Cimzia®) is a PEGylated protein registered for clinical use that is manufactured using cysteine specific PEGylation via insertion of a C-terminal cysteine residue into a Fab′ (Fab prime) fragment targeted to TNF-a to treat rheumatoid arthritis. The Fab′ is a Fab fragment containing a free sulfhydryl group in the hinge region where it would have been part of the IgG. The conjugation occurs via a *C*-terminal cysteine reaction with a maleimide PEG based reagent [144]. Certolizumab pegol was approved for the treatment of Crohn's disease in 2008 and rheumatoid arthritis in 2009. The dosing regimen after initial treatment is a 400 mg maintenance dose every 4 weeks [144], which is one of the highest doses of a PEGylated protein registered to date indicating the safety for mono-PEGylated proteins.

Insertion of a free cysteine to give a free thiol in a protein does have some disadvantages. Free cysteine residues can affect a variety of factors such as protein structure and function, these functions include thermal stability, dimerization and enzyme catalysis [145]. The two main limitations however are disulfide scrambling and protein misfolding. The inserted unpaired free cysteine can cause disulfide scrambling due to the free cysteine thiol undergoing disulfide exchange reactions with the native disulfide within a protein [146]. Misfolding may occur via the formation of non-native intramolecular disulfide bonds because of the presence of the free thiol, this can lead to aggregation and precipitation of the protein [147].

A method for site-specific PEGylation that does not require any modification to the structure of a protein is PEGylation of proteins via native accessible disulfide bonds (Scheme 1). This approach exploits the thiol chemistry provided by cysteine sulfur atoms that make up accessible disulfide bonds.
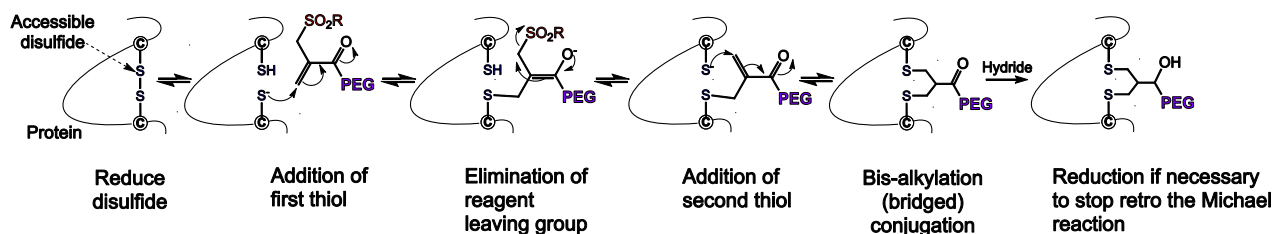
Scheme 1: Scheme for the conjugation of a *bis-alkylating* reagent to two reduced cysteine sulfur atoms via a series of addition and elimination reactions

The PEGylation involves two distinct steps which are reduction of the disulfide bond to liberate free thiols from an accessible disulfide and a *bis*-alkylation reaction on a cross-functionalise conjugation moiety that is capable of two Michael thiol

additions. The result is to create a three-carbon bridge which covalently conjugates the PEG reagent to each cysteine thiol to essentially re-anneal the original disulfide [148]. The reagents work by generation of an α,β-double bond conjugated to an electron withdrawing carbonyl. The generation of the double bond occurs by elimination of sulfone leaving groups (Scheme 2) at mild pH values (e.g. 6.5-7.0).
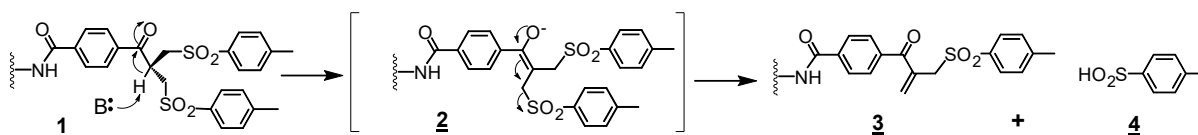
Scheme 2: Scheme for the elimination of toluene sulfinic acid **4** from the *bis*-sulfone conjugation moiety **1** to give a *mono*-sulfone conjugation moiety **3** containing a a,b-double bond which occurs through an enolate intermediate **2** at mild pH values (6.5-7.0).

The Michael reaction is reversible which means in proteins with multiple free disulfides, it is possible to re-bridge the correct cysteines [149]. A key advantage of the *bis*-sulfone conjugation moiety **1** is that the electron-withdrawing carbonyl can be reduced to hydroxide with mild hydride reagents (Scheme 1) to stop the retro-Michael reaction, and thus deconjugation. Although it is not possible to lock the conjugation in this manner with maleimide reagents that are used for *mono* or *bis*-thiol conjugations, several manufacturing processes in protein modification using other conjugation moieties utilise an analogous final reduction step. For example, the PEGylation of granulocyte colony-stimulating factor (GCSF) that is used to make the product Neulasta® (Amgen) is by reductive amination of an engineered aldehyde at the terminus of the protein. The process for the manufacture of Neulasta requires a hydride reduction step like that shown in Scheme 1.

Since the *bis*-alkylation conjugation to re-bridge disulfides is thought to be driven by a large component of the equilibria of the Michael reaction and protein conformation, it has been found that many proteins do not generally require the final reduction step to maintain the 3-carbon bridge that results from bis-alkylation conjugation. Proteins such as cytokines and Fabs appear to be quite resistant to deconjugation after disulfide rebridging. In the case of Fabs, the accessible interchain disulfide is the only available disulfide for conjugation and there are considerable intramolecular interactions between the light and heavy chains to help maintain protein structure. Molecular modelling of the three-carbon bridge formed after conjugation indicated that a re-bridged disulfide was more flexible than the unmodified disulfide [150], so if there are enough intramolecular interactions to maintain protein structure,

it has generally been found unnecessary to reduce the electron withdrawing carbonyl after conjugation.

The *bis*-alkylation approach is relevant for therapeutic proteins because they often have paired disulfides but seldom have a free cysteine residue [151]. Typically, these proteins have an even number of cysteines that pair up as disulfides [151–153]. The *bis*-alkylation approach for protein conjugation is especially appropriate for the interchain disulfide in Fabs because this conjugation approach exploits the chemical reactivity of both sulfur atoms from an accessible disulfide bond. Conjugation at the Fab interchain disulfide is as far as possible within the Fab to its epitope binding CDR region.

While disulfides influence a protein's properties in complex ways [154], it is thought that the accessible disulfides mainly contribute to the stability of the protein, rather than to its structure or its function [151]. In contrast, the disulfides that are present in a protein's hydrophobic interior [151,155] typically contribute to the maintenance of its tight packing and its function. Most of the work described in this thesis is focused on the disulfide-re-bridging conjugation of the accessible interchain disulfide. Since the focus of this thesis is to conjugate two Fabs as a means to make bispecific antibody mimetics, di-functional reagents such as **5** are of importance (Figure 13) [148]. The molecular weight of the PEG element in reagents such as **5** is generally in the range of 5-10 kDa which is less than the molecular weight of PEG used in protein PEGylation. The function of the PEG linker element in reagent **5** is to provide water-solubility for the reagent and to provide a linker between the conjugation moieties that is biocompatible.
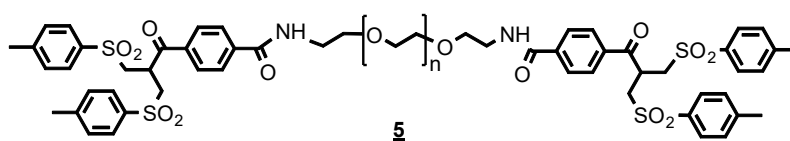
Figure 13: Example of a PEG di-*bis*-sulfone dimerisation reagent **5** (also known as BisB1) [148]. Two Fabs can be conjugated to this dimerisation reagent **5**, one Fab on each end of the PEG linker.

The di-*bis*-sulfone dimerisation reagent **5** was used to prepare antibody mimetics called Fab-PEG-Fab (FpF) [156] (Figure 14). An FpF is a bivalent molecule comprised of two Fabs, each conjugated at a terminus of a linear linker molecule (e.g. short PEG) via their interchain disulfide. The Fab elements were obtained via proteolytic digestion of existing IgG antibodies [156]. An FpF synthesised from the Fab derived from bevacizumab showed promising binding characteristics when examined

using surface plasmon resonance (SPR). The affinity (K_D) of the FpF was similar to the parent IgG (e.g. bevacizumab). While the association rate (k_a) was found to be slower for the FpF than the unmodified IgG the dissociation rate (k_d) was found to be slower for the FpF than the IgG. These differences in k_a and k_d resulted in a similar K_D for both the FpF and the unmodified IgG [156]. FpF binding properties were further corroborated in an isothermal calorimetry study [157]. The slower dissociation rate indicates a potential for increased tissue residence time [158] and may be due to more efficient rebinding because the linker PEG may be more flexible than the Fc hinge of an IgG. Anti-VEGF FpFs inhibited in vitro angiogenesis [156] and anti-TNF-α FpFs inhibited inflammation in an ocular *in vivo* model [159].
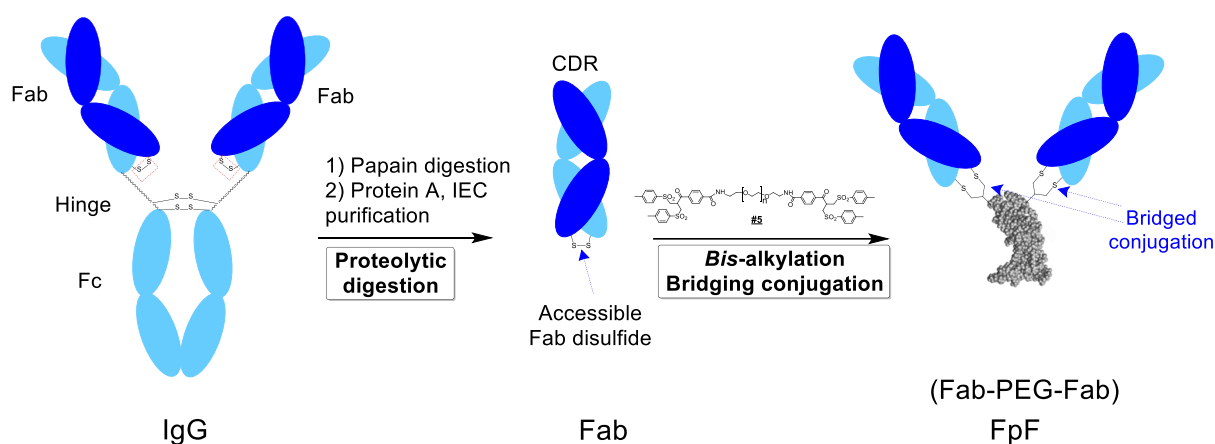
Figure 14: Structure of a Fab-PEG-Fab antibody mimetic [156] The FpF above is a homodimer made from two antibody Fab fragments conjugated to either end of the PEG di-*bis*-sulfone dimerisation reagent **5**. The Fab fragments are covalently bound to the reagent.

Another example of a bivalent PEGylated molecule prepared with the di-*bis*-sulfone dimerisation reagent **5** is a receptor binding region dimer called an RpR (Figure 15). An RpR was synthesised by proteolytically digesting aflibercept; an Fc-fusion protein targeted against VEGF. Aflibercept comprises 2 arms, each which comprise of the extracellular domains for the VEGF receptors 1 and 2. Each VEGF binding arm comprises domain 2 of VEGFR1 which binds to VEGF-A and domain 3 which binds to VEGF-A and to PIGF. Digestion of aflibercept to remove the Fc element resulted in isolation of the bind arms, each which possessed two hinge cysteines that could undergo disulfide re-bridging conjugation [160]. SPR binding studies using surface plasmon resonance revealed interesting and significant results. As with the FpF the association rate (k_a) was slower for the anti-VEGF RpR however the dissociation rate (k_d) was significantly slower for the RpR when compared to unmodified aflibercept. Binding affinity to VEGF was greater for the RpR than

aflibercept [160]. Again, the slower k_d may be due to a greater propensity for RpR rebinding than that possible for the unmodified Fc-fusion protein due to greater mobility of the PEG compared to the hinge region of the Fc-fusion protein.
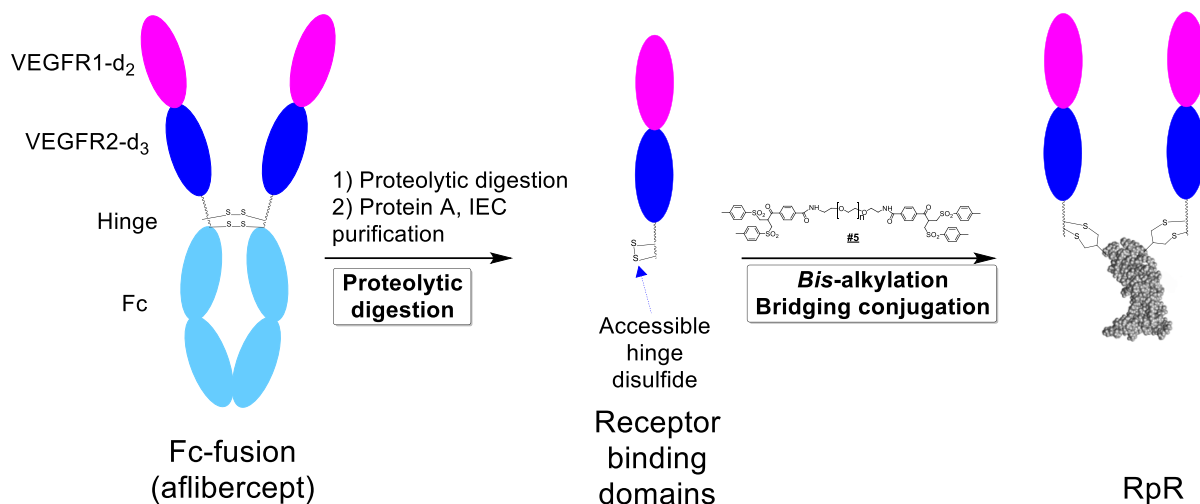
Figure 15: Structure of a receptor binding region-PEG-receptor binding region (RpR) [160] An RpR is a homodimer made by conjugating two receptor binding regions to either end of the PEG di-*bis*-sulfone protein dimerisation reagent **5**.

The protein dimerisation reagent **5** has been used to make Fab-PEG-Fabs (BsFpFs) previously by our research group with Scheme 3 showing the preparation of a BsFpF using the protein dimerisation reagent **5**.
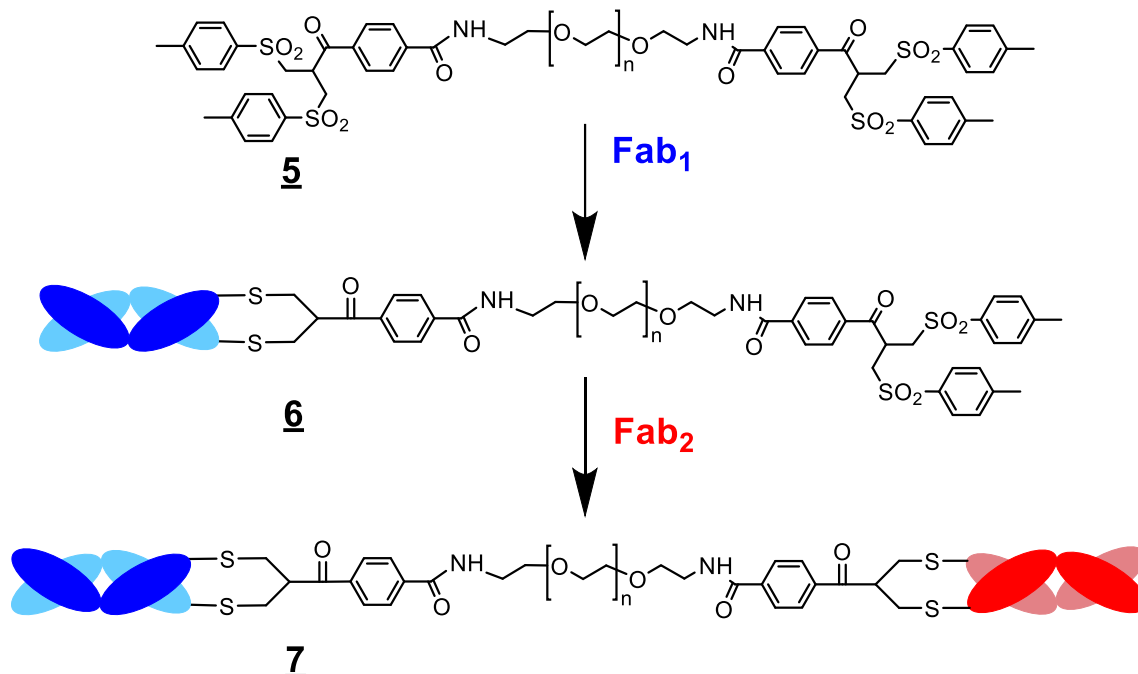
Scheme 3: Preparation of a bispecific FpF using the PEG di-*bis*-sulfone protein dimerisation reagent **5**. Fab₁ is reduced and combined with reagent **5** to prepare a Mono PEG-Fab **6** in which a single Fab is conjugated to the dimerisation reagent **5**. Fab₂ is then reduced and combined with the Mono PEG-Fab to form the bispecific FpF **7**.

However, a problem exists with this methodology in the form of a loss of reactivity after the first Fab is conjugated to the reagent. The loss of reactivity may occur because the already conjugated Fab provides a physical obstacle and covers the free bis-sulphone group or chemically the electronegative potential of the leaving group becomes reduced in some way. Although the BsFpF can be prepared using reagent **5** yields are extremely low meaning the molecule cannot be suitably characterised. It does however provide a proof of concept that a BsFpF can be prepared and is justification for further development.

Project hypothesis and aims

Monospecific antibody mimetics (FpF) have previously been shown to have comparable binding affinity and *in-vivo* functional efficacy to antibodies in the ocular mouse model [156,159,161]. Dual-targeting protein-based therapeutics, such as bispecific antibodies (bsAbs), possess the unique ability to simultaneously interact with two target epitopes and have the potential to increase the efficacy of intraocular medicines. Bispecific antibodies are suggested as an alternative to combination therapies within the eye, which have been shown to be ineffective [22,110]. To build upon this, the aim of this thesis was to synthesise bispecific Fab_1-PEG-Fab_2 (BsFpF) molecules capable of binding to two therapeutic targets within the eye. Fabs were obtained using proteolytically digestion of IgG molecules. Pro-angiogenic and proinflammatory targets including VEGF, TNF-α, IL-6R and IL-17A were selected because of their involvement in retinal degeneration diseases.

In this PhD it was hypothesised that:

1. A soluble form of papain can be used as an alternative to immobilised papain for obtaining Fabs via the digestion of IgGs. Using soluble papain will allow digestion of up to 100 mg of IgG in a single digestion.
2. Using PEG as scaffold and utilising chemical conjugation to combine two Fabs, a BsFpF can be synthesised effectively preserving the antigen binding properties of the individual Fabs.
3. The prepared BsFpF can be isolated from conjugation mixtures to give a final purified product free from impurities.

4. A BsFpF prepared by chemical conjugation, is stable in the intended storage condition with no deconjugation of Fabs from the PEG scaffold and light/heavy dissociation.

In order to test these hypotheses, the following research aims were listed:

1. Fabs will be obtained using enzymatic digestion of IgG. The main aim being to scale up IgG digestion to 100 mg IgG, hence different forms of soluble papain will be tested including crude and lyophilised forms. A suitable method for the purification of the digestion mixtures will need to be developed. Protein A, CH[1] affinity and protein L resins will be assessed for purification of the digestion mixture to obtain purified Fabs. To allow the digestion of 100 mg of IgG in a single experiment, purification using columns attached to AKTA systems will be investigated as digestion volumes are expected to be in excess of 50 mL. Different antibodies including infliximab, tocilizumab, bevacizumab and secukinumab will then be digested using optimised methods. Scheme 4 outlines the IgG digestion process.
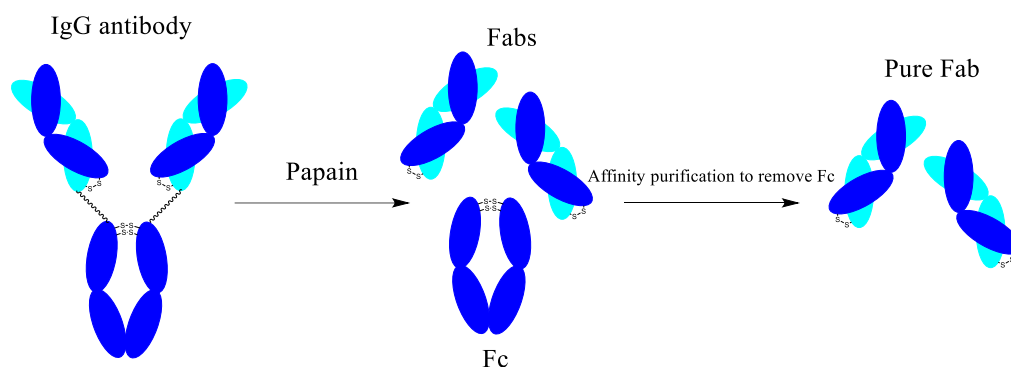
Scheme 4: Digestion of an IgG antibody using papain. The IgG is incubated with papain to obtain a crude digestion mixture containing Fabs and Fc. The Fc is purified from the mixture using an affinity purification to obtain pure Fab.

2. Using a PEG di-*bis*-sulfone protein dimerisation reagent **5** at molecular weights of 6 kDa and 20 kDa a BsFpF will be prepared. The interchain disulfide bond present in the Fabs will first be reduced in order to undergo chemical conjugation to either end of a PEG di *bis*-sulfone protein dimerisation reagent **5**. The process for conjugation of Fabs to reagent **5** to prepare a BsFpF is outlined earlier in Chapter 1 (Scheme 3).

3. Purification of the conjugation mixture containing the desired BsFpF will be performed using ion exchange chromatography (IEX). It is critical that the final

BsFpF is not contaminated with any impurities. Silver staining of SDS PAGE gels will be used to confirm purity.

4. The protein stability of BsFpFs will be analysed using SDS PAGE and dynamic light scattering at the intended storage temperature of 5°C and at a temperature of 37°C to mimic body temperature.

5. Different binding assays including Enzyme Immunosorbent Assays (ELISA), Surface Plasmon Resonance (SPR) and Microscale Thermophoresis (MST) will be used to measure the binding affinity of purified BsFpFs towards their targets and to determine if antigen binding properties have been retained when compared to PEG-Fab molecules. The mono PEG-Fab molecules will be prepared for binding comparison with a BsFpF.

6. Human umbilical vein endothelial cells (HUVECs) will be treated with both TNF-α and IL-17A. Expression of the inflammatory cell surface markers ICAM-1 and VCAM-1 will be measured using flow cytometry. Mixtures of TNF-α, IL-17A and a BsFpF targeting TNF-α and IL-17A will then be applied to HUVECs and the ICAM-1 and VCAM-1 expression measured again. This *in vitro* cell based assay will be used to evaluate the functional activity of an anti-TNF-α/IL-17A BsFpF.

Chapter 2 – Materials and methods

Materials

General lab reagents:

Sodium phosphate monobasic (cat no. S0751), Ethylenediaminetetraacetic acid calcium disodium salt (cat no. ED2SC), Sodium dihydrogen phosphate dihydrate (cat. no. 1063451000), Water, ACS reagent for ultratrace analysis (cat no. 14211), Sodium chloride – low endotoxin (cat no. 1.16224), Glycine (cat no. G7126), Sodium acetate trihydrate (cat no. S7670) and Trizma hydrochloride (cat no. T3253) were all purchased from Sigma Aldrich. Oxoid™ Phosphate Buffered Saline Tablets (cat no. BR10014G) were purchased from Thermofisher. HPLC grade water (cat no. 10043370) was purchased from Fisher. Type 1 water was obtained from in house water purification systems. 2M Sodium hydroxide solution and 2M Hydrochloric acid used for pH adjustments were obtained from in house technical services.

Antibody solutions:

Ranibizumab (10 mg/mL), Infliximab (10 mg/mL), Tocilizumab (20 mg/mL) and Eylea (40 mg/mL) were kindly donated as leftover therapeutic doses by hospitals. Bevacizumab (25 mg/mL) was obtained from existing stock within our research group. Secukinumab (150 mg/mL, cat. no. 730591) was purchased from Novartis.

Antibody digestion and purification materials:

Lyophilized papain (cat no. P4762), crude papain (cat no. P3375), L-Cysteine (cat no. 300-89) were purchased from Sigma Aldrich. Immobilized papain (cat. no. 20341) was purchased from Thermo Fisher. Hitrap Protein L column 1 mL (cat no. 29048665), Hitrap Protein L column 5 mL (cat no. 17547815) and Hitrap Protein A column 1 mL (cat no. 29048576) were purchased from Cytiva. CaptureSelect CH_1 affinity 1 mL column was obtained from existing stock within our research group.

Protein purification and buffer exchange materials:
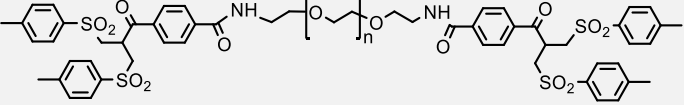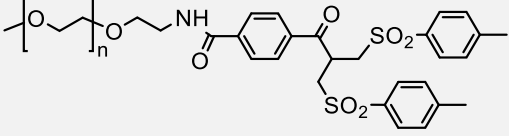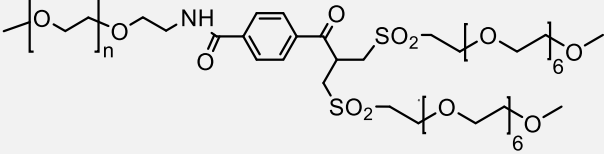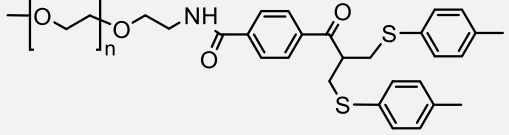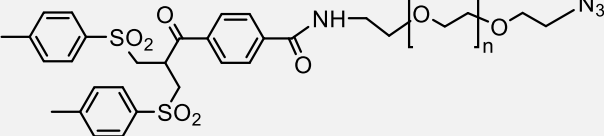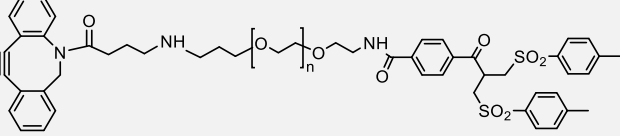
Disposable PD-10 Desalting columns (cat no. 11768488) were purchased from Fisher. Hitrap Macrocap SP cation exchange column (cat no. 15569244) was purchased from Thermo Fisher. Superdex 200 increase 10/300GL size exclusion column (cat no. 28990944) was purchased from Cytiva. Vivaspin 20 centrifugal concentrators, 30 kDa MWCO (cat no. Z614637) were purchased from Sigma.

Disulfide reducing agents:

DL-Dithiothreitol (cat no. D0632) was purchased from Sigma.

Bis-alkylating PEG reagents for protein conjugation.

A variety of *bis*-alkylating PEG reagents that were synthesised at UCL School of Pharmacy by our research group were kindly donated for use in this thesis. The reagents used for protein conjugation during this thesis were the PEG di-*bis*-sulfone protein dimerisation reagent **5**, PEG *bis*-sulfone **8**, PEG *bis*-sulfone glycol **12**, PEG *bis*-sulfide **17**, PEG *bis*-sulfone dibenzocyclooctyne (DBCO) **23**, PEG *bis*-sulfone Azide **22**, PEG *bis*-sulfone trans-cyclooctene (TCO) **26** and the PEG *bis*-sulfone tetrazine (Tz) **27** reagent, the reagents and their structures are summarised below in Table 3.

Reagent no.	Reagent Name	Structure
5	PEG di-*bis*-sulfone protein dimerisation reagent	 6 kDa and 20 kDa molecular weight reagents used for conjugation
8	PEG *bis*-sulfone	 5 kDa and 10 kDa molecular weight reagents used for conjugation
12	PEG *bis*-sulfone glycol	 10 kDa molecular weight reagent used for conjugation
17	PEG *bis*-sulfide	 10 kDa molecular weight reagent used for conjugation
22	PEG *bis*-sulfone azide	 3 kDa molecular weight reagent used for conjugation and ligation
23	PEG *bis*-sulfone DBCO	 5 kDa molecular weight reagent used for conjugation and ligation
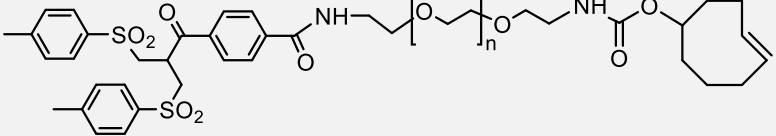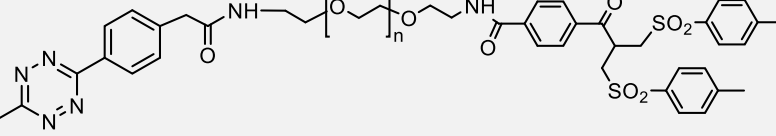
Reagent no.	Reagent Name	Structure
26	PEG *bis*-sulfone TCO	5 kDa and 10 kDa molecular weight reagents used for conjugation and ligation
27	PEG *bis*-sulfone Tz	5 kDa and 10 kDa molecular weight reagents used for conjugation and ligation

Table 3: Summary of the reagents used for protein conjugation during this thesis.

SDS page materials:

InstantBlue Coomassie Protein Stain (cat. no. ab119211) and 4-12% Bis-Tris Precast gels (cat. no. ab270467) were purchased from Expedeon. NuPAGE LDS sample buffer (4x) (cat. no. NP0007) and NuPAGE MOPS SDS running buffer (20x) (cat. no. NP0001) were purchased from Thermo Fisher. Barium Chloride (cat. no. 217565) was purchased from Sigma Aldrich. Iodine solution, 0.05M (cat. no. 12980754) was purchased from Fisher.

Surface plasmon resonance materials:

CM3 chips (cat. no. BR100541), NTA chips (cat. no. BR100034), NTA reagent kit (cat. no. 28995043), Glycine pH 2.0 (cat. no. BR100355), Acetate buffer, pH 5.5 (cat. no. BR100352) and HBS-EP+ (cat. no. 100826) were all purchased from Cytiva.

ELISA materials:

3,3′,5,5′-Tetramethylbenzidine (TMB) (cat. no. T0440), bovine serum albumin (cat. no. A2153) and Tween 20 (cat. no. P7949) were all purchased from Sigma Aldrich. Goat F(ab')2 Anti-Human IgG H&L (HRP) (cat. no. ab98525) was purchased from Abcam.

Microscale thermophoresis materials:

Monolith Protein Labelling Kit RED-NHS (Amine Reactive) (cat. no. MO-L001) and Monolith NT.115 Capillaries (cat. no. MO-KO22) were both purchased from NanoTemper.

Ligands:

Human vascular endothelial growth factor$_{165}$ (hVEGF$_{165}$) (cat. no. 100-20) was purchased from Peprotech. Human IL-17A, his-tag (cat no. 12047-H07Y), His-tagged human interleukin 6-receptor (IL-6R) (cat no. 10398-H08H) were purchased from Sino Biological. His-tagged human tumor necrosis factor alpha (TNF-α) (cat no. 15827837) was purchased from Fisher.

Cell culture materials:

Pooled human umbilical vein endothelial cells (HUVECs) (cat no. C-12203) were purchased from PromoCell. PromoCell endothelial growth medium (cat no. C22010) with supplement mix included and PromoCell detach kit (cat no. C-41200) were purchased from Sigma. Trypan blue, Sterile DMSO and heat inactivated fetal bovine

serum were sourced from existing stocks in our research group. Enzyme free cell dissociation buffer (cat. no. 13151014) was purchased from Thermo Fisher.

Materials for tagging of cell surface markers:

Human TruStain FcX (cat. no. 422302) was purchased from BioLegend. Mouse anti-human CD31 antibody (APC tagged) (cat no. 15577906) was purchased from Fisher. Mouse anti-human ICAM-1 antibody (APC tagged) (cat. no. 10346-MM01-A) and rabbit anti-human VCAM-1 antibody (APC tagged) (cat. no. 10113-R601-A) were purchased from Sino Biological.

Methods:

SDS page analysis:

4-12% bis-tris precast gels were used for analysis. Samples were prepared by combining 6.0 µl of LDS sample buffer with 20 µl of sample and vortexing until combined. The amount of sample loaded onto the gel was approximately 15 µL for 10/12 well gels and 10 µL for 15/17 well gels. MOPs (50 mL in 1.0 L distilled water) was used as the running buffer. The voltage applied for analysis was 200 V and the run time was approximately 1.0 hr. 5.0 µL of a pre-stained protein standard was loaded onto the first well of each gel.

For protein visualisation, approximately 30 mL of Instant Blue stain was used to stain the SDS-page gels. The gels were left in the gel for at least 1 hour, after which the gels were rinsed using water.

For the visualisation of PEG, a barium iodide stain was used as follows. The SDS-page gel was incubated with a 5% solution of barium chloride for 10 minutes. The container was gently shaken by hand throughout the 10 minutes. After 10 minutes iodine solution was added dropwise until PEG related bands began to appear. The gel was then rinsed using water. PEG bands have brown coloured bands using a barium iodide stain and PEGylated antibodies show green coloured bands.

Silver staining was performed to evaluate the purity and also when protein concentrations were too low to be detected using coomassie instant blue staining. The solutions required were (i) 30% ethanol:10% acetic acid in distilled water, (ii) 10% ethanol, (iii) sensitiser working solution (50 µL sensitiser with 25.0 mL water), (iv) working stain solution (0.5 mL enhancer with 25.0 mL stain), (v) working developer solution (0.5 mL enhancer with 25.0 mL developer) and (vi) stop solution (5% acetic acid in distilled water). The gel was thoroughly washed twice with ultrapure water for 5 mins and the gel was fixed with 30% ethanol: 10% acetic acid solution for 15 mins. The gel was washed twice with 10% ethanol and twice with water (5 mins per wash). After washing, the gel was incubated with sensitiser working solution for 1 min and washed twice with ultrapure water (1 min each). Stain working solution was added to the gel and incubated for 30 mins. The gel was washed twice with ultrapure water (1 min each). Developer working solution was added and the gel was incubated till protein bands appeared (usually within 2-15 mins). When the required band intensity

was achieved, the stop solution (5% acetic acid) was added for 10 mins and the final gel was washed with water.

Ion exchange chromatography (IEX) method

Two buffers were prepared; buffer A (100 mM sodium acetate, pH 4.0) and buffer B (100 mM sodium acetate, 1 M sodium chloride, pH 4.0) were prepared using HPLC grade water. Both buffer A and B solutions were filtered using a millipore filter flask with a cellulose nitrate membrane filter (0.45 µm).

Samples to be purified were concentrated using a vivaspin centrifuge tube (MWCO 10 kDa) to volumes of no more than 1 mL. The concentrated sample was then made up to a volume of no more than 2 mL using buffer A. The pH of the sample was then checked to ensure it was approximately pH 4.0 using litmus paper. The sample was then loaded using a syringe onto a 5 mL sample loop. Once the sample was loaded onto the sample loop a pre-programmed method with the settings shown in Table 4 was used for IEX purification. A Hitrap Macrocap SP cation exchange column attached to an AKTA prime plus system was used for all IEX purifications.

Breakpoint	Time (mins)	Concentration of buffer B (%)	Flow rate (mL)	Injection port position
1	0	0	1.0	Inject
2	12	0	1.0	Load
3	42	100	1.0	Load
4	50	100	1.0	Load

Table 4: Chromatography settings used for ion exchange purification.

Size exchange chromatography (SEC) method

Phosphate buffered saline was prepared as the SEC mobile phase by dissolving 5 Oxoid™ Phosphate Buffered Saline Tablets in 500 mL of type 1 water.

Samples to be purified were concentrated using a vivaspin centrifuge tube (MWCO 10 kDa) to volumes of no more than 0.5 mL. The sample was then loaded using a syringe onto a 2 mL sample loop. Once the sample was loaded onto the loop a pre-programmed method with the settings shown in Table 5 was used for purification. A Superdex 200 increase 10/300 GL size exclusion column attached to a AKTA purifier was used for all SEC purifications.

Breakpoint	Time (mins)	Concentration of buffer B (%)	Flow rate (mL)	Injection port position
1	0	0	1.0	Inject
2	10	0	1.0	Load
3	60	0	1.0	Load

Table 5: Chromatography settings used for size exclusion purification.

Representative digestion of humanised IgG antibodies using lyophilised papain – 15mg scale:

Pre-digestion buffer (200 mL, 20 mM NaH_2PO_4, 10 mM EDTA) pH 7.0 was prepared as follows. 372 mg EDTA and 312 mg phosphate dibasic dissolved in 200 mL of type 1 water and adjusted to pH 7.0 using sodium hydroxide. 50 mL of digestion buffer was prepared by dissolving 0.303 g of cysteine in 50 mL of pre-digestion buffer. The pH of the solution was checked to ensure it remained at pH 7.0±0.5 and was adjusted if necessary. 15 mg of humanised IgG antibody was diluted to a volume of 6 mL with digestion buffer. To this 150 µL of a 5 mg/mL lyophilised papain stock solution was added, equating to a 1:20 papain:IgG ratio. The digestion sample was placed into an incubator at 37°C for 30 minutes. The crude digestion mixture was purified using Protein L chromatography (Hitrap Protein L). For this, two buffers were prepared:

Buffer A (100 mM sodium phosphate, 150 mM sodium chloride, 500 mL, pH 7.2) was prepared by dissolving 6.89 g of sodium phosphate monobasic monohydrate and 4.38 g of sodium chloride in 500 mL of type 1 water, the pH of the solution was adjusted to 7.2.

Buffer B (100 mM glycine, 500 mL, pH 2.5) was prepared by dissolving 3.75 g of glycine in 500 mL of type 1 water, the pH of the solution was adjusted to 2.5. Both buffers were vacuum filtered using 0.45 µM filter paper prior to use.

The digestion mixture was injected straight onto an AKTA prime plus system; no sample preparation was performed. The following chromatography method listed in Table 6 was used:

Breakpoint	Time (mins)	Concentration of buffer B (%)	Flow rate (mL/min)	Injection port position
1	0	0	0.5	Inject
2	15	0	1	Load
3	15.1	100	1	Load
4	35	100	1	Load

Table 6: Chromatography settings used for Protein L purification of digested IgGs.

Eluted fractions were collected and monitored using SDS PAGE. To each elution fraction Tris-HCl (pH 8.0, 1 M) was added at a ratio of 60 µl to every 1 mL of eluted fraction to neutralize sample pH. The fractions containing the Fab fragment were then further purified using a SEC (Superdex 200 Increase 10/300 GL) with a flow rate of 0.5 mL/min using PBS as the mobile phase. Eluted fractions were collected and monitored using SDS PAGE.

The yield of purified Fab was calculated by measuring UV absorbance at 280 nm. To calculate yield the quantity of Fab contained in the parent IgG was used. For example 1 mg of IgG contains 0.66mg of Fab. Therefore if 0.33mg of purified Fab was obtained from digestion the final yield would be 50%.

Preparation of conjugation buffer:

Conjugation buffer was prepared by dissolving 240 mg of NaH_2PO_4 and 372 mg EDTA in 100 mL ultrapure water and adjusting to pH 7.6. The same buffer was used for the monospecific and bispecific preparations.

*Representative preparation of a PEG-Fab using a PEG20 bis-sulfone reagent **8** – 1 mg scale:*

In an Eppendorf tube (1.5 mL) approximately 1.5 mg of DTT was dissolved in 1 mL of 1 mg/mL Fab solution. The Fab fragment was diluted to a 1 mg/mL concentration using conjugation buffer. The Fab and DTT solution was then incubated at ambient temperature for 30 minutes. After 30 minutes the DTT was removed from the solution using a PD-10 desalting column equilibrated with conjugation buffer. A representative procedure to remove the DTT from a volume of 1.0 mL of reaction mixture using a PD-10 column was as follows: first a PD-10 column was equilibrated by allowing conjugation buffer to elute through the column. Then, the protein solution with DTT (1.0 mL) was loaded onto the equilibrated PD-10 column and the protein solution was allowed to elute from the PD-10 column. After this, 1.5 mL of conjugation buffer was

added to the PD-10 column and allowed to elute. Finally, the protein solution was recovered by addition of a 3.3 mL conjugation buffer to the PD-10 column. The same DTT removal procedure was used for all antibody conjugate preparations.

The PEG *bis*-sulfone reagent **8** (3.0 mg) was dissolved into distilled water (1.0 mL) prior to PEGylation. The PEG *bis*-sulfone reagent **8** (0.17 mL, 3.0 mg/mL in distilled water, 20 kDa reagent MW) was added to the solution containing the reduced Fab at a molar ratio of 1.5:1 reagent to Fab and left to incubate at room temperature for approximately 6 hours, the conjugation was monitored using SDS PAGE.

*Representative preparation of a monospecific FpF molecule using a PEG6 di-bis-sulfone protein dimerisation reagent **5** – 1 mg scale:*

In an Eppendorf tube (1.5 mL) approximately 1.5 mg of DTT was dissolved in 1 mL of 1 mg/mL Fab solution. The Fab fragment was diluted to a 1 mg/mL concentration using conjugation buffer. The Fab and DTT solution was then incubated at ambient temperature for 30 minutes. After 30 minutes the DTT was removed from the solution using a PD-10 desalting column equilibrated with conjugation buffer.

The PEG di-*bis*-sulfone protein dimerisation reagent **5** (3.0 mg) was dissolved into distilled water (1.0 mL) prior to use for conjugation. The PEG di-bis-sulfone protein dimerisation reagent **5** (0.06 mL of 3.0 mg/mL stock, 6 kDa, 0.5 molar eq.) was added to the solution containing the reduced Fab and left to incubate at room temperature for approximately 18 hours.

*Representative preparation of a monospecific FpF molecule using ligating PEG bis-sulfone TCO **26** and PEG bis-sulfone Tz reagents **27**:*

1 mg of a Fab fragment was diluted to a volume of 1 mL using the prepared conjugation buffer, to this 1 mg of DTT was added. Once the DTT was added the Fab was left to reduce at ambient temperature for 30 minutes. After which the DTT was removed using a PD-10 desalting column. The reduced Fab was split in half and to one aliquot PEG bis-sulfone TCO **26** reagent was added at a molar ratio of 1.5:1 reagent to Fab. To the other aliquot PEG bis-sulfone Tz **27** was added at a molar ratio of 1.5:1 reagent to Fab. The conjugations were left for approximately 6 hours at ambient temperature to react. The conjugations were monitored using SDS PAGE.

*Representative preparation of bispecific FpF molecule using ligating PEG bis-sulfone TCO **26** and PEG bis-sulfone Tz reagents **27**:*

0.5 mg of Fab_1 was diluted to a volume of 1 mL with the prepared conjugation buffer. 0.5 mg of Fab_2 was diluted to a 1 mL volume with conjugation buffer. To both Fab dilutions 1 mg of DTT was added and the Fabs were left to reduce at ambient temperature for 30 minutes. After which the DTT was removed from both dilutions using PD-10 desalting columns. To Fab^1 PEG bis-sulfone TCO **26** was added at a molar ratio of 1.5:1 reagent to Fab. To Fab^2 PEG bis-sulfone Tz **27** was added at a molar ratio of 1.5:1 reagent to Fab. The conjugations were left for approximately 6 hours at ambient temperature to react. The conjugations were monitored using SDS PAGE.

Representative purification steps for FpF and bispecific FpFs:

The conjugation reaction mixtures containing Fabs and ligating PEG *bis*-sulfone TCO **26** and PEG *bis*-sulfone Tz reagents **27** were first purified using the IEX method described in the method section to remove unconjugated PEG *bis*-sulfone TCO **26**, PEG- *bis*-sulfone Tz **27** and other impurities. The IEX-purified TCO functionalized Fab **28** and Tz functionalized Fab conjugates **29**, were then combined and the ligation reaction allowed to proceed, for 24 hours at 4°C. The ligation reaction was monitored using SDS PAGE.

The resulting monospecific **13** or bispecific **7** FpFs formed via the ligation reaction between the TCO and Tz functional groups were first purified using IEX to remove any remaining TCO functionalized Fab **28** and Tz functionalized Fab conjugates **29** from the reaction mixture. Size-exclusion chromatography (SEC) was then used for further purification. The eluted fractions were collected and assessed.

Immobilisation of VEGF onto a CM3 chip for surface plasmon resonance:

Immobilisation was carried out in manual mode. A flow rate of 5 µL/min was used for all steps. The chip was first washed with 50 mM NaOH for 60 seconds. The dextran surface was activated by injecting a 1:1 mixture of EDC and NHS (1 of each aliquot combined) for 200 seconds. HBS-EP buffer was then allowed to pass over the chip for 200 seconds. VEGF solution (0.5 µg/mL in pH 5.5 acetate buffer) was injected for 200 seconds and finally ethanolamine HCl was injected for 180 seconds to deactivate any remaining active groups on the surface.

SPR Binding assay for anti-VEGF molecules:

A series of at least 7 serial dilutions of anti-VEGF molecules were prepared using HBS-EP as a diluent. These were then run on over a CM3 chip which had been functionalised with human VEGF at low immobilisation level. A contact time of 180s and a dissociation time of 1200s were used. The CM3 chip was regenerated using a pH 2.0 Glycine solution with a contact time of 30s and a stabilisation period of 60s. Anti-VEGF binding assays were performed using a Biacore X100 system.

SPR Binding assay for anti-TNF-α and anti-IL-6R molecules:

A series of at least 7 serial dilutions of anti-TNFα or anti-IL-6R molecules were prepared using HBS-EP as a diluent. These were then run over an NTA chip functionalised with TNFα and IL-6R previously as describe here: A 5 µg/mL solution of his-tagged ligand was passed over an NTA chip for 180s to capture the ligand. Then a single serial dilution was passed over the captured ligand with a contact time of 120s and a dissociation time of 1200s. In between each serial dilution a fresh his-tagged ligand was captured onto the NTA chip. Regeneration of the chip at the end of each cycle was performed by passing a 350 mM EDTA solution (from NTA reagent kit) over the chip for 60s. Anti-TNF-α and anti-IL-6R binding assays were performed using a Biacore X100 system.

ELISA binding assay for anti-VEGF or anti-IL-6R molecules:

A flat bottom 96 well plate was coated with VEGF or IL-6R (100 µL of a 1 µg/mL VEGF solution, 0.1 µg VEGF per well or 100 µL of a 1 µg/mL IL-6R solution, 0.1 µg IL-6R per well) and incubated overnight at 4°C. The next day, the VEGF or IL-6R solutions were removed and without washing, blocking buffer (300 µL, PBS with 1% w/v BSA and 0.05% Tween 20) was added into each well and incubated at ambient temperature for 2.0 h. After this, blocking buffer was aspirated and the plate was washed once with washing buffer (300 µL, PBS with 0.05% w/v Tween 20). and then test compounds, which were prepared in PBS at a range of concentrations, were added into each well (100 µL). The plate was incubated for 2.0 h at ambient temperature. After 2.0 h incubation, the protein solutions were removed, and wells washed with washing buffer (300 µL) three times. Then, anti-human Fab₂ (Fab specific)-peroxidase (100 µL, 1/5000 dilution) was added into each well and incubated for 1.0 h at ambient temperature. The solutions were then removed, and the plate was washed off with

washing buffer three times. TMB (100 µL) was then added, and development of the blue colour was monitored. After approximately 5 mins, when the blue colour was visible enough for each well, HCl (50 µL, 1.0 M) solution was added to produce a constant yellow colour. The plate was then read using a plate reader at 450 nm wavelength. The data was processed using graph pad prism (V9) and affinities generated using a one site – specific binding fitting method.

MST Binding assays:

Antibodies and bispecific antibodies were labelled as per the instructions found in the monolith amine reactive protein labelling kit as follows. Protein concentration was adjusted to a concentration of 2-20 µM using the included labelling buffer. The dye was dissolved by adding 30 µL of 100% DMSO to the dye and vortexing thoroughly. The dye solution was then diluted to a concentration approximately 2-3 times higher than the protein concentration using the included labelling buffer. The diluted dye solution and protein solution was then mixed in a 1:1 volumetric ratio (200 µL final volume) and left to incubate for 30 minutes at room temperature and protected from light. To purify the protein/dye solution the included purification column was equilibrated using PBS solution. The protein/dye solution was then applied to the middle of the purification column and the flow through discarded. PBS (600 µL) was then applied to the purification column and the eluent collected in 200 µL fractions.

Final protein concentration and degree of labelling (DOL) was calculated first by measuring the UV absorbance of the protein solution at 280 nm and at 650 nm. Protein concentration was determined using the equation shown below, $\varepsilon Protein$ is the molar extinction coefficient which in this case was 210,000, d relates to path length which in this case was 1.

$$c(M) = A_{280} - (A_{650} \times 0.04) \div \varepsilon Protein \times d$$

Degree of labelling was calculated using the equation shown below. The value of 195,000 $M^{-1}cm^{-1}$ is the molar extinction coefficient of the dye used to label the protein, c(M) is the concentration of protein calculated using the equation above.

$$DOL = A_{650} \div 195,000 M^{-1}cm^{-1} \times c(M)$$

If a DOL of between 0.5-1.0 was calculated the labelled protein was suitable for use in MST assays. If the DOL fell outside of this range the sample was discarded and the labelling procedure repeated with fresh protein.

The same MST assay method was used for all molecules tested, assays were performed as follows. An MST assay buffer (50 mM Tris, 150 mM NaCl, 10 mM $MgCl_2$, pH 7.4, 0.05% w/v Tween 20) used to dilute the labelled bevacizumab or labelled infliximab to a concentration of 2.5 mg/mL. The pH of the solution was adjusted to pH 7.4. Labelled antibodies were diluted to a concentration of 5 nM with the MST assay buffer and used for all assays. Serial dilutions of relevant ligands (VEGF, TNF-α and IL-6R) were combined with the labelled antibodies and their conjugates in glass capillaries ready for measurement. The ligand concentration was determined by the MST software and was typically within the range of $1.0x10^{-6}$ to $1.52x10^{-11}$M. Assays were performed using an LED power of 15% and with laser power set to high. A Monolith Pico system was used for all MST measurements.

Culturing of human umbilical vein endothelial cells (HUVECs):

HUVEC cells were removed from liquid nitrogen and placed on ice. The cryovial was run under cold water until the frozen cells began to melt. Once completely melted the cells were split evenly into two vented T-75 flasks giving a concentration of 350,000 cells per T-75 flask. To each flask 10 mL of supplemented endothelial cell medium was added, supplement was added at a ratio of 1.22 mL supplement to 50 mL of endothelial cell medium. The flasks were then placed into a CO2 incubator set at 37°C and 5.0% CO2. The growth of the cells was monitored using a microscope daily and pictures were taken, the growth medium was replaced every 24-48 hrs. Once confluent the cells were harvested using a PromoCell detach kit, as per the kit instructions. The cells were counted by diluting 10 μL of cell suspension with 40 μL of trypan blue, the cell dilution was placed onto a hemocytometer and the cells were counted. After counting the average of the four quadrants was calculated and the total amount of cells was determined using the following formula:

(Average amount of cells x dilution factor) x mLs of cell suspension x 10^4
For example 27x5 (dilution factor when diluting with trypan blue) x2 (2 mL of cell suspension) x10^4 = 2,700,000 cells.

Cells were placed into two new flasks for growth at a concentration of 350,000 cells per T-75 and the remaining cells were frozen down using a freezing mix of 10% DMSO, 50% FCS (heat inactivated) and 40% of endothelial growth medium. The cryovials were first placed into a Mr. Frosty containing IPA at -70°C for at least 48 hours, after which they were placed into liquid nitrogen for long term storage.

Treatment of human umbilical vein endothelial cells (HUVECs) with anti-CD31 antibodies and flow cytometry:

HUVEC cells were grown to confluence in a T-75 flask using the culturing method described previously. HUVECs at passage no. 2 were used for this method.

Once confluent growth medium was aspirated from the T-75 flask and discarded. Then 5 mL of PBS was added to the flask and the flask gently rocked to bathe the cells for 60 seconds. After 60 seconds the PBS was aspirated and discarded. Next 5 mL of enzyme free cell dissociation buffer was added to a T-75 flask. The flask was gently agitated for two minutes after which the enzyme free cell dissociation was aspirated and discarded. The T-75 flask was firmly tapped against using the palm of the hand to dislodge the cells from the surface of the flask. Detachment was checked under a microscope. Once detached the cells were suspended in 10 mL of endothelial growth medium. The suspended detached cells were transferred to a centrifuge tube and then centrifuged at 220 g for 3 minutes. The supernatant was aspirated and discarded, and the pellet resuspended in 1 mL of endothelial growth medium. Cells were then counted using the same counting method described previously.

After cell counting detached HUVECs were added to 6 wells of a round bottom 96 well plate, 100,000 cells per well. To 4 wells Human TruStain FcX (0.5 µL) was added after which the 96 well plate was left on ice for 20 minutes. After incubation on ice mouse anti-human CD31 antibody (0.5 µL, APC tagged) was added to 2 of the Fc blocked wells. The 96 well plate was then incubated on ice for a further 20 minutes. While the well plate was incubating, FACs buffer (100 mL, PBS 1 mM EDTA, 2% heat inactivated fetal calf serum (FCS)) was prepared by dissolving 1 Oxoid™ Phosphate Buffered Saline Tablet and 37.4 mg of EDTA in 98 mL of type 1 water. To the PBS/EDTA solution, FCS (2 mL) was added, and the container inverted several times to mix.

Post incubation the wells were washed two times using 100 µL of FACs buffer per well, the plate was centrifuged at 4°C for 5 minutes at 1300rpm in between wash cycles. 200 µL of FACs buffer was added to each well, cells resuspended and transferred into LP4 tubes. Each sample was tested with an Accuri C6 flow cytometer using the FL4 flow channel as the anti-CD31 antibody was tagged with APC. Data was collected until a total of 10,000 events had occurred. Flow cytometer data was analysed using FlowJo analysis software.

Treatment of human umbilical vein endothelial cells (HUVECs) with TNF, IL-17A, Infliximab, Secukinumab and flow cytometry:

HUVEC cells (passage no.2) were seeded in 12 well plates (60,000 cells per well) and grown to confluence, a total of three 12 well plates were seeded. Once confluent the HUVECs were treated with proinflammatory ligands and/or neutralising antibodies, dilutions of ligands and antibodies were prepared using endothelial growth medium as a diluent. The ligands and antibodies added to the wells (final solution volume within each well of 1 mL) and their concentrations within the wells are now listed with a duplicate of each well being prepared to allow for staining using both anti-ICAM-1 and anti-VCAM-1 antibodies.

- 2 wells TNF-α 20 ng/mL
- 2 wells TNF-α 10 ng/mL
- 2 wells TNF-α 1 ng/mL
- 2 wells IL-17A 20 ng/mL
- 2 wells IL-17A 10 ng/mL
- 2 wells IL-17A 1 ng/mL
- 2 wells TNF-α 20 ng/mL and IL-17A 20 ng/mL
- 2 wells TNF-α 10 ng/mL IL-17A 10 ng/mL
- 2 wells TNF-α 1 ng/mL IL-17A 1 ng/mL
- 2 wells TNF-α 20 ng/mL and Infliximab 100 ng/mL
- 2 wells IL-17A 20 ng/mL and Secukinumab 150 ng/mL
- 2 wells TNF-α 20 ng/mL and IL-17A 20 ng/mL, Infliximab 100 ng/mL and Secukinumab 150 ng/mL

Once the HUVECs were treated with either a ligand or ligand/antibody mixture they were left to incubate for 24 hours in a CO_2 incubator set at 37°C and 5.0% CO2. After 24 hours of incubation microscopy images were taken. Then the solution in each

well was aspirated and discarded after which 1 mL of PBS was added per well and the plate gently rocked to bathe the cells for 60 seconds. After 60 seconds the PBS was aspirated and discarded. Next 1 mL of enzyme free cell dissociation buffer was added to each well and the plate gently agitated for two minutes after which the enzyme free cell dissociation buffer was aspirated and discarded. The 12 well plate was firmly tapped using the palm of the hand to dislodge the cells from the surface of the well plate. Once detached the cells in each well were suspended in 300 µL of endothelial growth medium. The detached suspended cells were then transferred from the 12 well plate to a round bottom 96 well plate with the contents of a single well of the 12 well plate being transferred to a single well of the round bottom 96 well plate. In total 32 wells of the round bottom 96 well plate were filled with detached HUVECs and the plate labelled according plate layout shown in Figure 16.

Figure 16: Round bottom 96 well plate layout used for the staining of HUVECs treated with TNF-α, IL-17A, Infliximab and Secukinumab. Anti-ICAM-1 and anti-VCAM-1 (both APC tagged) antibodies were used to stain the relevant wells. Empty wells have been excluded from the well plate layout.

To all the wells, except from *"blank control"*, Human TruStain FcX (0.5 µL) was added after which the 96 well plate was left on ice for 20 minutes. To the 14 wells in Figure 16 labelled with ICAM-1, 5 µL of mouse anti-human ICAM-1 antibody (APC tagged) was added. To the 14 wells of Figure 16 labelled with VCAM-1, 2.5 µL of rabbit

anti-human VCAM-1 antibody (APC tagged) was added. The 96 well plate was then left to incubate on ice for 30 minutes.

Post incubation the wells were washed two times using 100 µL of FACs buffer per well, the plate was centrifuged at 4°C for 5 minutes at 1300rpm in between wash cycles. 200 µL of FACs buffer was added to each well, cells resuspended and transferred into LP4 tubes. Each sample was tested with an Accuri C6 flow cytometer using the FL4 flow channel as the anti-ICAM and VCAM antibodies were tagged with APC. Data was collected until a total of 10,000 events had occurred. Flow cytometer data was analysed using FlowJo analysis software. It should be noted that although the samples were prepared for flow cytometry samples with TNF-α, IL-17A or TNF-α/IL-17A mixtures at concentrations of 10 ng/mL or 1 ng/mL were not run.

Chapter 3 – Digestion of IgG antibodies using soluble papain

The preparation of bispecific antibody fragments in this project involved the utilization of antigen binding fragment (Fab). While Fabs can be engineered using bacterial expression systems or recombinant methods, the expression of Fabs containing essential disulfide bonds, required for their activity and stability, presents a challenge using an *Escherichia coli (E. coli)* system [162,163]. Recombinant methods for producing Fabs sometimes encounter limitations in terms of yield, folding and functionality.

An alternative approach involves the enzymatic digestion of monoclonal antibodies to obtain Fabs [164–166]. This strategy offers the opportunity to conduct a direct binding comparison between Fabs in IgG and Fabs within the prepared bispecific antibody fragment. In this project, we employed enzymatic digestion of IgG to obtain pure Fabs. The use of papain, a proteolytic enzyme with a molecular weight of 23 kDa, has long been studied for the enzymatic digestion of IgG. Papain is originally derived from crude papaya (*carica papaya*) latex obtained from the unripe papaya fruit [167]. It cleaves monoclonal antibodies above the hinge region, resulting in the cleavage of the Fc (fragment crystallisable region) and the generation of two Fabs. The enzymatic digestion process is illustrated in Scheme 5.
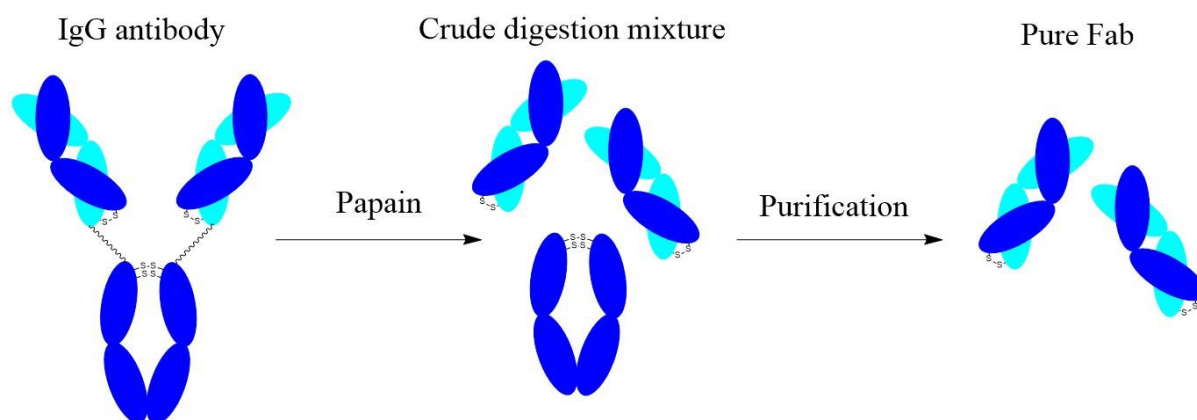
Scheme 5: A scheme for the digestion of an IgG antibody using papain

Papain is an enzymatic non-specific thiol-endopeptidase composed of 212 amino acids and stabilised by three disulfide bonds [167]. Within its active site, papain possesses a sulfhydryl group that requisites reduction to its active form for proteolytic activity. Consequently, cysteine is used as a reducing agent in the digestion buffer when employing papain. While papain is a non-specific endopeptidase, there are other highly specific enzymes available, such as gingisKHAN and FabULOUS, which can digest IgG at a single digestion site to obtain Fab. These enzymes have the advantage of being easily removed from the digested IgGs, because of the optimised

methodologies offered by Genovis. However, it is worth noting that the main drawback of these specific enzymes is their considerably higher cost. For instance, to digest 100 mg of IgG, 200,000 units of gingisKHAN are needed at the cost of £10,000. This expense limits their use in research, particularly when large quantities of Fabs are required.

In the past, the enzymatic digestion of IgG was commonly carried out using a soluble form of papain. However, this method presented several challenges, including purification difficulties and the risk of over digestion of the antibody. Over digestion can occur if the process is not properly controlled, resulting in breakdown of Fabs and Fc into smaller fragments with limited use. This issue arises from non-specific nature of the enzyme.

To address these challenges, immobilised forms of papain were developed, wherein the enzyme is attached to agarose beads. Immobilization aids in purification, as the enzyme can be easily removed via centrifugation. Despite the advantages of obtaining pure Fab, using immobilised papain for IgG digestion also has limitations, most notably slow digestion time (more than 7 h), and high cost which limits scalability within a research setting, as experienced previously by our research group [168].

Considering these factors, it became necessary to revisit the use of soluble papain during the first year of this PhD project. Reference experiments were first conducted, wherein 10 mg of tocilizumab, bevacizumab and infliximab were digested using immobilised papain. Figure 17 is an SDS PAGE gel showing the results of digesting 10 mg IgG, after a 7 hour digestion, using immobilised papain. Digestion mixtures (Figure 17, Lanes 2, 7 and 12) were further purified using a protein A column to separate Fabs from the Fc. Fractions F1-F3 (Figure 17, Lanes 3-5, 8-10 and 13-15) obtained from protein A columns, were for the purified Fabs. Protein A columns bind to Fc and elute Fabs. Using elution buffer (Glycine, pH 2.0), the Fc and undigested IgG were eluted from the protein A column, displayed in Figure 17, Lanes 6, 11 and 16.
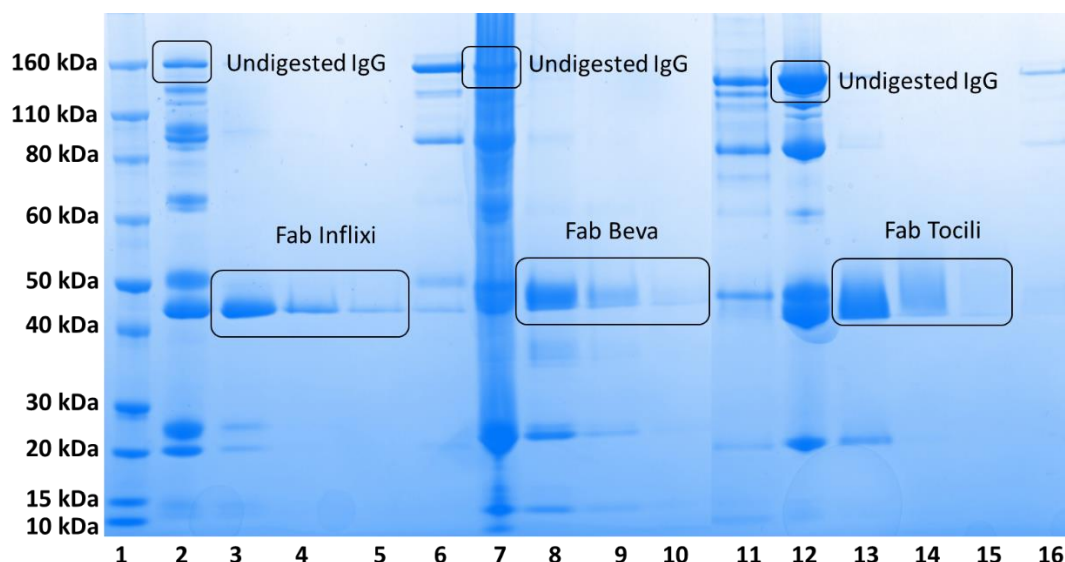
Figure 17: SDS PAGE gel of the digestion of infliximab, bevacizumab and tocilizumab using immobilised papain (7 hour digestion time) 10 mg of each antibody was digested. **Lane 1**: Protein marker, **2**: Crude infliximab digestion mixture, **3**: Pure $Fab_{Inflixi}$ fraction 1 (F1), **4**: F2, **5**: F3, **6**: E1, **7**: Crude bevacizumab digestion mixture, **8**: Pure Fab_{Beva} fraction 1 (F1), **9**: F2, **10**: F3, **11**: E1, **12**: Crude tocilizumab digestion mixture, **13**: Pure Fab_{Tocili} fraction 1 (F1), **14**: F2, **15**: F3, **16**: E1.

As observed in Figure 17 (Lanes 3-5, 8-10 and 13-15), the digestion of 10 mg of each antibody using immobilised papain resulted in the production of pure Fab. However, even after a digestion time of 7 hours, traces of undigested IgGs and IgG intermediates persisted in the crude digestion mixtures (Figure 17, Lanes 2, 7 and 12). Small quantities of Fabs are also present in the eluent lanes (Figure 17, Lanes 6, 11 and 16). Further washing of the protein A column may allow these Fabs to be collected. However further washing to try and obtain such a small quantity would not be recommended as it would result in the final purified Fabs being further diluted. Therefore, objectives were to reassess the soluble papain digestion process and explore potential optimisation methods to facilitate scaling up to 100 mg of IgG.

The first set of experiments using soluble papain was to determine which soluble form was most suitable as two forms of soluble papain are readily available. The first form is a crude, impure form of papain and the second a highly pure lyophilised form. An experiment to compare the two forms of soluble papain was carried out. The result of a digestion of tocilizumab using crude soluble papain is shown in Figure 18. Digestion was carried out for a total of 4 hours with samples taken at different timepoints throughout.
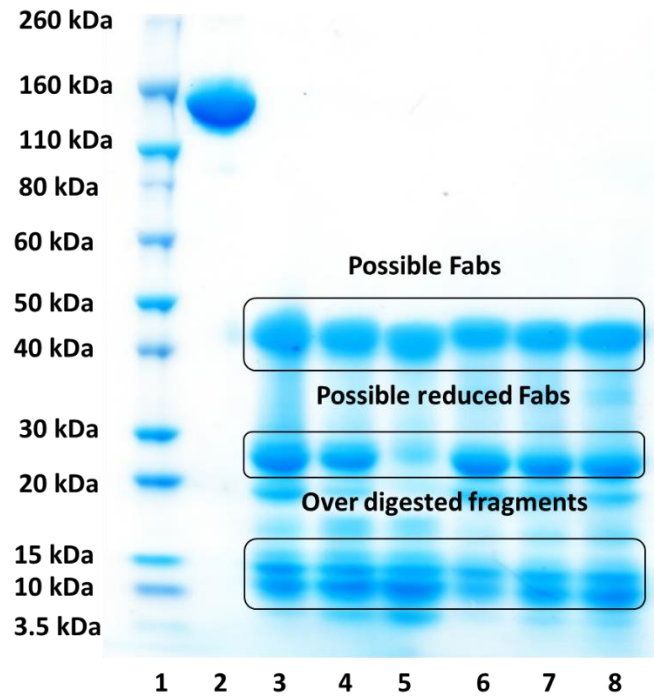
Figure 18: SDS PAGE gel of the digestion of 5 mg tocilizumab using a crude form of soluble papain for a total of 4 hours. **Lane 1:** Protein marker, **2:** 1 mg/mL tocilizumab, **3:** 10 min, **4:** 20 min, **5:** 30 min, **6:** 1 hr, **7:** 2 hrs, **8:** 4 hrs

As can be seen from Figure 18 (Lanes 3-8), tocilizumab was completely digested into smaller fragments with possible Fabs and reduced Fabs being present. It was concluded that complete digestion had occurred due to the lack of a band at approximately 160 kDa in Figure 18 Lanes 3-8. Smaller over digested fragments are also present in the same lanes at low molecular weights, over digestion is a known issue when using soluble papain to digest IgGs [169,170]. These fragments are illustrated in Figure 19.
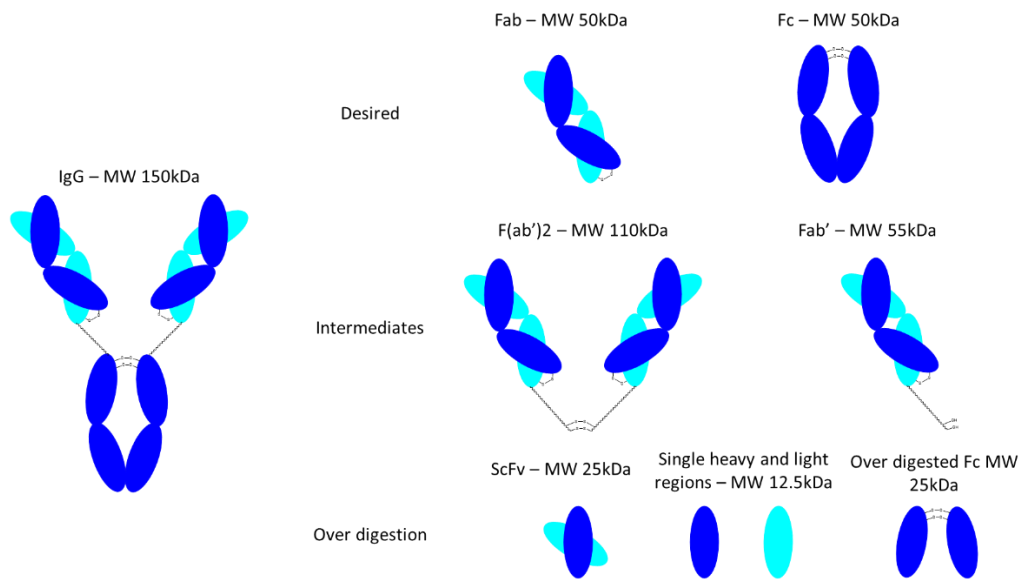
Figure 19: Possible antibody fragments obtained during digestion of an IgG using papain

In this experiment, iodoacetamide was added to each sample with the aim of blocking the activity of papain [171] to halt the digestion process. This addition was intended to allow for the evaluation of different digestion times. Iodoacetamide is commonly used as an alkylating agent to modify cysteine residues and prevent disulfide bond formation. In the context of papain digestion, iodoacetamide was used to modify any remaining cysteine residues in the papain, affecting the activity of the enzyme.

It was observed that the addition of iodoacetamide did not effectively cease the digestion process, as visually all the samples taken at different digestion times (Figure 18, Lanes 3-8) appeared similar. If the activity of the enzyme was blocked successfully, clear differences would have been expected. For example, after 10 minutes of digestion, a significant amount of undigested tocilizumab would have remained, with the quantity decreasing as time progressed and more digestion products formed. A key finding from this experiment however was the rapid rate at which the crude form of soluble papain digested tocilizumab. The antibody was completely digested within 4 hours, which is twice as fast as comparable digestions performed with immobilised papain.

Another form of soluble papain available was lyophilised soluble papain. In this experiment the pH of the samples taken at different timepoints was adjusted to pH 2.0 to halt the activity of papain after digestion time. The samples were also frozen to further halt the digestion. No iodoacetamide was used in this experiment. A pH of 2.0 was chosen as the enzymatic activity is greatly reduced or possibly halted at such an

acidic pH recommended in [172], the ideal pH for papain activity is 7.0. The result of a digestion of tocilizumab with lyophilised soluble papain with adjusted pH 2.0, is shown in Figure 20.
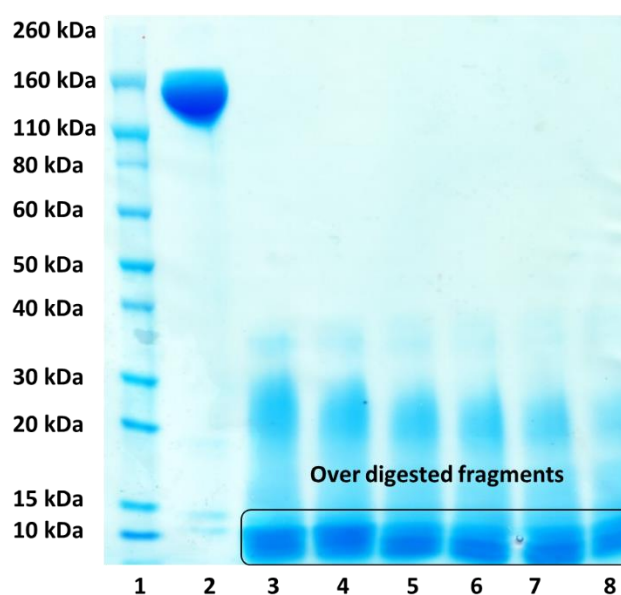
Figure 20: SDS PAGE gel of the digestion of 5 mg tocilizumab using a lyophilised form of soluble papain for a total of 4 hours. **Lane 1:** Protein marker, **2:** 1 mg/mL tocilizumab, **3:** 10 min, **4:** 20 min, **5:** 30 min, **6:** 1 hr, **7:** 2 hrs, **8:** 4 hrs.

As can be seen from Figure 20, tocilizumab has been completely digested. Again, visually the samples taken at different timepoints (Figure 20, Lanes 3-8) are similar with the greatest concentration of protein being over digested. This means that adjustment of pH and subsequent freezing did not halt the digestion process. Further reading of literature revealed that papain's activity may actually retain up to 50% of its residual activity at pH 2.0 [173] meaning the previous literature stating papain activity is reduced at low pH may be incorrect [172]. Over digestion of IgG was observed after 10 minutes incubation with lyophilised soluble papain at 37°C, over digestion was also observed after 10 minutes when using crude papain however to a lesser degree.

After completion of these two experiments, it was decided to use lyophilised soluble papain. This was because of two reasons, firstly the lyophilised papain digested IgGs faster than the crude papain and secondly because of its purity. Crude papain was impure, upon dissolving it in the digestion buffer it appeared to be a cloudy solution as shown in Figure 21 whereas lyophilised papain appeared to be a clear solution when it was dissolved in water.

Figure 21: Appearance of a crude papain solution. Crude papain was dissolved in digestion buffer at a concentration of 6.5 mg/mL.

The separation and purification of papain from the digestion mixture posed an additional challenge when utilising soluble papain, whether in crude or lyophilised form. Unlike, immobilised papain, which can be easily removed from the digestion mixture through centrifugation, soluble papain cannot be removed using this method. Consequently, when using soluble papain, it was not possible to analyse the digestion mixture in SDS PAGE without papain being present. This limitation hindered the characterization of the digestion mixture without the interference of papain, as demonstrated in [9], where immobilized papain was used.

It was important to investigate what purification technique could be used to remove the used papain and yield pure Fabs using a soluble papain digestion process. Initially CH[1] affinity chromatography was used to purify the digestions. CH[1] affinity resins bind to the CH[1] region present on a Fab allowing separation of Fabs and IgGs from a reaction mixture [174], Figure 22 shows an SDS PAGE gel from the CH[1] purification of tocilizumab digested with lyophilised soluble papain for 20 minutes. It should be noted that from here on the term soluble papain refers to the lyophilised form of the enzyme, the crude form was no longer experimented with.

69
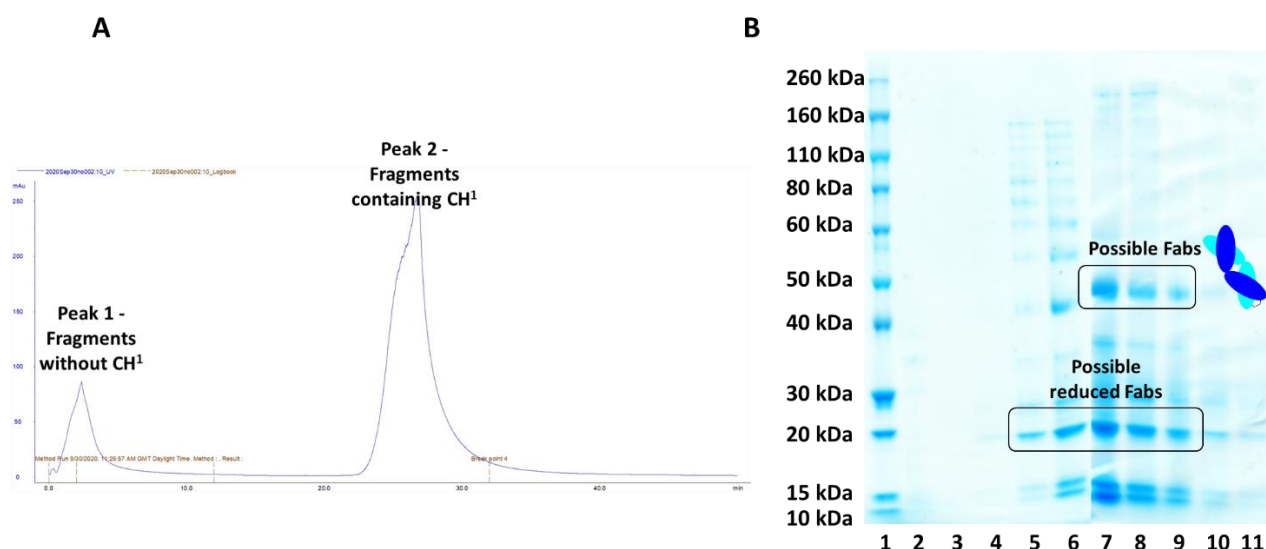
Figure 22: (A) CH^1 chromatogram from the purification of tocilizumab digested using soluble papain. **(B)** SDS PAGE gel of CH^1 purification of tocilizumab digested using soluble papain (5 mg scale, 20 min digestion time), **Lane 1**: Protein marker, **2:** Peak 1, **3:** Peak 2 fraction 1 (F1), **4:** F2, **5:** F3, **6:** F4, **7:** F5, **8:** F6, **9:** F7, **10:** F8, **11:** F9. Peak 2 fractions were collected every minute between 22.70-30.70 min of method run time.

As shown in the gel no bands are present for fraction collected for peak 1 (Figure 22B, Lane 2) despite a peak being present on the chromatogram. It was expected that the Fc or subunits of the Fc would be present in this fraction because it does not contain a CH^1 group and therefore would not bind to the column. Some of the fractions collected for peak 2 (Figure 22B, Lanes 5-9) contain bands that relate to the molecular weights of Fabs and reduced Fabs, for visualisation the bands corresponding to the Fabs have been annotated with a picture of a Fab. Also within these lanes are smaller molecular weight entities which are likely to be the result of over digestion.

Faint bands are also present at a higher molecular weight than the Fab bands, these bands relate to undigested or partially digested IgG. However, judging by the faintness of these bands most of the parent tocilizumab was digested. To further purify the possible Fab fragments, the fractions (Figure 22B, Lanes 5-9) were combined and concentrated to a volume of 0.5 mL and injected onto a SEC column. The results of the SEC purification are shown in Figure 23 below.
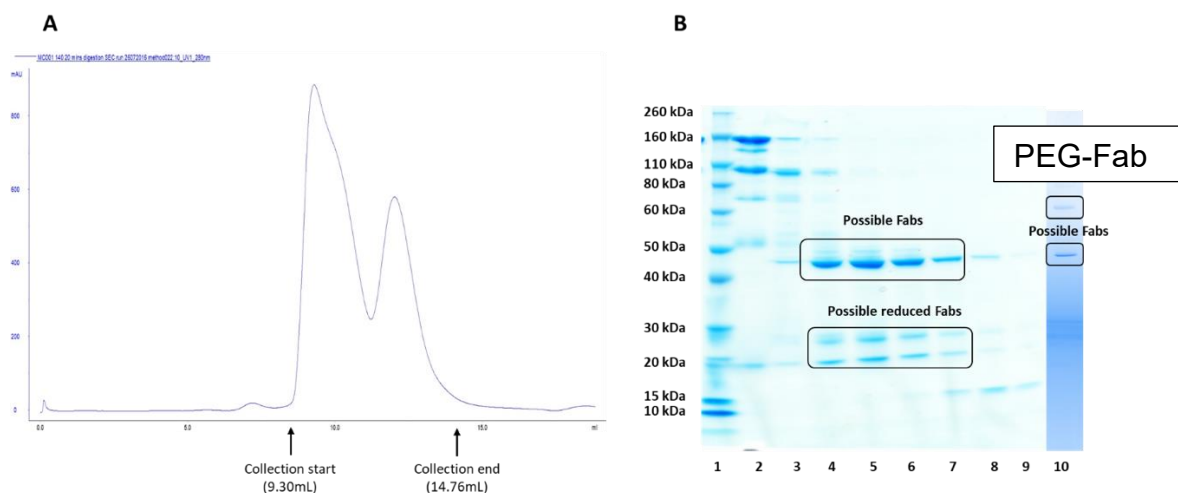
Figure 23: (A) SEC chromatogram from the purification of lanes 5-9, Figure 22B. **(B)** SDS PAGE gel of the SEC purification of lanes 5-9, Figure 22B, **Lane 1**: Protein marker, **2**: Fraction 1 (F1), **3**: F2, **4**: F3, **5**: F4, **6**: F5, **7**: F6, **8**: F7, **9**: F8, **10**: Conjugation of possible Fab_{Tocili} to a PEG_{20} *bis*-sulfone reagent **8**. Fractions were collected every 30 seconds between 9.30-14.76 mL of method volume.

As can be seen in lanes 4-7 (Figure 23B) SEC was able to purify most of the higher molecular weight bands from the possible Fab and reduced Fab. The quantity of Fab fragments was measured via UV absorption at 280 nm and a yield calculated, which in this case was 17%. This yield is significantly lower than what can be obtained when digesting tocilizumab using immobilised papain with yields of 50% being achieved consistently. The poor yield could be attributed to the binding capacity of the CH^1 resin. During this experiment a pre packed column containing CaptureSelect CH^1 affinity resin was used however the manufacturer has since released an improved version which in its datasheet states it has improved binding capacity [175] using the improved resin may help to improve yield. Before trying that however the Fabs obtained during this experiment were used for a conjugation experiment to assess the integrity of the Fab interchain disulfide bonds. Fab_{Tocili} was conjugated to a PEG_{20} *bis*-sulfone reagent **8** (Figure 24). The synthesis and functionality of reagent **8** is described in greater detail in Chapter 4.

8
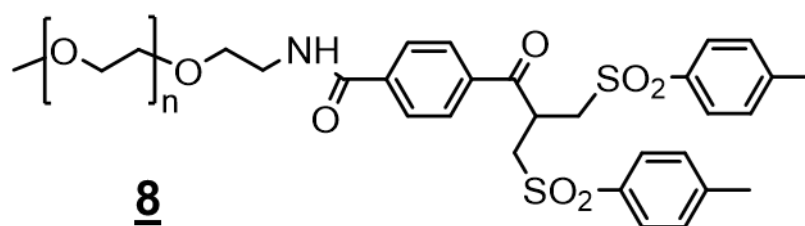
Figure 24: Structure of the PEG *bis*-sulfone reagent **8** used for the conjugation of Fab_{Tocili} obtained from the digestion of tocilizumab with soluble papain.

This experiment was carried out to check if the terminal disulfide bond present on the Fab remained healthy after digestion. The results of the conjugation are shown in Figure 23B, Lane 10. As can be seen very little PEG-Fab has formed suggesting there may be a problem with the Fab disulfide and that it has become damaged during digestion.

Because of the poor yield and conjugation experiments, a different approach was proposed to purify the soluble papain digestion mixtures. It was thought to try and mimic the purification method used for digestions using immobilised papain by using a prepacked Protein A column. Protein A binds to the Fc of IgGs meaning separation of the Fabs and Fc should be possible especially as this is an established purification technique. Figure 25 below shows an SDS PAGE gel and a chromatogram from the purification of a soluble papain digestion using Protein A chromatography.
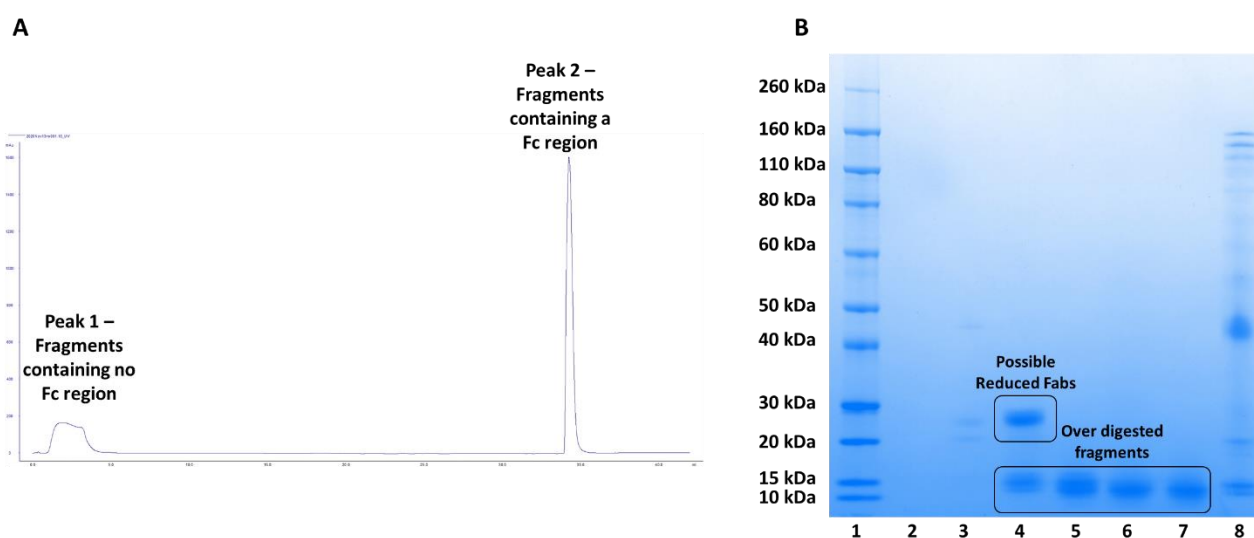
Figure 25: (A) Protein A chromatogram from the purification of tocilizumab digested using soluble papain. **(B)** SDS PAGE gel of protein A purification of tocilizumab digested using soluble papain (5 mg scale, 20 min digestion time), **Lane 1**: Protein marker, **2**: Peak 1 fraction 1 (F1), **3**: F2, **4**: F3, **5**: F4, **6**: F5, **7**: F6, **8**: Peak 2. Peak 1 fractions were collected every 30 seconds between 1-3 min of method run time.

In the SDS-PAGE gel (Figure 25B, Lane 4) two bands at approximately 25 and 12.5 kDa are visible. The 25 kDa band corresponds to the expected molecular weight of reduced Fabs. The 12.5 kDa band suggests the presence of a single heavy or light chain fragment, an indication of over digestion caused by the non-specific nature of papain. These bands are also observed in lanes 5-7.

Over digestion occurs because while protein A separates Fab from Fc, it is unable to separate Fab from papain. In Figure 25A, Peak 1 consists of unbound fragments lacking an Fc. However, within this unbound material, papain is still present as it does not bind to protein A resin. Consequently, post-purification, the Fab remains in solution with the enzyme, resulting in over digestion.

An alternative purification resin used in this study was Protein L. Protein L can bind specifically to the kappa light chain present in Fab fragments. By employing this type of affinity chromatography, it was anticipated that the soluble enzyme could be separated from the Fab, as papain is not expected to bind to the protein L resin. In the next section, the results of the soluble papain digestions, purified using Protein L resins, will be presented.

Protein L chromatography for the purification of soluble papain digestion

Initially small-scale digestions using 5 mg of tocilizumab were carried out and the digestion mixtures purified using a Protein L column. Figure 26 shows an SDS PAGE gel of 3 digestions of tocilizumab after purification of the crude digestion mixtures with a protein L column and a typical chromatogram generated using this methodology.
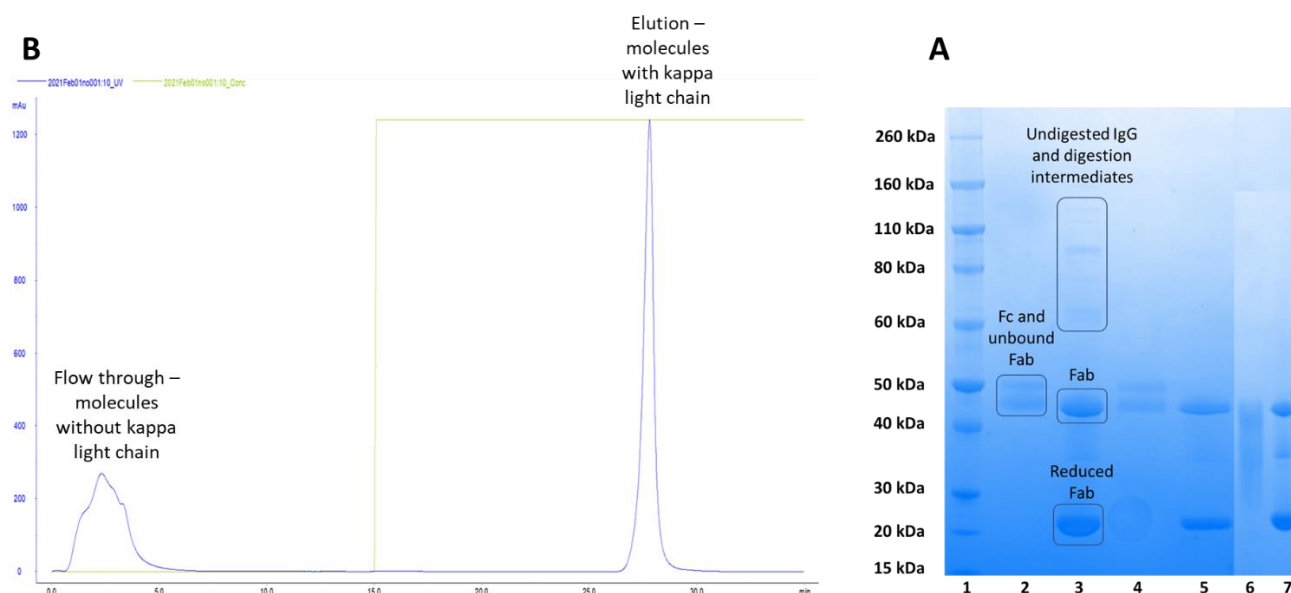
Figure 26: (A) Protein L chromatogram from the purification of tocilizumab digested using soluble papain. **(B)** SDS PAGE gel of protein L purification of tocilizumab digestions using soluble papain (5 mg scale, 30, 40 and 50 min digestion time), **Lane 1**: Protein marker, **2:** 30 min flow through, **3:** 30 min elution, **4:** 40 min flow through, **5:** 40 min elution, **6:** 50 min flow through, **7:** 50 min elution.

The results depicted in Figure 26B illustrate that increasing the digestion time leads to more complete digestion, as evidenced by the absence of undigested IgGs and intermediates at the 40- and 50-minute digestion times. The desired Fab fractions are present as shown by the band observed between 40-50 kDa in Figure 26B, lanes 3, 5 and 7. Additionally, a band of lower molecular weight, approximately 25 kDa is visible in these lanes, representing the reduced form of the Fab. The chromatogram (Figure 26A) exhibits two distinct elution peaks, indicating effective separation of molecules containing the kappa light chain and those lacking it. To ensure the removal of any high molecular weight impurities, the elution fractions underwent further purification using SEC. The yield of purified Fab following each digestion was calculated using the UV absorption at 280 nm. The yields are summarised in Table 7.

Digestion time (min)	Amount of Fab (mg)	Yield (%)
30	1.23	37
40	1.11	34
50	1.35	41

Table 7: Yields of purified Fab fragments from the digestions of 5 mg tocilizumab, 30, 40 and 50 minute digestion times.

The yields obtained in this set of experiments were higher compared to those observed previously when CH1 column was used. The yields for the digestions were closer to the expected values obtained when digesting tocilizumab using immobilised papain. Among the various digestion times evaluated, a 50 minute digestion time gave the highest yield and therefore was deemed the most suitable digestion time going forward. This is likely due to the longer digestion time ensuring complete digestion of the IgG, thereby maximising yield of Fab.

The subsequent step in this experiment involved using some of the obtained Fabs in a conjugation experiment using *bis*-alkylating reagents to assess the integrity of the interchain disulfide bonds. Fab$_{Tocili}$ was conjugated to a PEG *bis*-sulfone reagent **8**, Two separate conjugations were performed with 5 kDa MW and 10 kDa MW variants of the PEG *bis*-sulfone reagent **8** (Figure 27).
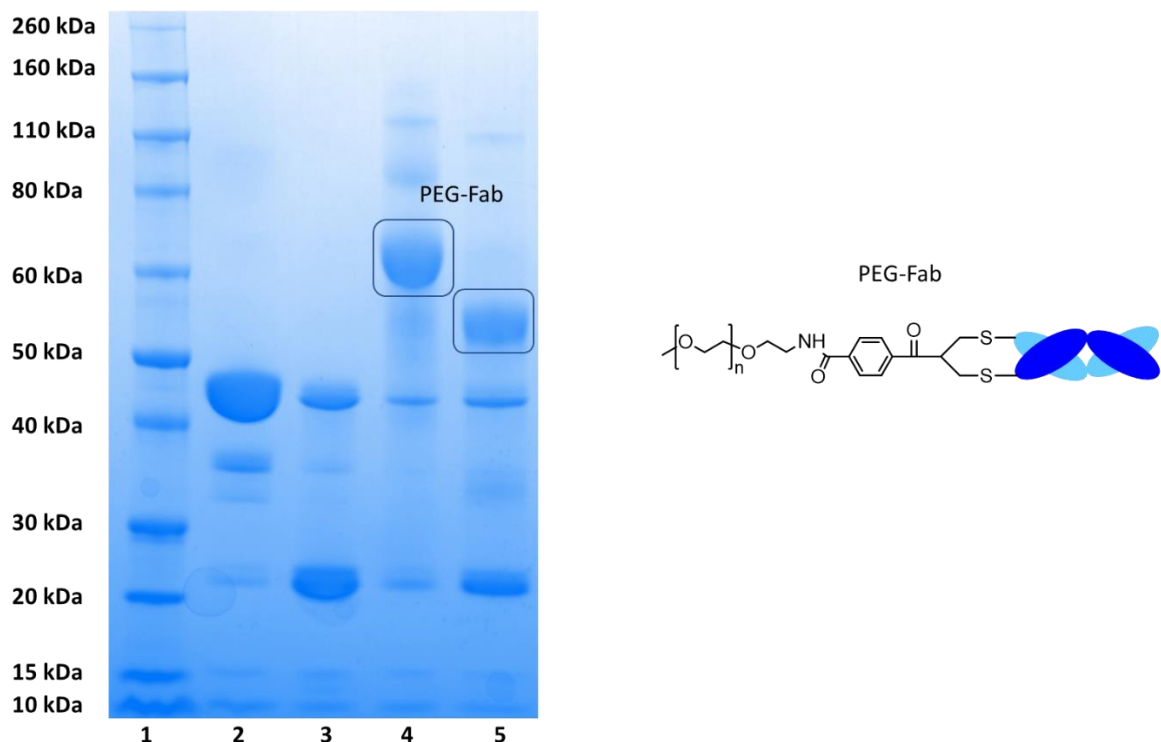
Figure 27: SDS PAGE gel of the conjugation of 0.5 mg Fab$_{Toclili}$ prepared using soluble papain to PEG$_{10}$ and PEG$_5$ *bis*-sulfone **8** using 1.5 molar equivalents of PEG reagent at pH 7.6. 6-hour conjugation time and a representation of a PEG-Fab molecule, **Lane 1**: Protein marker, **2:** Fab$_{Tocili}$, **3:** reduced Fab$_{Tocili}$, **4:** conjugation to PEG$_{10}$ *bis*-sulfone **8**, **5:** conjugation to PEG$_5$ *bis*-sulfone **8**.

As seen in Figure 27, the Fabs prepared and purified using protein L chromatography were able to conjugate to both the PEG$_{10}$ and PEG$_5$ *bis*-sulfone reagents **8** to form two PEG-Fab$_{Tocili}$ conjugates of differing molecular weights, Figure 27 (Lanes 4 and 5). The PEG$_{10}$-Fab$_{Tocili}$ highlighted in lane 4 was approximately 60 kDa MW (50 kDa Fab + PEG$_{10}$ *bis*-sulfone **8**) and the PEG$_5$-Fab$_{Tocili}$ highlighted in lane 5 was approximately 55 kDa MW (50 kDa Fab + PEG$_5$ *bis*-sulfone **8**). This demonstrated that the interchain disulfide bond in the prepared Fabs, remained healthy and intact and could react with the *bis-alkylating* functional group of the PEG *bis*-sulfone reagent **8**.

Different antibodies including bevacizumab and infliximab were subjected to digestion using soluble papain and subsequently purified using a Protein L column. Bevacizumab was selected due to its binding affinity to VEGF, which is a relevant ocular target. Moreover, bevacizumab demonstrated favourable properties in surface plasmon resonance (SPR) assays compared to another VEGF-binding molecule, ranibizumab (Chapter 5, Figures 87 and 88). Unlike ranibizumab, which exhibits a significantly slow dissociation rate from VEGF, making it a challenging molecule to study in SPR assay, bevacizumab does not possess this problem. Figure 28 features

an annotated chromatogram that represents a typical Protein L purification process applied to a bevacizumab digestion. Additionally, an SDS-PAGE gel provides characterisation of the flow-through and elution fractions obtained from digestion times of 30, 40 and 50 minutes.
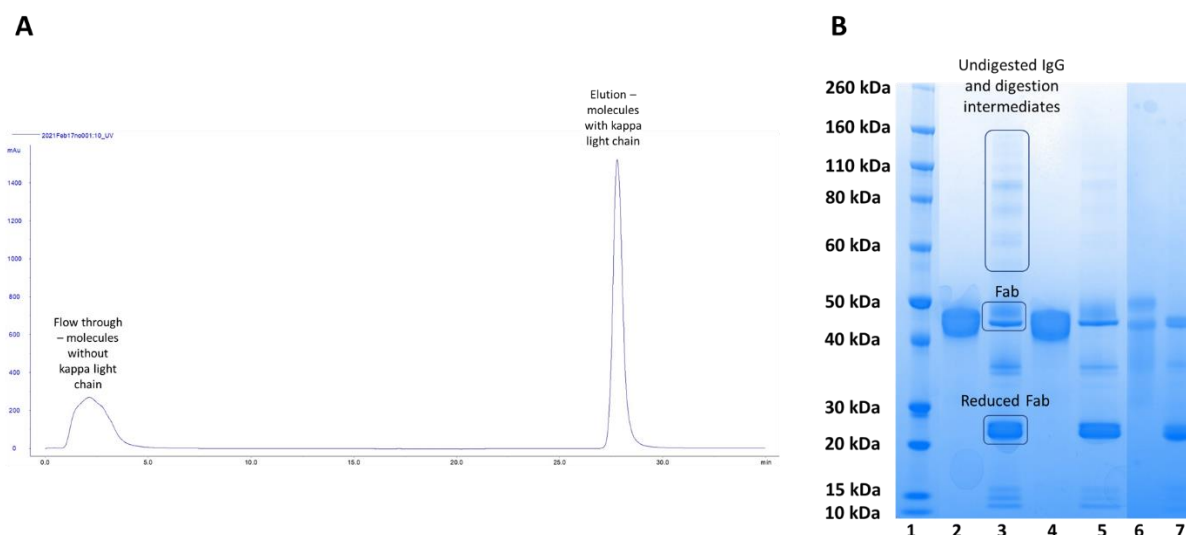
Figure 28: (A) Protein L chromatogram from the purification of bevacizumab digested using soluble papain. **(B)** SDS PAGE gel of protein L purification of bevacizumab digestions using soluble papain (5 mg scale, 30, 40 and 50 min digestion time), **Lane 1**: Protein marker, **2:** 30 min flow through, **3:** 30 min elution, **4:** 40 min flow through, **5:** 40 min elution, **6:** 50 min flow through, **7:** 50 min elution.

As can be seen from Figure 28B, extending the digestion time led to a more comprehensive digestion, as evidenced by the absence of undigested IgGs and intermediates. This result aligned with the observations made during the 5 mg digestions of tocilizumab. The % yields of purified Fab$_{Beva}$ are summarised in Table 8.

Digestion time (min)	Amount of Fab (mg)	Yield (%)
30	1.76	53
40	1.32	40
50	1.15	35

Table 8: Yields of purified Fab fragments from the digestions of 5 mg bevacizumab, 30,40 and 50 minute digestion time.

In contrast to the observations made with the tocilizumab digestions, it is noteworthy that a shorter digestion time has resulted in a higher yield for bevacizumab. The exact reason for this discrepancy remained unknown, but one possible explanation could be that the kappa light chain regions of bevacizumab are comparatively less stable than those of the tocilizumab molecule. As the digestion time increases, it is plausible that papain may cause damage to the bevacizumab kappa light chains, thereby reducing the binding capacity of the Fab fragment to the Protein L column. Consequently, some of the Fabs could be washed off the column and elute in the flow-through fraction. The % yields obtained after a 30 minute digestion time were comparable to the yields observed when digesting bevacizumab with immobilised papain.

It has been demonstrated that tocilizumab and bevacizumab can be digested at small scale (5 mg). From here the next step was to digest these antibodies using soluble papain but at a larger scale.

Large scale digestions of IgG antibodies using soluble papain

Soluble papain digestions have demonstrated significantly faster processing times compared to immobilised papain (up to 50 min vs up to 8 hrs) and have also shown a considerable reduction in cost, with the soluble enzyme being approximately 90 times cheaper. To expand the scope of this methodology, large-scale digestions of antibodies were undertaken, scaling up to 100 mg IgG. The success of large-scale digestions would enable the preparation of larger quantities of bispecific antibody mimetics, as a greater number of starting Fab would be available. However, a modification was required for the protein L purification methodology to accommodate the larger sample size necessary for these scale-up experiments.

In a 5 mg digestion, the digestion sample volume of 1.7 mL can be easily injected onto the column using a 5 mL sample loop. However, for a 100 mg digestion, the sample volume increases to 34 mL, making it impractical to find a sample loop for such a volume. Therefore the methodology was adjusted to apply the sample to the system via buffer valve, following the instructions provided in the AKTA prime plus instruction manual [176] (page 51). By utilizing the buffer valve there is no limit to the volume of sample that can be applied, offering the potential to scale the method beyond 100 mg. The first antibody to undergo large-scale digestion was tocilizumab.

Digestion of 100 mg of tocilizumab

Tocilizumab was chosen for the 100 mg digestion experiment due to its availability within our research group and its relevant therapeutical use within the eye. Although not approved specifically for use in the eye, it has been used off-label to treat non-infectious uveitis [177] because of its binding to pro-inflammatory IL-6R. Figure 29 shows the results of a 100 mg digestion of tocilizumab and subsequent purification using a protein L column.
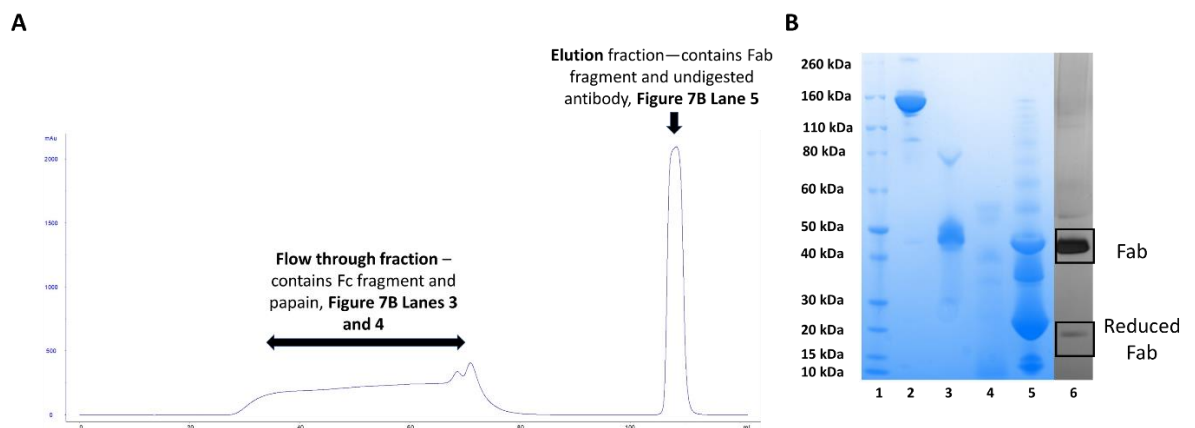
Figure 29: (A) Protein L chromatogram for the purification of a 100 mg tocilizumab digestion mixture, using soluble papain. **(B)** SDS PAGE analysis of flow through and elution fractions from the protein L purification, **Lane 1**: Protein marker, **2**: parent tocilizumab, **3** and **4**: flow through fractions containing Fc fragment and papain, they were collected in two parts due to the size of the column, **5**: elution fraction containing Fabs and undigested IgG, **6**: silver-staining of the purified Fab after SEC, reduced-Fab at 25 kDa observed due to presence of cysteine in the digestion buffer.

The flow-through and elution peaks shown in Figure 29A exhibit a similar pattern to what was observed in smaller-scale digestions of tocilizumab (Figure 26). The separation of the Fc and papain from the desired Fab fragments is evident, with the only distinction being the larger peak sizes due to the increased quantity of digested tocilizumab injected onto the protein L column. The flow-through fraction was substantial enough that it had to be collected in two samples for analysis, as shown in Figure 29B Lanes 3 and 4. In Figure 29B Lane 5, the elution fraction is displayed, and most of the Fabs appeared in a reduced form due to the presence of cysteine. The relatively poor resolution of the SDS PAGE for the elution fraction is attributed to its high concentration. Ideally, the elution fraction should have been diluted prior to SDS PAGE to give better resolution.

Subsequently, the elution fraction underwent further purification using SEC. Figure 29B Lane 6 showcases the silver staining of the final purified Fab. Although, the lane contains a small amount of reduced Fab due to the reduction of the disulfide

bond by cysteine which is present in the digestion buffer, the purified Fab solution itself does not contain cysteine. It is important to note that the reoxidation of the terminal disulfide bond does not happen instantaneously upon removal of the reducing agent.

A yield of 57.7% was achieved from this digestion, which was comparable to the yields obtained from small-scale soluble papain digestions. This yield corresponded to 38.5 mg of purified Fab which were stored in 1 mg aliquots at -20°C. Stability studies demonstrated that the Fabs remained stable for at least 5 months at -20°C shown in the SDS PAGE shown in Figure 30. Conjugations performed with these Fabs using *bis*-alkylating PEG reagents to assess if the interchain disulfide bond remained intact and healthy, results presented in the following chapter (Chapter 4). Protein-protein interaction experiments (Chapter 5) have also been performed with molecules containing these Fabs.
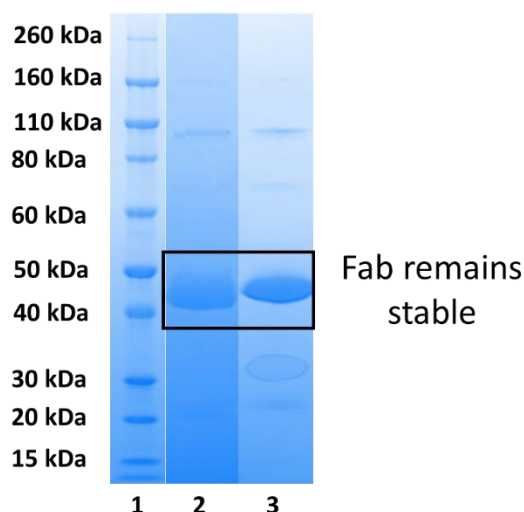
Figure 30: SDS PAGE gel showing the storage stability at -20°C of Fabs obtained from a 100 mg digestion of tocilizumab up to a 5 month timepoint, **Lane 1**: Protein marker, **2**: Initial, **3**: 5 months storage at -20°C

The 100 mg digestion of tocilizumab successfully showed that the soluble papain methodology could digest an IgG at large scale. It was then thought to perform another large scale digestion with a different antibody to ensure reproducibility. The anti-VEGF IgG, bevacizumab, was then selected.

Digestion of 37.5 mg of bevacizumab

Unfortunately, only 37.5 mg of bevacizumab was available for this experiment, however this amount is still significantly larger than the 5 mg bevacizumab digestions performed previously. Figure 31 shows the results of a 37.5 mg digestion of bevacizumab in the form of a protein L chromatogram and SDS PAGE gel.
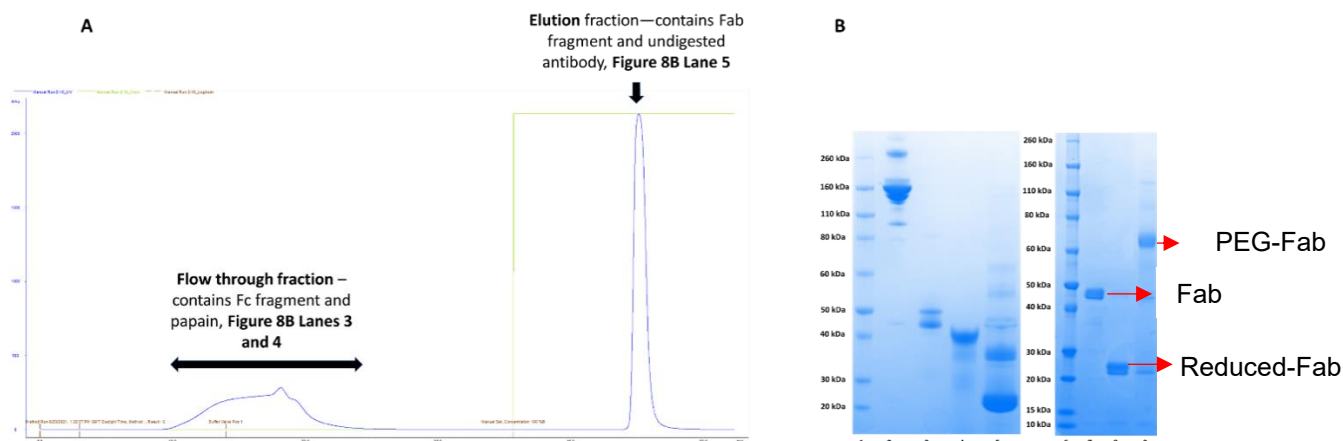
Figure 31: (A) Protein L chromatogram for the purification of a 37.5 mg bevacizumab digestion mixture, using soluble papain. **(B)** SDS PAGE analysis of flow through and elution fractions from the protein L purification and conjugation of the final purified Fab to a PEG$_{10}$ *bis*-sulfone reagent **8**, **Lane 1**: Protein marker, **2**: parent bevacizumab, **3** and **4**: flow through fractions containing Fc fragment and papain, they were collected in two parts due to the size of the column, **5**: elution fraction containing Fabs, most the Fabs are in the reduced form due to the presence of cysteine in the digestion buffer, **6**: Protein marker, **7**:Purified Fab$_{beva}$, **8**: Reduced Fab$_{beva}$, **9**: Fab$_{beva}$ conjugated to a PEG$_{10}$-B1 reagent.

The flow through and elution peaks observed in Figure 31A exhibited a similar profile to what was shown in Figure 29A, indicating clear separation. The SDS PAGE analysis of the flow through (Figure 31B Lanes 3 and 4) fractions and the elution (Figure 31B Lane 5) fractions resembled the results observed in Figure 29B, showing the reproducibility of the larger-scale method. A yield of 50% was achieved in this experiment.

In Figure 31B lanes 6-9, a conjugation of the final purified Fab$_{beva}$ to a PEG$_{10}$ *bis*-sulfone reagent **8** was displayed. The gel shows the purified Fab after further SEC purification (lane 7), that the Fab's disulfide bond reduces after being treated with DTT (lane 8) and finally the successful formation of a PEG$_{10}$-Fab$_{beva}$ conjugate (lane 9).

Binding of Fabs prepared using soluble papain and purified using a protein L column were further analysed using SPR kinetic assays with results being presented in Chapter 5.

In addition to bevacizumab and tocilizumab, which are humanised antibodies, we aimed to expand the application of the soluble papain method to other antibody

formats. Therefore, we conducted small-scale digestion of infliximab, a chimeric IgG antibody, and aflibercept, a Fc-fusion protein. In the next section, the results of small-scale digestions (up to 10 mg protein) of infliximab and aflibercept are presented.

Digestion of infliximab and aflibercept using soluble papain

Infliximab is a chimeric IgG and differs from humanised antibodies as it comprises of a mouse IgG with human complimentary determining regions (CDRs) grafted in place of the mouse CDRs. It has been reported that immobilised papain can successfully digest chimeric IgGs [178], hence it was worthwhile to see if soluble papain can also be suitable. Figure 32 shows SDS PAGE gels from digestions of 5 mg infliximab for 25 (Figure 32A) and 35 (Figure 32B) minutes.
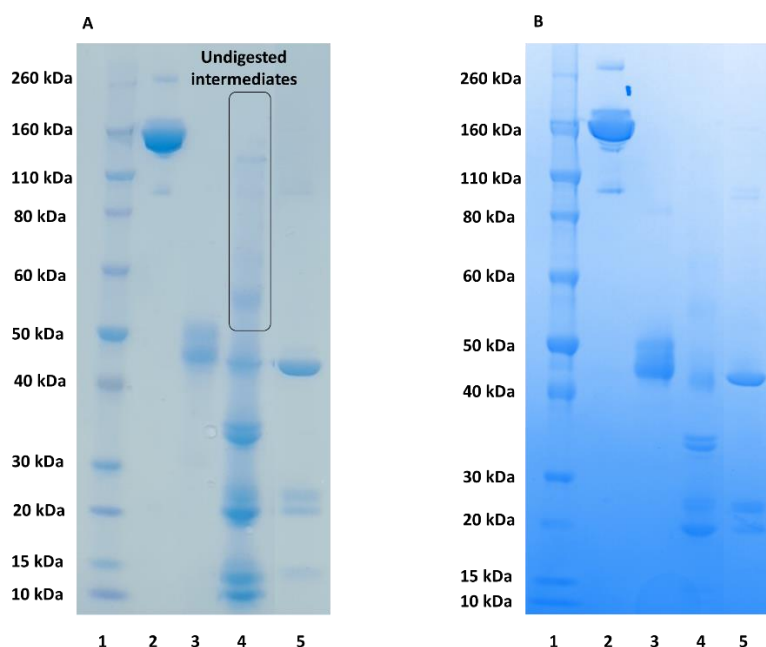
Figure 32: SDS PAGE gels showing digestions and purifications of 10 mg infliximab digested with soluble papain for 25 and 35min. **(A – 25 min digestion time) Lane 1:** Protein marker, **2:** parent infliximab, **3:** protein L flow through, **4:** protein L elution, **5:** final purified Fab. **(B – 35 min digestion time) Lane 1:** Protein marker, **2:** parent infliximab, **3:** protein L flow through, **4:** protein L elution, **5:** final purified Fab$_{inflixi}$.

In both Figure 32A and 32B, the digestion of infliximab using soluble papain is demonstrated. The flow through and elution fractions obtained from both digestions exhibited similarities to previous observations during the digestions of tocilizumab and bevacizumab in that clear flow-through and elution peaks were observed. The 35 minute digestion appeared to be more complete than the 25 minute digestion time. This was evident from presence of undigested intermediates in the elution fraction

82

from the 25 minute digestion (Figure 32A, Lane 4), while the 35- minute elution fraction showed no such intermediates. (Figure 32B, Lane 4).

After subjecting the digested samples to further purification using SEC, pure Fab$_{Inflixi}$ fractions (Figure 32A, Lane 5 and Figure 32B Lane 5) were isolated for both the 25 and 35 minute digestion. However, it is important to note that the yields obtained from both the 25 minute and 35 minute digestions of infliximab were considerably lower when compared to digestions of humanised IgGs. Specifically, the 25 and 35-minute digestions yielded 12.8% and 21.0% respectively.

A potential explanation for this discrepancy in yields could be attributed to the greater thermal stability [179] and physical stability [180] exhibited by humanised antibodies as compared to chimeric antibodies such as infliximab. These factors could potentially affect the efficiency of the digestion process and subsequent purification steps, resulting in lower yields.

Aflibercept, an Fc fusion protein, was also selected to evaluate if it can be digested using soluble papain. Figure 33 shows an SDS PAGE gel for the digestion and purification of 5 mg of aflibercept using soluble papain with 30 minutes of digestion time. For the purification, a combination of IEX and protein A was employed. Since aflibercept lacks kappa light chains and does not bind to protein L, IEX was first utilized to separate the digested aflibercept from papain. During the IEX process, papain does not bind to the column, while the digested aflibercept does, allowing for their separation.

Upon examining the IEX elution fractions (Figure 33, Lanes 3-10), it was evident that IEX alone was unable to completely purify the mixture, resulting in a combination of fragments. It is plausible that one of fragments corresponded to the Fc of aflibercept. To address this, protein A was chosen as a secondary purification step, as it binds to Fc regions, enabling further separation. Figure 33, Lane 11 depicts the final purified product obtained through this approach.

Based on its molecular weight, it appeared that this fragment may represent a single receptor binding region from the aflibercept molecule, lacking the necessary disulfide bonds. Consequently, this fragment does not hold any utility for site-specific conjugation or for my research purposes. To validate this hypothesis, conjugation of the fragment to a PEG *bis*-sulfone reagent **8** reagent could provide conformation.
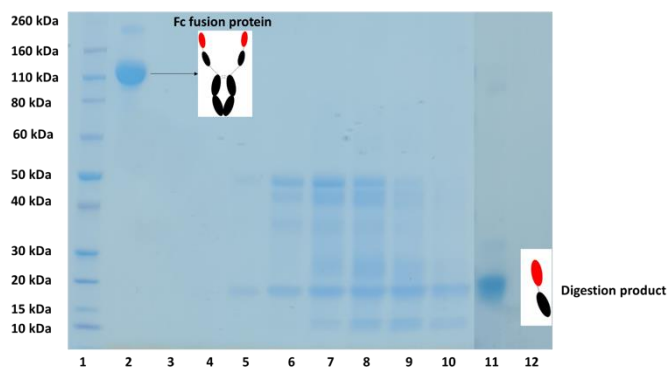
Figure 33: An SDS PAGE gel showing digestion of aflibercept (5 mg) using soluble papain (30 min), and purification fraction after IEX elution fractions were further purified using a protein A column. **Lane 1:** Protein marker, **2:** aflibercept, **3:** 40-41 mLs, **4:** 41-42 mLs, **5:** 42-43 mLs, **6:** 43-44 mLs, **7:** 44-45 mLs, **8:** 45-46 mLs, **9:** 46-47 mLs, **10:** 32.45-33.45 mLs, **11**: Protein A flow through, **12**: Protein A elution.

Conclusions

A digestion methodology utilising a soluble form of papain has been shown to be an effective way to obtain pure Fabs. Key to the success of the methodology was the correct choice of purification conditions. The use of protein L resin allowed fast effective separation of the soluble enzyme and Fc from the desired Fabs. A secondary purification using SEC allowed any higher molecular weight molecules containing kappa light chains to be separated from the Fabs. Key advantages of using soluble papain over immobilised papain were faster digestion speed, significantly reduced cost of enzyme and finally, and most critically, scalability with no loss in digested yield. Digestions using soluble papain have been performed using up to 100 mg of tocilizumab as starting material. Fabs obtained from the 100 mg digestion of tocilizumab have been shown to contain healthy disulfide bonds and are stable for up to 5 months. Bevacizumab was also digested using soluble papain up to a scale of 37.5 mg. Alongside the two humanised IgGs tocilizumab and bevacizumab, the chimeric IgG infliximab was also digested albeit with lower final isolated Fab yields of approximately 20%.

Fabs are required for the preparation of both monospecific and bispecific FpF molecules. The soluble papain digestion methodology allows for large quantities of Fabs to be obtained quickly and cheaply. This allows greater time to focus on FpF preparation and characterisation. Also, the scalability of the method means that if the preparation of the FpFs themselves was to ever be scaled up, the quantities of Fab required should not be a stumbling block. Fabs obtained from soluble papain digestions are used in the following chapter which focuses on conjugation activities.

Chapter 4 – Preparation of bispecific antibody mimetics

Conjugation experiments were first conducted with the PEG *bis*-sulfone reagent **8** [161,168] with Fabs that were obtained by the enzymatic digestion of full antibodies that had been obtained as leftovers from clinic (described in Chapter 3). Ranibizumab, which is a Fab (also termed Fab$_{rani}$), was used directly. It was difficult to obtain enough ranibizumab from clinical left-overs as each vial would contain less than *ca* 30 mL. It was necessary to evaluate the *mono*-functionalised *bis*-sulfone reagent **8** (Figure 34) to gain experience and to understand what was achievable with the associated conjugation and purification methodologies experiments.

8
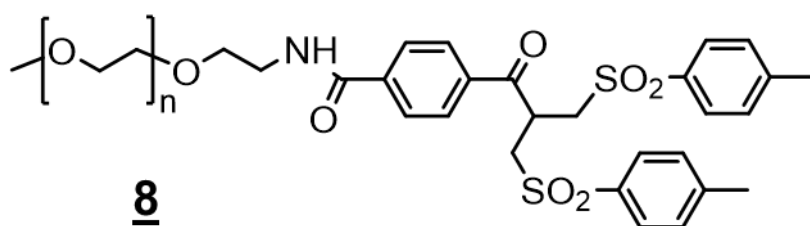
Figure 34: Chemical structure of the PEG *bis*-sulfone reagent **8**

Preparation of the PEG *bis*-sulfone reagent **8** was achieved by following published methods [181] that were modified by using a mixed anhydride coupling reagent **9**, 2-Isobutoxy-1-isobutoxycarbonyl-1,2-dihydroquinoline (IIDQ) (Scheme 6). Since the precursor PEG molecular weight can be varied, specific reagents will be denoted as follows: PEG$_{10}$-*bis* sulfone **8** is the *mono*-functionalised reagent derived from a 10 kDa PEG precursor (e.g. PEG amine **10** in Scheme 6 below). Synthesis of the carboxylic acid *bis*-sulfone precursor **11** was accomplished by published procedures [181] and was provided by colleagues in our research group.
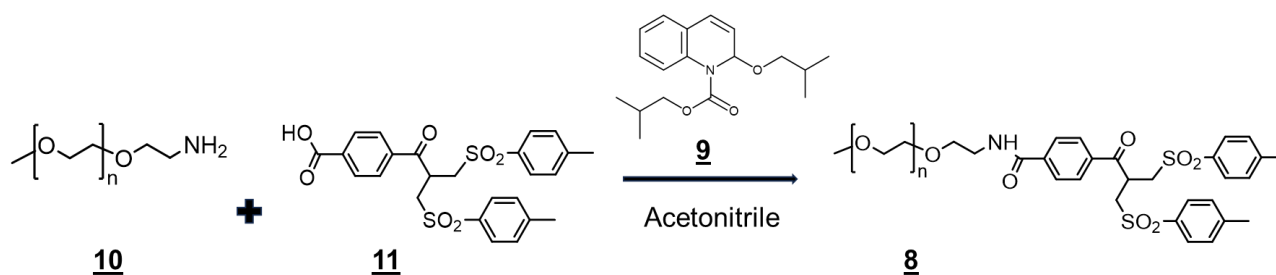
Scheme 6: Synthesis of mono functional PEG bis-sulfone reagents **8**.

Scouting conjugations with ranibizumab were conducted using PEG$_{10}$-*bis* sulfone **8** (Figure 35). The interchain disulfide in ranibizumab was first reduced with dithiothreitol (DTT) and carefully eluted over a PD10 column to remove excess DTT while minimising reoxidation of the interchain disulfide. The starting Fab with the intact

oxidised interchain disulfide appears as a band at approximately the 50 kDa marker. The reduced interchain disulfide Fab appears between the 20 and 30 kDa markers in the non-reducing SDS-PAGE gels shown in Figure 35. Once the Fab interchain disulfide is reduced and mixed with SDS (sodium dodecyl sulfate), which is an anionic surfactant that coats polypeptides, the tight, non-covalent interactions between the Fab light and heavy chains are disrupted and separated. Since each individual chain is about 25 kDa, the reduced Fab appears as a single band at approximately 25 kDa. When Fab is exposed to only DTT, there are no protein denaturing agents such as SDS in solution, so the light and heavy chains maintain their non-covalent interactions. This means the Fab remains intact as a 50 kDa protein in solution. However, it is imperative to remove excess DTT from solution as any thiol exchange reagent will undergo reaction with any thiol reactive conjugation reagent, including *bis*-sulfone reagents.

The SDS-PAGE gels conducted throughout this PhD were all non-reducing gels which allow monitoring of the extent and maintenance of the reduction of the Fab interchain disulfide. Reoxidation of the Fab interchain disulfide means conjugation with the *bis*-sulfone conjugation moiety is greatly inhibited. *Bis*-sulfone reagents **8** do not readily undergo reaction with polypeptide amines at pH values where free thiols undergo reaction, so knowledge about the presence of the reduced Fab is important to monitor the extent of conjugation. If the extent of conjugation is low (i.e low conjugation conversion) and there is knowledge about the reduced interchain Fab present, then it is not possible to know whether low conjugation conversion is due to a problem with the purity of the *bis*-sulfone reagent or the absence of cysteine free thiol from the Fab, which can occur by re-oxidation of the Fab interchain disulfide. Interchain disulfide reoxidation can occur when there is oxygen or metal contamination during DTT removal. Being able to monitor the disappearance of the reduced Fab and appearance of the expected conjugate product is important for optimising scouting experiments.
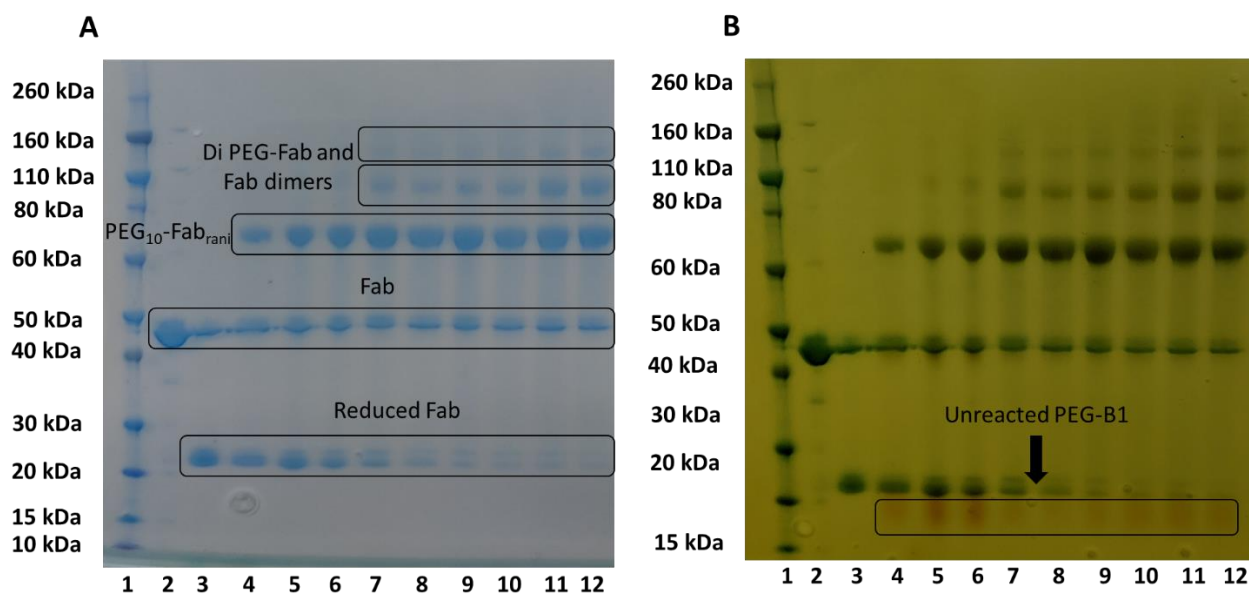
Figure 35: SDS PAGE gel showing the conjugation of 0.3 mg ranibizumab per conjugation (0.3 mg/mL ranibizumab concentration) with varying stoichiometries of PEG_{10}-*bis* sulfone **8** Ph 7.6 for 2-, 3- and 18-hour conjugation times. **(A)** Coomassie blue stain and **(B)** barium iodide stain; **Lane 1**: Protein marker, **2**: ranibizumab, **3**: reduced ranibizumab, **4**: 1.5 eq. reagent **8**, incubate 2 h, **5**: 1.5 eq. 3 h, **6**: 1.5 eq. 18 h, **7**: 2 eq. 2 h, **8**: 2 eq. 3 h, **9**: 2 eq. 18 h, **10**: 2.5 eq. 2 h, **11**: 2.5 eq. 3 h, **12**: 2.5 eq. 18 h.

As can be seen from Figure 35 the PEG_{10}-Fab conjugate appears as a band at approximately 70 kDa and is present in all the conjugation lanes (Lanes 4-12). The PEG has a more extended conformation in solution than that of a polypeptide with its repeating amide structure, so PEG migrates less than what is anticipated by the protein markers used in SDS-PAGE. Generally, PEG molecular weight in mono-PEG protein conjugates appears at about 2× in SDS-PAGE than the actual PEG molecular weight [150]. In the current example for PEG_{10}-Fab_{rani} conjugate, the Fab contributes ~50 kDa and the PEG_{10} which is 10 kDa, appears to contribute 20 kDa ((50+20) kDa=70 kDa) to the SDS-PAGE band that is observed for the conjugate.

As the stoichiometry of the PEG_{10} *bis*-sulfone reagent **8** was increased there was a decrease in the presence of the reduced Fab, indicating an increase conversion to the PEG_{10}-Fab conjugate. There was also the formation of two higher molecular weight bands, the first at approximately 100-110 kDa is thought to be PEG_{10} dimer of the Fab which is formed by the reaction of a second molecule of the PEG_{10} *bis*-sulfone **8** with the Fab. Since conjugation occurs by a series of addition and elimination steps (Scheme 1, Chapter 1), after addition of the first PEG_{10} *bis*-sulfone **8** to one of the interchain cysteine thiols, elimination of the second sulfone must occur followed by addition of second cysteine thiol to give the desired bridged conjugate. It is possible that a second PEG_{10} *bis*-sulfone **8** adds to the second cysteine thiol before re-bridging

of the first molecule of the reagent has occurred. This competitive reaction would give a Fab conjugated to two PEG molecules. Rates of sulfone elimination from the PEG reagent and rates of conjugation are dependent on temperature, incubation times, and concentrations of protein and reagent [150]. The need to optimize protein conjugation conditions is necessary for all types of conjugation reagents and tends to be protein dependent.

The faint band (Figure 35) that can be observed at higher molecular weights (~130 kDa) for the experiments conducted with the higher PEG$_{10}$ *bis*-sulfone **8** equivalence and conjugation incubation times is thought to be non-specific conjugation of at least another molecule of the PEG$_{10}$ *bis*-sulfone **8** probably to the unbridged PEG dimer conjugate of Fab$_{rani}$. As reagent stoichiometry and conjugation incubation time increases, the amount of free Fab$_{rani}$ decreases resulting in the formation of undesired conjugates. Prior work on the PEGylation of Fabs with the PEG *bis*-sulfone reagent **8** shows that optimal conditions result in high conversion (> 80%) to the PEG-Fab conjugate which can be easily purified to good yields by ion exchange chromatography [150,161,182]

Additional scouting reactions with ranibizumab were conducted with PEG *bis*-sulfone reagent **8** (Figure 36). Three different pH values and conjugation reagent derived from two different molecular weight PEG precursor amines were used: PEG$_{10}$ and PEG$_{20}$ *bis*-sulfone **8**. Figure 36A (2 h incubation time) shows that conjugation proceeds more quickly at higher pH for both PEGylation reagents (Figure 36A Lanes 4-6 and 7-9). The same conjugations were allowed to undergo incubation for 18 hours (Figure 36B Lanes 2-4 and 5-7). The greatest quantity of conjugate has formed at pH 8 (Figure 36B, Lane 6). This is indicated by the densest PEG$_{20}$-Fab$_{rani}$ band and by the fact that the pH 8 lanes contain the smallest quantity of remaining reduced Fab with little evidence of the presence of reoxidised Fab$_{rani}$. Conjugations proceed faster and to greater completion at pH 8 for both the 10 and 20 kDa reagents in these scouting experiments.
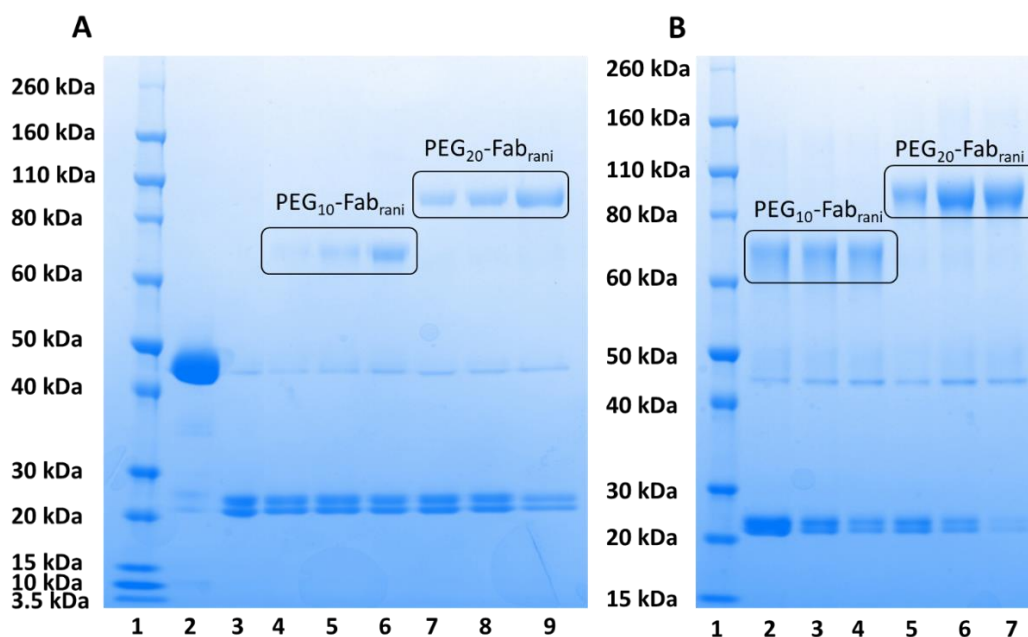
Figure 36: (A) SDS PAGE gel showing the conjugation of 0.3 mg ranibizumab per conjugation (0.3 mg/mL) to 1.5 eq. PEG_{10} and PEG_{20} *bis*-sulfone **8** at pH 6, 7 and 8 after **(A)** 2 hours conjugation time and **(B)** 18 hours conjugation time. **(A) Lane 1**: Protein marker, **2**: ranibizumab, **3**: reduced ranibizumab, **4**: pH 6 PEG_{10}, **5**: pH 7 PEG_{10}, **6**: pH 8 PEG_{10}, **7**: pH 6 PEG_{20}, **8**: pH 7 PEG_{20}, **9**: pH 8 PEG_{20}. **(B) Lane 1**: Protein marker, **2**: pH 6 PEG_{10}-, **3**: pH 7 PEG_{10}-, **4**: pH 8 PEG_{10}, **5**: pH 6 PEG_{20}, **6**: pH 7 PEG_{20}, **7**: pH 8 PEG_{20}.

There is a limit to how high a pH value should be used to conduct conjugations with thiol specific reagents such as the *bis*-sulfone reagents. Increasing the pH in excess of 8.0 can result in the deprotonation of lysine ammonium ions resulting in non-specific conjugation. While use of pH 8 and above can certainly result in the formation of di or multi-PEG conjugation, it is also possible that the mono-PEG Fab_{rani} conjugates will comprise a mixture of the desired re-bridged thiol conjugate along with non-specific mono-PEG Fab_{rani} conjugates. Increased hydroxide concentration may also cause hydrolysis of the bis-sulfone reagent which essentially kills the reagent to further re-bridging conjugation to the protein. One encouraging observation of the scouting reaction shown in Figure 36 is there appears to be a relatively wide process window for conjugation. Figure 36B (Lanes 2-7) show that conjugation does occur between pH 6-8 for both *bis*-sulfone reagents and that no higher molecular weight conjugates appear to have formed.

Ranibizumab was used as the Fab for these scouting reactions because it could be obtained in small quantities and no digestion was needed. Digestion often results in Fabs with different heavy chain structures due to proteolytic cleavage variation. Ranibizumab is homogeneous and does not contain "digestion tails", so it was thought

that it would be easier, when possible, to correlate and optimise conditions more accurately. It was necessary after the scouting conjugation to perform conjugations with a Fab obtained by the proteolytic digestion (Figure 37), which in this case was Fab$_{inflixi}$ that was obtained by the proteolytic digestion of infliximab. Using PEG$_{20}$ bis-sulfone **8**, the conjugation with Fab$_{inflixi}$ was conducted n=4 times.
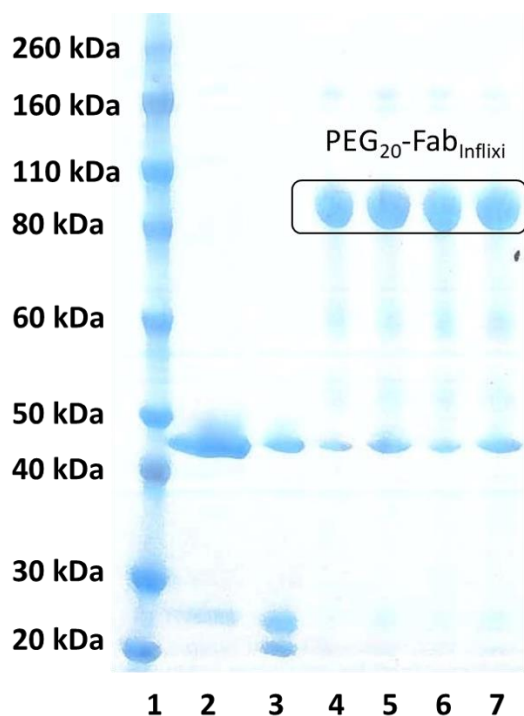
Figure 37: SDS PAGE gel showing the conjugation of 0.5 mg Fab$_{inflixi}$ per conjugation (0.60 mg/mL) to 1.5 eq of PEG$_{20}$ *bis*-sulfone **8**, pH 7.6, 4 replicates, 18 hour conjugation time. **Lane 1**: Protein marker, **2**: Fab$_{infilxi}$, **3**: reduced Fab$_{infilxi}$, **4**: conjugation 1, 18 h, **5**: conjugation 2, 18 h, **6**: conjugation 3, 18 h, **7**: conjugation 4, 18 h.

Formation of the desired conjugate, PEG$_{20}$-Fab$_{inflx}$ occurred in each reaction (Figure 37) with what appear to be quite high [150,168] and equal conversion, indicating the conjugation methodology that was followed is reproducible and robust.

There was some concern about the hydrophobicity of the toluene sulfinic acid leaving groups in the *bis*-sulfone reagents. For the di *bis*-sulfone reagent **5** that was going to be used to try to make bispecific FpFs, there was concern that end-group hydrophobicity might cause polymer conformations, where an end-group could become less solvent accessible, by a process not dissimilar to unimolecular polymer micellation. Although PEG mono-terminal functionalised *bis*-sulfone reagents are effective for protein conjugation it was not clear how effective conjugation would be with the di *bis*-sulfone reagent **5** on either the first or second protein conjugation.

It is possible to use *bis*-sulfone conjugation reagents with different leaving groups which can be important for different applications. For example, the reagents were utilised to conjugate selectively by bis-alkylation histidine tags, where leaving group variation was important for slowing the elimination reaction, to allow conjugation

to occur. Another example are *bis*-sulfone reagents that have been used to make antibody drug conjugates. The leaving groups in these reagents are based on a few repeat units of ethylene glycol to reduce potential hydrophobic effects. Scouting experiments were conducted with the PEG$_{10}$ *bis*-sulfone glycol reagent **12** (Figure 38).

Figure 38: Chemical structure of the PEG *bis*-sulfone glycol reagent **12**

Scouting conjugations were performed at pHs ranging from 5-8 and the conjugations were left to undergo reaction for up to 21 hours (Figure 39). The results from the SDS PAGE analysis indicates the PEG$_{10}$ *bis*-sulfone glycol reagent **12** performs best at pH 8.0. Very little reduced Fab could be observed at the 6-hour timepoint (Lane 20). Even after 21 hours with 1.5 equivalents of the PEG$_{10}$ *bis*-sulfone glycol reagent **12** there were no higher molecular weight conjugation impurities that appeared to have been formed. Both PEG$_{10}$ *bis*-sulfone **8** and PEG$_{10}$ *bis*-sulfone glycol **12** visually displayed similar conjugation performance with Fab$_{rani}$ (Figure 40). While the same conjugation media was used, there was more reoxidised Fab$_{rani}$ in the conjugations that were conducted with PEG$_{10}$ *bis*-sulfone glycol **12** than the corresponding conjugation with PEG$_{10}$ *bis*-sulfone **8** (Figure 40). Since the synthesis of the PEG$_{10}$ *bis*-sulfone **8** is well established it was decided to continue with the toluene sulfinic acid leaving groups.

Figure 39: SDS PAGE gel showing the conjugation of 0.3 mg ranibizumab per conjugation (0.3 mg/mL) to 1.5 eq of PEG_{10} *bis*-sulfone glycol **12** at pHs 5-8. **Lane 1.** Protein marker, **2**: ranibizumab, **3**: reduced ranibizumab pH 5, **4**: reduced ranibizumab pH 6, **5**: reduced ranibizumab pH 7, **6**: reduced ranibizumab pH 8, **7**: pH 5 conjugation 2 h , **8**: pH 6 2 h, **9**: pH 7 2 h, **10**: pH 8 2 h, **11**: Protein marker, **12**: pH 5 4 h, **13**: pH 6 4 h, **14**: pH 7 4 h, **15**: pH 8 4 h, **16**: Protein marker, **17**: pH 5 6 h, **18**: pH 6 6 h, **19**: pH 7 6 h, **20**: pH 8 6 h, **21**: Protein marker, **22**: pH 5 21 h, **23**: pH 6 21 h, **24**: pH 7 21 h, **25**: pH 8 21 h.
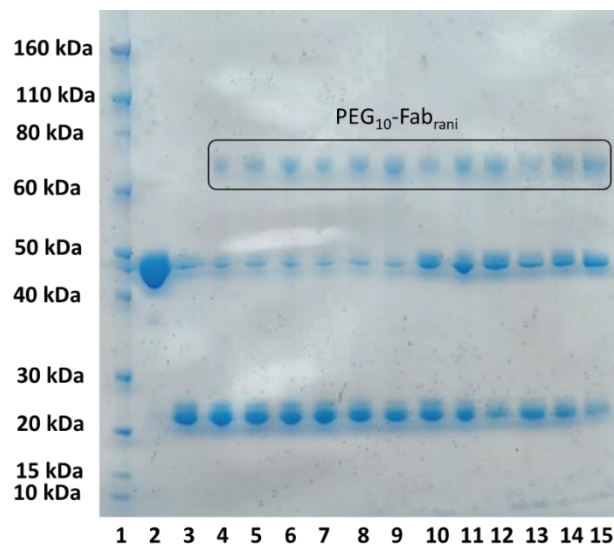
Figure 40: SDS PAGE gel showing results from conjugations of 0.3 mg ranibizumab per conjugation (0.30 mg/mL) with varying stoichiometries of PEG_{10} *bis*-sulfone **8** (lanes 4-9) and PEG_{10} *bis*-sulfone glycol **12** (lanes 10-15) pH 8.0 for 2 and 4-hour conjugation times. **Lane 1**: Protein marker, **2**: ranibizumab, **3**: reduced ranibizumab, **4**: PEG_{10} *bis*-sulfone **8** 1 eq 2 h, **5**: 1.5 eq 2 h, **6**: 2 eq 2 h, **7**: 1 eq 4 h, **8**: 1.5 eq 4 h, **9**: 2 eq 4 h, **10**: PEG_{10} *bis*-sulfone glycol **12** 1 eq 2 h, **11**: 1.5 eq 2 h, **12**: 2 eq 2 h, **13**: 1 eq 4 h, **14**: 1.5 eq 4 h, **15**: 2 eq 4 h.

93

Scouting reactions to prepare a mono-specific, bivalent FpF **13** (Scheme 7) derived from Fab_rani were then conducted with the known [159,161,183] PEG_6 di *bis*-sulfone reagent **5**.
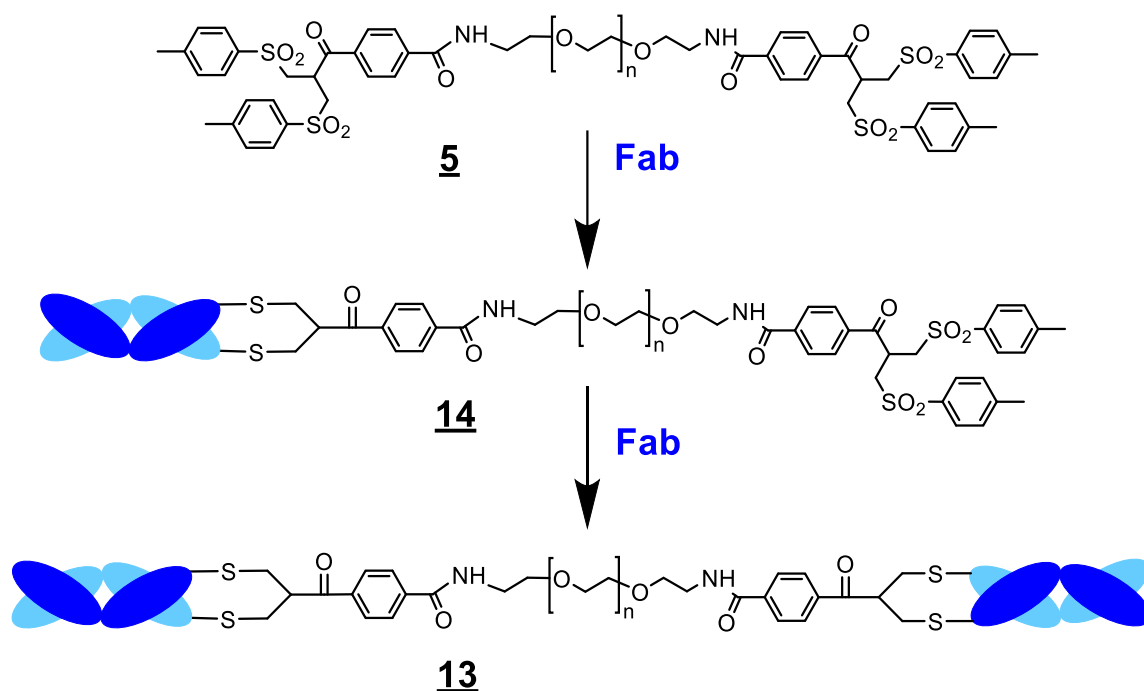
Scheme 7 Preparation of a monospecific FpF **13** via the conjugation of Fabs to both ends of PEG di *bis*-sulfone **5**. The mono-conjugate **14** is an intermediate molecule.
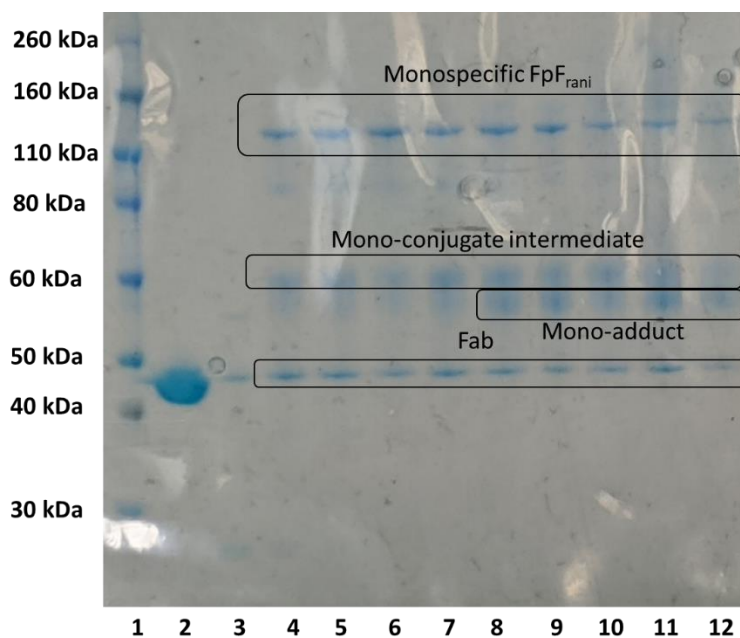
Figure 41: SDS PAGE gel showing the conjugation of 0.3 mg ranibizumab per conjugation (0.30 mg/mL) with varying stoichiometries to PEG_6 di *bis*-sulfone **5** pH 7.6 for 3,6- and 18-hours conjugation times. **Lane 1**: Protein marker, **2**: ranibizumab, **3**: reduced ranibizumab, **4**: 0.5 eq 3 h, **5**: 0.5 eq 6 h, **6**: 0.5 eq 18 h, **7**: 1 eq 3 h, **8**: 1 eq 6 h, **9**: 1 eq 18 h, **10**: 1.5 eq 3 h, **11**: 1.5 eq 6 h, **12**: 1.5 eq 18 h.

Reagent stoichiometry ranged from 0.5 to 1.5 equivalents of di *bis*-sulfone **5** to Fab$_{rani}$. All the reduced Fab was consumed and higher conversion to the desired FpF occurred when using 0.5 equivalent of reagent **5**. Higher conversion to the desired FpF was expected when using 0.5 eq of reagent **5**. A reagent stoichiometry of 0.5 equivalents means that for every molecule of reagent 2 Fabs are available for conjugation favoring formation of the desired FpF. Interestingly there was considerable conversion to the desired FpF with 1.0 equivalent of the PEG$_6$ di *bis*-sulfone reagent **5**. However, the mono-conjugate intermediate **14** also appeared to be formed in higher conversion, which was expected. But with longer incubation times at higher stoichiometry, another, slightly lower molecular weight band for a mono-conjugate appeared. It was thought this band was a cyclic, unbridged mono-adduct.

The PEG di *bis*-sulfone reagent **5** was then used to prepare a BsFpF (Scheme 8).
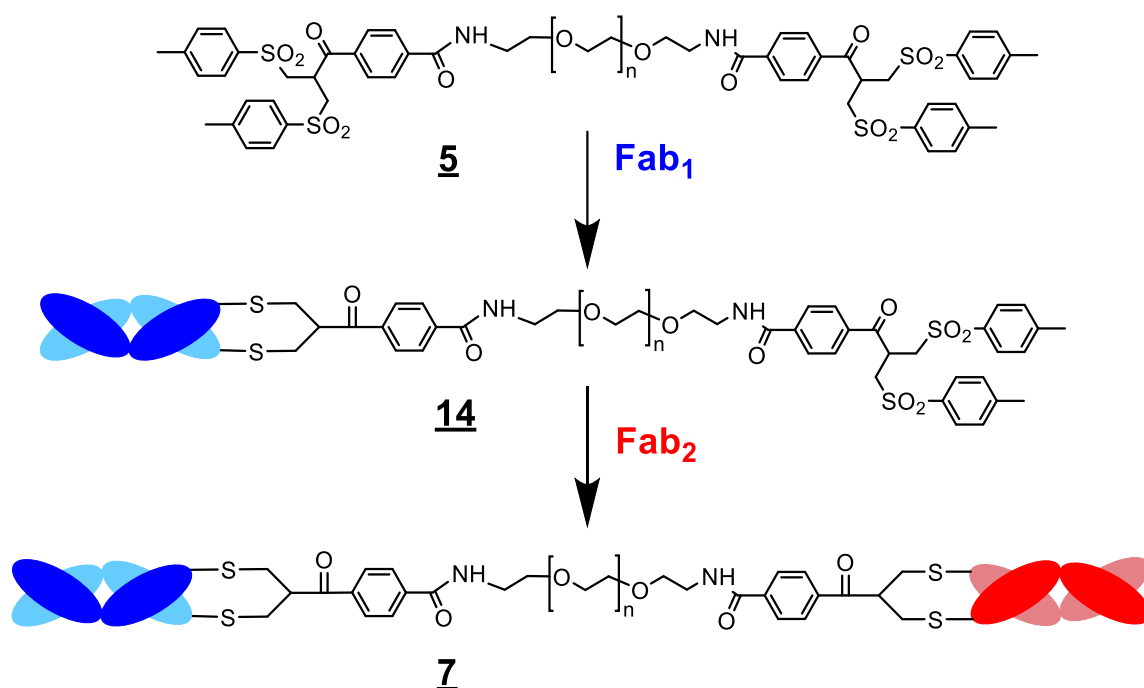
Scheme 8: Preparation of a BsFpF **7** via the conjugation of Fab$_1$ and Fab$_2$ to PEG di *bis*-sulfone **5**. The BsFpF **7** forms after the conjugation of Fab$_2$ to the *bis*-sulfone PEG-Fab$_1$ intermediate **14**.

A first Fab is allowed to react with an excess of the di *bis*-sulfone reagent **5**, followed by eluting the conjugating mixture over an IEX column to give an enriched solution of the *bis*-sulfone PEG-Fab$_1$ intermediate **14** by removing excess reagent, Fab and any FpF that forms. Fab$_2$ is then added to undergo reaction with the *bis*-sulfone PEG-Fab$_1$ intermediate **14** to give the desired BsFpF **7**.

Using Fab$_{rani}$ and 1 equivalent of PEG$_{20}$ di *bis*-sulfone reagent **5** both the desired *bis*-sulfone PEG-Fab$_{rani}$ intermediate **14** and undesired Fab$_{rani}$ derived FpF can be seen in lane 3 (Figure 42). It may be possible to prepare greater quantities of the desired *bis*-sulfone PEG-Fab$_{rani}$ intermediate **14** with higher stoichiometries of the starting di *bis*-sulfone reagent **5**. The PEG-Fab$_{rani}$ intermediate **6** was purified by IEX and the fraction collected (Lane 5) still contained a small quantity of FpF. Lane 6 shows the fraction containing most of the FpF. The fraction containing PEG-Fab$_{rani}$ intermediate **14** was combined with reduced Fab$_{inflixi}$ and incubated for 18 hours at pH 8.0. The pH for the second conjugation was increased to increase the reactivity of the remaining free conjugation moiety, although the risk was that competitive hydrolysis would occur leading to a non-reactive chain end in the PEG-Fab$_{rani}$ intermediate **14**.
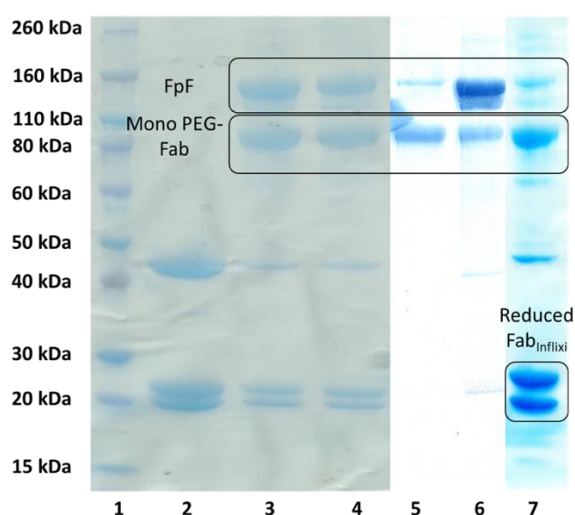
Figure 42: SDS PAGE gel showing an attempt to prepare an anti-VEGF/TNF BsFpF derived from Fab$_{rani}$ and Fab$_{inflixi}$ using a PEG$_{20}$ di bis-sulfone reagent **5**. **Lane 1**: Protein marker, **2**: reduced ranibizumab, **3**: conjugation of 1 mg (1 mg/mL) Fab$_{rani}$ to reagent **5** (1 eq, pH 7.6, 18 h), **4**: conjugation of 1 mg (1 mg/mL) Fab$_{rani}$ to reagent **5** (1 eq, pH 7.6, 18 h) n=2, **5**: IEX purified PEG$_{20}$-Fab$_{rani}$ intermediate **14**, **6**: IEX fraction containing monospecific FpF$_{rani}$, **7**: conjugation of Fab$_{inflixi}$ to PEG$_{20}$-Fab$_{rani}$ intermediate **14**

Fab$_{inflixi}$ was added in excess at a molar ratio of approximately 1.5:1 (Fab$_{inflixi}$ to intermediate **14**). Unfortunately, while there was a large amount of reactive, reduced Fab$_{inflixi}$ present, there was no evidence that significant amounts of the desired BsFpF had formed (lane 7).

To try to suppress the formation of unwanted FpF during addition of the first Fab and the possible dead chain ends that could form due to hydrolysis during the first IEX purification to isolate the intermediate **9**, the di functional reagent **15** was considered (Scheme 9).
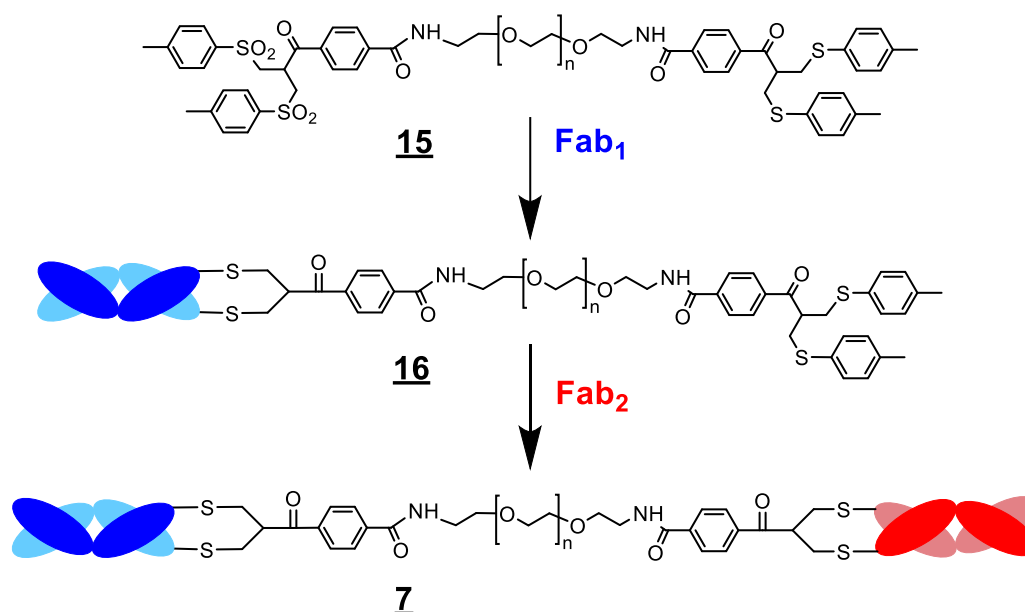
Scheme 9 Preparation of a BsFpF **7** via the conjugation of Fab$_1$ and Fab$_2$ to a di functional reagent **15**. Fab$_1$ conjugates to the *bis*-sulfone moiety to form intermediate **16**. pH could then be increased to allow conjugation of Fab$_2$ to the *bis*-sulfide moiety giving a BsFpF **7**

Conjugation of Fab$_1$ would be favoured on the *bis*-sulfone terminus as the toluene sulfinic acid groups were expected to be better leaving groups than the toluene thiols on the other terminus of the reagent. So physiological pH values could be used to first conjugate Fab$_1$. Then the pH could be increased and Fab$_2$ would then be conjugated to the *bis*-sulfide terminus (e.g. intermediate **16**). The PEG$_{10}$ *bis*-sulfide reagent **17** was evaluated using Fab$_{rani}$ for re-bridging conjugation (Figure 43).
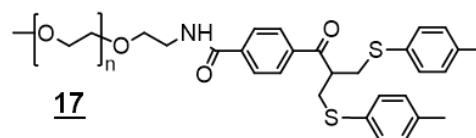
Chemical structure of the PEG *bis*-sulfide reagent **17**
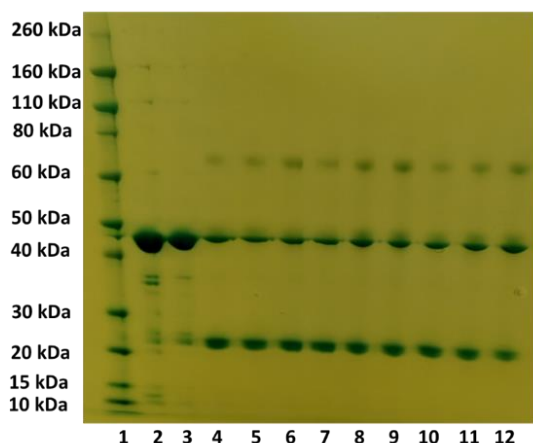
Figure 43: SDS PAGE gel showing the conjugation of 0.3 mg ranibizumab per conjugation (0.30 mg/mL) with varying stoichiometries to PEG$_{10}$ *bis*-sulfide **18** pH 8.2 for 2, 3 and 18 hours conjugation times – Coomassie blue, then barium iodide stain **Lane 1:** Protein marker, **2**: ranibizumab, **3**: reduced ranibizumab, **4**: 1.5 eq 2 h, **5**: 1.5 eq 3 h, **6**: 1.5 eq 18 h, **7**: 2 eq 2 h, **8**: 2 eq 3 h, **9**: 2 eq 18 h, **10**: 2.5 eq 2 h, **11**: 2.5 eq 3 h, **12**: 2.5 eq 18 h.

Scouting reactions with PEG$_{10}$ *bis*-sulfide **17** were conducted with variation in reagent stoichiometry and conjugation incubation at a pH of 8.2 (Figure 43), which was considered quite high [184] as most conjugations with Fabs have been conducted at pH 7.4 or less [168]. Little conjugation occurred (lanes 4-12) even at the higher stoichiometries of PEG$_{10}$ *bis*-sulfide **17** that were examined (i.e. 2.5 equivalents reagent to Fab). Interestingly, there was no evidence of higher molecular weight conjugates formed. The results of Fab conjugation to PEG$_{10}$ *bis*-sulfide **17** suggests the thiol toluene moieties are not a suitable leaving group for use in re-bridging conjugation.

Conjugation-ligation

The utilisation of a single difunctional reagent such as PEG di *bis*-sulfone **5** to prepare BsFpF appeared to be limited, so another approach was examined (Scheme 10). Di-functional reagents capable of a 2-step process to give the desired BsFpFs was envisaged. Di-functional reagents would have the *bis*-sulfone moiety on one terminus for re-bridging conjugation to the Fab interchain disulfide. The other terminus would have orthogonal reactive moieties which would subsequently undergo reaction (i.e. ligation) to form the BsFpF. The ligation reactive moieties would not undergo reaction with the Fab, only with a paired reactive moiety as shown in Scheme 10.
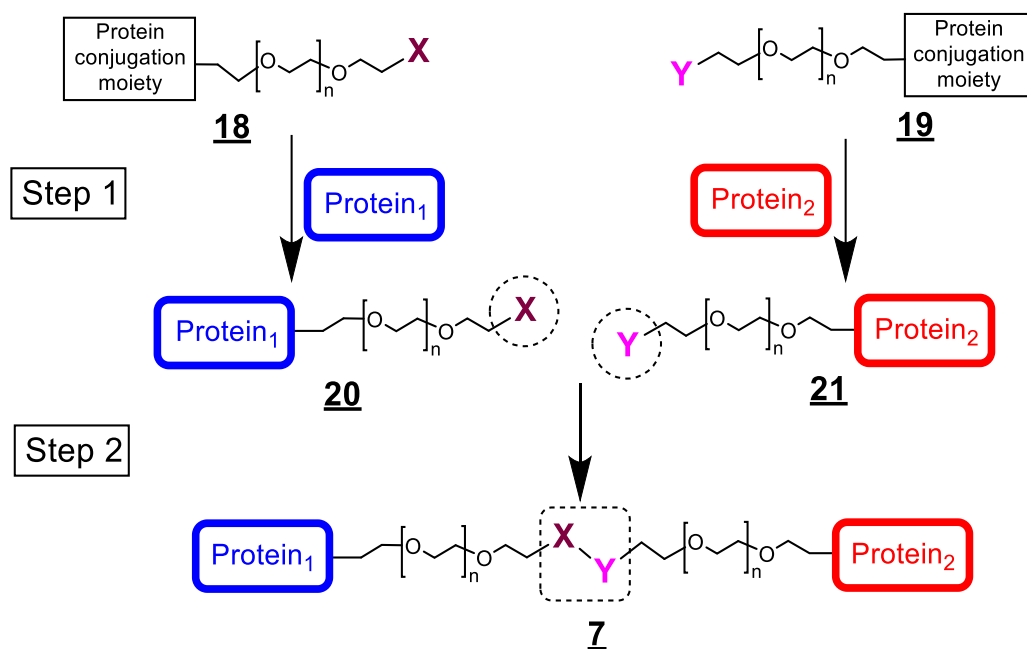
Scheme 10: Formation of a BsFpF **7** via conjugation-ligation. Protein$_1$ and Protein$_2$ are first conjugated to di-functional reagents **18** and **19**. The two functionalised protein conjugate intermediates **20** and **21** are combined and the orthogonal reactive moieties (X and Y) ligate to from a single molecule, a BsFpF **7**.

Another student in our group had examined ways to conjugate two different proteins together by the general strategy shown in Scheme 10 (e.g. interferon-Fab$_{rani}$ or amylase-lipase) [182] Orthogonal reactions studied were hydrazone ligation and copper catalysed azide-alkyne cycloaddition (CuAAC), often called a click reaction. CuAAC reactions are selective and occur in mild conditions. An issue is the presence of the copper catalyst which can lead to metal mediated fragmentation of IgGs [185]. The key finding was it was not possible to ligate two proteins with these types of reagents. It was found that copper complexed to the PEG element in the bi-functional reagents and to protein, so it was thought the cycloaddition was inhibited by competitive copper complexation.

Strain-promoted azide-alkyne cycloaddition (SPAAC) does not require the presence of copper. It was found that if the reactivity of alkynes was increased by using ring strain, then it could be possible to enable an azide-alkyne cyclo reaction without the need for a copper catalyst [186]. Dibenzo cyclooctyne (DBCO) and azide (N$_3$) are moieties that have been described for SPAAC and these moieties were used with two difunctional reagents **22** and **23** prepared by colleagues in our research group (Scheme 11). Two separate conjugation reactions are first conducted and then intermediates **24** and **25** are allowed to undergo cycloaddition to ligate the two Fabs giving the BsFpF **7**.
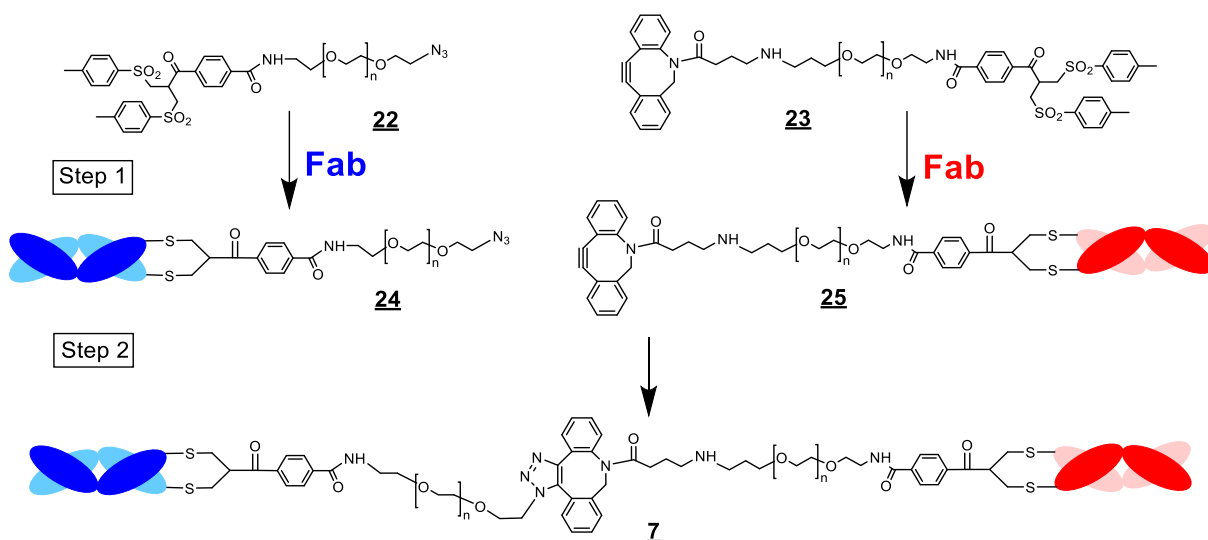
Scheme 11: Preparation of a BsFpF using PEG *bis*-sulfone azide **22** and PEG *bis*-sulfone DBCO **23**. Two different Fabs are conjugated to reagents **22** and **23** to form azide **24** and DBCO **25** functionalised Fab conjugates. Intermediates **24** and **25** are combined to allow the azide and DBCO moieties to ligate and form a BsFpF **7**.

Prior to moving onto to further discussion of conjugation-ligation strategies a distinction needs to be made. In theory, conjugation of a Fab fragment to either PEG *bis*-sulfone azide **22** or PEG *bis*-sulfone DBCO **23** would form a conjugated Fab with similarities to a PEGylated Fab (PEG-Fab) prepared via Fab conjugation to PEG *bis*-sulfone **8** as demonstrated earlier in this chapter. A PEG-Fab in which the molecular weight and hydrodynamic radius of the Fab is increased, can lead to increased ocular residence times and systemic half-live, alongside other benefits such as improved chemical and thermal stability [187]. The purpose of the intermediate molecules termed as azide **24** and DBCO **25** functionalised Fab conjugates is very different in that they are being prepared as intermediate molecules which can then ligate to form a BsFpF possibly overcoming the limitations experienced when attempting to prepare a BsFpF using PEG di *bis*-sulfone **5** dimerization reagents. It should also be noted that none of the di-functional reagents have molecular weights in excess of 10 kDa, PEGylation reagents would typically have higher molecular weights, for example a reagent with a molecular weight of 20 kDa was used earlier in this chapter.

An alternative to the azide and DBCO moieties (Scheme 11) that react via SPACC, are moieties that ligate via inverse-electron-demand Diels-Alder (iEDDA) reactions [186], which also do not require the presence of a copper catalyst. Ligation via iEDDA is known to proceed at a faster rate than ligation via SPACC [188], this faster rate may lead to faster BsFpF preparation methods. Trans-cyclooctene (TCO) and tetrazine (Tz) are two moieties that are known to react with each other via iEDDA.

Two difunctional reagents containing TCO **26** and Tz **27** were kindly prepared by colleagues in our research group. Similarly to difunctional reagents **22** and **23**, two separate conjugation reactions are carried out (Scheme 12) and intermediates **28** and **29** are combined and allowed to ligate to form a BsFpF **7**.
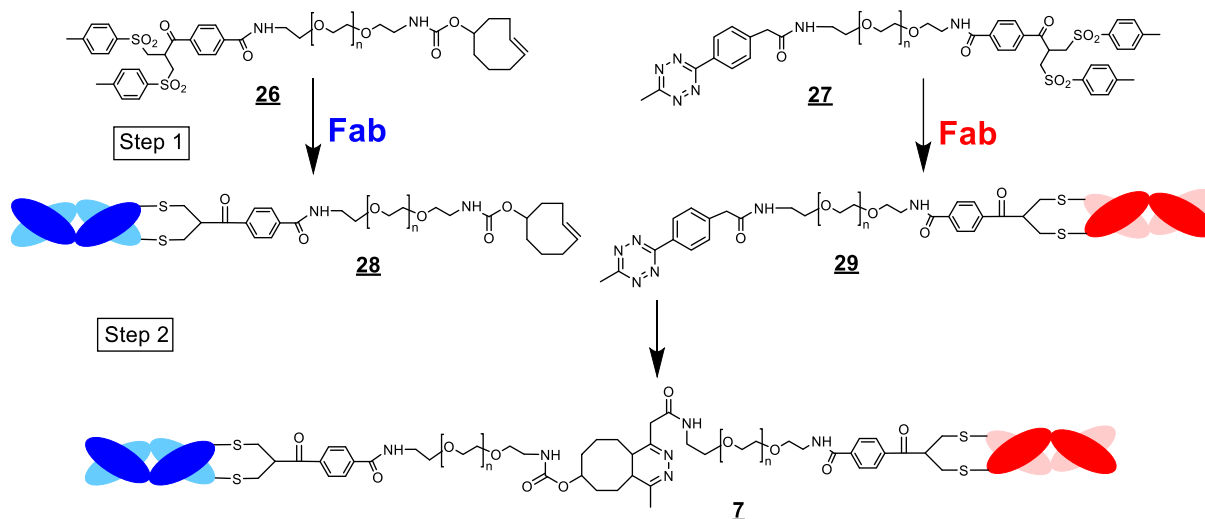
Scheme 12: Preparation of a BsFpF using PEG *bis*-sulfone TCO **26** and PEG *bis*-sulfone Tz **27**. Two different Fabs are conjugated to reagents **26** and **27** to form TCO **28** and Tz **29** functionalised Fab conjugates. Intermediates **28** and **29** are combined to allow the TCO and Tz moieties to ligate and form a BsFpF **7**.

The first set of experiments carried out with the difunctional reagents were focused on whether the ligation reaction between the DBCO and azide orthogonal moieties did in fact proceed. To understand this a methoxy (MeO) PEG$_{10}$ DBCO reagent **30** (Figure 44A) was combined with a PEG$_3$ *bis*-sulfone azide reagent **22** in solution at pH 7.6 (Figure 44B).
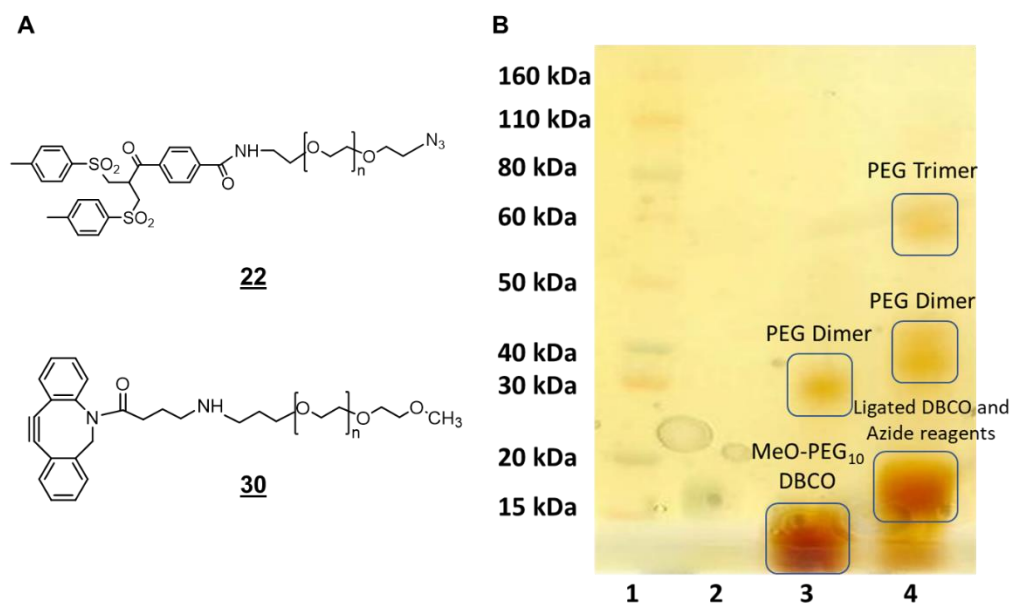
Figure 44: (A) Chemical structure of PEG *bis*-sulfone azide **22** and MeO PEG DBCO **30** **(B)** SDS PAGE gel showing ligation of MeO PEG$_{10}$ DBCO **30** and PEG$_3$ *bis*-sulfone azide **22** at a 1:1 molar ratio stained with barium iodide. **Lane 1**: Protein marker, **2**: PEG$_3$ *bis*-sulfone azide **22**, **3**: MeO PEG$_{10}$ DBCO **30**, **4**: Ligation reaction between PEG$_3$ *bis*-sulfone azide **22** and MeO PEG$_{10}$ DBCO **30**.

It is evident that ligation reaction between MeO PEG$_{10}$ DBCO **30** and PEG$_3$ *bis*-sulfone azide **22** proceeded successfully. This is indicated by the appearance of a band (Figure 44B, Lane 4) at a molecular weight between 15-20 kDa. This band is a at a higher molecular weight than what was observed in lane 3 (Figure 44B) containing solely MeO PEG$_{10}$ DBCO **30**, a band no more than 15 kDa molecular weight was observed for this reagent. No band was observed in the lane containing solely PEG$_3$ *bis*-sulfone azide **22** (Figure 44B, Lane 2) this is due to the di-functional reagent **22** containing a PEG backbone with a molecular weight of 3 kDa, which is too small to visualise using this type of SDS PAGE gel. Bands at molecular weights of approximately 30 kDa (Figure 44B, Lane 3) and at approximately 40 and 60 kDa (Figure 44B, Lane 4) can also be observed. These are likely to be as the result of higher molecular weight impurities contained within the PEG$_3$ *bis*-sulfone azide **22** and MeO PEG$_{10}$ DBCO **30** namely PEG dimers and trimers.

Next, reagent only ligation reactions were performed using PEG$_5$ *bis*-sulfone TCO **26** and PEG$_5$ *bis*-sulfone Tz **27** reagents (Figure 45). This experiment was carried out to answer 2 questions. Firstly, whether the TCO and Tz moieties present on reagents **26** and **27** were able to ligate and secondly to ascertain whether the ligation would proceed at a range of different pHs.
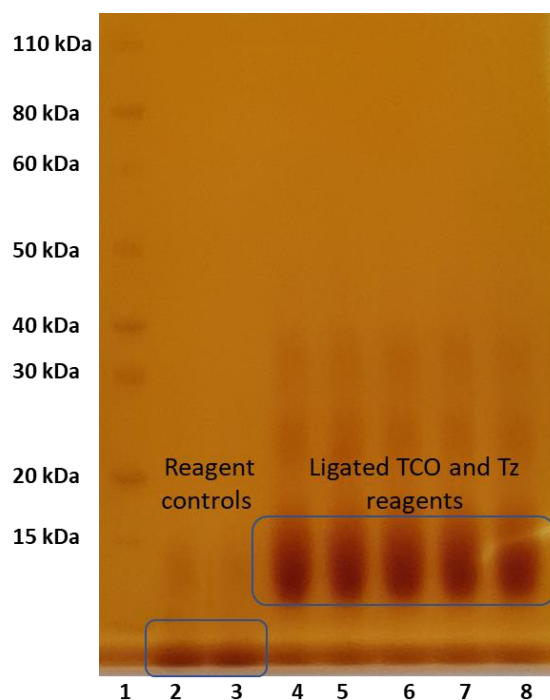
Figure 45: SDS PAGE gel showing ligation of PEG$_5$ *bis*-sulfone TCO **26** and PEG$_5$ *bis*-sulfone Tz **27** ,1:1 molar ratio stained with barium iodide at a range of different pHs, 2 hour reaction time. **Lane 1**: Protein marker, **2**: PEG$_5$ *bis*-sulfone TCO **26**, **3**: PEG$_5$ *bis*-sulfone Tz **27**, **4**: pH 5, **5**: pH 6, **6**: pH 7, **7**: pH 8, **8**: pH 9.

The cycloaddition reaction between using PEG$_5$ *bis*-sulfone TCO **26** and PEG$_5$ *bis*-sulfone Tz **27** proceed well (Figure 45, Lanes 4-8) at the range of pHs (5-9) tested in this experiment. Similar to observations made previously for ligation between reagents **22** and **30** a band has appeared at a molecular weight of approximately 15 kDa, this band is not present in the reagent control lanes (Figure 45, Lanes 2 and 3). The fact that the cycloaddition between the TCO and Tz moieties proceeds comparably at a range of different pHs is quite advantageous in terms of purification. A common way to purify a protein conjugated to PEG is IEX [189,190] which requires pHs as low as 5 and as high as 9 to function properly as the methodology requires the protein to be in an ionised state. As the ligation reaction between PEG$_5$ *bis*-sulfone TCO **26** and PEG$_5$ *bis*-sulfone Tz **27** reaction proceeds well at pHs 5 and 9, it gives some confidence that if IEX was used to purify TCO and Tz containing molecules the ability of the functional groups to ligate would not be diminished. The faint bands present in Figure 45 Lanes 4-8 at molecular weights between 20-40 kDa are likely due to impurities within the reagents.

Having determined that ligation reactions between reagents **21** and **30** and reagents **26** and **27** proceeded successfully in the absence of protein, Fab$_{rani}$ was conjugated to PEG$_{10}$ *bis*-sulfone TCO **26** and PEG$_5$ *bis*-sulfone Tz **27** reagents at pH 7.6 (Figure 46). The formed intermediate TCO **28** and Tz **29** functional Fab conjugates were then combined and incubated at 5°C for approximately 18 hours. Conjugation of Fab$_{rani}$ to reagents **26** and **27** yielded some of the required intermediates (Figure 46, Lanes 4 and 5), however relatively large quantities of reduced Fab remained, it is likely that by increasing the equivalents of reagents **28** and **29** to 1.5 more of the reduced Fab would convert. Upon mixing of intermediates **28** and **29** no ligation occurred (Figure 46 Lane 6). It was expected that a band would appear with a molecular weight of approximately 110 kDa. If intermediate **28** (60 kDa MW, Figure 46, Lane 4) and intermediate **29** (50 kDa MW, Figure 46, Lane 5) did indeed ligate, a band at 110 kDa is probable.
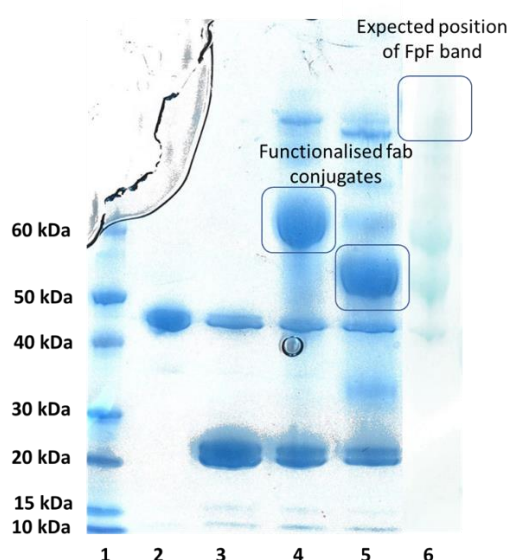
Figure 46: SDS PAGE gel showing the conjugation of 0.5 mg Fab$_{rani}$ per conjugation (0.30 mg/mL) to PEG$_{10}$ *bis*-sulfone TCO **26** and PEG$_5$ *bis*-sulfone Tz **27** pH 7.6, 1 eq, 18 hours conjugation time and the combination of the Fab$_{rani}$ TCO **28** and Fab$_{rani}$ Tz **29** functionalised Fab conjugates. **Lane 1**: Protein marker, **2**: Fab$_{rani}$, **3**: reduced Fab$_{rani}$, **4**: conjugation of Fab$_{rani}$ to reagent **26**, **5**: conjugation of Fab$_{rani}$ to reagent **27**, **6**: Ligation reaction mixture of intermediates **28** and **29**

TCO and Tz are a well-established pair of functional moieties capable of undergoing inverse electron demand Diels–Alder (iEDDA) reactions [191]. This fact coupled with the results of reagent only ligation reactions (Figure 45) show that TCO and Tz moieties can undergo cycloaddition in the presence of each other. Previous research into the use of bio-orthogonal moieties, specifically hydrazines for the preparation of heterodimeric protein molecules [182] found that efficiency of coupling was higher when reagents were coupled together in absence of protein. This implies that when a protein is present it can create a shielding effect in which the protein can sterically hinder the two bio-orthogonal moieties from coming into close enough contact with each other to couple. The same may be occurring in this example in which

Fab$_{rani}$ may be hindering the interaction of the free TCO and Tz groups present in intermediates **28** and **29**.

Another issue could be that a quantity of free, unconjugated PEG$_{10}$ *bis*-sulfone TCO **26** and PEG$_5$ *bis*-sulfone Tz **27** reagents are present within the ligation reaction mixture containing intermediates **28** and **29** (Figure 46, Lane 6). This could mean that instead of intermediates **28** and **29** ligating intermediate **28** may ligate to reagent **27** and vice versa for intermediate **29** and reagent **26**. A band in Figure 46, Lane 5 at approximately 60 kDa suggests that this may be occurring, considering that the Fab$_{rani}$ Tz functionalised conjugate **29** has a molecular weight of approximately 50 kDa and the PEG$_{10}$ *bis*-sulfone TCO reagent has a molecular weight of close to 10 kDa. Ligation of intermediate **29** and reagent **26** would form a different intermediate molecule termed a Fab PEG TCO-Tz PEG *bis*-sulfone intermediate **31** (Figure 47).
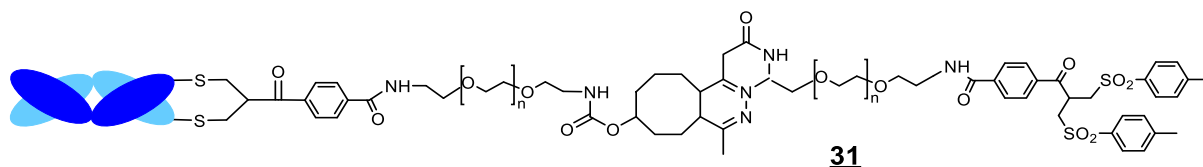
Figure 47: Chemical structure of the Fab PEG TCO-Tz PEG *bis*-sulfone intermediate **31**

This could suggest that a large molecule (functionalised Fab conjugate) prefers to ligate to a smaller molecule (free reagent) over ligating to another large molecule (functionalised Fab conjugate). Therefore, it was decided to try and remove any free reagents **26** and **27** from the TCO **28** and Tz **29** functionalised Fab conjugation mixtures prior to combination. Because the molecular weights of reagents **26** and **27** are no more than 10 kDa it was decided to remove them from the respective conjugation reactions using vivaspin centrifugation columns with a molecular weight cut off (MWCO) of 30 kDa. The choice of a 30 kDa MWCO would allow free reagent **26** and **27**) to pass through the membrane but ensure that the TCO **28** and Tz **29** functionalised Fab conjugates (MW greater than 50 kDa) would not pass through, allowing for separation.

Ranibizumab was conjugated to PEG$_{10}$ *bis*-sulfone TCO **26** and PEG$_5$ *bis*-sulfone Tz **27** (Figure 48A, Lanes 5 and 6). Also within this experiment ranibizumab was conjugated to PEG$_5$ *bis*-sulfone azide **21** and PEG$_5$ *bis*-sulfone DBCO **22** (Figure 48A, Lanes 3 and 4). Both sets of ligation reagents were included in this experiment with the aim of providing a direct comparison. The better performing pair of di functional reagents would then be evaluated with the aim of preparing BsFpFs.

Azide **24**, DBCO **25**, TCO **28** and Tz **29** functionalised Fab conjugates were then prepared. Prior to combination of intermediates **24** and **25** and intermediates **28** and **29** all the functionalised Fab conjugates were individually washed using a vivaspin centrifugation column (30 kDa MWCO). Combining washed intermediates **24** and **25** led to the appearance of a band at a molecular weight of approximately 130 kDa (Figure 48B Lanes 3 and 4), close to the expected molecular weight of an FpF as the azide **24** and DBCO **25** functionalised Fab conjugates had approximate molecular weights of 60 kDa and 70 kDa respectively.
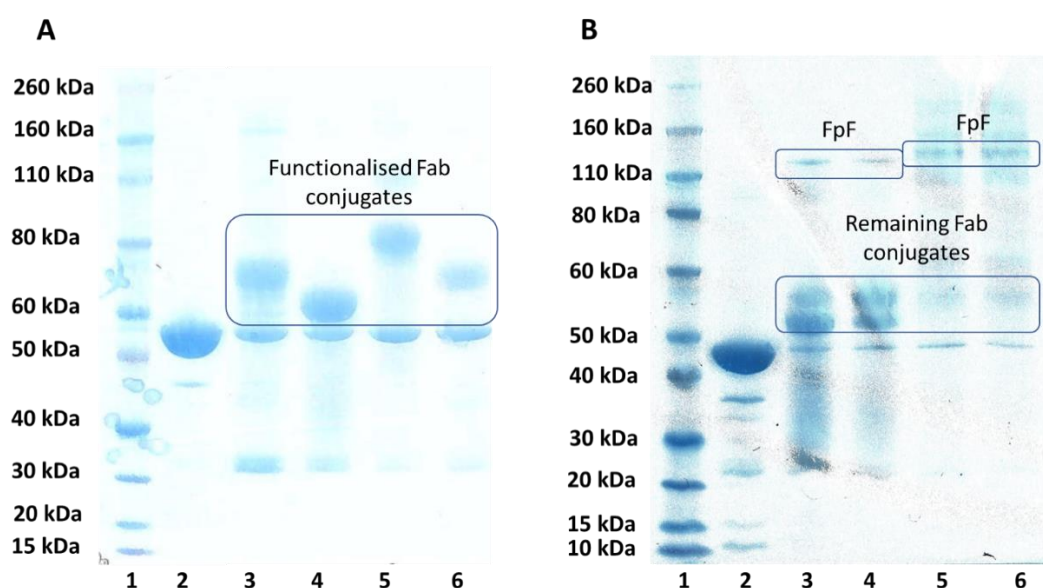
Figure 48: (A) SDS PAGE gel showing the conjugation of 0.5 mg per conjugation ranibizumab (0.60 mg/mL) to PEG$_5$ *bis*-sulfone DBCO **22**, PEG$_3$ *bis*-sulfone azide **21**, PEG$_{10}$ *bis*-sulfone TCO **26** and PEG$_5$ *bis*-sulfone Tz **27** reagents pH 7.6, 1 eq, 18 hr conjugation time) **(B):** SDS PAGE gel showing the ligation of intermediates **23** and **24** and **28** and **29**, 18 hour reaction time, PBS. **(A) Lane 1**: Protein marker, **2**: ranibizumab, **3**: conjugation to PEG$_5$ *bis*-sulfone DBCO **22**, **4**: PEG$_3$ *bis*-sulfone azide **21**, **5**: PEG$_{10}$ *bis*-sulfone TCO **26**, **6**: PEG$_5$ *bis*-sulfone Tz **27**. **(B) Lane 1**: Protein marker, **2**: ranibizumab, **3**: ligation of intermediates **23** and **24** , **4**: ligation of intermediates **23** and **24** n=2, **5**: ligation of intermediates **28** and **29**, **6**: ligation of intermediates **28** and **29** n=2.

The combination of the TCO and Tz intermediates (**28** and **29**) also led to the formation of bands (Figure 48B, Lanes 5 and 6) at a higher molecular weight indicating the presence of an FpF. These bands in Figure 48B, lanes 5 and 6 are at a slightly higher molecular weight than was observed in lanes 3 and 4 because the TCO **28** and Tz **29** functionalised Fab conjugates had higher molecular weights due to increased length of the PEG backbone used for conjugation. Both ligations between the intermediates pairs were performed twice with little difference between the replicates.

The presence of the FpF bands (Figure 48B Lanes 3-6) was encouraging and showed that removal of free difunctional reagent prior to ligation was a critical step.

Visually the ligation between the TCO **28** and Tz **29** intermediates (Figure 48B Lanes 5 and 6) appears to be superior to the ligation between the DBCO **25** and azide **26** intermediates as indicated by the concentration of FpF present in lanes 5 and 6. Because of this result no further work with the PEG *bis*-sulfone DBCO **23** and PEG *bis*-sulfone azide **22** reagents was performed.

This experiment served as a good starting point and gave justification for optimising the click reaction process. Moving forward, an experiment was performed looking at the effect of different equivalents of PEG$_{10}$ *bis*-sulfone TCO **26** and PEG$_5$ *bis*-sulfone Tz **27** used for conjugation to Fabs, and to see its subsequent effect on FpF yield. It was thought that increasing the molar equivalent of reagent would drive greater formation of the functionalised Fab intermediates. With greater intermediate concentrations available for ligation there is the possibility that in turn greater concentrations of FpFs may form.
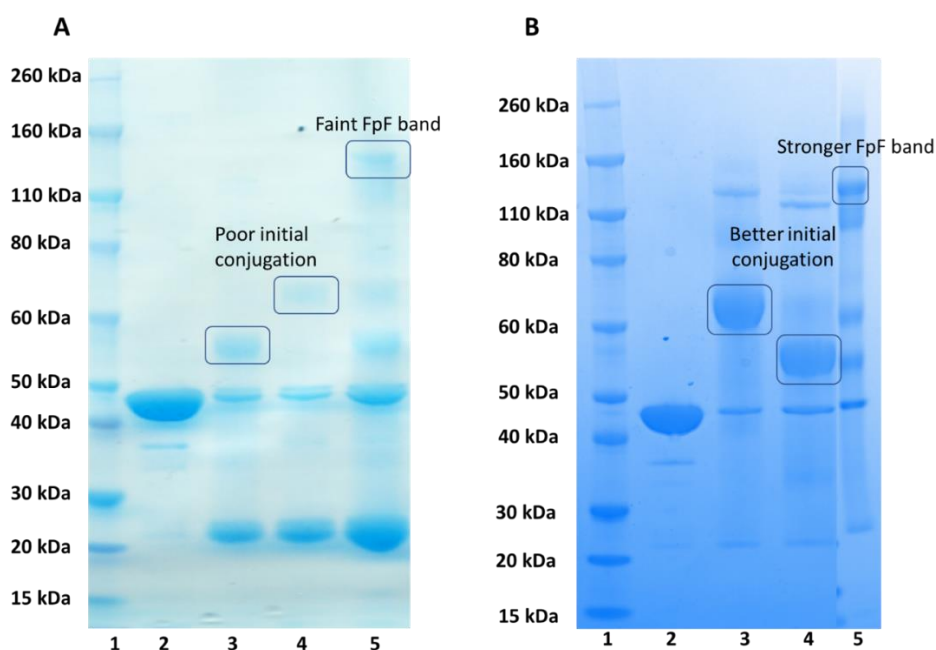
Figure 49: (A) SDS PAGE gel showing the conjugation of 0.5 mg ranibizumab per conjugation to 1 eq PEG$_{10}$ *bis*-sulfone TCO **26** and PEG$_5$ *bis*-sulfone Tz **27** pH 7.6 18 hours conjugation time and ligation of intermediates **28** and **29** **(B)** SDS PAGE gel showing the conjugation of 0.5 mg ranibizumab per conjugation to 1.5 eq PEG$_{10}$ *bis*-sulfone TCO **26** and PEG$_5$ *bis*-sulfone Tz **27** pH 7.6 18 hours conjugation time and ligation of intermediates **28** and **29**.**(A)**: Protein marker, **2**: ranibizumab, **3**: conjugation to PEG$_5$ *bis*-sulfone Tz **27**, **4**: PEG$_{10}$ *bis*-sulfone TCO **26**, **5**: ligation of intermediates **28** and **29**. **(B) (A)**: Protein marker, **2**: ranibizumab, **3**: conjugation to PEG$_{10}$ *bis*-sulfone TCO **26**, **4**: PEG$_5$ *bis*-sulfone Tz **27**, **5**: ligation of intermediates **28** and **29**.

Results shown in Figure 49 did indeed show this was the case. Performing the conjugation of Fab$_{rani}$ to 1.5 eq of PEG$_{10}$ *bis*-sulfone TCO **26** and PEG$_5$ *bis*-sulfone Tz **27** (Figure 49B Lanes 3 and 4) resulted in greater formation of TCO **28** and Tz **29** functionalised Fab conjugates than when 1 eq (Figure 49A Lanes 3 and 4) of reagents **26** and **27** were used. Use of 1.5 eq of both reagents has driven the formation of intermediates **28** and **29** as more of the *bis*-sulfone conjugation moiety is available to bridge to the reduced ranibizumab. When combined the intermediates prepared using 1.5 eq of reagent **26** and **27** ligated to form an FpF Figure 49B lane 5 in greater quantities than that observed for ligation of the same intermediates that were prepared via conjugation using 1 eq of the same reagents.

A caveat for using 1.5 eq of PEG *bis*-sulfone TCO **26** and PEG *bis*-sulfone Tz **27** is the presence of bands at higher molecular weights in the conjugation mixtures (Figure 49B Lanes 3 and 4). The exact nature of these bands is unknown but judging from their molecular weights of between 120-130 kDa they are likely to be a dimeric molecule in which 2 Fabs have conjugated to a single molecule of either reagent **26** or **27**. One Fab may have conjugated as normal through a reduced disulfide, the other is likely a result of a non-specific interaction. Fabs are complex molecules, and it is possible for PEG based reagents to interact with amino acid residues [192] present on the surface of the antibody fragment. This molecule, despite likely being dimeric in nature, cannot be called an FpF. The orientation of the second Fab would likely be random, meaning CDR regions may be shielded.

After establishing that using 1.5 eq of PEG *bis*-sulfone TCO **26** and PEG *bis*-sulfone Tz **27** is optimum for the preparation of an FpF via conjugation-ligation the next challenge was to try and isolate an FpF from a ligation reaction mixture (i.e. Figure 49B Lane 5) and obtain a purified final product. IEX chromatography was chosen as a purification method. Upon PEGylation of a protein PEG is known to impart a steric shielding effect [193], this shielding effect extends to IEX chromatography, with longer PEG chains providing a greater shielding effect [194]. In short this means that a protein conjugated to PEG has a weaker interaction with an IEX column than the free protein, meaning a lower concentration of competitor ion is required to elute the conjugated protein from the IEX column. FpFs are known to behave more like Fabs during IEX [183] with the shielding effect of PEG being reduced as it only makes up a relatively small part of the molecule. A functionalised Fab conjugate is likely to behave like a PEGylated Fab during IEX, these differences in behaviour may allow an FpF and any

leftover TCO **28** and Tz **29** functionalised Fab conjugates within the ligation mixture to be separated.

An FpF was prepared via conjugation-ligation using Fab$_{inflixi}$ and PEG$_{10}$ *bis*-sulfone TCO **26** and PEG$_5$ *bis*-sulfone Tz **27** reagents, using 1.5 eq of each reagent for the initial conjugation. An attempt was then made to purify the monospecific anti-TNF-α monospecific FpF from the ligation mixture using IEX (Figure 50) with collected fractions assessed using SDS PAGE.
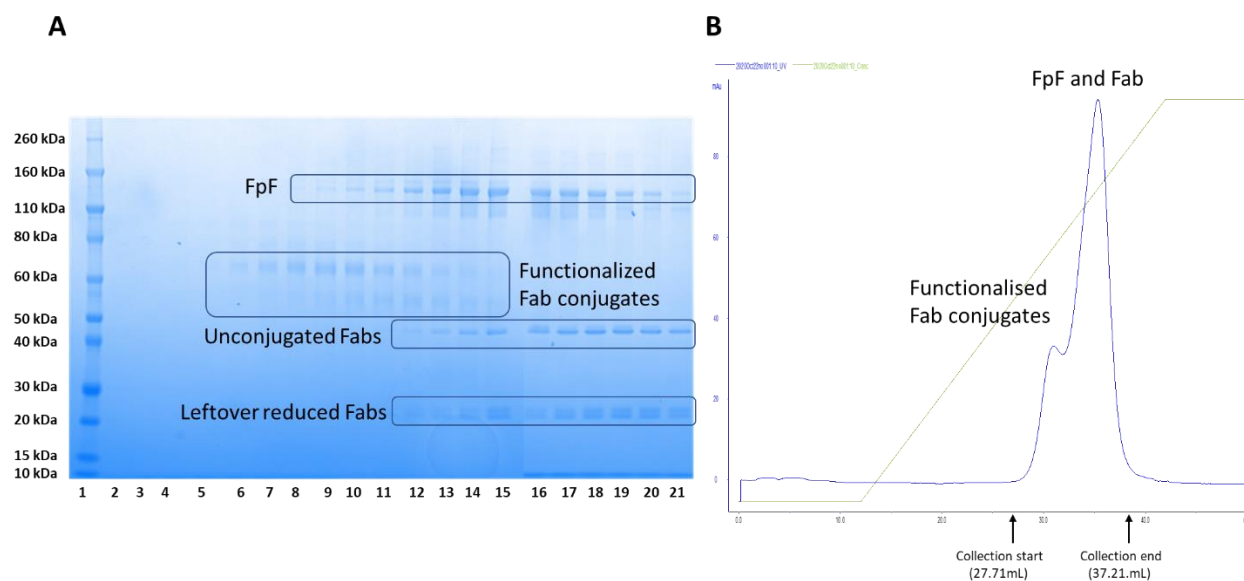
Figure 50: (A) SDS PAGE gel showing the fractions collected during the IEX purification of the ligation reaction mixture of an FpF prepared using Fab$_{inflixi}$. **Lane 1**: Protein marker, **2**: 27.71 mL, **3**: 28.21 mL, **4**: 28.71 mL, **5**: 29.21 mL, **6**: 29.71 mL, **7**: 30.21 mL, **8**: 30.71 mL, **9**: 31.21 mL, **10**: 31.71 mL, **11**: 32.21 mL, **12**: 32.71 mL, **13**: 33.21 mL, **14**: 33.71 mL, **15**: 34.21 mL, **16**: 34.71 mL, **17**: 35.21 mL, **18**: 35.71 mL, **19**: 36.21 mL, **20**: 36.71 mL, **21**: 37.21 mL. **(B)** IEX chromatogram from the purification of the click reaction mixture, 0.5 mL fractions were collected between 27.71-37.21 mL of method volume, the green line is the concentration of competitor ion (Na+).

It was possible to partially purify the FpF contained in the ligation mixture using IEX. Figure 50A, Lanes 16-21 contain bands corresponding to the FpF, leftover unconjugated Fabs and leftover reduced Fabs, it was possible to remove the TCO **28** and Tz **29** functionalised Fab conjugates from these fractions. The ratio of PEG to protein is less in an FpF as it contains two Fabs. This means the steric shielding effect has been limited and the molecule behaves like the native Fab on the IEX column. Figure 50B shows the IEX chromatogram from this purification, of interest is the green line which indicates the concentration of competitor ion. Once the competitor ion reaches a certain concentration the TCO **28** and Tz **29** functionalised Fab conjugates elute from the column, then once the ion concentration increases the FpF and unconjugated Fabs elute.

A secondary purification step was required to separate the desired FpF from the remaining Fab impurities. Size exclusion chromatography (SEC) was the method of choice as the large differences in molecular weights between the Fab (50 kDa) and the FpF (approx. 120 kDa) mean that it should be able to separate them based upon their size or, more specifically, hydrodynamic radius.

Affinity chromatography with protein A is not suitable for this as an FpF does not contain the Fc group found in conventional IgGs. Protein L was also not be suitable as both molecules contain Fab fragments. To purify using SEC the fractions shown in Figure 50A, Lanes 16-21 were combined and concentrated to a volume of no more than 0.5 mL as per instructions provided with the SEC column, the fractions were concentrated using vivaspin centrifugation tubes. It should be noted that lanes 16-21 were chosen as they contain the smallest concentrations of the remaining TCO **28** and Tz **29** functionalised Fab conjugates. The chosen strategy was to minimise the amount of functionalised Fab conjugate in the sample being injected on the SEC column. This direction was chosen because the molecular weight difference between the functionalised Fab conjugate and native Fab is too small for them to be effectively separated using SEC.

This strategy however does come with a caveat in that yield is being sacrificed in place of attaining a highly purified product. The fractions sent to waste (Figure 50A Lanes 6-15) contain the desired FpF, these fractions could be repurified using IEX to try and maximise yield however that would be a laborious process and would not be viable if this process was ever to be scaled up, in an industrial setting these fractions would likely be considered as waste. Moving on, the concentrated sample (Figure 50A Lanes 16-21) was injected onto the SEC column for further purification using PBS as the mobile phase.

SEC was able to successfully purify the FpF from the remaining impurities (Figure 51A, Lanes 6 and 7). The SEC chromatogram from this purification (Figure 51B) shows the elution order of the FpF, functionalised Fab conjugates and Fabs. The elution order is based upon molecular weight, with larger molecules eluting first as they do not travel as far into the pores of the SEC resin.
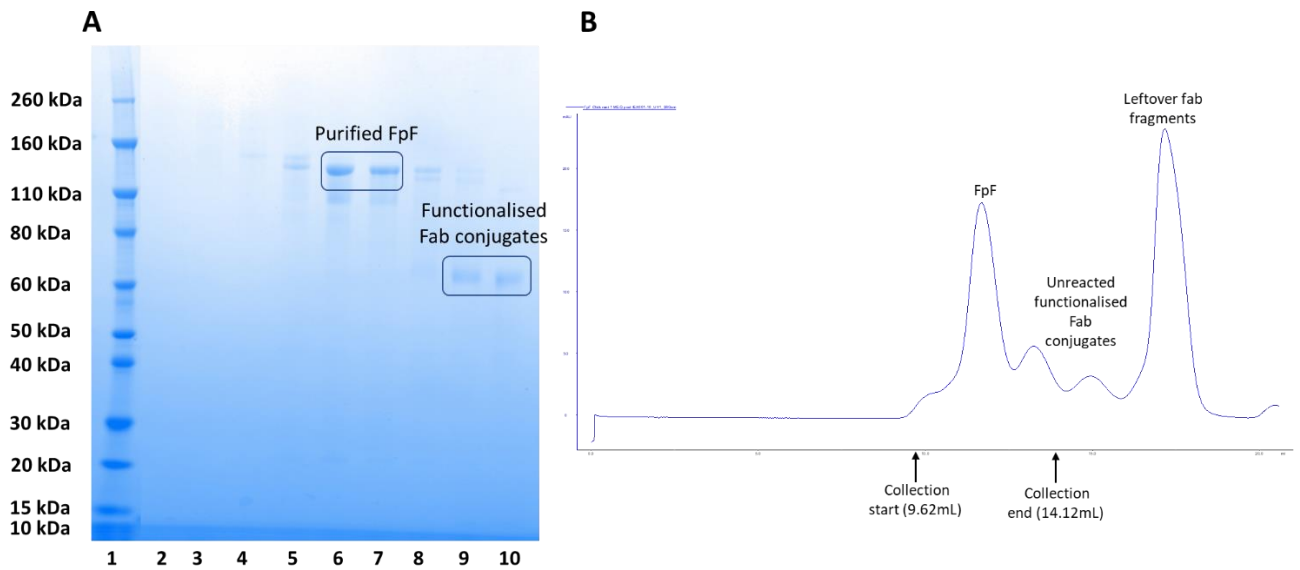
Figure 51: (A) SDS PAGE gel showing the fractions collected during the SEC purification of the sample prepared by combining fractions shown in lanes 16-21 Figure 50A. **Lane 1**: Protein marker, **2**: 9.62 mL, **3**: 10.12 mL, **4**: 10.62 mL, **5**: 11.12 mL, **6**: 11.62 mL, **7**: 12.12 mL, **8**: 12.62 mL, **9**: 13.12 mL, **10**: 13.62 mL, **(B)** SEC chromatogram from the purification of the sample prepared by combining lanes 16-21 Figure 50A, 0.5 mL fractions were collected between 9.62-14.12 mL of method volume.

Fractions were not collected any later than 14.12 mLs of elution volume meaning that the Fab fragments (peak shown on Figure 51B) collected during this purification were not visualised using SDS PAGE in this example. From the experiments performed during the development of the soluble papain digestion method (Chapter 3) it is known that Fab fragments elute after 16 mL of method volume corresponding with the elution volume of the labelled Fab peak in Figure 51B.

Once the FpF was purified a suitable quantification method needed to be used to determine FpF concentration and give a final isolated yield. Typically for antibodies UV absorbance is measured at 280 nm because the amino acids tyrosine and tryptophan allow direct measurement of antibody concentration at this wavelength. However PEG absorbs UV light at 280 nm [195] meaning that any absorbances at 280 nm may be exaggerated leading to falsely high concentrations of FpFs. A suitable method for quantification is the micro-BCA assay. The micro-BCA assay is a modified version of the BCA assay. The components are modified to allow the quantification of less concentrated protein samples. The assay works by using bicinchoninic acid (BCA) to detect reduced copper ions which are formed due to the presence of a protein, the BCA and the copper ions chelate to form a complex which is purple in colour.

This complex can be measured at 562 nm and behaves in a linear manner, PEG shows minimal absorbance at 562 nm, meaning a true concentration of FpF can

be determined. To quantify the FpF, first a calibration curve was prepared using unconjugated Fabs as the control, a linear trendline was then added to the calibration curve and the unknown concentrations were determined by using the equation of the trend line. Figure 52 shows a typical micro-BCA calibration curve and the trend line equation used to work out the concentration and subsequent yield of FpF.
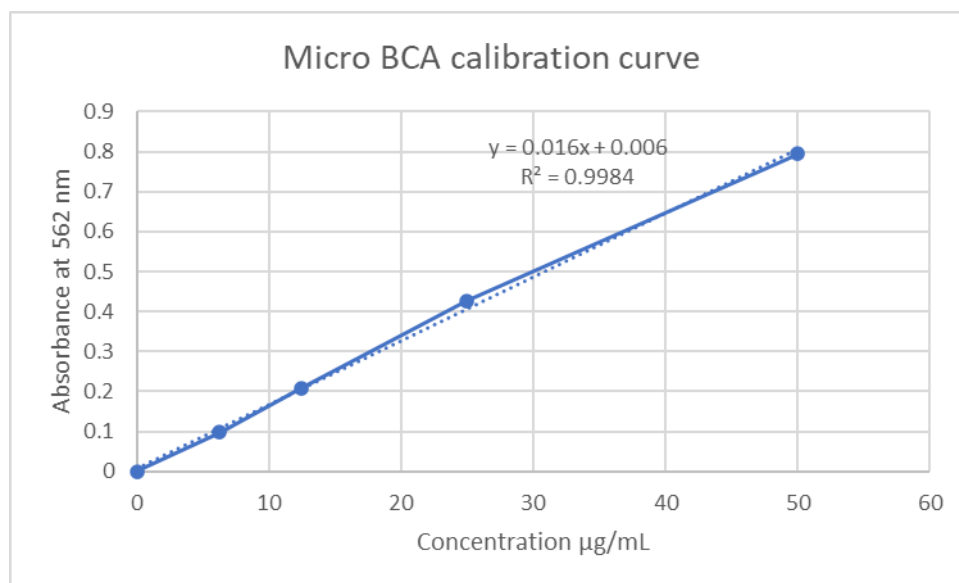
Figure 52: Micro-BCA calibration curve prepared using unconjugated Fab. The resulting equation is used to calculate unknown concentrations based upon their absorbances.

As can be seen from Figure 52 the micro-BCA assay is linear up to a concentration of 50 µg/mL when using Fabs to construct a calibration curve, this is evident by the R^2 value of 0.9984. When the absorbance of the purified $FpF_{inflixi}$ (Figure 51A, Lanes 6 and 7) was measured using micro-BCA the average absorbance was found to be 0.335, this equated to a concentration of 13 µg/mL. As the FpF was diluted 10× prior to measurement the actual concentration of the FpF stock was 130 µg/mL. A 10× dilution was used firstly to ensure the concentration of the measured solution did not exceed 50 µg/mL and secondly to preserve as much of the FpF stock solution as possible, it is not possible to recover the sample solution after use in a micro-BCA assay. In total 1 mL of a 130 µg/mL monospecific anti-TNF-α FpF derived was prepared. This equated to a yield of 6.5% as a total of 2 mg $Fab_{inflixi}$ had been used to prepare the molecule.

To summarise, it has been demonstrated that an FpF can be prepared via a conjugation-ligation strategy. The final ligation reaction mixture can be purified to obtain a pure final FpF. The conjugation-ligation concept is summarised in Figure 53. Starting Fab (Figure 53, Lane 1) is reduced using DTT. The reduced Fab (Lane 2) is

conjugated to PEG *bis*-sulfone TCO **26** and PEG *bis*-sulfone Tz **27** to prepared TCO **28** and **29** functionalised Fab conjugates which are then combined after having any free remaining reagent **26** and **27** removed via filtration centrifugation. Intermediates **28** and **29** then ligate to form an FpF (Lane 6).
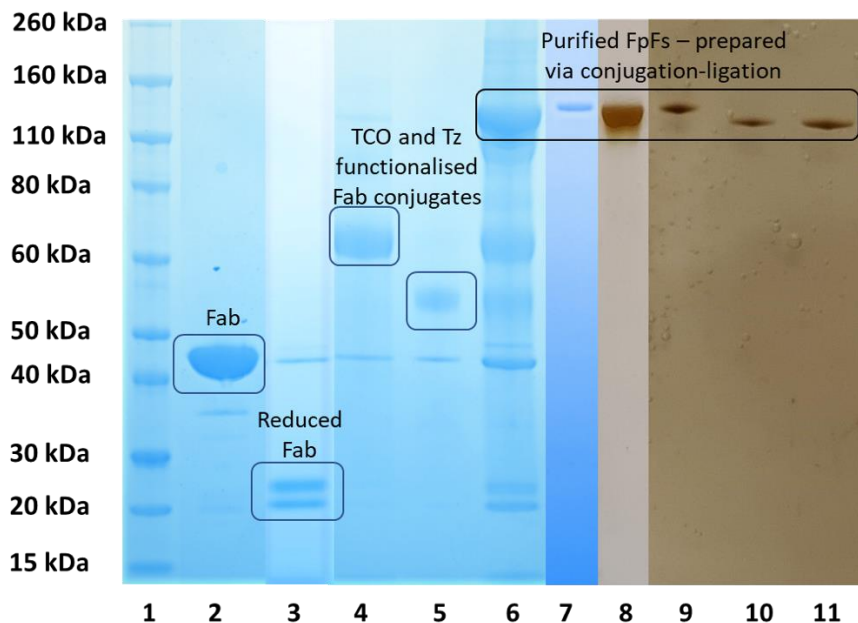
Figure 53: SDS PAGE gel showing the preparation and purification of monospecific and bispecific FpFs via conjugation-ligation. **Lane 1**: Protein marker, **2**: parent Fab, **3**: reduced Fab, **4**: Fab conjugated to difunctional reagent 1, **5**: Fab conjugated to difunctional reagent 2, **6**: combination of TCO **28** and Tz **29** functionalised Fab conjugates, **7**: anti-VEGF monospecific FpF – Coomassie blue, **8**:purified anti-VEGF monospecific FpF – silver stained, **9**: purified anti-VEGF/IL-6R BsFpF – silver stained, **10**: purified anti-VEGF/TNF BsFpF – silver stained, **11**: purified anti-TNF/IL-6R BsFpF – silver stained.

The ligation mixture is then purified using a mixture of IEX and SEC to attain a purified final product, an FpF (Figure 53, Lanes 7-11). Lanes 7-11 show examples of 4 different FpFs including 3 BsFpFs prepared via conjugation-ligation. SDS PAGE gels that have been silver stained are shown in Figure 53 to demonstrate that highly purified monospecific and bispecific FpFs can be prepared. Silver staining can detect as little as 0.25 ng of protein [196] making it suitable for detecting small traces of impurities, coomassie blue would not be suitable for this purpose as this dye detects proteins at a minimum concentration of 0.1 µg.

Being able to prepare a highly purified BsFpF via conjugation-ligation is of high importance. Firstly, there is a requirement for pharmaceutical medicines to be highly purified. Secondly, impurities may make characterisation of the FpFs difficult. For example, the presence of remaining functionalised Fab conjugate in an FpF sample may skew affinity data during protein-protein binding assays. Briefly looking back at

113

Figure 53 the bands in lanes 8 and 9 are at slightly higher molecular weights than bands in lanes 10 and 11. This is because the molecular weights of PEG *bis*-sulfone TCO **26** and PEG *bis*-sulfone Tz **27** used for conjugation to Fabs were greater. For clarity, descriptions of the molecules present in Figure 53 are shown below in Table 9.

Name	Derived from	Molecular weight	Lane in Figure 53
Anti-VEGF monospecific FpF	Fab$_{Rani}$	120 kDa	7 and 8
Anti-VEGF/IL-6R BsFpF	Fab$_{Beva}$ Fab$_{Tocili}$	120 kDa	9
Anti-VEGF/TNF BsFpF	Fab$_{Beva}$ Fab$_{Inflixi}$	110 kDa	10
Anti-TNF/IL-6R BsFpF	Fab$_{Inflixi}$ Fab$_{Tocili}$	110 kDa	11

Table 9: Descriptions of monospecific and BsFpFs presented in Figure 53. 4 purified FpFs prepared via conjugation-ligation are presented in Figure 53, Lanes 7-11. The FpFs were prepared from a range of different therapeutic Fabs including Fabs obtained from the digestion of bevacizumab, tocilizumab, and infliximab. Differences in molecular weight are due to the length of the PEG backbone present in reagents **26** and **27**.

There was however one issue during the preparation of the BsFpFs which needed to be addressed, namely the formation of high molecular weight impurities during the conjugation of Fabs to PEG *bis*-sulfone TCO **26** and PEG *bis*-sulfone Tz **27**.

Optimisation of the conjugation-ligation methodology to prepare BsFpFs of greater purity.

A key step in the preparation of monospecific and BsFpFs is the removal of free PEG *bis*-sulfone TCO **26** and PEG *bis*-sulfone Tz **27** reagent post conjugation. The original method used vivaspin columns with a molecular weight cut off (MWCO) of 30 kDa. This method was effective at removing free reagents **26** and **27** however a problem exists which filtration centrifugation is not able to solve.

During the conjugation of Fab$_{inflixi}$ to PEG$_{10}$ *bis*-sulfone TCO **26** and PEG$_5$ *bis*-sulfone Tz **27** reagents (Figure 54, Lanes 2 and 3) bands at molecular weights of approximately 110 and 120 kDa form. These are likely to be dimeric molecules in which 2 Fabs are conjugated to a single molecule of either reagent **26** or **27**. The molecular weight of the high molecular weight (HMW) molecule is like the molecular weight of the FpF formed via conjugation-ligation. This could mean that the final purified FpF could be contaminated with the HMW impurity.
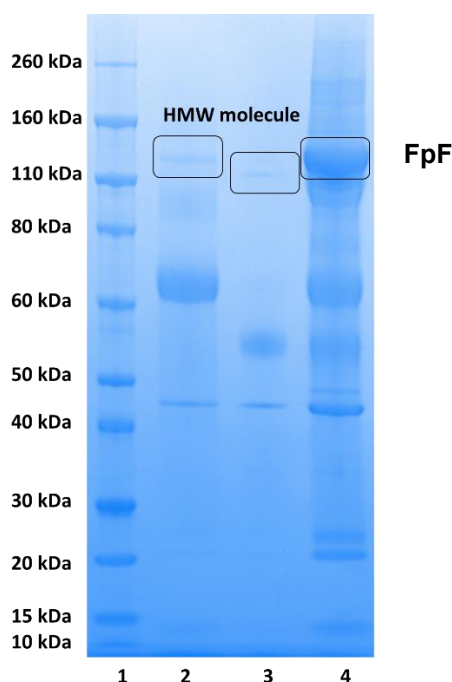
Figure 54: SDS PAGE gel showing a conjugation of Fab$_{inflixi}$ to PEG$_{10}$ *bis*-sulfone TCO **26** and PEG$_5$ *bis*-sulfone Tz **27** reagents and ligation of the TCO **28** and Tz **29** functionalised Fab conjugates. **Lane 1:** Protein marker, **2:** Conjugation of Fab$_{inflixi}$ to PEG$_{10}$ *bis*-sulfone TCO **26**, **3:** Conjugation of Fab$_{inflixi}$ to PEG$_5$ *bis*-sulfone Tz **27**, **4:** Ligation reaction mixture of the TCO **28** and Tz **29** functionalised Fab conjugates.

To see if the formation of the HMW impurity during conjugation of Fabs to PEG *bis*-sulfone TCO **26** and PEG *bis*-sulfone Tz **27** was pH sensitive, a pH scouting experiment (Figure 55) was performed. It was thought that if it was proven that HMW formation was pH sensitive, the pH used for conjugation using reagents **26** and **27** could be adjusted to limit or eliminate the formation of the HMW impurity. Fab$_{rani}$ was

conjugated (Figure 55) to PEG$_5$ *bis*-sulfone TCO **26** and PEG$_5$ *bis*-sulfone Tz **27** at a range of pH values.
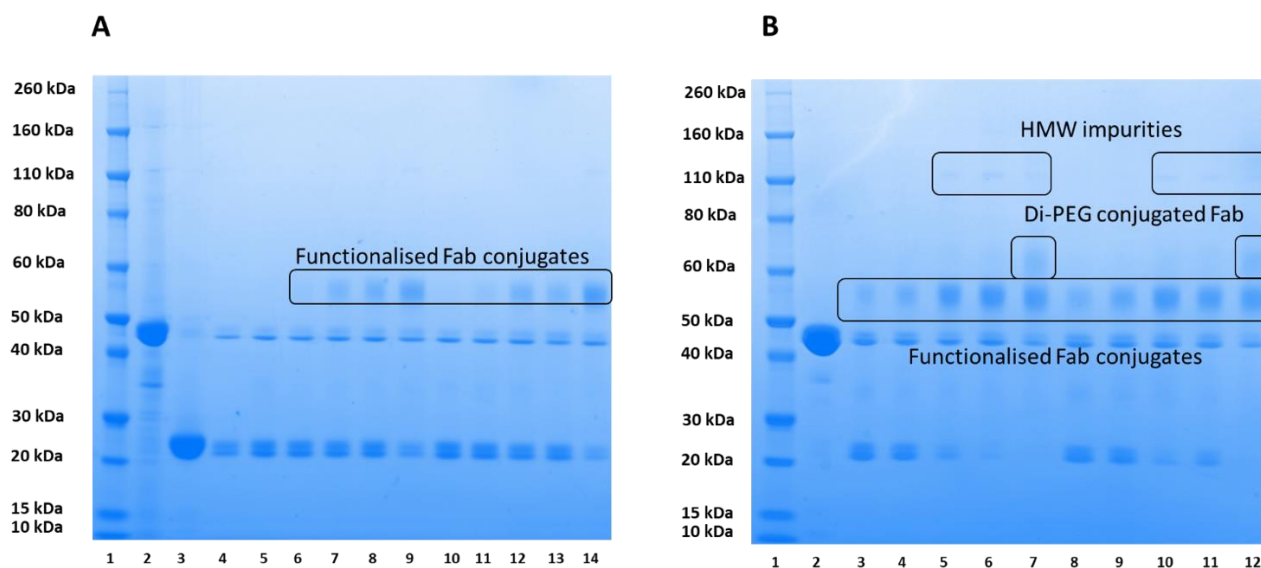
Figure 55: (A) SDS PAGE gel stained with Coomassie blue showing results from conjugations of 0.3 mg ranibizumab per conjugation (0.30 mg/mL) to 1.5 eq. of PEG$_5$ *bis*-sulfone TCO **26** and PEG$_5$ *bis*-sulfone Tz **27** at different pHs,3.5 hour reaction time. **(B)**: 24 hour reaction time. **(A) Lane 1**: Protein marker, **2**: ranibizumab, **3**: reduced ranibizumab no DTT removal, **4**: reduced ranibizumab, **5**: PEG$_5$ *bis*-sulfone TCO **26** pH 5, **6**: pH 6, **7**: pH 7, **8**: pH 8, **9**: pH 9, **10**: PEG$_5$ *bis*-sulfone Tz **27** pH 5, **11**: pH 6, **12**: pH 7, **13**: pH 8, **14**:pH 9. **(B) Lane 1**: Protein marker, **2**: ranibizumab, **3**: PEG$_5$ *bis*-sulfone TCO **26** pH 5, **4**: pH 6, **5**: pH 7, **6**: pH 8, **7**: pH 9, **8**: PEG$_5$ *bis*-sulfone Tz **27** pH 5, **9**: pH 6, **10**: pH 7, **11**: pH 8, **12**: pH 9.

After 3.5 hours of reaction time conjugation proceeds fastest at pHs of 8 and 9 for both reagents (Figure 55A, Lanes 8 and 9 and Lanes 13 and 14) as indicated by the density of the bands for the TCO **28** and Tz **29** functionalised Fab conjugates. No HMW impurities are seen in Figure 55A. However, when incubation time is extended to 24 hours (Figure 55B) conjugations between both reagents **28** and **29** have proceeded to a greater extent. At pH 5 and 6 (Figure 55B Lanes 3 and 4 and Lanes 8 and 9) small quantities of TCO **28** and Tz **29** functionalised Fab conjugates have formed. At pHs 7, 8 and 9 (Figure 55B Lanes 5 to 7 and Lanes 10 to 12) greater concentrations of intermediates **28** and **29** have formed. Also present in these lanes, although at low concentrations, are HMW impurities. So, formation of the HMW impurities could be eliminated by conducting conjugations at pHs of 5 or 6 (Figure 55B, Lanes 3 and 4 and Lanes 8 and 9). If this strategy was adopted FpF yield would likely be negatively affected quite significantly as the concentration of TCO **28** and Tz **29** functionalised Fab conjugates formed at pHs 5 and 6 (Figure 55B, Lanes 3 and 4 and Lanes 8 and 9) is low as indicated by the faintness of the bands. Based upon the results from the pH scouting experiment (Figure 55) it was decided not to modify

conjugation pH from 7.6 and it was decided to attempt to remove the HMW impurity prior to the combination of the TCO **28** and Tz **29** functionalised Fab conjugates.

IEX was use to remove the HMW impurity. This is because if the HMW impurity contains two Fabs, as suspected, it should elute later from an IEX column than the TCO **28** and Tz **29** functionalised Fab conjugates. Fab$_{Inflixi}$ was conjugated to a PEG$_{10}$ *bis*-sulfone TCO **26** reagent. The conjugation mixture was then buffered exchanged into pH 4.0 acetate buffer and injected onto a cation exchange column. Eluted fractions were collected and characterised using SDS PAGE (Figure 56).
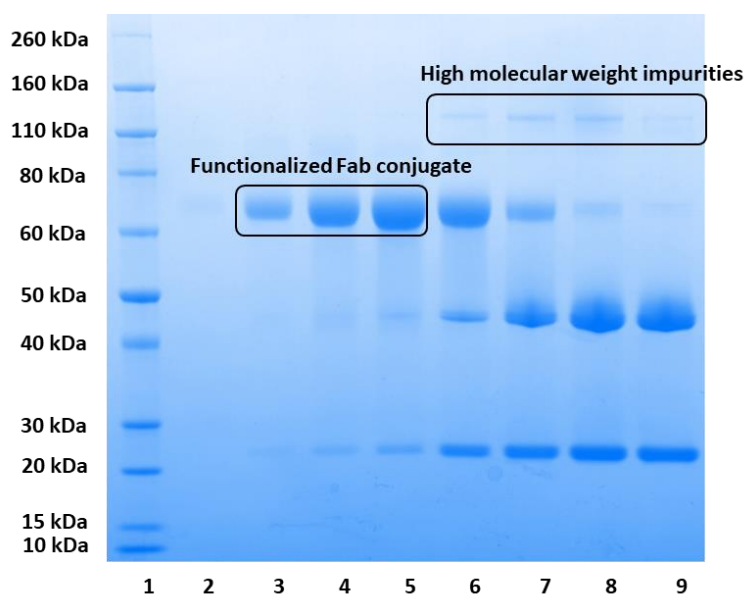
Figure 56: An SDS PAGE gel showing collected fractions from the IEX purification of a Fab$_{Inflixi}$ TCO functionalised Fab conjugate **28**. **Lane 1:** Protein marker, **2:** 25.45-26.45 mLs, **3:** 26.45-27.45 mLs, **4:** 27.45-28.45 mLs, **5:** 28.45-29.45 mLs, **6:** 29.45-30.45 mLs, **7:** 30.45-31.45 mLs, **8:** 31.45-32.45 mLs, **9:** 32.45-33.45 mLs.

Using IEX for this purpose allowed separation of the TCO functionalised Fab conjugate **28** from the HMW impurities. Considering this result, the filtration centrifugation step to remove free reagents **26** and **27** was replaced by IEX. It was assumed the same result would occur if a conjugation mixture containing a Tz functionalised Fab conjugate **29** was purified using IEX.

In total 18 different FpFs were prepared using a conjugation-ligation methodology. Table 10 summarises both the monospecific and BsFpFs that were prepared and their respective final isolated yields.

No.	Name and target(s)	Derived from	Molecular weight	Yield (%)	Purification methodology
1	Anti-VEGF monospecific FpF	Ranibizumab	120 kDa	2.5	Vivaspin-IEX-SEC
2	Anti-VEGF monospecific FpF	Ranibizumab	120 kDa	20.1	Vivaspin-IEX-SEC
3	Anti-TNF monospecific FpF	Fab$_{Inflixi}$	115 kDa	7.8	Vivaspin-IEX-SEC
4	Anti-VEGF/IL-6R Bispecific FpF	Ranibizumab Fab$_{Tocili}$	115 kDa	0.6	Vivaspin-IEX-SEC
5	Anti-VEGF/TNF Bispecific FpF	Ranibizumab Fab$_{Inflixi}$	115 kDa	1	Vivaspin-IEX-SEC
6	Anti-VEGF/IL-6R Bispecific FpF	Fab$_{Beva}$ Fab$_{Tocili}$	115 kDa	14.9	IEX-IEX-SEC
7	Anti-VEGF/TNF Bispecific FpF	Fab$_{Beva}$ Fab$_{Inflixi}$	115 kDa	15.7	IEX-IEX-SEC
8	Anti-TNF/IL-6R Bispecific FpF	Fab$_{Inflixi}$ Fab$_{Tocili}$	115 kDa	14.4	IEX-IEX-SEC
9	Anti-VEGF monospecific FpF	Fab$_{Beva}$	115 kDa	11.5	IEX-IEX-SEC
10	Anti-IL-6R monospecific FpF	Fab$_{Tocili}$	115 kDa	8.0	IEX-IEX-SEC
11	Anti-VEGF monospecific FpF	Ranibizumab	115 kDa	6.5	IEX-IEX-SEC
12	Anti-VEGF/IL-6R Bispecific FpF	Fab$_{Beva}$ Fab$_{Tocili}$	115 kDa	11.2	IEX-IEX-SEC
13	Anti-VEGF/IL-6R Bispecific FpF	Fab$_{Beva}$ Fab$_{Tocili}$	115 kDa	7.8	IEX-IEX-SEC
14	Anti-VEGF/IL-17A Bispecific FpF	Fab$_{Beva}$ Fab$_{Secu}$	115 kDa	10.1	IEX-IEX-SEC
15	Anti-TNF/IL-17A Bispecific FpF	Fab$_{Inflixi}$ Fab$_{Secu}$	115 kDa	10.6	IEX-IEX-SEC
16	Anti-IL-17A Monospecific FpF	Fab$_{Secu}$	115 kDa	15.0	IEX-IEX-SEC
17	Anti-VEGF monospecific FpF	Fab$_{Beva}$	115 kDa	13.9	IEX-IEX-SEC
18	Anti-TNF monospecific FpF	Fab$_{Inflixi}$	115 kDa	12.1	IEX-IEX-SEC

Table 10: Summary of monospecific and BsFpFs prepared via conjugation ligation using PEG *bis*-sulfone TCO **26** and PEG *bis*-sulfone Tz **27** reagents.

It should be noted that interleukin-17A (IL-17A) is listed as a target in Table 10 (molecules 14, 15 and 16). FpFs were prepared using Fabs isolated from the digestion of secukinumab, an anti-IL-17A IgG antibody. The relevance of IL-17A as an ocular target has been discussed previously in Chapter 1. Also referenced in Table 10 is the purification methodology used to isolate the FpFs. Vivaspin-IEX-SEC means that free reagent (PEG *bis*-sulfone TCO **26** and PEG *bis*-sulfone Tz **27**) was removed from the TCO **28** and Tz **29** functionalised Fab conjugation mixtures via centrifugation filtration, then post combining of the TCO **28** and Tz **29** functionalised Fab conjugates IEX and SEC were used to obtain a purified FpF. IEX-IEX-SEC means that the free reagent (reagents **26** and **27**) removal step was performed using IEX. The majority of FpFs were purified using the IEX-IEX-SEC sequence.

FpFs purified using the vivaspin-IEX-SEC purification sequence (Table 10, Samples no. 1-5) gave yields of between 0.6-20.1%. This is a large range and little consistency in yields was observed using this methodology. It is likely that the variation in yields is due to the performance of the filtration centrifugation step. As seen previously the removal of free PEG *bis*-sulfone TCO **26**, free PEG *bis*-sulfone Tz **27** (Figure 46) and concentration of TCO **28** and Tz **29** functionalised Fab conjugates are key to maximising the final yield of purified FpF.

It is possible that the vivaspin column used for centrifugation does not perform consistently, there may be loss of functionalised Fab conjugate through the membrane even though the MWCO of 30 kDa used suggests that should not happen. Removal of free reagents **26** and **27** may also not be consistent. This may help to explain the low yields of 2.5%, 0.6% and 1% (Table 10, Samples 1, 4 and 5) obtained using vivaspin-IEX-SEC.

Changing to an IEX-IEX-SEC purification strategy improved the consistency of purified yields obtained (Table 10, Samples 6-18). Yields ranged between 6.5-14.9%, with most experimental yields being in the 10-15% range. This consistency is likely due to IEX being extremely effective at removing free PEG *bis*-sulfone TCO **26** and free PEG *bis*-sulfone Tz **27** reagents from their conjugation mixtures. Reagents **26** and **27** do not bind to the surface of the IEX column and typically elute within five minutes of method run time. The TCO **28** and Tz **29** functionalised Fab conjugates elute in a controlled way (elution requires addition of competitor ion, Na$^+$) after approximately 30 minutes of run time.

To give context regarding FpF yield. If the FpF conjugation-ligation process was started with a total of 1 mg Fab, a final yield of 10% would equate to 100 µg of FpF. 100 µg of FpF would be enough to characterise the molecule. This quantity would certainly be enough to assess purity via silver stained SDS PAGE and to assess binding kinetics using both SPR and ELISA. Quantities required for *in vitro* assays are also typically quite small and within nanomolar ranges, so yields of up to 15% (excluding the anomalous 20.1% yield) are high enough to be able to characterise the molecule and make conclusions on binding kinetics and stability. However, as a therapeutic molecule this yield is probably not acceptable, a comparable and relatable example of this would be Faricimab. A 50 µL dose of Faricimab contains 6 mg[197] of drug, to obtain 6 mg of a BsFpF **7**, assuming a yield of 10%, 60 mg of starting material (Fabs) would be needed, losing 54 mg of starting material to produce a single dose is unlikely to be acceptable.

Prior to performing any characterisation of BsFpFs **7** prepared via conjugation-ligation several control reactions were performed. In this case a control reaction is when an unreduced Fab with an intact disulfide bond are incubated together. SDS PAGE is then used to examine if any non-specific conjugation has occurred.

The control reactions were carried out as it was thought that impurities formed (Figure 54) during conjugation of Fabs to PEG *bis*-sulfone TCO **26** and PEG *bis*-sulfone Tz **27** were due to non-specific conjugation which could be pH sensitive Control reactions have been performed previously by our research group [148] using PEG based reagents containing a *mono*-sulfone conjugation moiety **3** with no non-specific conjugation occurring at a range of pHs between 6-8.6. Performing control reactions using PEG *bis*-sulfone TCO **26** and PEG *bis*-sulfone Tz **27** would allow comparison with previous work and help to better understand the behaviour of reagents **26** and **27** during conjugation. A pH scouting experiment focusing on the ligation between intermediates **28** and **29** was also performed. Reagent only reactions (Figure 45) had shown the ligation reaction was not sensitive to pH, it was therefore interesting to see if the presence of protein made any difference.

Control reactions and pH scouting experiments

Ranibizumab was incubated with PEG$_5$ *bis*-sulfone TCO **26** and PEG$_5$ *bis*-sulfone Tz **27** for 2 hours (Figure 57) at a range of different pHs (5-9). The accessible disulfide bond present in ranibizumab was not reduced prior to combination with reagent **26** and **27**. After a 2 hour incubation time faint bands at a molecular weight in excess of the parent Fab (approx. 55 kDa) are beginning to form at pHs 7, 8 and 9 (Figure 57, Lanes 5-7 and Lanes 10-12) for reactions with both reagents **26** and **27** with the greatest concentrations forming at pH 9 (Figure 57, Lanes 7 and 12).
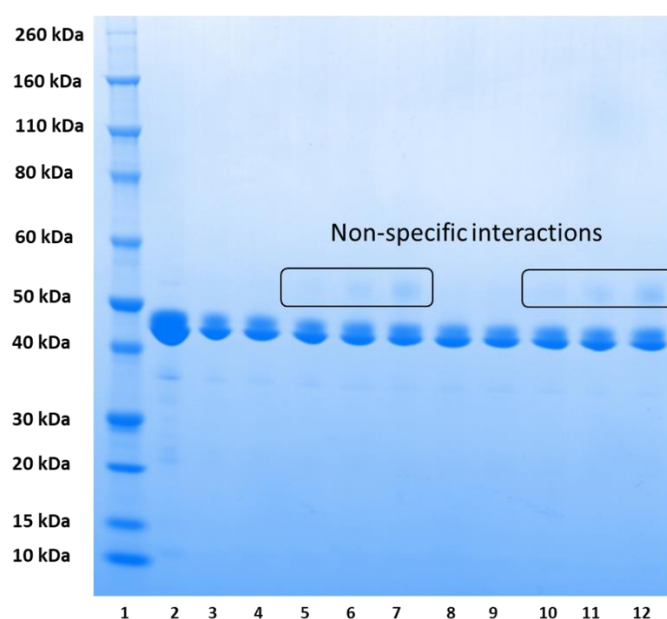
Figure 57 SDS PAGE gel showing results from control reactions of 0.3 mg ranibizumab per reaction (0.30 mg/mL) incubated with 1.5 eq. PEG$_5$ *bis*-sulfone TCO **26** and PEG$_5$ *bis*-sulfone Tz **27** at range of pHs, 2 hour reaction time. **Lane 1**: Protein marker, **2**: ranibizumab, **3**: PEG$_5$ *bis*-sulfone TCO **26** pH 5, **4**: pH 6, **5**: pH 7, **6**: pH 8, **7**: pH 9, **8**: PEG$_5$ *bis*-sulfone Tz **27** pH 5, **9**: pH 6, **10**: pH 7, **11**: pH 8, **12**: pH 9.

The presence of the faint band at approximately 55 kDa shows that nonspecific conjugations between Fab$_{rani}$ and PEG$_5$ *bis*-sulfone TCO **26** and PEG$_5$ *bis*-sulfone Tz **27** are occurring, likely involving lysine groups present on the surface of the Fab molecule. The greatest quantity of non-specific conjugation is seen at pH 9 because at this pH the surface lysine groups are deprotonated. The control reactions were left to incubate for 24 hours to see how the reactions proceeded with results being shown in Figure 58.
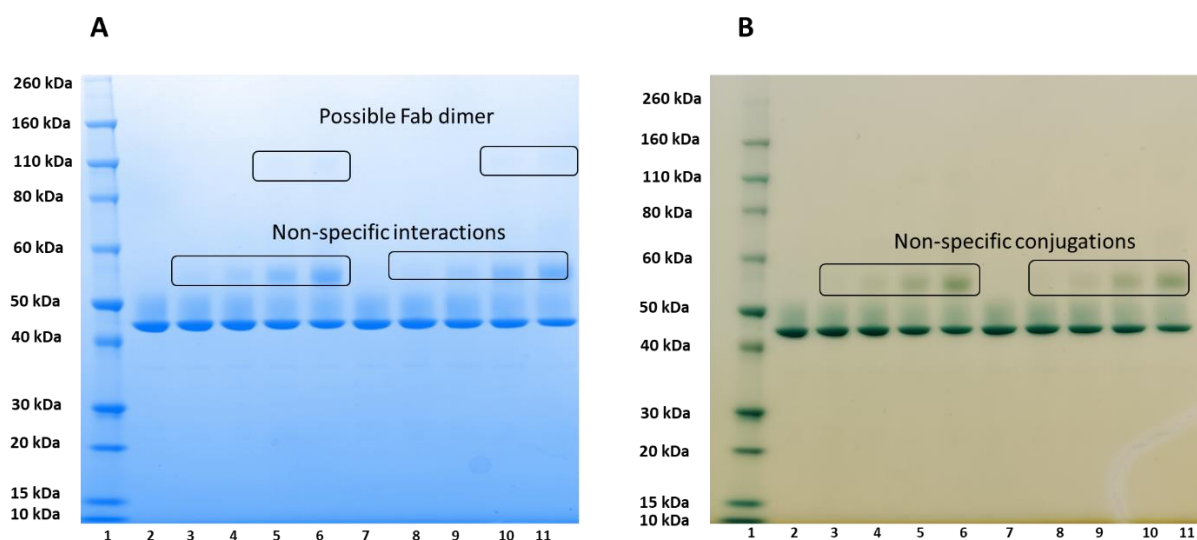
Figure 58: SDS PAGE gel showing results from control reactions of 0.3 mg ranibizumab per reaction (0.30 mg/mL) incubated with 1.5 eq. PEG$_5$ *bis*-sulfone TCO **26** and PEG$_5$ *bis*-sulfone Tz **27** at range of pHs, 24 hour reaction time, stained with Coomassie blue **(A)** and **(B)** barium iodide. **Lane 1**: Protein marker, **2**: PEG$_5$ *bis*-sulfone TCO **26** pH 5, **3**: pH 6, **4**: pH 7, **5**: pH 8, **6**: pH 9, **7**: PEG$_5$ *bis*-sulfone Tz **27** pH 5, **8**: pH 6, **9**: pH 7, **10**: pH 8, **11**: pH 9.

After incubation for 24 hours the nonspecific conjugation has continued to proceed at pHs 7, 8 and 9 as indicated by the increased concentration of the bands at approximately 55 kDa (Figure 58A, Lanes 4-6 and Lanes 9-11) for both reagent **26** and **27**. Within these lanes faint bands at a molecular weight of 110 kDa have begun to form which is likely a dimeric molecule containing 2 Fabs and a single molecule of reagents **26** and **27**. Faint bands (approximately 55 kDa) have also begun to form for control reactions performed at pH 6 (Figure 58A, Lanes 3 and 8).

Barium iodide staining was used to confirm that the bands at approximately 55 kDa (Figure 58A, Lanes 3-6 and Lanes 8-11) were a type of precursor Fab conjugate that had formed. The annotated bands (Figure 58B Lanes 3-6 and Lanes 8-11) turned a green colour whereas the remaining native Fab remained blue. The green colour formation is a mixture of brown PEG related and blue protein related bands, the presence of green bands indicates that conjugation, although non-specific, has occurred. Non-specific conjugations of Fab fragments with PEG *bis*-sulfone TCO **26** and PEG *bis*-sulfone Tz **27** reagents are not ideal as this behaviour can be unpredictable.

Control reactions between Fab$_{rani}$ and the PEG *bis*-sulfone TCO **26** and PEG *bis*-sulfone Tz **27** reagents show that non-specific conjugations are occurring, with most prevalence occurring at pH 8 and 9, higher than conditions in which conjugations

122

have typically been taking place (pH 7.6). This behaviour is different to what has been previously observed [148,161].

Another point of interest was the pH sensitivity of the iEDDA ligation reaction between the TCO **28** and Tz **29** functionalised Fab conjugates. Ranibizumab was conjugated to PEG_{10} *bis*-sulfone TCO **26** and PEG_5 *bis*-sulfone Tz **27** reagents. Intermediates **28** and **29** were purified using IEX and combined and allowed to ligate at a pH range of 5-9 (Figure 59, Lanes 2-6). pH had no impact upon the ligation reaction in the presence of protein. Bands of equal concentration were formed at pHs 5 through to 9 (Figure 59, Lanes 2-6). In addition to variation of pH ligations performed in which either the TCO **28** or Tz **29** functionalised Fab conjugates were in molar excess of each other (2:1 molar ratio) (Figure 59, Lanes 7 and 8) showed that the presence of either intermediate **28** or **29** in excess had no impact on FpF yield, with band concentrations being of similar intensity. Lastly a ligation reaction was performed at pH 7 but at an elevated temperature of 37°C (Figure 59, Lane 9). Again elevated temperature had little impact upon the ligation reaction with the formed band being of similar concentration to the band formed during the ligation reaction at the same pH (Figure 59, Lane 4) but at ambient temperature.
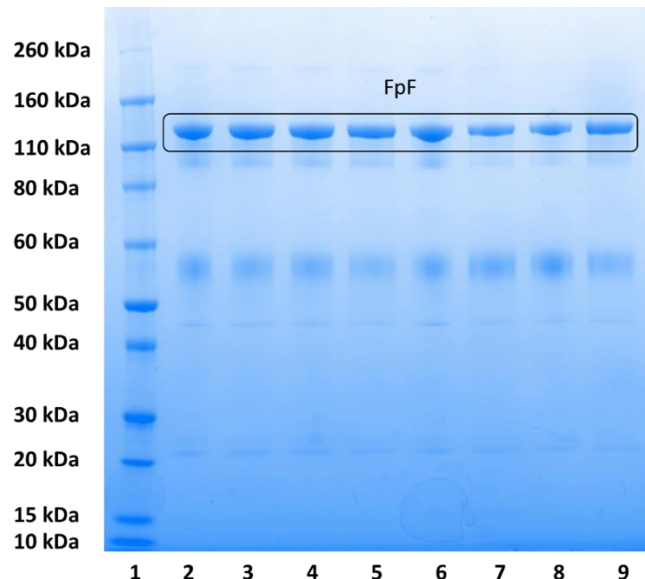
Figure 59: SDS PAGE gel showing results from ligation scouting reactions between TCO **28** and Tz **29** functionalised Fab_{rani} at a range of pHs, intermediate excesses and elevated temperature, 2 hour reaction time. **Lane 1**: Protein marker, **2**: pH 5, **3**: pH 6, **4**: pH 7, **5**: pH 8, **6**: pH 9, **7**: 2:1 TCO **28** functionalised Fab conjugate: Tz **29** functionalised Fab conjugate, **8**: 2:1 Tz **29** functionalised Fab conjugate: TCO **28** functionalised Fab conjugate, **9**: 1:1 ratio of TCO **28** functionalised Fab conjugate and Tz **29** functionalised Fab conjugate, pH 7 at 37°C.

The experiment performed (Figure 59) showed that the ligation reaction in the presence of protein is not pH sensitive, which is consistent with reagent only ligation

reactions (Figure 45). Incubation time was extended to 24 hours with no change in the concentrations of FpFs for all conditions examined, meaning that the ligation reaction between intermediates **28** and **29** proceeds to completion within 2 hours.

An ideal result would have been to determine an optimum condition for the ligation reaction to improve FpF yield. What can be taken from this experiment is that the ligation reaction is robust and does not require exacting conditions to proceed. Another thought was to attempt to prepare a BsFpF using an alternative methodology leveraging results observed during initial attempts to prepare a FpF via conjugation-ligation (Figure 48). Observations showed that a large molecule (intermediate **28** or **27**) has preference to ligate to a smaller molecule (reagent **26** or **27**).

Preparation of a BsFpF using an alternative methodology

Up to this point BsFpFs have been prepared by conjugating 2 different Fabs to PEG *bis*-sulfone TCO **26** and PEG *bis*-sulfone Tz **27** reagents and the subsequent ligation of the resulting TCO **28** and Tz **29** functionalised Fab conjugates. Alternatively, a different methodology (Scheme 13) was proposed.
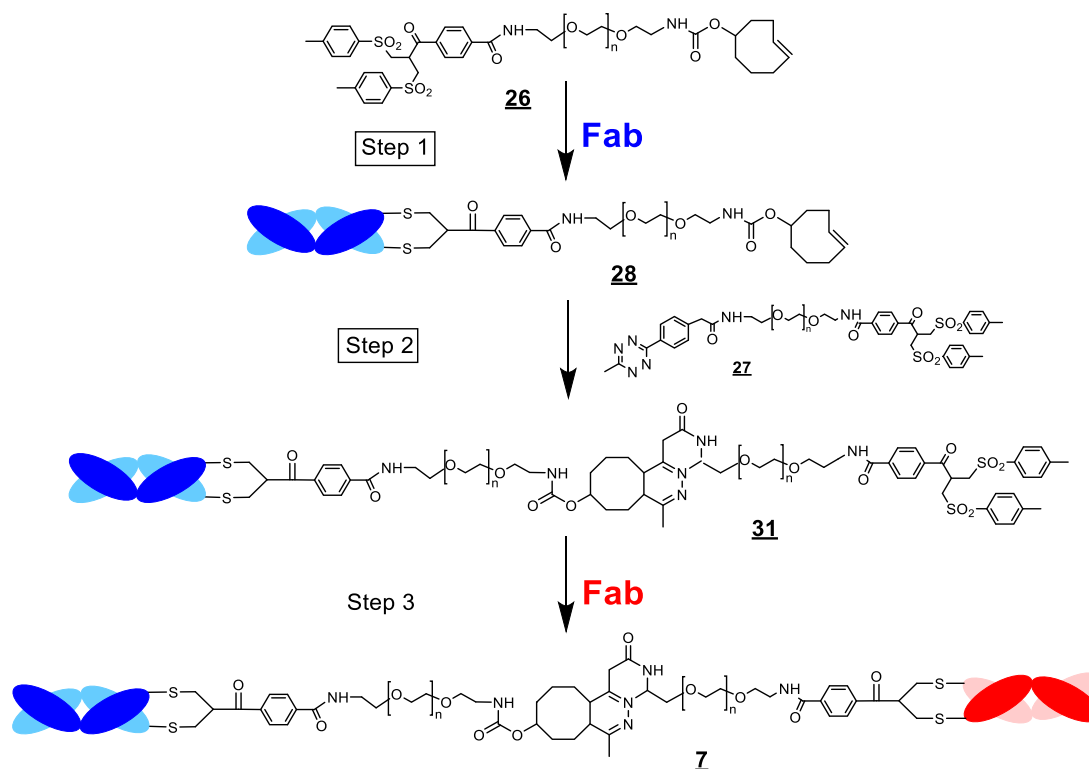
Scheme 13: Preparation of a BsFpF **7** via an alternative methodology. A TCO functionalised Fab conjugate is prepared by conjugating a Fab to PEG *bis*-sulfone TCO **26**. Intermediate **28** is ligated to PEG *bis*-sulfone Tz **27** to form a Fab PEG TCO-Tz PEG *bis*-sulfone intermediate **31**. A second, non-identical Fab is then conjugated to the free *bis*-sulfone group present in intermediate **31** to prepare a BsFpF **7**.

A TCO functionalised Fab conjugate **28** is prepared via conjugation of Fab_1 to PEG *bis*-sulfone TCO **26**. Intermediate **28** is ligated to a PEG *bis*-sulfone Tz **27** reagent to prepare a Fab PEG TCO-Tz PEG *bis*-sulfone intermediate **31**. Finally, Fab_2 is reduced and introduced to intermediate **31** to prepare the final BsFpF **7**. The ligation between the TCO functionalised Fab conjugate **28** and PEG *bis*-sulfone Tz **27** is seen as the most interesting part of this methodology as it tries to exploit the preference of something large (intermediate **28**) preferentially ligating to something small (reagent **27**). It was thought that exploiting this preference would drive the formation of intermediate **31**. If large quantities of intermediate **31** did indeed form, plenty of BsFpF **7** should form upon incubation of intermediate **31** with reduced Fab_2 via the free *bis*-sulfone conjugation moiety.

An attempt to prepare a BsFpF using the methodology outlined in Scheme 13 was performed (Figure 60). Ranibizumab was conjugated to a PEG_{10} *bis*-sulfone TCO **26** to form the required TCO functionalised Fab conjugate **28** (Figure 60, Lane 4). Intermediate **28** was purified using IEX (Figure 60, Lane 5) to remove free reagent **26** and any HMW impurities. Upon incubation of intermediate **28** with 1.5 molar equivalents of PEG_5 *bis*-sulfone Tz **27** (Figure 60, Lane 6) the intended Fab PEG TCO-Tz PEG *bis*-sulfone intermediate **31** formed, indicated by the appearance of a band at approximately 70 kDa, more than the molecular weight of intermediate **28** (approximately 60 kDa MW). Intermediate **31** was purified using IEX to remove any free PEG_5 *bis*-sulfone Tz **27**.

Intermediate **31** was quantified using micro-BCA to allow a suitable quantity of Fab_{Tocili} to be used during conjugation. A quantity of Fab_{Tocili} was reduced and incubated with intermediate **31** at pH 7.6 for 18 hours, this led to formation of a BsFpF **7** (Figure 60, Lane 7). To remain consistent with the conjugation reaction to prepare the TCO functionalised Fab conjugate **28,** the amount of Fab_{Tocili} used was set to ensure intermediate **31** was in a 1.5 molar excess of reduced Fab.
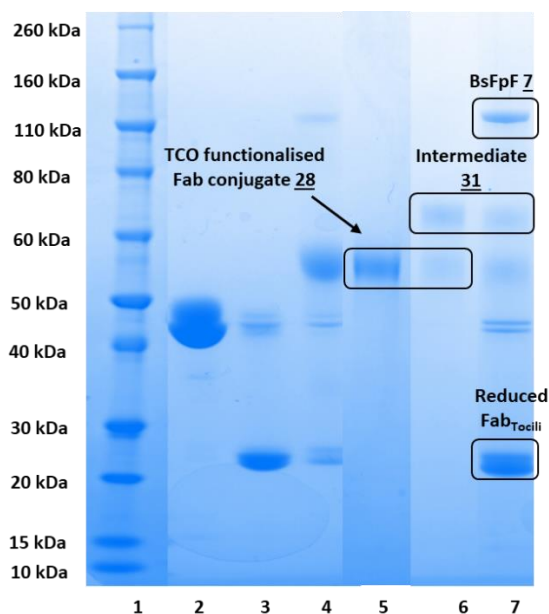
Figure 60: An SDS PAGE gel showing the preparation of a BsFpF **7** using an alternative method. **Lane 1:** Protein marker, **2:** ranibizumab, **3:** reduced ranibizumab, **4:** conjugation of reduced ranibizumab to 1.5 eq. PEG$_{10}$ *bis*-sulfone TCO **26**, pH 7.6, 18 hours, **5:** purified TCO functionalised Fab$_{rani}$ conjugate **28**, **6:** Ligation of intermediate **28** to PEG$_5$ *bis*-sulfone Tz **27**, **7:** conjugation of reduced Fab$_{Tocili}$ to the Fab$_{rani}$ PEG TCO-Tz PEG *bis*-sulfone intermediate **31**.

Visually the yield of BsFpF **7** (Figure 60, Lane 7) was no greater than BsFpFs **7** prepared using the standard conjugation-ligation methodology which was disappointing and meant that this methodology was not adopted Visually comparing 2 different SDS PAGE gels may not have been the best way to compare between the 2 methodologies. A better way would have been to use an internal standard to quantitatively compare. However, some interesting observations could be made from this experiment. During the ligation (Figure 60, Lane 6) of intermediate **28** to PEG$_5$ *bis*-sulfone Tz **27** not all of intermediate **28** was consumed despite reagent **27** being added in a 1.5 molar excess. Also, after the conjugation (Figure 60, Lane 7) between intermediate **31** and reduced Fab$_{Tocili}$ an amount of intermediate **31** remained despite the Fab also being added in excess. Intermediate **28** and intermediate **31** should have been completely consumed during the respective ligation (Figure 60, Lane 6) and conjugation (Figure 60, Lane 7) reactions, the source of the incomplete conversion is likely to be the purity of the PEG *bis*-sulfone TCO **26** and PEG *bis*-sulfone Tz **27** reagents which could also help to explain why final purified BsFpF yields (Table 10) do not exceed 15%.

The synthesised PEG *bis*-sulfone TCO **26** and PEG *bis*-sulfone Tz **27** reagents are likely mixtures of 3 different molecules (Figure 61). Taking the PEG *bis*-sulfone TCO **26** as an example there is likely a mixture of the desired reagent **26**, a PEG X

126

TCO molecule **32** and finally a PEG *bis*-sulfone X molecule **33**. The X in the reagent names is used to signify dead, unreactive chain ends.

26

32

33
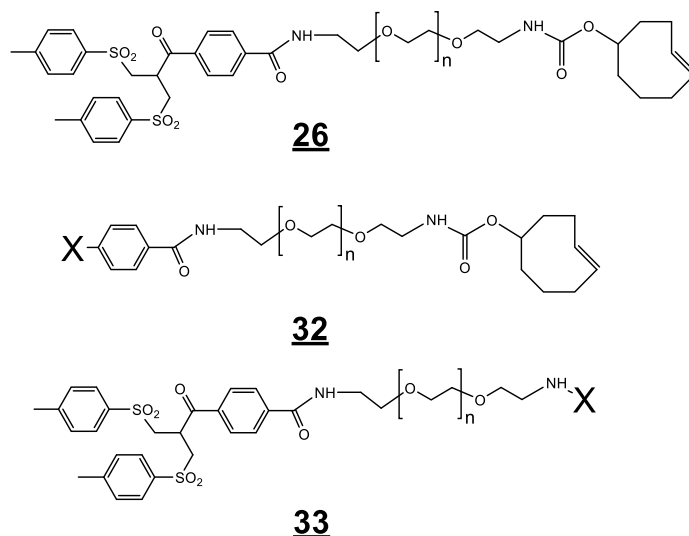
Figure 61: Chemical structure of PEG *bis*-sulfone TCO **26**, PEG X TCO **32** and PEG *bis*-sulfone X **33**. PEG X TCO **32** can ligate but not conjugate, PEG *bis*-sulfone X **33** is able to conjugate but not ligate.

PEG X TCO **32** would influence the yield of TCO functionalised Fab conjugate **28** as it lacks the *bis*-sulfone moiety **1** required for conjugation. To put this into perspective if 1.5 eq. of PEG *bis*-sulfone TCO **26** was used in a conjugation reaction, only a proportion of the added reagent **26** would contain the required *bis*-sulfone moiety **1**. Say the ratio of reagent **26** to impurity **32** was 1:1 (0.75 eq. reagent **26**, 0.75 eq. impurity **32**). This would mean Fab would be in excess of PEG *bis*-sulfone TCO **26**. At most, assuming an optimistic efficiency of 100%, only 75% of the reduced Fab would be able to conjugate, limiting the yield of TCO functionalised Fab conjugate **28**. As demonstrated earlier in this chapter (Figure 49) the quantity of TCO functionalised Fab conjugate **28** is key in maximising the final yield of FpF.

The incomplete consumption of the TCO functionalised Fab conjugate **28** (Figure 60, Lane 6) during ligation to PEG$_5$ *bis*-sulfone Tz **27** is likely due to PEG *bis*-sulfone X **33**. During the conjugation of Fab$_{rani}$ to PEG$_{10}$ *bis*-sulfone TCO **26** two different intermediates have likely formed (Figure 62), the desired TCO functionalised Fab conjugate **28** and a Fab conjugate lacking the TCO ligating moiety **34** (Fab$_{rani}$ + PEG *bis*-sulfone X **33**).
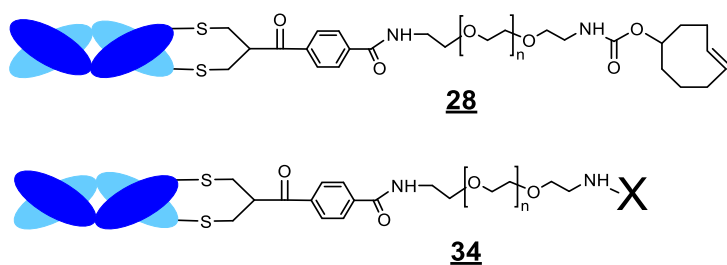
Figure 62: Chemical structure of a TCO functionalized Fab conjugate **28** and a Fab conjugate lacking a TCO ligating moiety **34**. Impurity **34** is not able to undergo ligation reactions.

Fab conjugate **34** is not able to ligate as it lacks the required TCO moiety. Therefore, when conjugate **34** is incubated with PEG *bis*-sulfone Tz **27** the ligation reaction would not occur. It is likely that conjugate **34** is responsible for the band observed at approximately 55 kDa in Figure 60, Lane 6. SDS PAGE would not be able to discern between conjugate **28** and conjugate **34** because of the similarities in molecular weight. A more appropriate technique may be Matrix-Assisted Laser Ionisation-Time-of-Flight (MALDI-TOF) which can be used to directly measure molecular weight of antibodies with great accuracy [198].

The incomplete conversion of intermediate **31** to BsFpF **7** (Figure 60, Lane 7) occurs due to the PEG *bis*-sulfone Tz **27** containing a similar mixture of impurities (Figure 63) as the PEG *bis*-sulfone TCO **26** reagent.
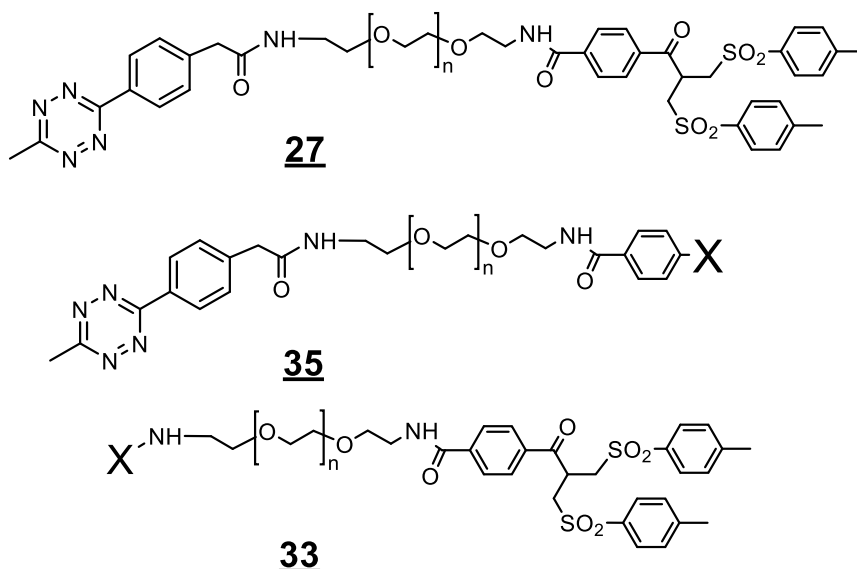
Figure 63: Chemical structure of PEG *bis*-sulfone Tz **27**, PEG X Tz **35** and PEG *bis*-sulfone X **33**. PEG X Tz **35** can ligate but not conjugate, PEG *bis*-sulfone X **33** is able to conjugate but not ligate.

During the ligation of the TCO functionalised Fab conjugate **28** to PEG *bis*-sulfone Tz **27** (Figure 60, Lane 6) a mixture of conjugates forms, including the desired Fab PEG TCO-Tz PEG *bis*-sulfone intermediate **31** and a Fab PEG TCO-Tz PEG X impurity **36** (Figure 64), which does not contain a free *bis*-sulfone moiety **1** and therefore is not capable of conjugating to a second reduced Fab. This explains why a

128

band corresponding to intermediate **31** remains (Figure 60, Lane 7) even when it is incubated with an excess of Fab, the band for intermediate **31** is a mixture of the two molecules illustrated in Figure 64.
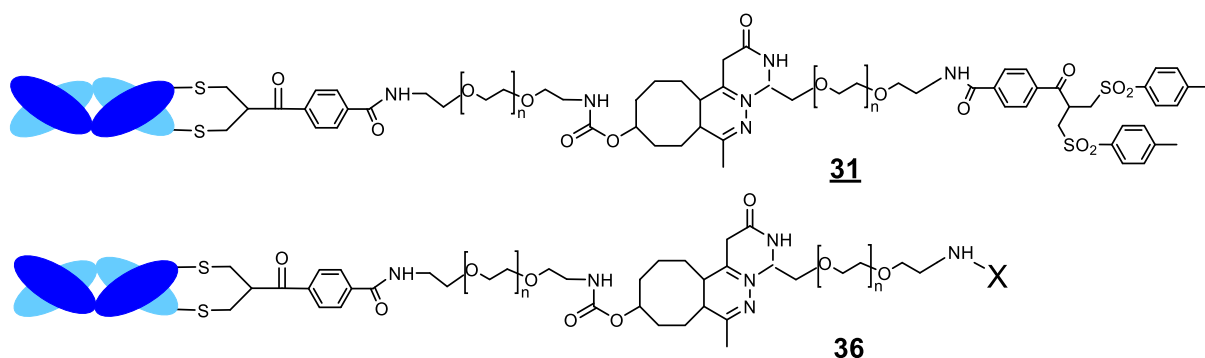
Figure 64: Chemical structure of a Fab PEG TCO-Tz PEG *bis*-sulfone intermediate **31** and Fab PEG TCO-Tz PEG X **36** impurity. Impurity **36** is not able to conjugate to a Fab due to a lack of the *bis*-sulfone **1** group.

Discussion of the results presented in Figure 60 prove that the purity of the PEG *bis*-sulfone TCO **26** and PEG *bis*-sulfone Tz **27** reagents limits the yield of final purified BsFpF that can be obtained. Impurities present in reagents **26** and **27** limit the yield of TCO **28** and Tz **29** functionalised Fab conjugate, which in turn limits FpF yield when intermediates **28** and **29** are combined and allowed to ligate. Once reagent synthesis improves, leading to purer reagents, yields should begin to increase, HPLC purification is a way that the di-functional reagents could be purified prior to use in conjugation and subsequently ligation experiments. Moving forward, experimentation characterising FpFs including BsFpFs **7** prepared via conjugation-ligation were performed.

Stability of an FpF and BsFpF prepared via conjugation-ligation

The stability of a monospecific anti-VEGF FpF prepared via conjugation-ligation was assessed by storing the conjugate for 6 months (24 weeks) at a storage temperature of 5°C. The anti-VEGF FpF was prepared via conjugation-ligation using ranibizumab as the source of Fab. Prior to setting down the anti-VEGF FpF on stability the molecule was treated with sodium triacetoxyborohydride (STAB) to stabilise the conjugate by reducing the linker carbonyl group to an alcohol group. This is a key step as it can prevent a potential de-conjugation occurring between the PEG polymer backbone and Fab via a retro-Michael addition reaction.

The anti-VEGF FpF was set down on stability in a partially formulated state. A 0.1% w/v concentration of Tween 20 was added to the FpF solution (PBS, pH 7.2).

Tween 20 is a non-ionic surfactant with prevalence of use in therapeutic antibody formulations [199] and can limit protein aggregation by providing a steric shielding effect, in essence the surfactant coats surfaces and provides a physical barrier to interactions. Samples of the anti-VEGF FpF were taken at pre-determined time points and characterised using SDS PAGE (Figure 65).
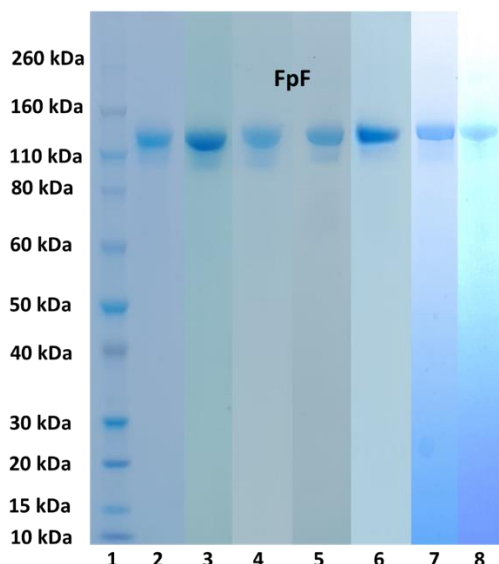
Figure 65: An SDS PAGE gel showing results from the storage of a monospecific anti-VEGF (derived from ranibizumab) FpF at 5°C for 24 weeks at a concentration of 0.2 mg/mL, treated with STAB prior to stability set down. The FpF was set down dissolved in PBS (pH 7.2) with 0.1% w/v Tween 20. **Lane 1:** Protein marker, **2:** Initial timepoint, **3:** 1 week timepoint, **4:** 2 weeks, **5:** 4 weeks, **6:** 6 weeks, **7:** 12 weeks, **8:** 24 weeks.

The anti-VEGF FpF remained physically stable for up to 24 weeks (6 months), no signs of aggregation or de-conjugation were observed. If aggregation of two FpFs had occurred a band at a molecular weight of approximately 230 kDa would be visible. The covalent bond formed during ligation reaction is stable as no bands corresponding TCO **27** or Tz **28** functionalised Fab conjugates are present. If the covalent bond formed during ligation had broken two bands would appear on the gel, one at 60 kDa and another at 55 kDa.

Next a storage temperature of 37°C was assessed as this simulates internal body temperature and gives an indication of the stability of the FpF post dosing. Figure 66 shows an SDS PAGE gel of same anti-VEGF FpF after storage at 37°C for 4 weeks. Despite antibodies having intravitreal half-lives of approximately 7 days [73] the study at 37°C was extended to 28 days as it is feasible for patients to have monthly injections of anti-VEGF therapeutics [73]. The study would have been extended beyond 28 days but was halted due to a lack of material.
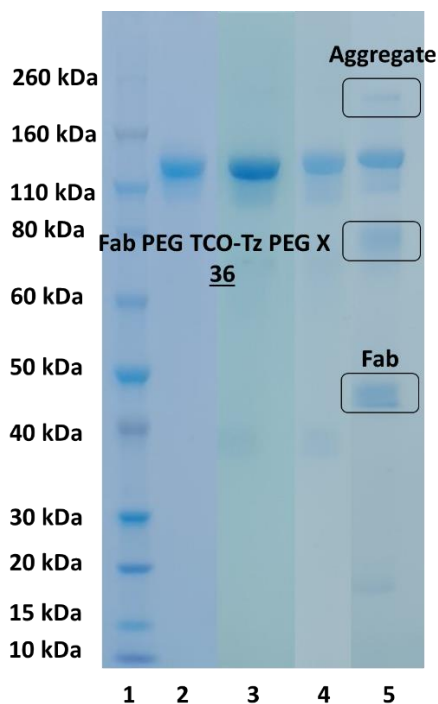
Figure 66: An SDS PAGE gel showing results from the storage of a 0.2 mg/mL monospecific Anti-VEGF (derived from Fab$_{Rani}$) FpF at 37°C for 28 days, treated with STAB prior to stability set down. The FpF was set down dissolved in PBS (pH 7.2) with 0.1% w/v Tween 20 **Lane 1:** Protein marker, **2:** Initial timepoint, **3:** 7 days, **4:** 14 days, **5:** 28 days.

Unlike storage at 5°C, degradation of the anti-VEGF FpF did occur after being stored for 28 days at 37°C (Figure 66, Lane 5). A faint band at approximately 240 kDa is likely an aggregate in which 2 FpF molecules (120 kDa each) are entangled with each other. Aggregation of monoclonal antibodies tends to occur when partial unfolding of the tertiary structure occurs exposing residues which can allow monomers to aggregate [200]. Antibody aggregation can be accelerated by an increase in temperature [201]

Evidence of Fab dissociation is also present as indicated by the faint band (Figure 66, Lane 5) with a molecular weight of just less than 80 kDa which corresponds to a Fab PEG TCO-Tz PEG X **36** impurity. It is assumed that the STAB reaction was not entirely effective and did not proceed to completion allowing some retro Michael-addition reactions to occur. Despite some evidence of instability, a relatively large amount of the parent anti-VEGF FpF (Figure 66, Lane 5, band at approximately 120 kDa MW) remains intact.

A stability study at 5°C was also carried out with an anti-VEGF/IL-6R BsFpF. The BsFpF was prepared via conjugation ligation using ranibizumab and Fab$_{Tocili}$ as the source of Fabs. This study ran for 24 weeks with samples being collected at pre-determined timepoints and assessed using SDS PAGE. SDS PAGE showed that the anti-VEGF/IL-6R BsFpF remained stable after 24 weeks storage at 5°C (Figure 67). No signs of BsFpF aggregation or deconjugation were detected.

131
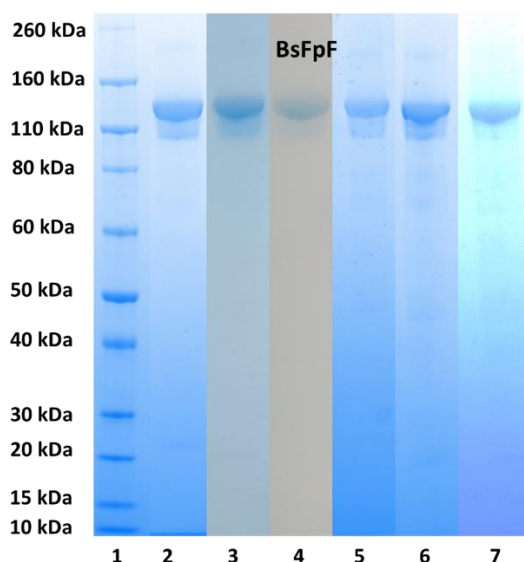
Figure 67: An SDS PAGE gel showing results from the storage of a 0.5 mg/mL Anti-VEGF/IL-6R (derived from ranibizumab and Fab$_{tocili}$) BsFpF FpF at 5°C for 24 weeks , treated with STAB prior to stability set down. The FpF was set down dissolved in PBS (pH 7.2) with 0.1% w/v Tween 20 **Lane 1:** Protein marker, **2:** Initial, **3:** 2 weeks, **4:** 4 weeks, **5:** 8 weeks, **6:** 12 weeks, **7:** 24 weeks.

Further characterization of BsFpFs, specifically measuring their affinity to their intended targets is presented in Chapter 5. The next section of this chapter presents efforts to prepare a bivalent bispecific molecule, a construct which is distinct from a BsFpF.

Attempts to prepare a bivalent bispecific molecule

A monospecific IgG antibody is a bivalent molecule containing two identical binding arms. Bivalency allows a single IgG to bind to more of its intended target leading to greater target neutralisation [202] compared to a monovalent Fab. The BsFpFs prepared during this research are monovalent molecules mimicking approved bispecific therapeutics such as Faricimab. Faricimab is a monovalent bispecific containing one anti-VEGF and one anti-ANG-2 binding arm. The use of ligation reactions is not exclusive to fab fragments. Wagner et al. [203] synthesised a bispecific antibody from full length monospecific IgG molecules using a combination of sortase transpeptidation and click chemistry. The conjugation of the IgG molecules occurred at the C-terminus creating a C-C fused IgG heterodimer. Using this methodology two anti-influenza A antibodies with activities against different virus subgroups were linked to form a bispecific. The bispecific retained the anti-viral activities of the two parent monospecific antibodies.

It was proposed to try and prepare a bivalent bispecific molecule which would contain 2 binding arms for target A and 2 binding arms for target B (Scheme 14).
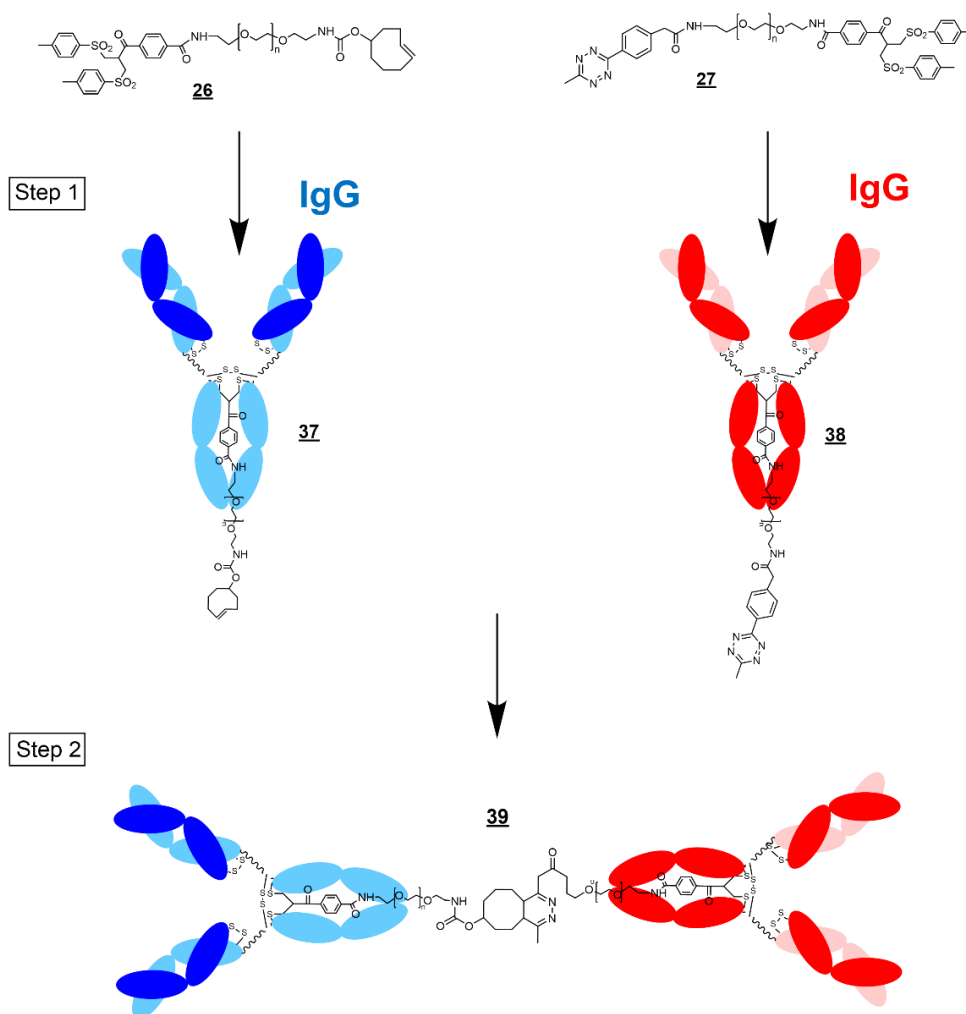
Scheme 14: Preparation of a Bivalent bispecific molecule **39** via conjugation ligation. An IgG is conjugated to PEG *bis*-sulfone TCO **26** to prepare a TCO functionalised IgG **37**. A second IgG is conjugated to PEG *bis*-sulfone Tz **27** to form a Tz functionalised IgG **38**. In this example conjugation of reagents **26** and **27** to both IgGs has occurred at one of the hinge disulfide bonds. Intermediates **37** and **38** are combined and allowed to ligate to form a bivalent bispecific molecule **39**. The bivalent bispecific **39** would have a molecular weight of approximately 300 kDa.

The proposed method of preparation is similar to the scheme proposed for the conjugation-ligation of Fabs (Scheme 12) to prepare a BsFpF with the only difference being the use of complete IgGs. Using complete IgGs for this methodology does create some complexity. IgG antibodies contain four reducible disulfide bonds available for conjugation. Reduction of IgGs with DTT causes all four of the disulfide bonds to reduce. Therefore, it would be possible and probable for multiple molecules of either reagent **26** or **27** to conjugate to a single IgG, Scheme14 outlines a scenario in which a single molecule of reagent **26** or **27** has conjugated to an IgG. The initial strategy for the preparation of bivalent bispecific **39** involved using 1.5 eq. of PEG *bis*-sulfone TCO **26** and PEG *bis*-sulfone Tz **27** for conjugation with the hope that a low eq. of reagent

would favour the formation of a mono conjugated IgG (an IgG conjugated to a single molecule of reagent **26** or **27**).

Infliximab and tocilizumab were conjugated (Figure 68A, Lanes 3 and 5) to 1.5 eq. of PEG$_{10}$ *bis*-sulfone TCO **26** and PEG$_5$ *bis*-sulfone Tz **27**. TCO **37** and Tz **28** functionalised IgGs were formed as an increase in molecular weight was observed (Figure 68A, Lanes 3 and 5) when compared to the source infliximab and tocilizumab (Figure 68A, Lanes 2 and 4). Intermediates **37** and **38** were combined (Figure 68A, Lane 6) and allowed to ligate for 18 hours. A band at a notably higher molecular weight did form. This could be because of ligation between intermediates **37** and **38**. The ligation reaction mixture was purified using SEC (Figure 68B). The highlighted band (Figure 68B, Lane 4) in excess of 260 kDa could be the desired molecule of interest **39**. Visually the yield is quite low as indicated by the intensity of the band.
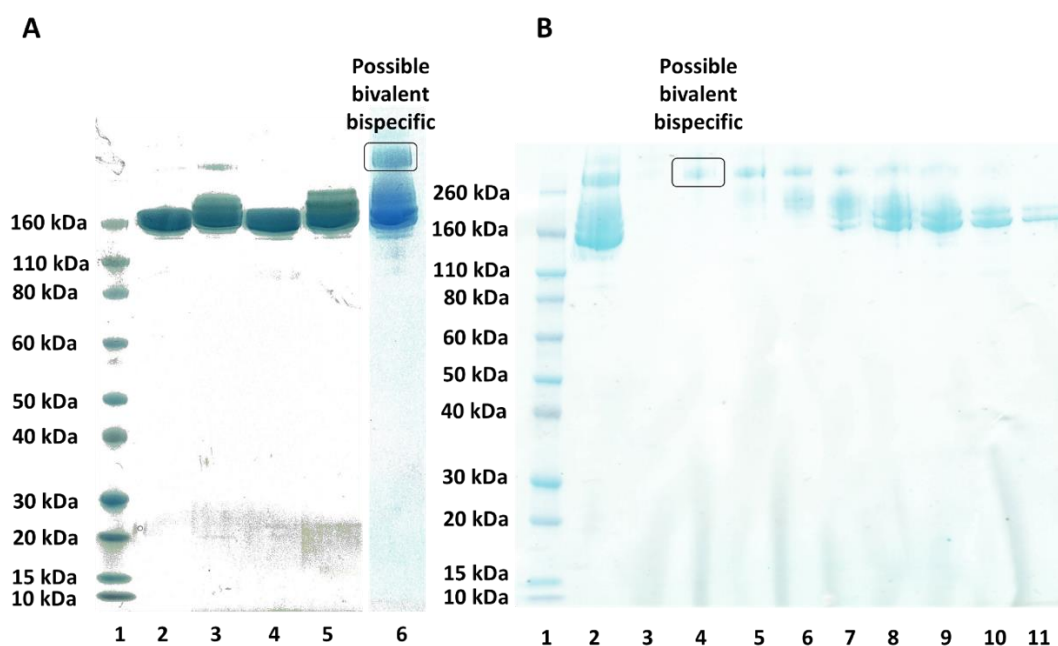
Figure 68: **(A)** SDS PAGE gel showing conjugation of 1 mg tocilizumab (0.30 mg/mL) and 1mg (0.30 mg/mL) infliximab to 1.5 eq. of PEG$_5$ *bis*-sulfone Tz **27** and PEG$_{10}$ *bis*-sulfone TCO **26**, pH 7.6, 18 hours and ligation of the formed TCO **37** and Tz **38** functionalised IgGs. **(B)** SEC purification of the ligation reaction mixture (Figure 68A, Lane 6). **(A) Lane 1:** Protein marker, **2:** infliximab, **3:** infliximab, 1.5 eq. PEG$_5$ *bis*-sulfone Tz **27**, **4:** tocilizumab, **5:** tocilizumab, 1.5 eq. PEG$_{10}$ *bis*-sulfone TCO **26**, **6:** ligation of intermediates **37** and **38**. **(B) Lane 1:** protein marker, **2:** ligation mixture (Figure 68A, lane 6), **3:** SEC fraction 1 (F1), **4:** F2, **5:** F3, **6:** F4, **7:** F5, **8:** F6, **9:** F7, **10:** F8, **11:** F9.

Another attempt to prepare a bispecific bivalent molecule **39** was made (Figure 69) using infliximab and secukinumab as the source of IgGs. Infliximab and secukinumab were used due to their availability at the time. Two different conjugations were performed using secukinumab and tocilizumab. One set of conjugations used 1.5 eq. of reagents **26** and **27** (Figure 69A, Lanes 2 and 4) and the other set 4 eq. of reagents **26** and **27**. 4 eq. of reagents **26** and **27** were added to try and conjugate all 4 of the IgG disulfide bonds to try and increase the amount of TCO **37** and Tz **38** functionalised IgGs prepared, which when subsequently ligated may lead to greater formation of a bivalent bispecific **39**. It was evident that using 4 eq. (Figure 69, Lanes 3 and 5) of reagents **26** and **27** increased the quantity of TCO **37** and **38** IgG conjugates that were formed, compared to when 1.5 eq. was used (Figure 69, Lanes 2 and 4), as a greater concentration of bands in excess of 160 kDa were present. The bands are not well defined and appear more like a smear, this is likely because a mixture of mono, di and multi conjugated IgGs has formed due to 4 eq. of reagents **26** and **27** being used.
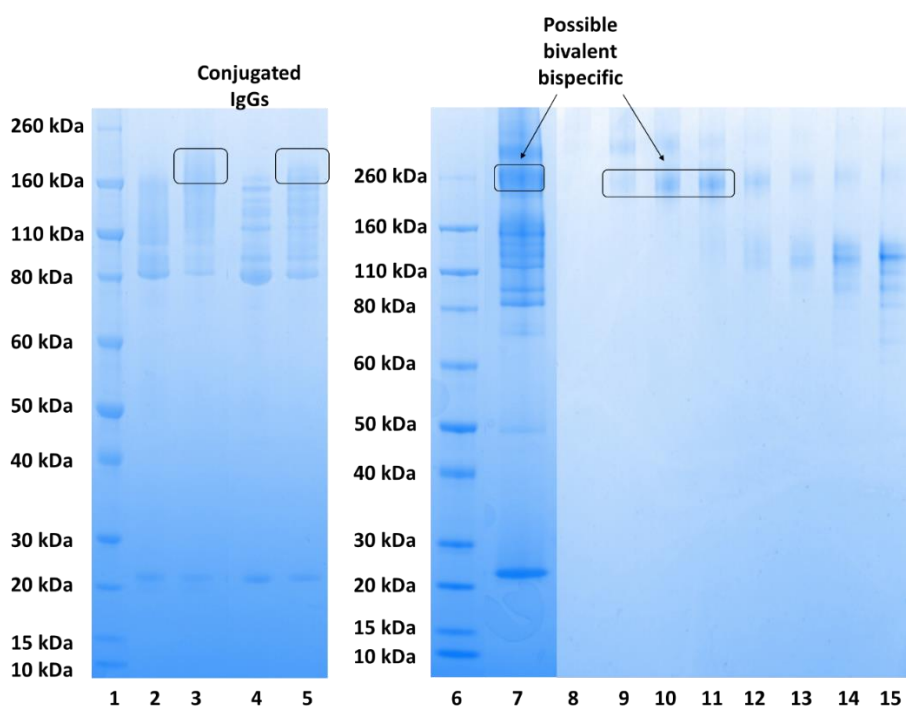
Figure 69: SDS PAGE gel showing conjugation of 1 mg (0.30 mg/mL) secukinumab to 1.5 eq. and 4 eq. of PEG$_{10}$ *bis*-sulfone TCO **26** and 1 mg tocilizumab (0.30 mg/mL) to 1.5 eq. and 4 eq. PEG$_5$ *bis*-sulfone Tz **27**, pH 7.6, 18 hours, ligation of the formed TCO **37** and Tz **38** functionalised IgGs and SEC purification of the ligation reaction mixture. **Lane 1:** Protein marker, **2:** secukinumab, 1.5 eq. PEG$_{10}$ *bis*-sulfone TCO **26** , **3:** secukinumab, 4 eq. PEG$_{10}$ *bis*-sulfone TCO **26**, **4:** tocilizumab, 1.5 eq. PEG$_5$ *bis*-sulfone Tz **27** **5:** tocilizumab, 4 eq. PEG$_5$ *bis*-sulfone Tz **27**. **6:** protein marker, **7:** ligation mixture, **8:** SEC fraction 1 (F1), **9:** F2, **10:** F3, **11:** F4, **12:** F5, **13:** F6, **14:** F7, **15:** F8.

The TCO **37** and Tz **38** functionalised IgGs prepared using 4 eq. of reagents **26** and **27** were combined and allowed to ligate forming a number of bands in excess of 260 kDa (Figure 69, Lane 7). One band has been annotated as it was thought this may be the bivalent bispecific **39**. Bands with higher molecular weights are also present in Lane 7. Ligation between TCO **37** and Tz **38** functionalised IgG conjugates containing multiple reagent molecules are likely responsible for this. For example, if a TCO functionalised IgG **37** was a conjugate containing 2 molecules of reagent **26** it could ligate to 2 Tz functionalised IgGs **38** creating a trivalent molecule with a molecular weight of around 500 kDa. The ligation reaction mixture (Figure 69, Lane 7) was purified using SEC with the purification not being particularly successful, as when the fractions were analysed using SDS PAGE (Figure 69, Lanes 8-15) multiple bands were present in each fraction.

The results presented in Figures 68 and 69 indicate that it may be possible to prepare a bivalent bispecific **39** using conjugation-ligation. However, it was thought that the bivalent bispecific **39** could be modified to make it more suitable for use as a potential intra-ocular therapy, it was proposed to try and remove the Fc region from the bivalent bispecific **39** to prepare a bispecific Fab2 (BsFab2, Figure 70) **40**
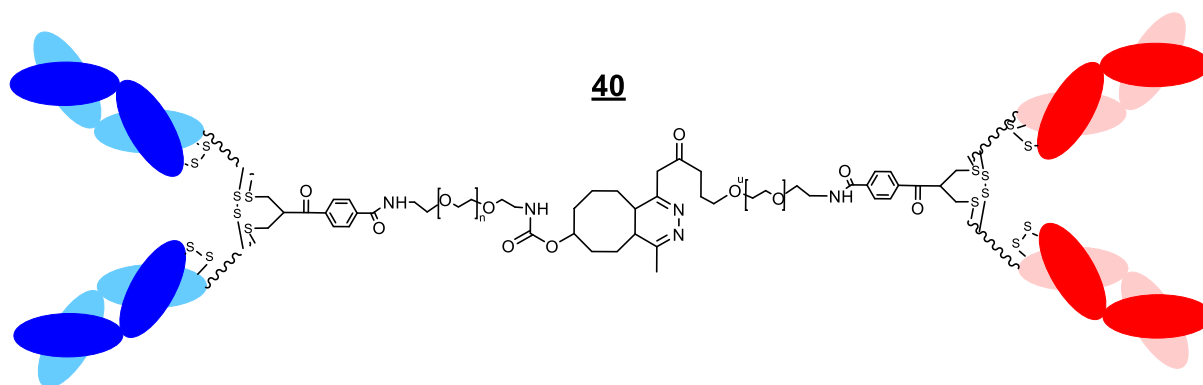
Figure 70: Structure of a bispecific Fab2 (BsFab2) molecule **40** with an estimated molecular weight of approximately 200 kDa.

Attempts to prepare a bispecific Fab2 _40_ via conjugation ligation and digestion with Pepsin

Neonatal Fc receptors (FcRn) are expressed within the eye [204] which may affect the half-life and distribution of molecules containing Fc which are injected intravitreally. One route of IgG elimination from the eye is via the central retinal vein, IgGs eliminated via this route enter systemic circulation. Removal of the Fc would reduce systemic half life post ocular elimination and also eradicate any potential pro-inflammatory effector functions [205], Faricimab has its Fc functionality disabled via amino acid exchange during development for these reasons [205].

Performing amino acid exchange was not a viable option to disable the Fc functionality of the bivalent bispecific **39**. Instead, it was proposed to remove the Fc region via enzymatic digestion. One enzyme that can perform this task is pepsin. Pepsin digests IgGs below the hinge region yielding a Fab2 molecule. This enzyme could be used to digest the bivalent bispecific **39** to prepare an Fc free molecule. Digestion of the ligation reaction mixture would reduce the molecular weight of all components of the mixture which may allow for easier purification using SEC. Before trying to digest a bivalent bispecific **39,** pepsin was used to digest an unmodified IgG, in this case tocilizumab, (Figure 71)
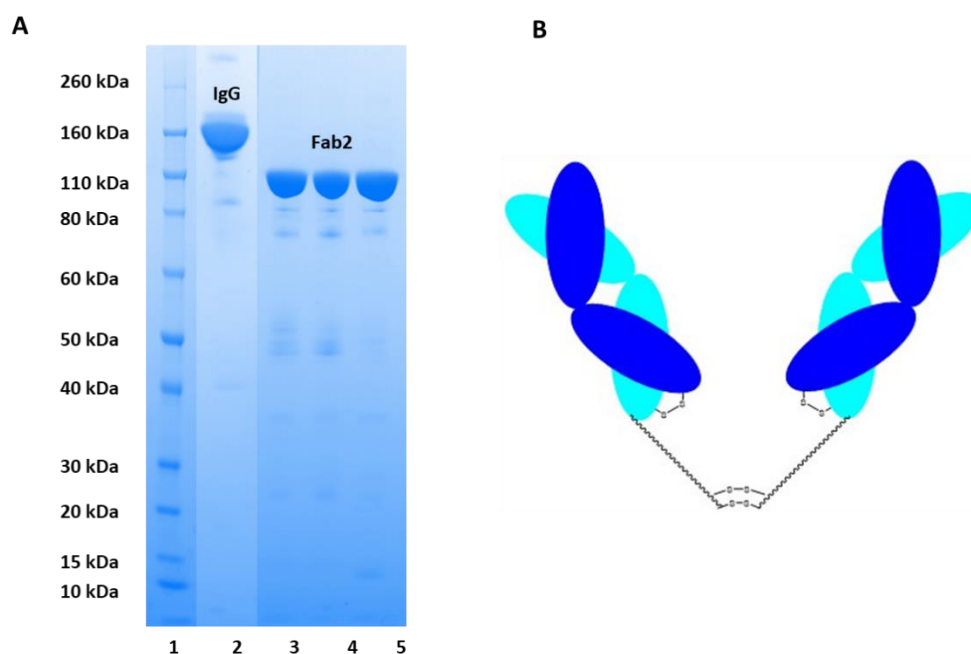
Figure 71: (A) SDS PAGE gel showing results from digestion of 1 mg tocilizumab (1 mg/mL) with soluble pepsin at pH 3, 3.5 and 5, 37°C, 15-hour digestion time. **Lane 1:** Protein marker, **2:** parent tocilizumab, **3:** pH 3.0, **4:** pH 3.5, **5:** pH 4.0 **(B)** The structure of a Fab2 molecule.

Tocilizumab was successfully digested to a Fab2 molecule at a variety of pHs using pepsin (Figure 71A, Lanes 3-5). This can be determined by the decrease in molecular weight to approximately 100 kDa. Pepsin is active at acidic pHs so a pH range of between 3-4 was used. During digestions using pepsin the Fc is not preserved and is digested into many small fragments which are too small to see on this type of SDS PAGE gel. Visually the digestion at pH 4.0 has the greatest yield of Fab2. Yield was not measured quantitively. Based upon the success of this experiment it was decided to prepare a bivalent bispecific **39** and subsequently digest the molecule using pepsin to form a BsFab2 **40** with an expected molecular weight of around 200 kDa.

Infliximab and tocilizumab were conjugated to 4 eq. of PEG$_{10}$ *bis*-sulfone TCO **26** and 4 eq. PEG$_5$ *bis*-sulfone Tz **27** respectively (Figure 72A, Lanes 2 and 3). The resulting TCO **37** and Tz **38** functionalised IgGs were combined and allowed to ligate (Figure 72A, Lane 4). The ligated intermediates **37** and **38** were digested using pepsin (Figure 72B, Lane 2) for 15 hours (pH 4.0, 37°C), the SDS PAGE characterisation of the digestion mixture did not reveal much information, no distinct bands could be identified. However, when the digestion mixture was purified using SEC (Figure 72B, Lanes 4-13), better defined bands were revealed. The bands highlighted (Figure 72B, Lanes 10-13) have molecular weights likely close to 200 kDa, the expected molecular weight of the BsFab2 **40**.
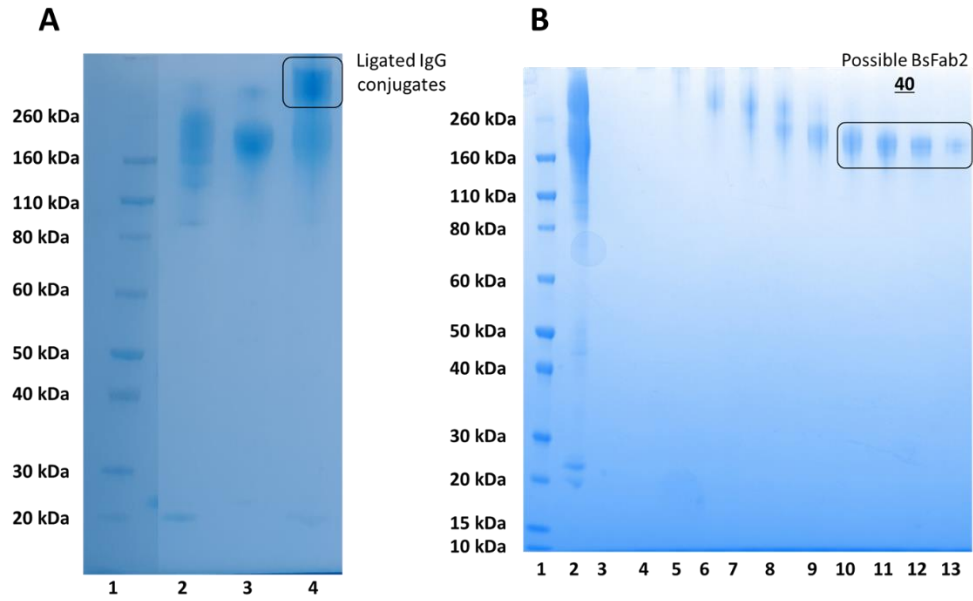
Figure 72: (A) SDS PAGE gel showing conjugation of 1 mg (0.30 mg/mL) tocilizumab to 4 eq. of PEG_{10} *bis*-sulfone TCO **26** and 1 mg infliximab (0.30 mg/mL) 4 eq. PEG_5 *bis*-sulfone Tz **27**, pH 7.6, 18 hours, ligation of the formed TCO **37** and Tz **38** functionalised IgGs **(B)** Digestion of ligation mixture (Figure 72B, Lane 2) with pepsin, 15 hours, pH 4.0, 37°C and SEC purification of the digestion mixture. **(A)** **Lane 1:** Protein marker, **2:** tocilizumab, 4 eq. PEG_{10} *bis*-sulfone TCO **26**, **3:** infliximab, 4 eq. PEG_5 *bis*-sulfone Tz **27**. **4:** ligation mixture. **(B) Lane 1:** Protein marker, **2:** digestion of ligation mixture with pepsin, **3:** SEC purification of digested ligation mixture fraction 1(F1) **4**: F2, **5**: F3, **6**: F4, **7**: F5, **8**: F6, **9**: F7, **10**: F8, **11**: F9, **12**: F10, **13**: F11.

The same gel was analysed using Biorad Image Lab software to the molecular weights of the bands (Figure 72B, Lanes 10-13) more accurately, the analysis is shown below (Figure 73)
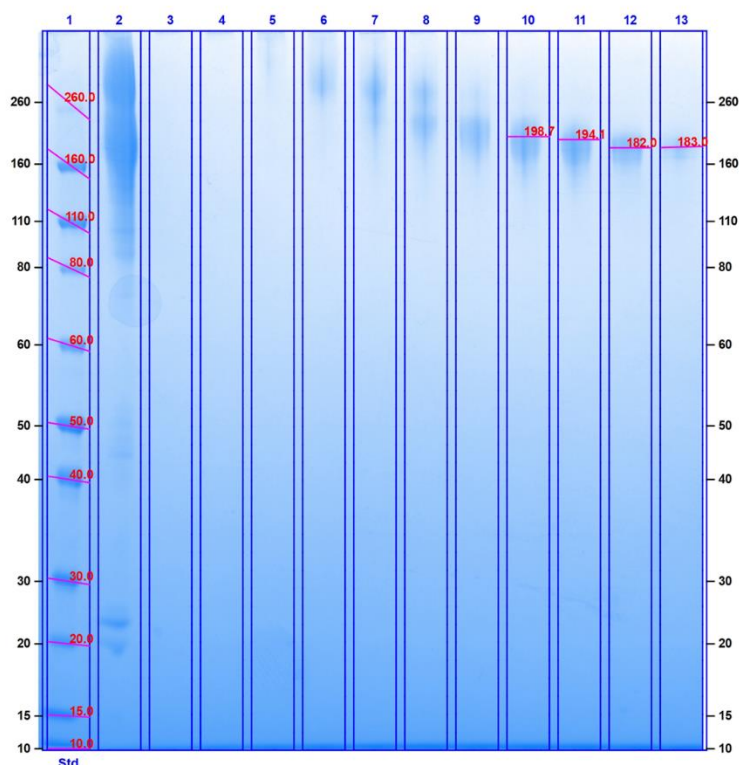
Figure 73: SDS PAGE gel showing molecular weight analysis of Figure 72B, Lanes 10-13 using Biorad Image Lab software (ver 6.1). Lane arrangement identical to Figure 72B.

The bands in lanes 10-13 (Figure 73) have molecular weights of between 182.0-198.7 kDa. As the expected weight of a BsFab2 **40** molecule would be close to 200 kDa this gives some confidence that these bands represent the desired BsFab2 **40**, in which one Fab2 derived from infliximab is present and the other derived from tocilizumab making it an anti-TNF-α/IL-6R BsFab2 **40**. The bands (Figure 73, Lanes 10-13) were combined and the absorption at 280 nm was measured, it was calculated that 35 µg of BsFab2 **40** had been prepared. Ideally quantification should have been carried out using micro-BCA as PEG has some interference at 280 nm, however micro-BCA is a destructive test.

Future work would include characterising this molecule further. 2 experiments that could be performed to help characterise the molecule would be MALDI-TOF to help confirm molecular weight and an SPR kinetic assay comparison with Fab conjugates such as PEG-Fabs derived from infliximab and tocilizumab. A comparison would be helpful because in theory a BsFab2 **40** should dissociate slower because of

its bivalent nature, if this was shown experimentally it would go some way to confirming a bivalent bispecific has been prepared.

Conclusions:

Attempts to prepare a BsFpF **7** using a PEG di-*bis*-sulfone protein dimerisation reagent **5** were not successful to the extent necessary to prepare BsFpFs that were envisaged. It was thought that a heterodimeric reagent **15** may be able to overcome the limitations of reagent **5** when preparing BsFpFs, however experimentation with PEG *bis*-sulfide **17** and PEG *bis*-sulfone glycol **12** lead to this strategy not being adopted because of the low reactivity of the PEG *bis*-sulfide **17**.

Instead, it was proposed to try and prepare a BsFpF **7** via a conjugation ligation strategy using pairs of difunctional reagents. Two sets of difunctional reagents, PEG *bis*-sulfone DBCO **23**, PEG *bis*-sulfone azide **24** and PEG *bis*-sulfone TCO **26,** PEG *bis*-sulfone Tz **27** were compared for their conjugation and ligation properties. It was possible to form BsFpFs at greater concentrations using reagents **26** and **27** so these reagents were used for subsequent experimentation.

Four monospecific FpFs and 14 BsFpFs **7** were successfully prepared via conjugation ligation using reagents **26** and **27** with typical isolated yields in the range of between 10-15%. Experimentation showed that the purity of the PEG *bis*-sulfone TCO **26** PEG *bis*-sulfone Tz **27** may be a limiting factor precluding higher isolated yields of the final BsFpF being possible. Key to FpF preparation was driving the formation of the TCO **28** and Tz **29** functionalised Fab conjugates during the conjugation step and the removal of free reagent **26** and **27** prior to ligation. It was possible to prepare highly purified BsFpFs using IEX and SEC. An anti-VEGF/IL-6R BsFpF was shown to be stable for up to 6 months when stored at 5°C, with no aggregation or deconjugation occurring.

Chapter 5 – Protein-protein binding interaction studies

Determining the binding affinity and kinetic properties between antibody-based molecules and their targets is a critical aspect of developing new antibody medicines. Hence, various binding assays including surface plasmon resonance (SPR), enzyme linked immunosorbent assays (ELISA) and microscale thermophoresis (MST) were utilised to assess the binding affinity and kinetic properties of BsFpFs prepared during this PhD. Table 11 summarises the list of all bispecific FpFs and other antibody conjugates that had their binding affinity and kinetic properties measured during this PhD.

Molecule	Derived from	Reagent(s) used for preparation	Target Ligand(s)	Molecular weight	Technique(s) used	Experimental replicates
Anti-VEGF/IL-6R bispecific FpF	Fab$_{Beva}$	PEG *bis*-sulfone TCO reagent **27**	VEGF	115 kDa	ELISA SPR MST	2 3 2
	Fab$_{Tocili}$	PEG *bis*-sulfone Tz reagent **28**	IL-6R			
Anti-VEGF/IL-6R bispecific FpF	Fab$_{Rani}$	Reagent **27** Reagent **28**	VEGF	115 kDa	SPR	1
	Fab$_{Tocili}$		IL-6R			
Anti-VEGF/TNF bispecific FpF	Fab$_{Beva}$	Reagent **27** Reagent **28**	VEGF	115 kDa	SPR	1
	Fab$_{Inflixi}$		TNF			
Anti-VEGF/TNF bispecific FpF	Fab$_{Rani}$	Reagent **27** Reagent **28**	VEGF	115 kDa	SPR	1
	Fab$_{Inflixi}$		TNF			
Anti-TNF/IL-6R bispecific FpF	Fab$_{Inflixi}$	Reagent **27** Reagent **28**	TNF	115 kDa	SPR	1
	Fab$_{Tocili}$		IL-6R			
Anti-VEGF TCO functionalised Fab conjugate **28**	Fab$_{Beva}$	PEG *bis*-sulfone TCO **26**	VEGF	60 kDa	ELISA SPR MST	2 3 2
Anti-IL-6R Tz functionalised Fab conjugate **27**	Fab$_{Tocili}$	PEG *bis*-sulfone Tz **26**	IL-6R	60 kDa	ELISA SPR MST	2 3 2
Anti-VEGF FpF	Fab$_{Beva}$	Reagent **27** Reagent **28**	VEGF	115 kDa	ELISA SPR	1 1
Anti-VEGF FpF	Fab$_{Rani}$	Reagent **27** Reagent **28**	VEGF	115 kDa	SPR	1
Anti-VEGF FpF	Fab$_{Beva}$	PEG di-*bis*-sulfone protein dimerisation reagent **5**	VEGF	120 kDa	ELISA SPR	1 1
Anti-VEGF FpF	Fab$_{Rani}$	Reagent **5**	VEGF	120 kDa	SPR	1

Table 11: List of prepared bispecific FpFs which had their binding affinities characterised using different binding assays.

Techniques used to measure the binding affinity of antibodies to their intended targets

(i) ELISA. ELISA is a technique used to determine the binding affinity and binding specificity of an antibody to its target. Direct, indirect, sandwich and competitive are all formats of ELISA. However, the indirect ELISA has previously shown to be suitable for measuring the binding affinity of certolizumab pegol [206], a commercial PEGylated Fab fragment targeting TNF-α, and hence it was used in this study.

Indirect ELISA involves coating the wells of a suitable plate with a fixed concentration of antigen, the antibody of choice is then applied to the plate and binding detected using a suitable secondary antibody. ELISA can be used to measure the affinity of a molecule (K_D) to its target and could be used to gather data on the affinity of bispecific FpFs. A generic example of an indirect ELISA is shown in Figure 74.
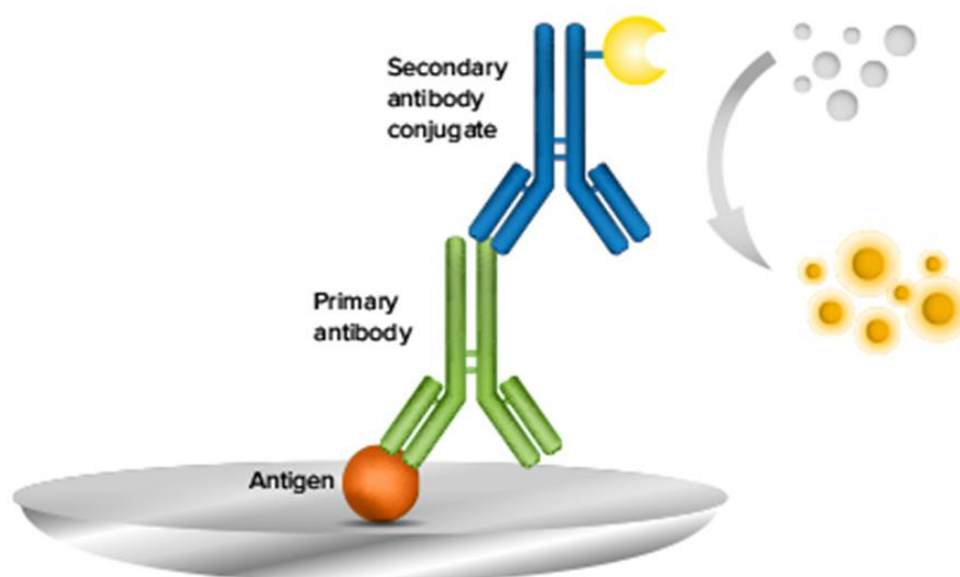
Figure 74: A scheme for an indirect ELISA. During an indirect ELISA the target antigen is captured onto a substrate. The primary antibody is introduced and binds to the antigen. A secondary antibody specific to the Fc region of the primary antibody is then introduced, the secondary antibody contains a tag which can be used to quantify the concentration of secondary antibody. The secondary and primary antibody should be present in a 1 to 1 ratio meaning measuring the concentration of secondary antibody indirectly measures the concentration of primary antibody. UV is usually the technique of choice for quantification.

(ii) SPR: SPR is a technique in which a ligand of choice is either immobilised or captured onto a chip. Attached to the surface of the gold chip is carboxymethylated dextran, the dextran surface can either be activated or functionalised with additional leaving groups to enable it to interact with a molecule. Once the ligand is immobilised

145

an analyte molecule is passed over the chip (Figure 75A) at a set flow rate and for a predetermined period after which analyte flow is halted and buffer is passed over the chip, from this a sensorgram (Figure 75B) is generated. This methodology enables SPR to generate outputs telling us how fast the analyte binds to its ligand (association rate, k_a), how strongly the analyte binds to the ligand (dissociation rate, k_d) and affinity of the molecule (K_D) to its target.
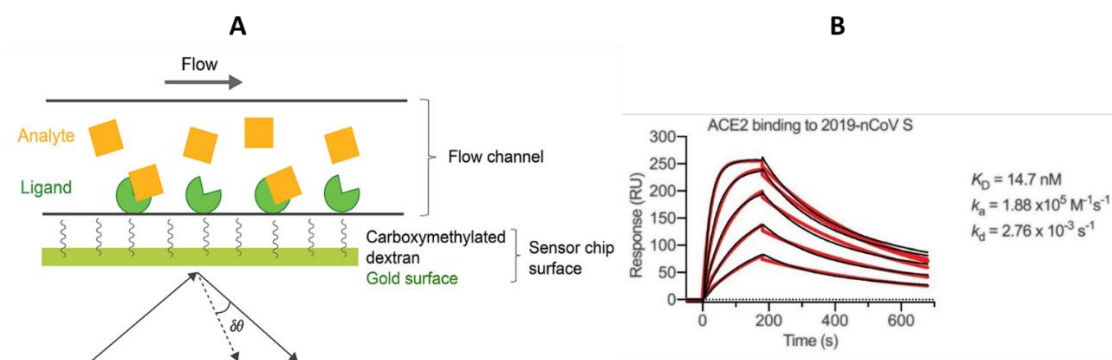
Figure 75: (A) Surface plasmon resonance methodology in which the ligand is immobilised to a dextran coated chip and the analyte of interest passed over the immobilised ligand, **(B)** An example SPR sensorgram, the binding of ACE2 to 2019-nCoV S with the affinity (K_D), association rate (k_a) and dissociation rate listed (k_d)

The kinetic properties k_a and k_d were measured using SPR. SPR is a technique that allows low and precise immobilisation levels of ligands to be achieved. In this study, we adopted a methodology previously developed by our research group to immobilise VEGF to a CM3 chip at a very low immobilisation level [183]. Low immobilisation level is needed to avoid mass transport limitations and to minimise re-binding effects in which the analyte rebinds to the ligand after dissociating, this allows the sensitivity of the assay to be enhanced. A low immobilisation level also ensures that the ligand is sparsely distributed on the sensor surface. This allows for better access of the analyte to the binding sites and helps with reducing the potential for ligand-ligand interactions or steric hindrance between closely packed ligand molecules. The sensorgram below (Figure 76) shows the steps during the immobilisation of VEGF onto a CM3 chip.
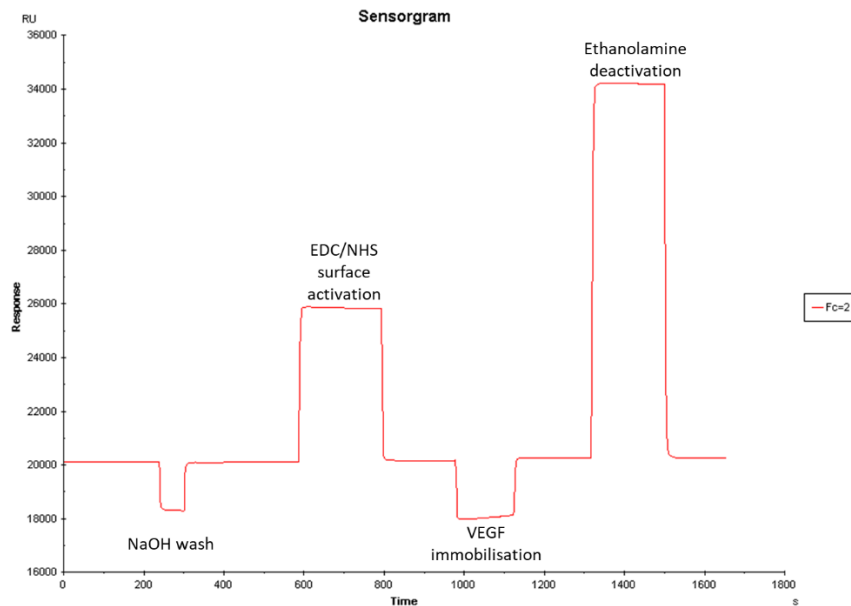
Figure 76: Sensorgram showing each step of the immobilisation of VEGF to a CM3 chip. Moving left to right, the first step is application of NaOH to ensure the chip surface is clean from any impurities. Then an EDC/NHS solution is applied to the chip surface for activation. VEGF at a concentration of 0.5 µg/mL was applied to the chip surface. The final step is deactivation of any remaining binding sites on the chip surface using an ethanolamine solution.

Firstly, NaOH was applied to ensure the surface of the chip was free from any impurities. The next step is activation of chip surface as the CM3 chip contains carboxy groups (-COOH) on its surface which need to be activated by creating reactive ester groups, which can then react with the primary amine of the ligand. This is typically achieved using a mixture of 1-Ethyl-3-(3-dimethylaminopropyl)carbodiimide (EDC) and N-Hydroxysuccinimide (NHS). If chip surface is not activated by EDC/NHS, the chip is not able to be functionalised with the ligand. The third step is to run a ligand solution of VEGF at a concentration of 0.5 µg/mL over the activated chip surface, the VEGF was diluted to this concentration using a pH 5.5 acetate buffer. VEGF contains primary amine groups which require specific buffer conditions to maintain their stability and activity during immobilisation. The final step is Ethanolamine deactivation, this step deactivates any free sites on the chip surface making them unreactive and ensuring they do not interfere with any subsequent assays. Figure 77 is an annotated sensorgram showing how the immobilisation level or RU of VEGF upon the chip is calculated.

147
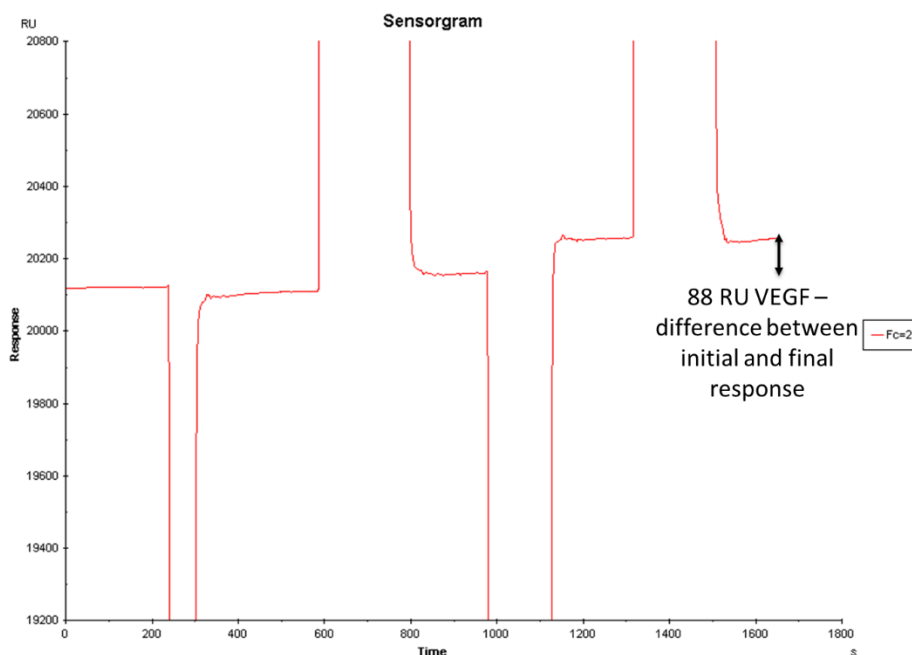
Figure 77: Sensorgram illustrating how the immobilisation level is derived from the immobilisation sensorgram (88 RU VEGF in this case). To determine the immobilisation level the increase between initial response pre NaOH wash, and the response post ethanolamine deactivation was calculated.

To determine the immobilisation level the difference between the initial response, obtained prior to the NaOH wash, and the final response after ethanolamine deactivation was calculated. In this study, the immobilisation level of VEGF was found to be 88 RU. Additionally, another chip was immobilised with VEGF with an immobilisation level of 95.9 RU. As explained, it was crucial to maintain the immobilisation level below 100 RU for kinetic assays [207]. This was to limit rebinding events during kinetic measurement to avoid its impact on the accurate measurement of the molecule's dissociation rate and, consequently, its overall affinity.

Other ligands such as TNF-α, IL-6R were captured (and not immobilised using amine-coupling) over an NTA-Chip, a CM3 chip is not suitable for capturing of ligands. Capturing also requires that the ligands of interest contain a histidine tag (his-tag). In this method, the sensor chip NTA (nitrilotriacetic acid) was employed which is composed of NTA covalent immobilised onto a carboxymethylated dextran surface. To enable the capture of TNF-α (as an example) over an NTA chip, we had to obtain histidine-tagged TNF-α and activate the NTA chip with a nickel (Ni^{+2}) solution to form a nickel-chelated NTA group. Anti-TNF-α antibody molecules (IgG, FpF and Bs-FpF) were passed over the chip's surface which has been functionalised with his-tagged TNF-α, and the binding kinetics were evaluated.

To regenerate the chip for a new analysis cycle, the NTA surface was washed with an EDTA solution after each run. This regeneration was followed by refreshing the chip with fresh Ni^{2+} solution and his-tagged TNF-α. For the kinetic purposes, the aim was to minimise the amount of his-tagged TNF-α captured onto the surface of the NTA chip, hence a low concentration of his-tagged TNF-α (5 μg/mL) was used for capture.

(iii) MST. Measurement of binding affinity for antibody conjugates can also be achieved using Microscale Thermophoresis (MST). MST offers distinct advantages over other methods such as ELISA and SPR. Notably, MST is a solution-based technique that eliminates the need for immobilisation of ligands on a sensor chip (as in SPR) or coating of ligands onto a plate (as in ELISA), providing a better mimicry of *in vivo* conditions.

In MST, either the antigen or the antibody is labelled with a fluorescent tag, the experimental set up involves the addition of the antibody and ligand to glass capillary tubes. The concentration of the labelled partner is kept constant, while the concentration of the unlabelled partner is varied. The principle underlying MST is based on thermophoresis, which describes the movement of molecules along temperature gradients resulting in a measurable change in the local concentration of the target molecules. By employing fluorescence measurements, these concentration changes can be easily monitored since the target molecules are fluorescently labelled prior to an MST measurement.

This directed movement of molecules in MST is influenced by their molecular size, charge, and hydration shell. Binding of a ligand to a target molecule induces changes in at least one of these parameters, consequently leading to an altered thermophoretic movement of the target-ligand complex compared to the single molecules alone [208]. MST can be used to measure the binding affinity of an antibody and generates a K_D value. For instance, the binding affinity of anti-TNF-α antibody, Humira, and the anti-HER2 antibody, Herceptin, was determined using MST and reported in an application note [209].

The first binding assay used to measure binding affinity of the prepared antibody conjugates, was ELISA as presented in the following section.

ELISA to measure binding affinity:

ELISA of anti-VEGF FpFs:

As described in the BsFpF preparation chapter (Chapter 4), antibody conjugates have been prepared using the di-*bis*-sulfone protein dimerization reagent **5** and via the ligation of functionalised Fab conjugations prepared via the conjugation of Fabs to PEG *bis*-sulfone TCO **26** and PEG bis-sulfone Tz **27** reagents. An important question to ask was whether binding affinity of an FpF prepared using reagent **5** was comparable to a binding affinity of FpF prepared using reagents **26** and **27**. To try and answer this question the binding affinity of anti-VEGF monospecific FpFs prepared using reagent **5** and reagents **26** and **27** were measured used ELISA and SPR. Figure 78 shows the results from an ELISA comparison of the anti-VEGF FpFs prepared using the two different methodologies. Both molecules were anti-VEGF, monospecific FpFs prepared using Fab_{beva} obtained from the digestion of bevacizumab. The FpFs were applied over a 96-well plate which was pre-coated with VEGF.
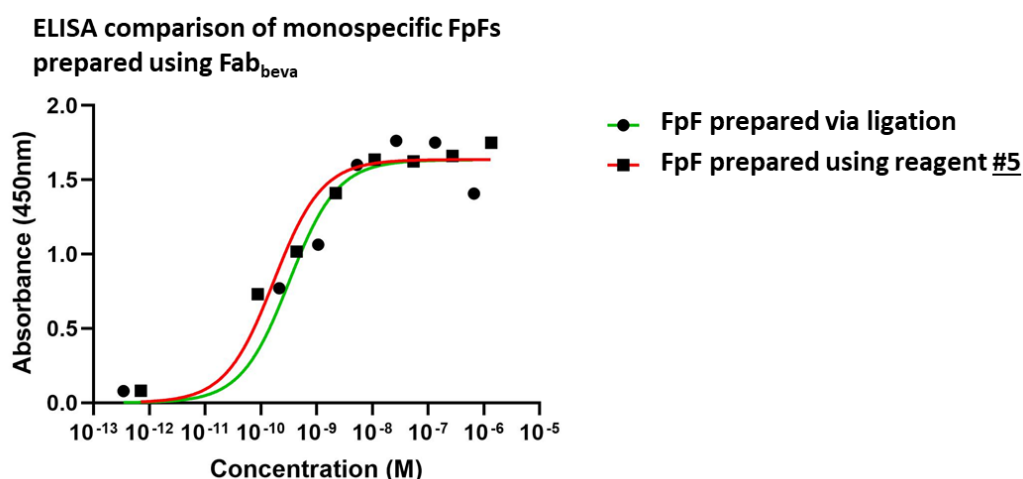
Figure 78: ELISA curves from plates coated with VEGF, treated with FpF_{beva} homodimers prepared using a PEG_{20} di-*bis*-sulfone dimerization reagent **5** and via ligation of TCO **28** and Tz functionalised **29** Fab_{beva} conjugates, n=1. FpF_{beva} prepared using reagent **5** applied at concentrations ranging from 1.4×10^{-6} to 7.0×10^{-13}M, FpF_{beva} prepared via ligation applied at concentrations ranging from 6.7×10^{-7} to 3.4×10^{-13}M.

As seen in Figure 78, both the FpF_{beva} prepared via ligation and FpF_{beva} prepared using reagent **5** were able to saturate the VEGF ligand during the ELISA experiment. This is evident by the plateau displayed for both molecules which begins between the 10^{-8} and 10^{-7} molar concentrations for both FpF molecules. To fit the data GraphPad Prism was used. A one site – specific binding data fitting method was applied to fit all the ELISA data presented in this thesis.

It was found that binding affinity (K_D) of the FpF_{beva} prepared using reagent **5** (0.17 nM) was lower than binding affinity of the FpF_{beva} prepared via ligation (0.33 nM), this is close to a 50% difference in affinity, which is an interesting finding as both molecules were derived from the same antibody. While this experiment was only carried out once and ideally more replicates are required, it suggested that the method of preparation used to prepare the FpFs might have an impact on the binding affinity of the molecules. We also performed SPR kinetic assays to measure the binding kinetics of FpF prepared using reagent **5** and ligation with the data being presented later in the chapter.

ELISA of an anti-VEGF/IL-6R bispecific FpF

An indirect ELISA methodology using VEGF as a ligand was used to measure binding affinity of an anti-VEGF/IL-6R BsFpF **7** prepared via conjugation-ligation. For control purposes the anti-VEGF IgG, bevacizumab, and Fab$_{beva}$ had their affinities to VEGF measured using ELISA (Figure 79). To ensure no non-specific binding occurred during the ELISA experiment a control using the anti-TNF-α IgG, infliximab was also applied to wells containing VEGF. Infliximab is a TNF-α neutralising molecule meaning it should not bind to VEGF and wash from the 96 well plate during the washing steps during the ELISA experiment. This should result in no absorbance being measured after application of the HRP conjugated antibody. Another control experiment was conducted by applying the anti-VEGF/IL-6R BsFpF **7** to wells containing PBS. The negative controls were carried out to establish if any non-specific binding was occurring during the ELISA experiment. Both negative controls demonstrated that no non-specific binding was occurring during ELISA experiments.
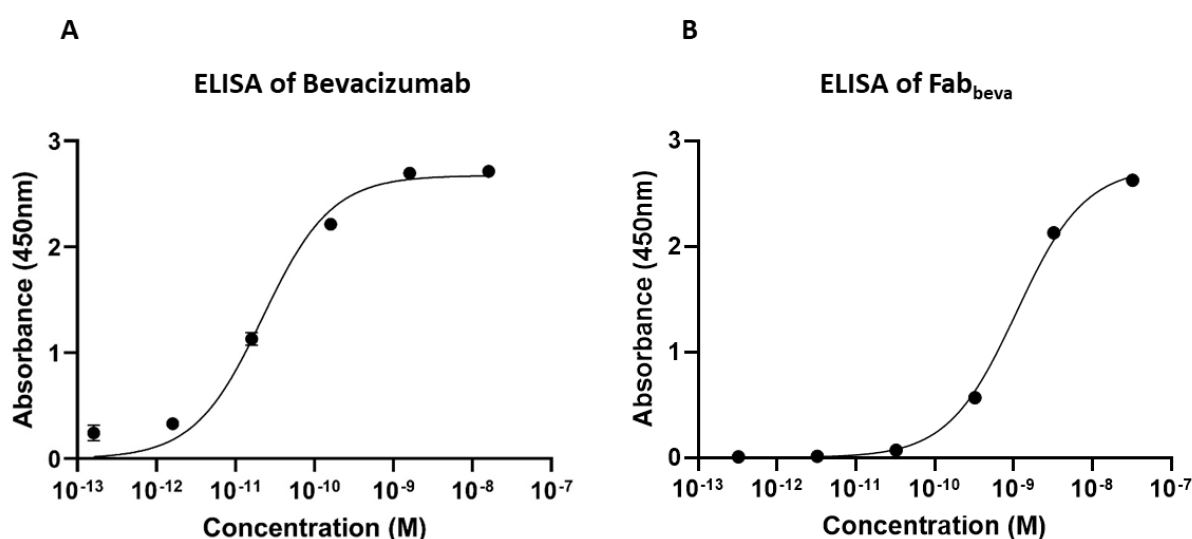
Figure 79: ELISA curves of a 96 well plate, each well coated with 0.1 µg of VEGF, treated with bevacizumab **(A)** and Fab$_{beva}$ **(B)**, n=1. Bevacizumab concentrations range from 1.6×10^{-8} to 1.6×10^{-13}M and Fab$_{beva}$ concentration range from 3.2×10^{-8} to 3.2×10^{-13}M

Absorbances were plotted against molar concentration to generate the ELISA curves. The calculated affinities (K_D) were 0.022 nM for bevacizumab and 1.09 nM for Fab$_{beva}$. A lower affinity was expected for bevacizumab as it is a bivalent molecule, containing two binding sites in comparison to the monovalent Fab$_{beva}$. As bevacizumab is bivalent it is expected that if bevacizumab and Fab$_{beva}$ were required to neutralise the same quantity of VEGF a lower molar concentration of bevacizumab would be needed.

To conduct an ELISA using IL-6R as a ligand, the VEGF ELISA protocol was altered to use IL-6R as the ligand. Incubation times and conditions post application of IL-6R to the 96 well plate was kept consistent, the amount of IL-6R applied per well (0.1 µg) was also kept consistent with the VEGF ELISA protocol. The anti-IL6R IgG, tocilizumab, and Fab$_{Tocili}$ were used to validate the IL-6R ELISA assay with the results being shown in Figure 80.
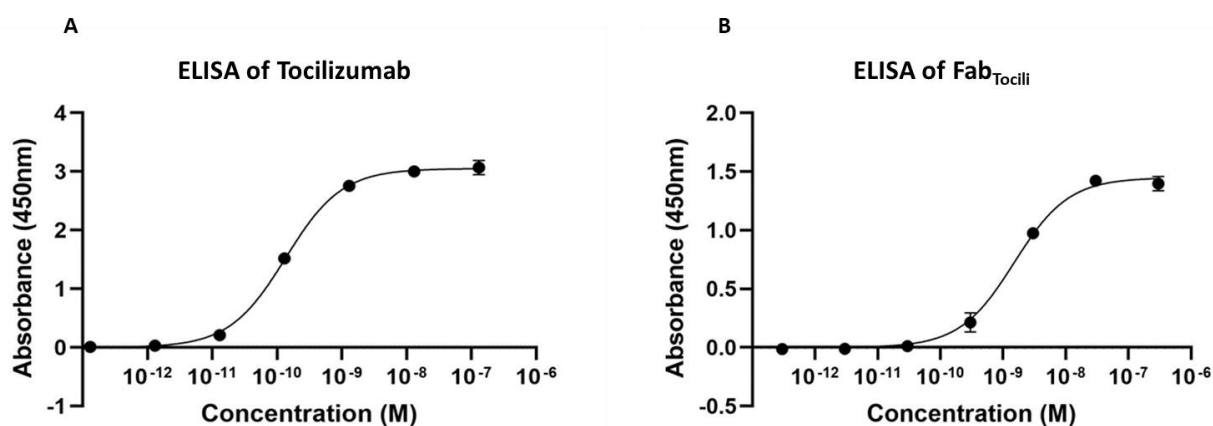
Figure 80: ELISA curves of a 96 well plate, each well coated 0.1 µg of IL-6R, treated with tocilizumab **(A)** and Fab$_{tocili}$ **(B)**, n=1. Tocilizumab concentrations range from 1.3×10^{-7} to 1.3×10^{-13}M and Fab$_{tocili}$ concentration range from 3.0×10^{-7} to 3.0×10^{-13}M

The calculated affinities (K_D) were 0.13 nM for tocilizumab and 1.50 nM for Fab$_{Tocili}$. As expected, a greater affinity was measured for tocilizumab as a bivalent IgG compared to the monovalent Fab$_{Tocili}$ which was consistent with results observed previously during ELISA comparisons of bivalent bevacizumab and monovalent Fab$_{beva}$ (Figure 79).

With ELISA methodologies available for both VEGF and IL-6R, the next step was to test an anti-VEGF/IL-6R bispecific FpF using the VEGF and IL-6R methodologies. The results of an ELISA in which an anti-VEGF/IL-6R BsFpF and an anti-VEGF TCO functionalised Fab conjugate **28** were tested using VEGF as the target ligand is shown in Figure 81. The anti-VEGF/IL-6R BsFpF in this example was prepared via ligation of TCO **28** and Tz **29** functionalised Fab conjugates prepared via the conjugation of Fab$_{beva}$ and Fab$_{Tocili}$ to PEG-*bis*-sulfone TCO **26** and PEG-*bis*-sulfone **27** Tz reagents. The anti-VEGF TCO functionalised Fab conjugate **28** was prepared via the conjugation of Fab$_{beva}$ to reagent **26**.

A

ELISA of Anti-VEGF/IL-6R BsFpF against VEGF

B

ELISA of Anti-VEGF TCO functionalised Fab conjugate 28 against VEGF
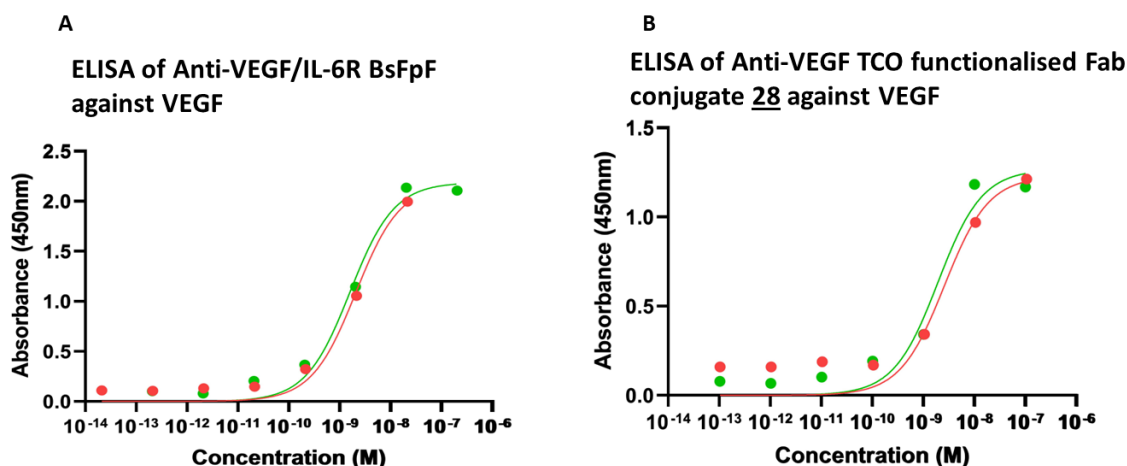
Figure 81: ELISA curves of a 96 well plate, each well coated with 0.1 µg of VEGF, treated with an anti-VEGF/IL-6R BsFpF **7 (A)** and an anti-VEGF TCO functionalised Fab conjugate **28 (B)**, n=2, red and green sample points and curves indicate separate experiments. Anti-VEGF/IL-6R bispecific concentration range from 2.1×10^{-7} to 2.1×10^{-13}M and anti- TCO functionalised Fab conjugate **28** concentration range from 1.0×10^{-7} to 1.0×10^{-13}M.

The calculated binding affinity of the anti-VEGF/IL-6R BsFpF **7** to VEGF (K_D:1.80 nM) was like the calculated affinity of the anti-VEGF TCO functionalised Fab conjugate **28** (K_D 2.25 nM). The affinities presented here are average affinities across the two replicates. The closeness of the affinities indicates that the FpF behaved in a similar fashion to the TCO functionalised Fab conjugate **28** when binding to VEGF. The IL-6R binding arm does not appear to be causing any interference. Another comparison can be made between the anti-VEGF/IL-6R BsFpF **7**, the anti-VEGF TCO functionalised Fab conjugate **28** and unmodified Fab$_{beva}$. Fab$_{beva}$ had a greater affinity towards VEGF (Figure 79, K_D 1.09 nM) than the BsFpF **7** (K_D 1.80 nM) and the anti-VEGF TCO functionalised Fab conjugate **28** (K_D 2.25 nM). This finding is not unusual and is quite typical when an antibody is conjugated to a scaffold containing PEG [161,210]. The effect occurs due to the PEG polymer chain creating a steric shielding effect.

The affinity of the same anti-VEGF/IL-6R BsFpF **7** towards its other intended target IL-6R was also measured using ELISA (Figure 82). The calculated binding affinity of the BsFpF **7** to IL-6R (K_D: 2.55 nM,) was close to the affinity of the anti-IL-6R Tz functionalised Fab conjugate **29** (K_D: 3.20 nM) towards IL-6R. Similar to the VEGF affinity measurements, the unmodified Fab_{Tocili} (K_D: 1.50 nM, Figure 80) had a greater affinity toward IL-6R than the anti-VEGF/IL-6R BsFpF and anti-IL-6R Tz functionalised Fab conjugate **29**.
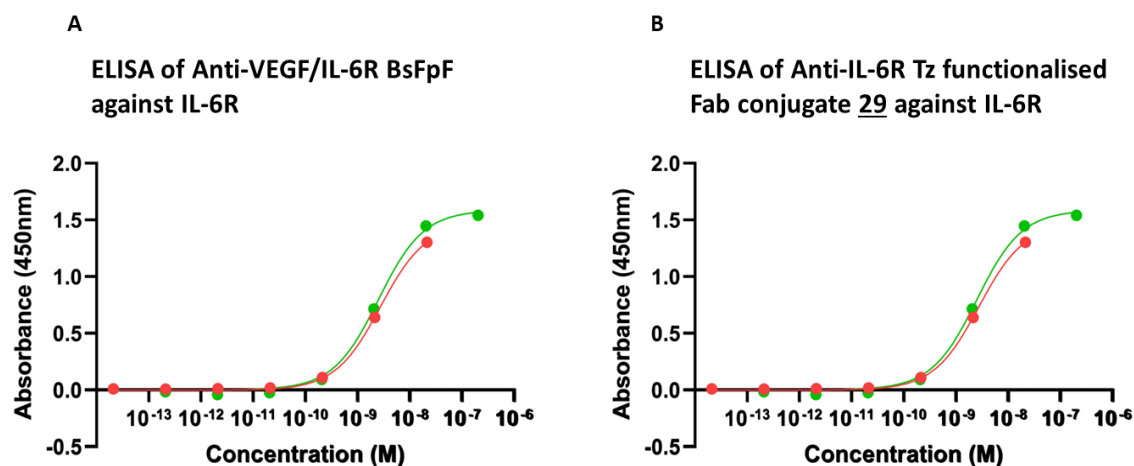
Figure 82: ELISA curves of a 96 well plate, each well coated with 0.1 µg of IL-6R, treated with an anti-VEGF/IL-6R BsFpF **7 (A)** and an anti-IL-6R Tz functionalised Fab conjugate **29 (B)**, n=2, red and green sample points and curves indicate separate experiments. Anti-VEGF/IL-6R bispecific concentration range from 2.1×10^{-7} to 2.1×10^{-13}M and anti-IL-6R PEG-Fab concentration range from 1.6×10^{-7} to 1.6×10^{-13}M.

To summarise the findings of the ELISA experiments (Figures 81 and 82) it appears that the anti-VEGF/IL-6R BsFpF **7** has similar affinity towards both VEGF and IL-6R compared to anti-VEGF and anti-IL-6R functionalised Fab conjugates **28** and **29**. This indicates that each of the binding arms present in the BsFpF can bind independently to their target without the other interfering. The binding activity of the Fab_{Beva} and Fab_{Tocili} used to prepare the BsFpF via conjugation-ligation have been preserved.

Another ELISA experiment was also performed in which a 96-well plate was treated with both VEGF and IL-6R simultaneously. Each well contained an equal concentration of VEGF and IL-6R and after the ligands were captured the anti-VEGF/IL-6R BsFpF was added (Figure 83). The objective of this experiment was to see if it could be determined that the BsFpF was capable of binding to both of its targets at the same time. If the BsFpF did indeed bind to both of its targets at the same

time it was thought that there may be a difference in affinity compared to when the anti-VEGF/IL-6R BsFpF was tested against single targets in VEGF and IL-6R ELISAs.
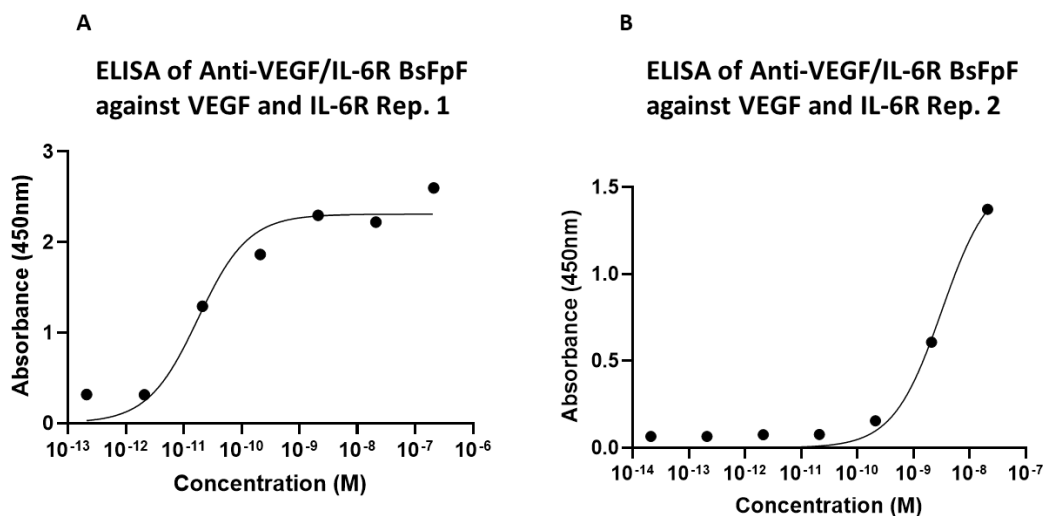
Figure 83: ELISA curves of a 96 well plate, each well coated with 0.1 μg of VEGF and 0.1 μg of IL-6R, treated with an anti-VEGF/IL-6R BsFpF **(A)** Replicate 1 **(B)**, Replicate 2. Anti-VEGF/IL-6R bispecific concentration range from 2.1×10^{-7} to 2.1×10^{-13}M, experimental conditions same for replicates 1 and 2.

The affinity of the BsFpF towards both VEGF and IL-6R was found to be 0.01 nM for the first replicate (Figure 83A), a significantly lower affinity than what had been seen in VEGF (K_D 2.25 nM) and IL-6R (K_D 2.55 nM) single target ELISA experiments. A lower affinity does make sense. A K_D value corresponds to the required concentration of a molecule to saturate 50% of the available binding sites. A BsFpF binding to both targets concurrently would mean a lower concentration of molecule would be required to saturate 50% of the binding sites in turn generating a lower K_D meaning greater affinity.

A second replicate (Figure 83B) using the same experimental conditions was performed to try and replicate the result from the first replicate (Figure 83A). The affinity derived from this experiment (Figure 83B) was significantly higher at 3.2 nM which does not corroborate the finding of the first experiment questioning its validity. It is likely that the method is sensitive to the arrangement of the VEGF and IL-6R ligands at the bottom of the well plate with a quantity of ligand being orientated to allow binding and another quantity not being orientated in such a way. Controlling ligand orientation using an indirect ELISA is not possible as the ligands are captured onto the well plate without any chemical interactions being exploited. It may be probable that the amount of ligand orientated to allow binding would be different for both of the

156

experimental replicates. An alternative to use instead of an indirect ELISA for measuring affinity to 2 ligands could be a bridging ELISA [211].

A more appropriate technique for measuring the affinity of BsFpFs to both of their intended targets in a single assay may be SPR. SPR allows greater control of ligand arrangement and orientation as immobilisation, or coupling to a chip surface required for SPR assays can be achieved using functional groups present in ligands which are not involved in binding. In the following section, SPR is used to measure not only the affinity of BsFpFs towards their targets but also kinetic parameters such as association and dissociation rates.

SPR to measure binding affinity and kinetic parameters:

As previously mentioned, the application of the SPR assay enabled the measurement of not only binding affinity, but also essential kinetic parameters, such as the associate rate constant and dissociation rate constant.

First presented in this section, is attempts at determining the binding kinetics of ranibizumab towards VEGF using the Biacore X100. Previous studies conducted by our research group [161], had encountered limitations in measuring the dissociation rate constant of ranibizumab using Biacore X-100, at 25°C, despite successfully measuring the association rate. According to previous studies reported in [212], it has been suggested that extending the duration of the dissociation phase of a kinetic assay to 3 hours, while conducting the assay at 37°C, enables the measurement of the dissociation rate for ranibizumab. The same experiment was conducted using a Biacore X100 to assess the effect of extending the dissociation phase and performing the assay at 37°C.

A serial dilution of ranibizumab was injected onto a CM3 chip immobilised with VEGF with the experimental temperature set at 37°C. The sensorgram (Figure 84A), contains large, sharp peaks which are likely due to formation of bubbles within the system. This behaviour is not usually observed when running kinetic SPR assays at 25°C. This likely occurs due to the presence of dissolved air within the SPR running buffers. As temperature increases the solubility of air in aqueous liquids decreases meaning that bubble formation is more likely to occur at 37°C than at 25°C. The sensorgram presented in Figure 84A was magnified to show greater detail (Figure 84B). As can be seen sharp peaks exist throughout the whole sensorgram at each ranibizumab concentration injected.

Because of the presence of these peaks, it was not possible to derive either association or dissociation constants from this sensorgram. This experiment was repeated a further two times to ensure this result was not an outlier. In both repeats the same results were observed. Because of this, attempts to derive a dissociation constant for ranibizumab or molecules derived from ranibizumab using SPR were halted. It was decided to use bevacizumab as a source of anti-VEGF Fabs for preparation of BsFpFs if the dissociation rate of a BsFpF from VEGF was to be measured.
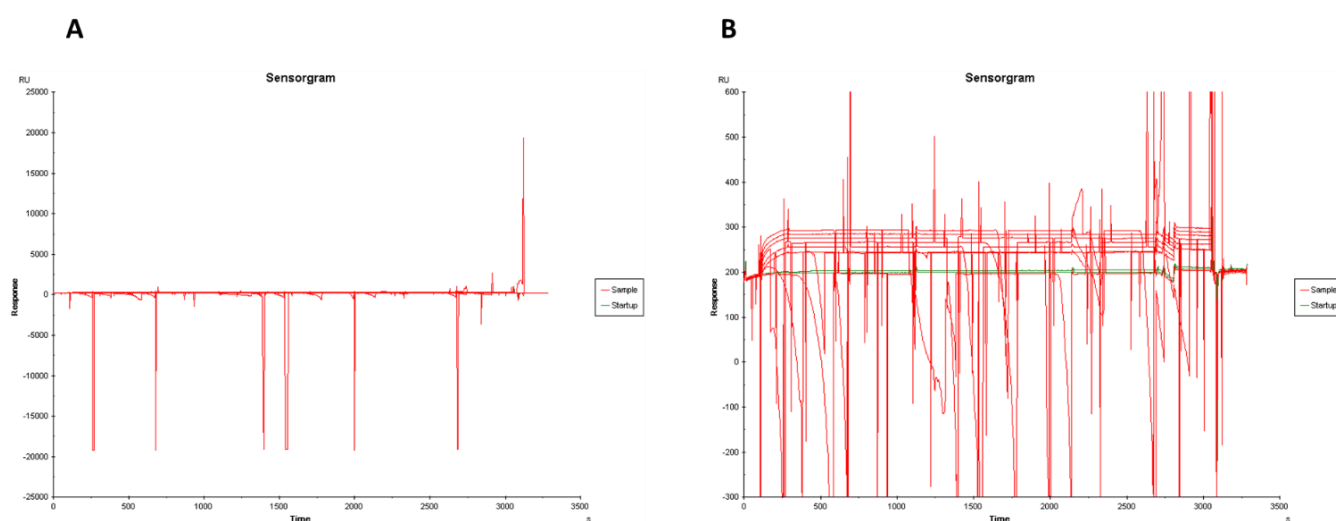
Figure 84: Sensorgrams showing the binding of ranibizumab to VEGF at 37°C, the VEGF. VEGF immobilised onto CM3 chip at 88RU.

Based upon experimentation showing that the use of ranibizumab to prepare FpFs was unlikely to allow accurate measurement of dissociation rates (Figure 84). 2 anti-VEGF monospecific FpFs derived from Fab$_{Beva}$ were tested in an SPR kinetic assay (Figure 85). The 2 FpFs were prepared using 2 different methodologies. One anti-VEGF monospecific FpF was prepared via the conjugation of Fab$_{Beva}$ to the PEG di *bis*-sulfone protein dimerisation reagent **5**. The second FpF was prepared via conjugation ligation using Fab$_{Beva}$ and the PEG *bis*-sulfone TCO **26** and PEG *bis*-sulfone Tz **27** reagents. It should be noted that the SPR binding data for the anti-VEGF monospecific FpF prepared using reagent **5** was kindly provided by another researcher from within our research group and is labelled subsequently in Table 12 as "legacy" data.
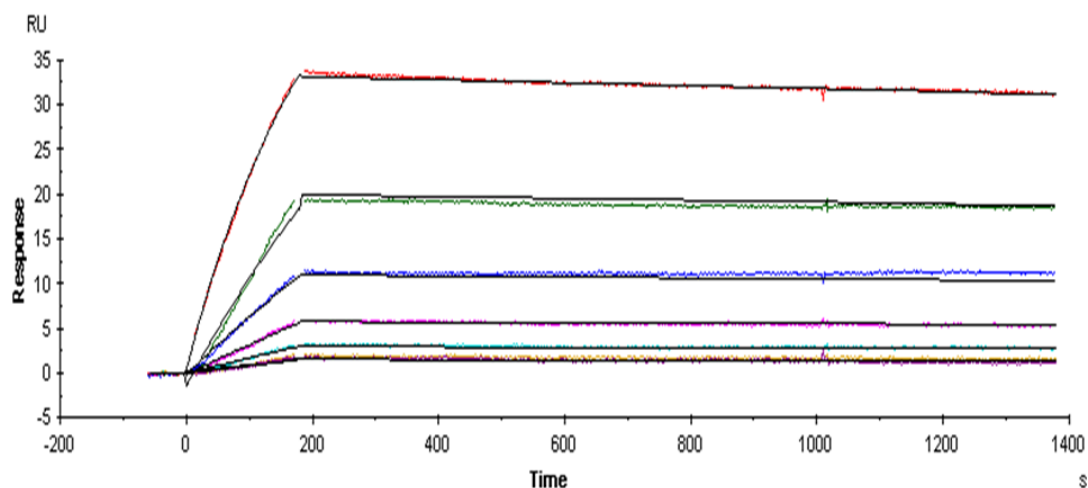
Figure 85: Sensorgram showing the binding of an anti-VEGF FpF to VEGF. VEGF immobilised onto CM3 chip at 95.9 RU. The FpF was prepared via conjugation ligation using Fab$_{Beva}$ and reagents **26** and **27**. The FpF was serially diluted and applied to the chip at concentrations of between 69-2.15 µg/mL. Red line – 69 µg/mL, green – 34.5 µg/mL, blue – 17.25 µg/mL, purple – 8.63 µg/mL, turquoise – 4.31 µg/mL, orange 2.15 µg/mL. Black lines represent the fitting of the binding model to the experimental data.

The anti-VEGF FpF prepared via conjugation ligation bound to VEGF in a concentration dependent manner (Figure 85), as concentration of FpF increased response also increased. No indication of rebinding events was seen. If a rebinding event was to occur in which an anti-VEGF FpF molecule was to dissociate from VEGF and the same molecule, then rebind would be visible as an increase in response after approximately 200 seconds of run time. Rebinding events can lead to inaccurate measurement of dissociation rate constants (K_d) [213] which in turn can lead to inaccurate affinities ($K_{D)}$ being calculated. The low immobilisation level of VEGF (95.9 RU) helps to ensure any rebinding events do not occur.

The sensorgram was fitted with a 1:1 binding model to derive the binding constants and affinity (Table 12). A 1:1 binding model was chosen for fitting of the kinetic data because it is likely each molecule of the anti-VEGF FpF would have bound to a single molecule of VEGF during the assay.

Molecule	Derived from	Reagent(s) used for preparation	K_a (1/Ms)	K_d (1/s)	K_D (nM)
Anti-VEGF monospecific FpF – 115 kDa MW	Fab$_{Beva}$	PEG *bis*-sulfone TCO reagent **26** PEG *bis*-sulfone Tz reagent **27**	7312	$5.10X10^{-5}$	7.0
Legacy Anti-VEGF monospecific FpF – 120 kDa MW	Fab$_{Beva}$	PEG di-*bis*-sulfone dimerization reagent **5**	19600	$3.00X10^{-5}$	1.53

Table 12: Binding constants for Anti-VEGF FpFs prepared via conjugation-ligation using reagents **26** and **27** and via conjugation to reagent **5**. Fab$_{Beva}$ was the source of anti-VEGF activity for both molecules.

It was found that the anti-VEGF monospecific FpF prepared using reagent **5** had greater affinity (K_D 1.53 nM) to VEGF than the anti-VEGF FpF (K_D 7.0 nM) prepared via conjugation ligation, corroborating the findings during an ELISA comparison of the same 2 molecules (Figure 78). The FpF prepared using reagent **5** has an association rate close to three times greater (K_a 19600 vs 7312) than the FpF prepared via conjugation ligation and a slower dissociation rate (K_d $3.00X10^{-5}$ vs $5.10X10^{-5}$). This indicates that the anti-VEGF FpF prepared using reagent **5** binds faster and in a stronger fashion to VEGF.

The exact reason why the anti-VEGF FpF prepared using reagent **5** has greater affinity towards VEGF is unknown. The FpF prepared via conjugation may be a more rigid molecule compared to the FpF prepared using reagent **5**. This could be responsible for the slower association rate as the potential rigidity limits the molecule to axial and radial movements instead of being able to bend and flex to reach binding sites. The difference in dissociation rate is harder to explain. It could be argued that the difference between the two dissociation rates (K_d $3.00X10^{-5}$ vs $5.10X10^{-5}$) is not large enough to be deemed significant and that they could be treated as equivalent. It could be that molecular weight is playing a role, the anti-VEGF FpF prepared using reagent **5** has a higher molecular weight (120 kDa vs 115 kDa) which would mean that the molecule dissociates slower simply due to its bulk.

Drawing definitive conclusions from this data (Table 12) is difficult as only a single experimental replicate was performed, however the trend seen during SPR experimentation does correlate with what was observed during ELISA (Figure 78). What can be said is that it should not be assumed that an FpF prepared using the di

bis-sulfone protein dimerisation reagent **5** and an FpF prepared via conjugation ligation have equivalent association rates, dissociation rates and affinities towards their targets.

Another SPR comparison (Figures 86 and 87) between an FpF prepared via conjugation ligation and an FpF prepared using reagent **5** was performed. The source of Fab for the FpF preparation was ranibizumab. It has been shown that measuring the dissociation rate of ranibizumab is not feasible using a Biacore X100 so the purpose of this experiment was to compare association rates.
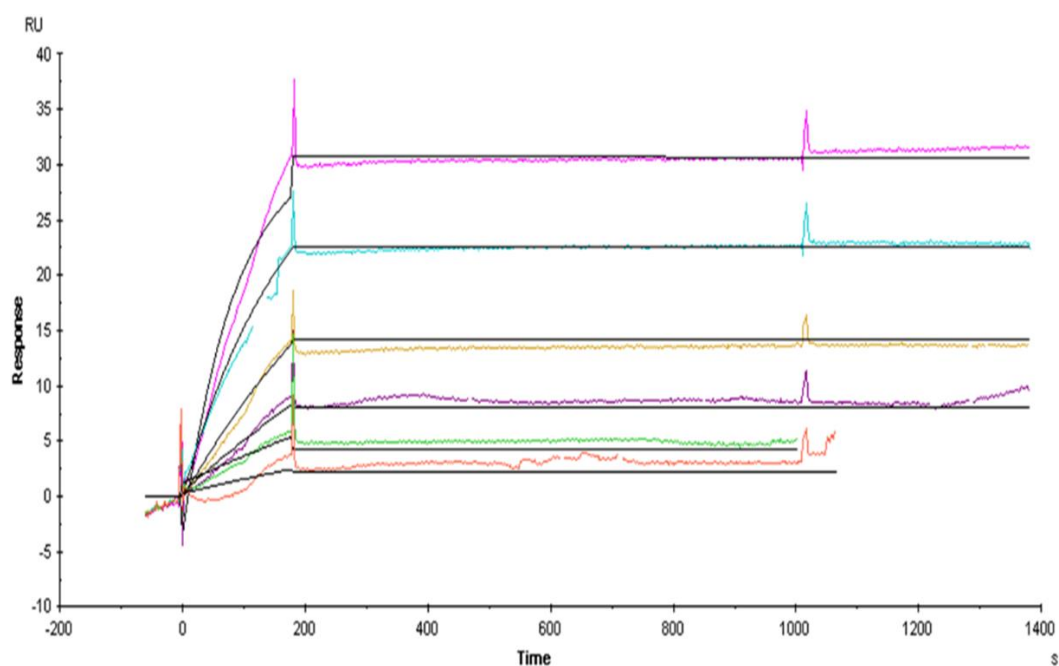
Figure 86: Sensorgram showing the binding of an anti-VEGF FpF to VEGF. The FpF was prepared via conjugation of Fab$_{Rani}$ to reagent **5**. VEGF immobilised onto CM3 chip at 88RU. The FpF was serially diluted and applied to the chip at concentrations of between 100-2.15 µg/mL. Purple line – 100 µg/mL, green – 50 µg/mL, orange – 25 µg/mL, purple – 12.5 µg/mL, brown – 7.25 µg/mL, orange, and pink 3.63 µg/mL. Black lines represent the fitting of the binding model to the experimental data.
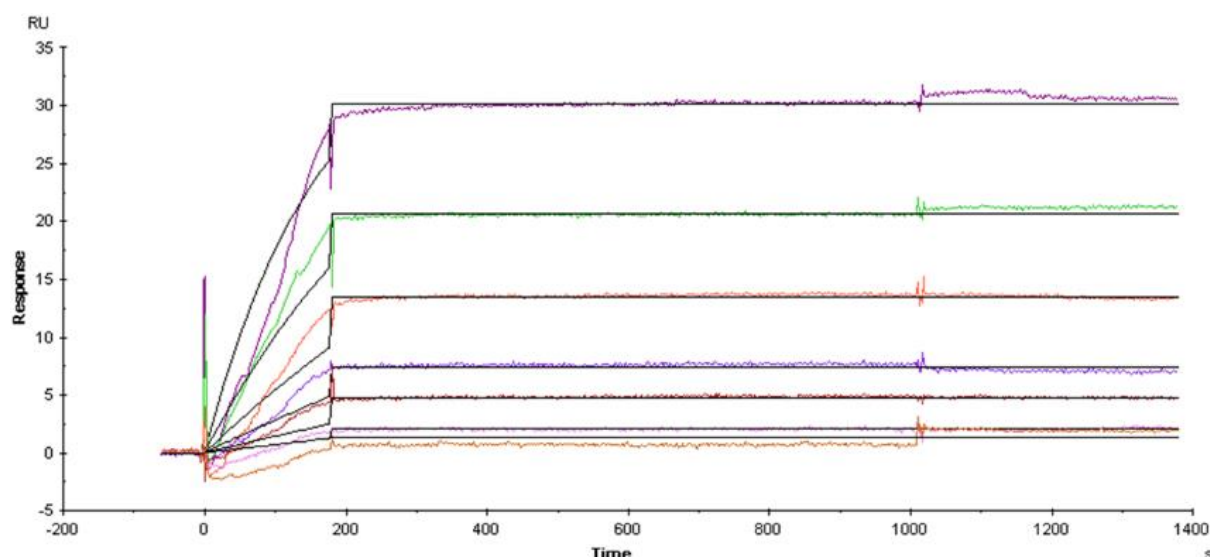
Figure 87: Sensorgram showing the binding of an anti-VEGF FpF to VEGF. The FpF was prepared via conjugation ligation using Fab$_{Rani}$ and reagents **26** and **27**. VEGF immobilised onto CM3 chip at 88 RU. The FpF was serially diluted and applied to the chip at concentrations of between 100-2.15 µg/mL. Purple line – 100 µg/mL, green – 50 µg/mL, orange – 25 µg/mL, purple – 12.5 µg/mL, brown – 7.25 µg/mL, orange, and pink 3.63 µg/mL. Black lines represent the fitting of the 1:1 binding model to the experimental data.

Both anti-VEGF FpFs derived from ranibizumab bind to VEGF in a concentration dependent manner (Figures 86 and 87). Rebinding events are visible on both sensorgrams at FpF concentrations of 100 and 50 µg/mL. Increases in response visible after approximately 1000 seconds of method run time relate to these rebinding events. Rebinding occurs when the anti-VEGF FpF binds to the immobilised VEGF and subsequently dissociates, however, the dissociated FpF then rebinds to a different VEGF molecule giving an increase in response. A rebinding event can significantly influence the measurement of dissociation kinetics [214] meaning obtaining reproducible, consistent data can be challenging.

A 1:1 binding model was used to fit the SPR sensorgrams (Figures 86 and 87) to generate binding constants (Table 13) for both anti-VEGF FpFs prepared using ranibizumab. From the fitting, association rates were obtained, the dissociation rate could not be measured as both FpFs were prepared using ranibizumab. As dissociation rate could not be determined the affinity of both FpFs to VEGF could not be calculated.

162

Molecule	Derived from	Reagent(s) used for preparation	K_a (1/Ms)	K_d (1/s)	K_D (nM)
Anti-VEGF monospecific FpF – 115 kDa MW	Fab$_{Rani}$	PEG *bis*-sulfone TCO reagent **26** PEG *bis*-sulfone Tz reagent **27**	5792	N.D.	N.D.
Legacy Anti-VEGF monospecific FpF – 120 kDa MW	Fab$_{Rani}$	PEG di-*bis*-sulfone dimerization reagent **5**	5486	N.D.	N.D.

Table 13: Binding constants for Anti-VEGF FpFs prepared via conjugation-ligation using reagents **26** and **27** and via conjugation to reagent **5**. Ranibizumab was the source of anti-VEGF activity for both molecules. N.D. means not determined.

The anti-VEGF FpF prepared via conjugation ligation was found to have a slightly faster association rate (K_a 5792 vs 5486) than the anti-VEGF FpF prepared using reagent **5,** however, this difference is so small that it is likely to be experimental error rather than a true result. The association rates for both anti-VEGF FpFs measured during this are lower than the measured association rates for both of the anti-VEGF FpFs derived from bevacizumab (Figure 85 and Table 12). Parent, unmodified ranibizumab is known to associate faster to VEGF than bevacizumab [215]. Also, a PEG-Fab$_{Rani}$ prepared in previous work using a PEG$_{20}$ *bis*-sulfone reagent **8** had a faster association rate to VEGF than a PEG-Fab$_{Beva}$ molecule also prepared using a PEG$_{20}$ *bis*-sulfone reagent **8**.

A possible explanation for the unexpectedly low association rates measured for both anti-VEGF FpFs derived from ranibizumab (Table 13) could be that the VEGF immobilised onto the chip was not in a healthy state and had begun to degrade limiting the binding activity of the ligand. It may have been better to immobilise another chip with VEGF immediately before using for this experiment.

To conclude, this set of SPR binding experiments comparing anti-VEGF FpFs prepared via conjugation-ligation and via conjugation to reagent **5,** it should not be assumed that FpFs prepared via the 2 different methodologies have equivalent binding performance (i.e., association, dissociation and affinity). The binding constants attained for the anti-VEGF FpFs prepared using Fab$_{Beva}$ suggest that an anti-VEGF FpF prepared using PEG di *bis*-sulfone **5** may have greater affinity towards VEGF, this finding correlates with ELISA experimentation (Figure 78). Making definitive

conclusions is difficult however as these experiments are single replicates, more experimental replicates are required to give a definitive answer.

SPR of BsFpFs prepared via conjugation-ligation

Several different BsFpFs were prepared using the conjugation-ligation methodology using PEG *bis*-sulfone TCO **26** and PEG *bis*-sulfone Tz **27** described in Chapter 4. Anti-VEGF/IL-6R, anti-VEGF/TNF-α and anti-TNF-α/IL-6R molecules were prepared and kinetically assessed using SPR to generate sensorgrams and binding constants. These three targets were chosen because of their relevance within ocular diseases. VEGF and TNF-α are known to contribute to the pathology of wet AMD [216,217]. TNF-α and IL-6R are both implicated in ocular inflammatory diseases such as uveitis [218,219]. More detailed discussion of the role of TNF-α and IL-6R as pro-inflammatory cytokines within the eye was made in Chapter 1. Single target SPR binding and kinetic assays were performed meaning each BsFpF the binding and kinetics of the BsFpF to both targets were measured separately.

Kinetics of an anti-VEGF/IL-6R BsFpF

An anti-VEGF/IL-6R BsFpF derived from Fab_{Rani} and Fab_{Tocili} had its binding to VEGF and IL-6R assessed using SPR. The sensorgram generated for binding to VEGF (Figure 88A) lacks clarity due to the concentration of the anti-VEGF/IL-6R BsFpF being too low (highest concentration 20.75 µg/mL). Low concentrations can impact the performance of the Biacore X100. The VEGF binding sensorgram (Figure 88A) does however show that the anti-VEGF/IL-6R BsFpF binds to VEGF in a concentration dependent manner, as concentration increases so does response.

The sensorgram derived from the binding of the anti-VEGF/IL-6R BsFpF to IL-6R (Figure 88B) shows that the BsFpF also binds to IL-6R in a concentration dependent manner. The responses measured in the IL-6R sensorgram are significantly higher because a considerably larger amount of his-tag IL-6R was captured on the surface of the NTA chip compared to the amount of VEGF immobilised onto the CM3 chip surface used for the VEGF binding experiment (88 RU). Although the exact amount of IL-6R that was captured was unknown it was certainly well more than the VEGF immobilisation level. It is important to note that capturing small amounts of his-tagged ligand onto the surface of an NTA chip is not feasible.

Figure 88: SPR sensorgrams for an Anti VEGF/IL-6R BsFpF prepared via conjugation-ligation with binding moieties derived from Fab$_{Rani}$ and Fab$_{Tocili}$. The BsFpF was serially diluted and applied to the chip at concentrations of between 20.75-2.59 µg/mL (against VEGF) and 20.75-1.29 µg/mL (against IL-6R), **(A)** VEGF sensorgram, VEGF immobilised onto CM3 chip at 88 RU, pink line 20.75 µg/mL. green 10.38 µg/mL, red 5.19 µg/mL, dark green and blue 2.59 µg/mL. **(B)** IL-6R sensorgram, orange line 20.75 µg/mL, purple line 10.38 µg/mL, dark orange line 5.19 µg/mL, pink line 2.59 µg/mL, red and blue line 1.29 µg/mL. Black lines on both sensorgrams represent the fitting of the 1:1 binding model to the experimental data.

Binding constants (Table 14) were derived from the VEGF and IL-6R sensorgrams (Figure 88). The binding constants along with the sensorgrams are presented to show that the Anti-VEGF/IL-6R BsFpF can bind to both of its targets. As the VEGF binding moiety was derived from ranibizumab, the dissociation rate and affinity could not be determined.

Molecule	Derived from	Target ligand	K_a (1/Ms)	K_d (1/s)	K_D (nM)
Anti-VEGF/IL-6R BsFpF – 115 kDa MW	Fab_{Ranii}	VEGF	3517	N.D.	N.D.
	Fab_{Tocili}	IL-6R	13442	2.48×10^{-4}	18

Table 14: Binding constants for an Anti-VEGF/IL-6R BsFpF prepared via conjugation-ligation using reagents **26** and **27**. N.D. means not determined.

Kinetics of an anti-VEGF/TNF-α BsFpF

Next an anti-VEGF/TNF-α BsFpF derived from Fab_{Rani} and $Fab_{Inflixi}$ had its binding to VEGF and TNF-α assessed. Again, the VEGF sensorgram (Figure 89A) was of poor quality due to the low concentration of BsFpF injected (highest concentration 20 µg/mL). Responses measured for binding to TNF-α (Figure 89B) were significantly higher because TNF-α containing a his-tag was captured onto the surface of an NTA chip, meaning the level of TNF-α on the chip surface could not be particularly well controlled. Both the VEGF (Figure 89A) and TNF-α (Figure 89B) sensorgrams showed that the anti-VEGF/TNF-α BsFpF derived from Fab_{Rani} and $Fab_{Inflixi}$ bound to both of its targets in a concentration dependent manner.

A − VEGF sensorgram

B − TNF-α sensorgram
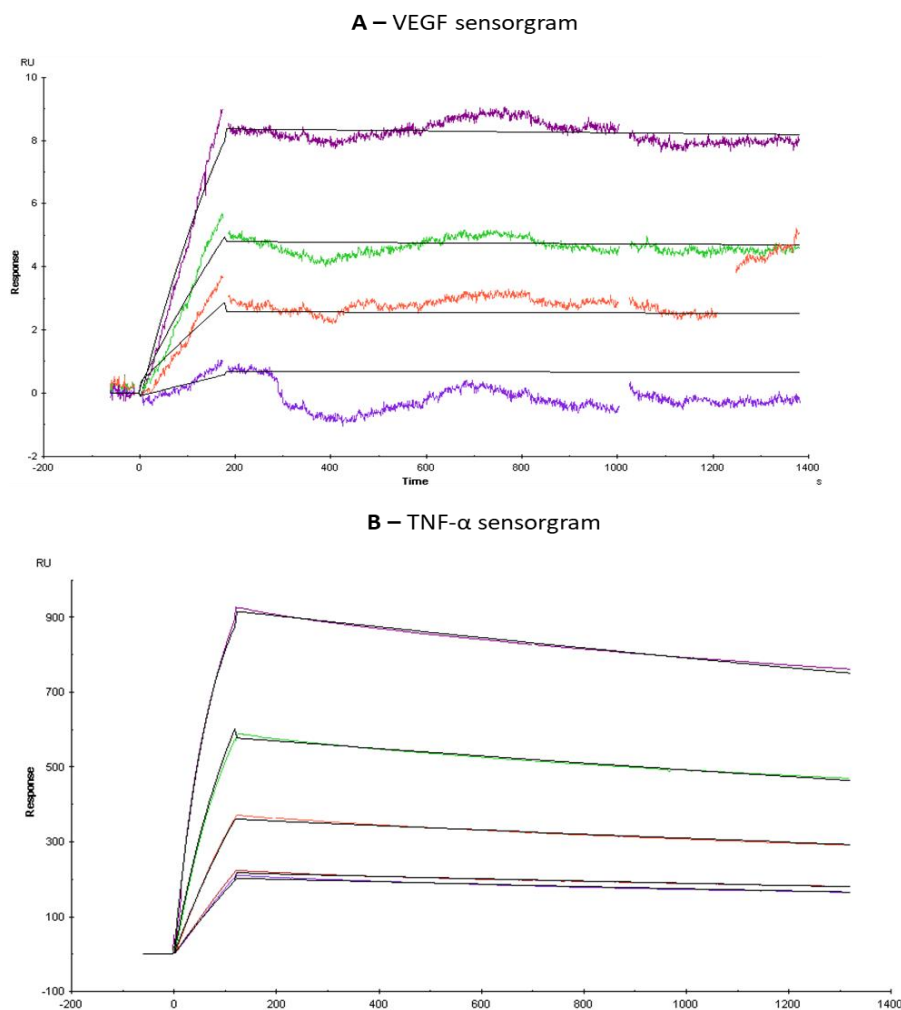
Figure 89: SPR sensorgrams for an Anti VEGF/TNF-α BsFpF prepared via conjugation-ligation with binding moieties derived from Fab_{Rani} and $Fab_{Inflixi}$. The BsFpF was serially diluted and applied to both chips at concentrations between 20-2.5 µg/mL. **(A)** VEGF sensorgram, VEGF immobilised onto CM3 chip at 88 RU, purple line 20 µg/mL. green 10 µg/mL, orange 5 µg/mL, light purple 2.5 µg/mL. **(B)** TNF-α sensorgram, pink line 20 µg/mL, green line 10 µg/mL, orange line 5 µg/mL, red and light purple line 2.5 µg/mL. Black lines on both sensorgrams represent the fitting of the 1:1 binding model to the experimental data.

After fitting the VEGF and TNF-α sensorgrams (Figure 89) with a 1:1 fitting model, binding constants and affinities were calculated (Table 15). The association rate of the anti-VEGF/TNF-α BsFpF to VEGF (K_a 2863) was found to be like that of the association rate of the anti-VEGF/IL-6R BsFpF to VEGF (K_a 3517), it was not possible, again, to calculate dissociation rate or affinity. The association of the anti-VEGF/TNF-α BsFpF to TNF-α (K_a 23801) was found to be faster than the association to VEGF.

Molecule	Derived from	Target ligand	K_a (1/Ms)	K_d (1/s)	K_D (nM)
Anti-VEGF/TNF-α BsFpF – 115 kDa MW	Fab$_{Rani}$	VEGF	2863	N.D.	N.D.
	Fab$_{Inflixi}$	TNF-α	23801	1.76×10^{-4}	7.4

Table 15: Binding constants for an Anti-VEGF/TNF-α BsFpF prepared via conjugation-ligation using reagents **26** and **27**. N.D. means not determined.

Kinetics of an anti-VEGF/TNF-α BsFpF

An anti-VEGF/IL-6R BsFpF derived from Fab$_{Beva}$ and Fab$_{Inflixi}$ was applied to a CM3 onto which VEGF had been immobilised at a concentration of 88 RU and also to an NTA chip to which his-tagged TNF-α had been captured. The sensorgrams for these 2 experiments are presented in Figure 90. A key difference was that this example of an anti-VEGF/TNF-α BsFpF was that it was prepared using Fab$_{Beva}$ meaning it should be possible to measure dissociation rates and affinities of the BsFpF towards VEGF, this was not possible previously (Table 15).

An immediate observation for the VEGF sensorgram (Figure 90A) is clarity of the sensorgram compared to previously presented sensorgrams for binding of BsFpFs to VEGF (Figures 88A and 89A), this occurred as the anti-VEGF-TNF-α BsFpF was applied to the chip at greater concentrations (up to 100 μg/mL) which in turn lead to a greater response.
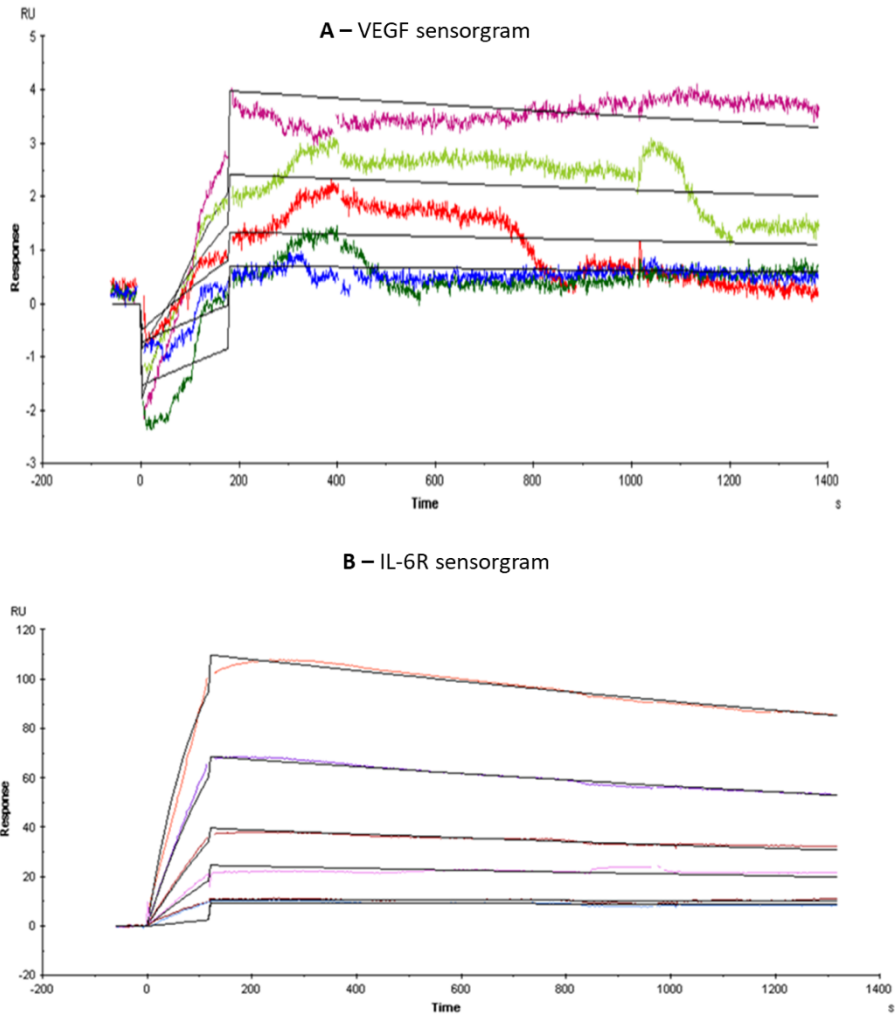
Figure 90: SPR sensorgrams for an Anti VEGF/TNF-α BsFpF prepared via conjugation-ligation with binding moieties derived from Fab$_{Beva}$ and Fab$_{Inflixi}$. The BsFpF was serially diluted and applied to both chips at concentrations between 100-6.25 µg/mL. **(A)** VEGF sensorgram, VEGF immobilised onto CM3 chip at 88 RU **(B)** TNF-α sensorgram. Red lines (both sensorgrams) 200 µg/mL, green 100 µg/mL, blue 50 µg/mL, pink 25 µg/mL, turquoise 12.5 µg/mL, orange and yellow 6.25 µg/mL. Black lines on both sensorgrams represent the fitting of the 1:1 binding model to the experimental data.

Binding constants derived from the sensorgrams (Figure 90) are presented in Table 16. Association rates, dissociation rates and affinities are available for both binding arms of the anti-VEGF/TNF-α BsFpF.

169

Molecule	Derived from	Target ligand	K_a (1/Ms)	K_d (1/s)	K_D (nM)
Anti-VEGF/TNF-α BsFpF – 115 kDa MW	Fab$_{Beva}$	VEGF	8087	8.40×10^{-5}	10.0
	Fab$_{Inflixi}$	TNF-α	70301	8.40×10^{-5}	2.4

Table 16: Binding constants for an Anti-VEGF/TNF-α BsFpF prepared using Fab$_{Beva}$ and Fab$_{Tocili}$ via conjugation-ligation using reagents **26** and **27**.

Kinetics of an anti-TNF-α/IL-6R BsFpF

Finally, the kinetics of an anti-TNF-α/IL-6R BsFpF derived from Fab$_{Inflixi}$ and Fab$_{Tocili}$ was measured. This was the first BsFpF not to contain a VEGF binding moiety. The anti-TNF-α/IL-6R bound to both TNF-α and IL-6R in a concentration dependent manner (Figure 91).

Figure 91: SPR sensorgrams for a Anti TNF-α/IL-6R BsFpF prepared via conjugation-ligation with binding moieties derived from Fab$_{Inflix}$ and Fab$_{Tocili}$. The BsFpF was serially diluted and applied to both chips at concentrations between 100-6.25 µg/mL. **(A)** TNF-α sensorgram, **(B)** IL-6R sensorgram. Red lines (both sensorgrams) 200 µg/mL, green 100 µg/mL, blue 50 µg/mL, pink 25 µg/mL, turquoise 12.5 µg/mL, orange and yellow 6.25 µg/mL. Black lines on both sensorgrams represent the fitting of the 1:1 binding model to the experimental data.

Binding constants and affinities for the anti-TNF-α/IL-6R BsFpF are shown in Table 17.

Molecule	Derived from	Target ligand	K_a (1/Ms)	K_d (1/s)	K_D (nM)
Anti-TNF-α/IL-6R BsFpF – 115 kDa MW	Fab$_{Inflixi}$	TNF-α	88070	5.34×10^{-4}	2.9
	Fab$_{Tocili}$	IL-6R	91591	2.63×10^{-4}	5.8

Table 17: Binding constants for an Anti- TNF-α /IL-6R BsFpF prepared via conjugation-ligation using reagents **26** and **27**.

To summarise the findings in this section it is evident that a range of BsFpFs prepared via conjugation ligation can bind to both of their intended targets in a concentration dependent manner. A pertinent question does arise regarding the extent of interference caused by the non-binding moiety, i.e. does the VEGF binding arm of an anti-VEGF/IL-6R BsFpF interfere during binding of the BsFpF to IL-6R. Results presented in the following section aimed to address this question.

SPR of an anti-VEGF/IL-6R BsFpF derived from Fab$_{Beva}$ and Fab$_{Tocili}$

Within this section the results of SPR binding and kinetic assays of an anti-VEGF/IL-6R BsFpF derived from Fab$_{Beva}$ and Fab$_{Tocili}$ and towards VEGF and IL-6R are presented. Each measurement was performed 3 times to see if binding constants were reproducible. More extensive testing of the anti-VEGF/IL-6R BsFpF using SPR was possible because large quantities of Fab$_{Beva}$ and Fab$_{Tocili}$ were available because large-scale digestions of bevacizumab and tocilizumab using soluble papain were performed (Chapter 3).

To determine if the VEGF and IL-6R binding arms of the BsFpF were able to bind independently of each other an anti-VEGF TCO functionalised Fab conjugate **28** and an anti-IL-6R Tz functionalised Fab conjugate **27** were prepared. The functionalised Fab conjugates essentially represent each half of the anti-VEGF/IL-6R BsFpF. Comparison of the association rates, dissociation rates and affinities of the BsFpF to the TCO **28** and Tz **27** functionalised Fab conjugates would allow judgements to be made as to whether the BsFpF is truly able to bind independently to VEGF and IL-6R. For clarity the structures of the 3 different antibody conjugates are presented in Figure 92.

Anti-VEGF/IL-6R BsFpF
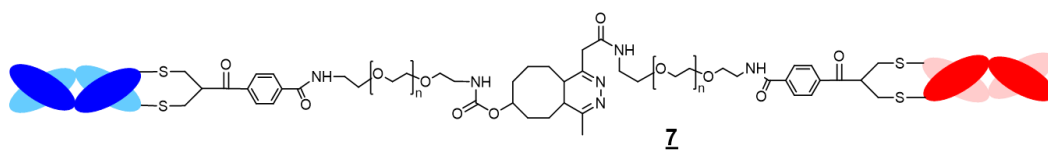
Anti-VEGF TCO functionalised Fab conjugate
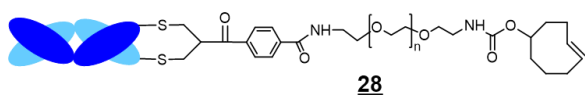
Anti-IL-6R Tz functionalised Fab conjugate
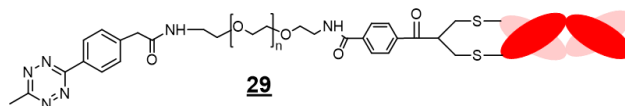
Figure 92: Structures of the Anti-VEGF/IL-6R BsFpF **7**, Anti-VEGF TCO functionalised Fab conjugate **28** and Anti-IL-6R Tz functionalised Fab conjugate **29** used in SPR kinetic assays. Fab$_{Beva}$ and/or Fab$_{Tocili}$ were used to prepare these antibody conjugates.

Sensorgrams for the binding of the anti-VEGF/IL-6R BsFpF and anti-VEGF TCO functionalised Fab conjugate **28** binding to VEGF (Figure 93) show that both molecules bind in a concentration dependent manner. 3 separate experimental replicates were performed with Figure 93 showing typical sensorgrams for the binding of the BsFpF and conjugated Fab **28** to VEGF. The same CM3 chip onto which VEGF was immobilised at a concentration of 95.9 RU was used for all experimentation.
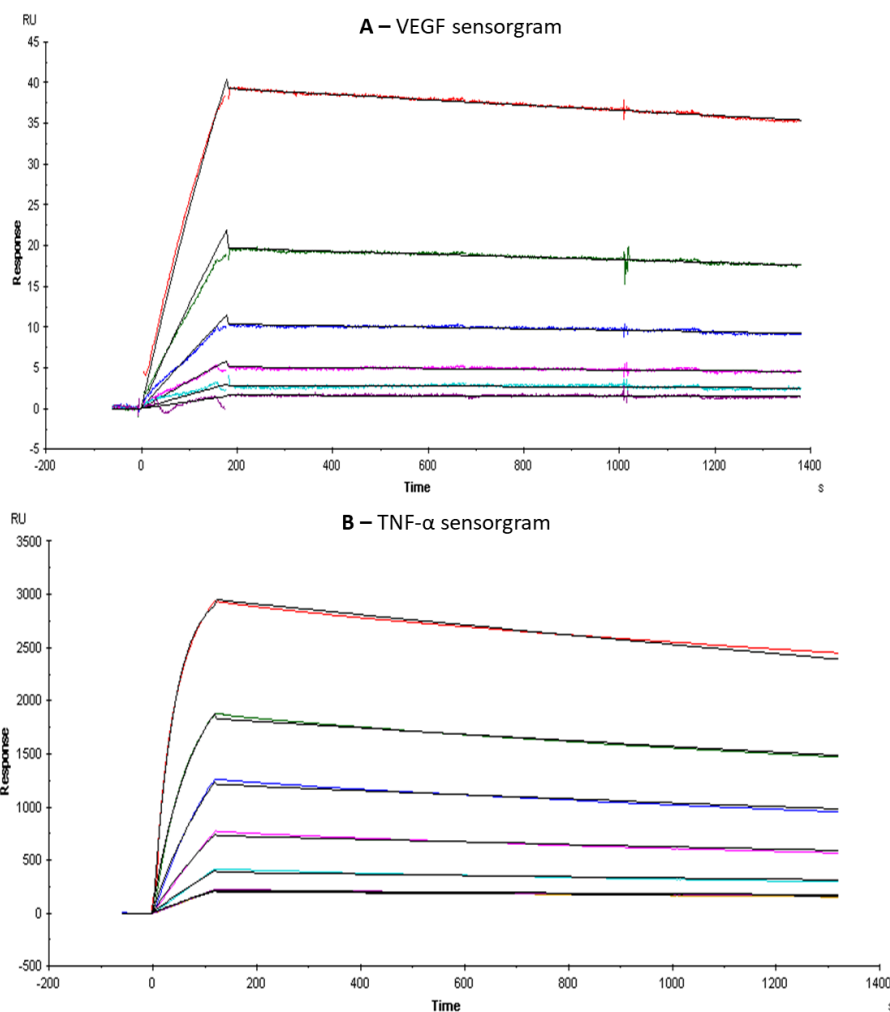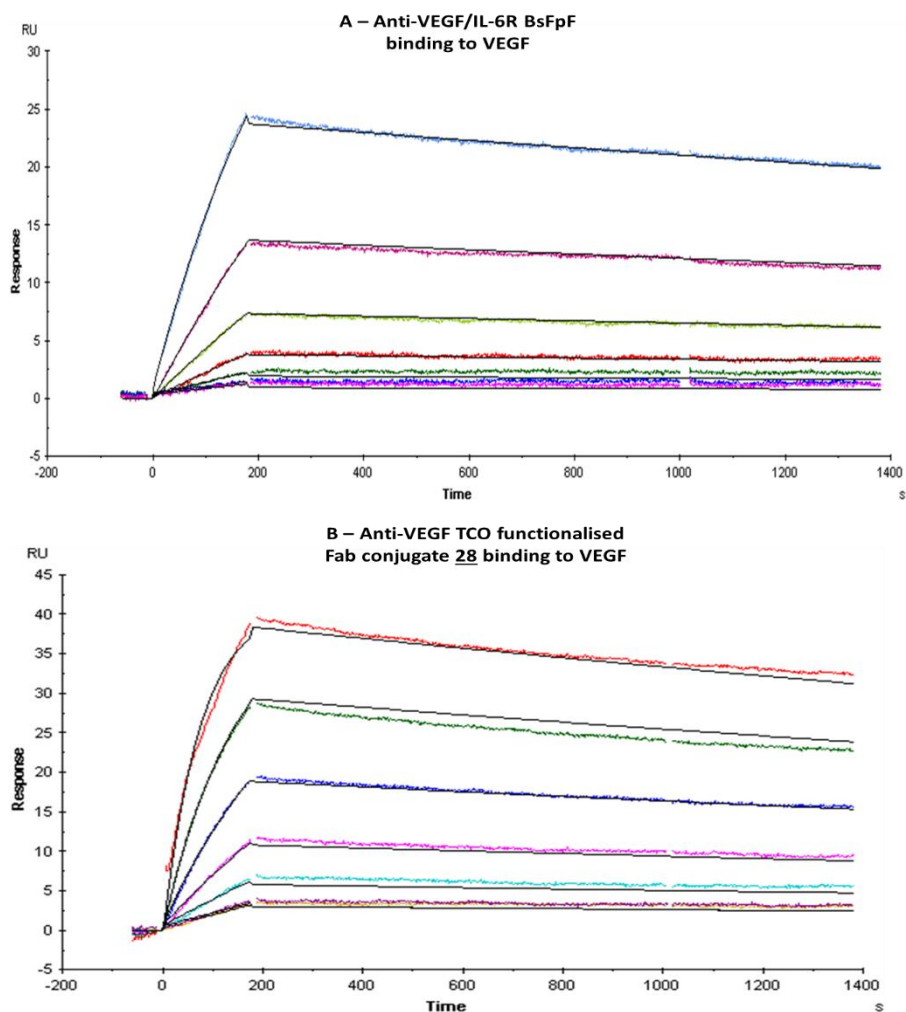
Figure 93: SPR sensorgrams for an Anti VEGF/IL-6R BsFpF prepared via conjugation-ligation with binding moieties derived from Fab$_{Beva}$ and Fab$_{Tocili}$ and for an anti-VEGF TCO functionalised Fab conjugate **28** – *VEGF binding*. The BsFpF was serially diluted and applied to the chip at concentrations of between 60-1.83 µg/mL. The Fab conjugate **28** was serially diluted at concentrations of between 62-1.93 µg/mL **(A)** BsFpF sensorgram, light blue line 60 µg/mL. pink 30 µg/mL, light green 15 µg/mL, red 7.5 µg/mL, green 3.75 µg/mL, blue and purple 1.83 µg/mL. **(B)** Fab conjugate **28** sensorgram, red line 62 µg/mL, green 31 µg/mL, dark blue 15.5 µg/mL, pink 7.75 µg/mL, brown and yellow 1.93 µg/mL. Black lines on both sensorgrams represent the fitting of the 1:1 binding model to the experimental data.

173

**A – Anti-VEGF/IL-6R
BsFpF binding to IL-6R**

**B – Anti-IL-6R Tz functionalised Fab
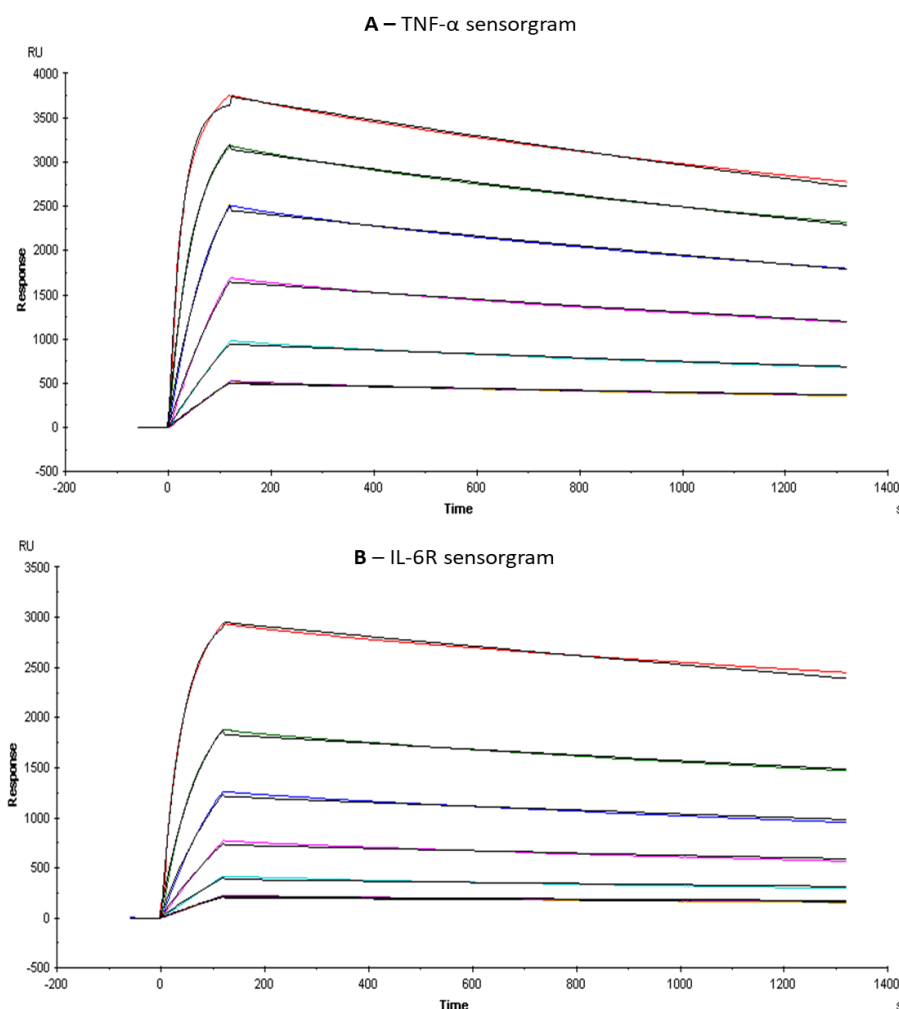conjugate 29 binding to IL-6R**
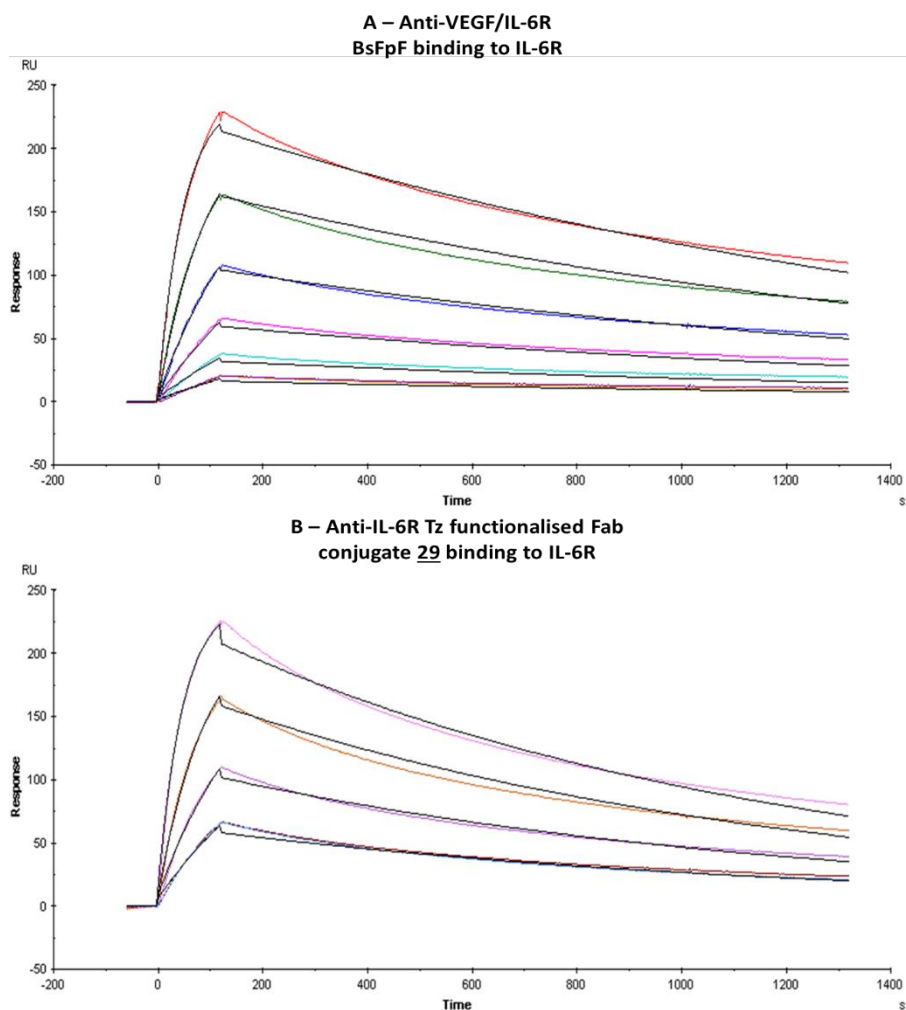
Figure 94: SPR sensorgrams for an Anti VEGF/IL-6R BsFpF prepared via conjugation-ligation with binding moieties derived from Fab$_{Beva}$ and Fab$_{Tocili}$ and for an anti-IL-6R Tz functionalised Fab conjugate **27** – *IL-6R binding*. The BsFpF was serially diluted and applied to the chip at concentrations of between 60-1.83 µg/mL. The Fab conjugate **27** was serially diluted at concentrations of between 92-2.94 µg/mL **(A)** BsFpF sensorgram, red line 60 µg/mL. green 30 µg/mL, blue 15 µg/mL, pink 7.5 µg/mL, light blue 3.75 µg/mL, brown and yellow 1.83 µg/mL. **(B)** Fab conjugate **27** sensorgram, pink line 92 µg/mL, orange 41 µg/mL, dark pink 20.5 µg/mL, light blue and brown 2.94 µg/mL. Black lines on both sensorgrams represent the fitting of the 1:1 binding model to the experimental data.

Both sets of sensorgrams (Figures 93 and 94) show that anti-VEGF/IL-6R BsFpF and TCO **28** and Tz **29** functionalised Fab conjugate molecules bind in a concentration dependent manner to VEGF and IL-6R. From these sensorgrams binding constants for the anti-VEGF/IL-6R BsFpF, anti-VEGF TCO functionalised Fab conjugate **28** and anti-IL-6R Tz functionalised Fab conjugate **29** were derived (Table 18).

174

Molecule	Derived from	Target ligand	K_a (1/Ms)	K_a (1/Ms) STDEV	K_d (1/s)	K_d (1/s) STDEV	K_D (nM)	K_D (nM) STDEV	Chi^2	R_{max}	Chi^2 % of R_{max}
Anti-VEGF/IL-6R BsFpF 115 kDa MW	Fab_{Beva} / Fab_{Tocili}	VEGF	8436	2701	1.00×10^{-4}	3.70×10^{-5}	13.0	7.8	0.12	52	0.23
Anti-VEGF TCO functionalised Fab conjugate **28** 60 kDa MW	Fab_{Beva}	VEGF	13136	581	1.45×10^{-4}	3.53×10^{-5}	10.9	3.0	0.52	42	1.23
Anti-VEGF/IL-6R BsFpF 115 kDa MW	Fab_{Beva} / $Fab_{Inflixi}$	IL-6R	28357	13083	5.73×10^{-4}	7.57×10^{-5}	23.3	14.4	12.50	241	5.18
Anti-IL-6R Tz functionalised Fab conjugate **27** 60 kDa MW	Fab_{Tocili}	IL-6R	39970	18353	1.25×10^{-3}	4.94×10^{-4}	38.1	29.6	10.57	234	4.51

**Table 18:** Average kinetic constants (n=3) of an anti-VEGF/IL-6R BsFpF prepared via conjugation-ligation using reagents **26** and **27**, anti-VEGF TCO functionalised Fab conjugate **28** and an anti-IL-6R functionalised Fab conjugate **29**. The averages are calculated from 3 separate experiments with standard deviations (STDEV) presented. Chi2, R_{max} and Chi2 % of R_{max} values are also average values (n=3).

A 1:1 binding model was used for the fitting of all experimental data to allow calculation of the binding constants. Chi^2 is a quantitative measure of how well the binding model fits to the experimental data, allowing accurate calculation of binding constants, Chi^2 values are presented in Table 18. In SPR, to say that fitting is optimal, a Chi^2 value should be within 10% of the R_{max}, R_{max} is a parameter that reflects the number of complexes formed between the analyte and ligand during the kinetic assay. Chi^2 values were within 10% of the R_{max} value (Table 18, final column) for all the kinetic assays performed in this series of experiments. A higher Chi^2 was recorded for the kinetic assays using IL-6R as the target ligand because a greater number of complexes were formed during these experiments leading to higher R_{max} values. This difference in response occurs because more ligand is present on the chip during the IL-6R kinetic assays than during the VEGF kinetic assays as the IL-6R is captured instead of being immobilised.

Focusing on the binding constants and affinities, the data presented in Table 18 shows that firstly the anti-VEGF TCO functionalised Fab conjugate **28** binds faster to VEGF (K_a 13136) than the anti-VEGF/IL-6R BsFpF (K_a 8436). The reasons for this could be due to the physical size of the molecules and the effect that it has upon mobility. The anti-VEGF/IL-6R BsFpF is close to two times the molecular weight of the anti-VEGF TCO functionalised Fab conjugate **28** (115 kDa vs 60 kDa) likely slowing

association as the BsFpF would take longer to encounter the chip surface. The same trend in association rates is also observed for binding to IL-6R with the anti-IL-6R Tz functionalised Fab conjugate **27** having a greater association rate (K_a 39970) than the anti-VEGF/IL-6R BsFpF (K_a 28357).

Another possible explanation could be that the non-binding arm is creating some sort of steric shielding effect slowing down association of the BsFpF with VEGF and IL-6R. This could occur in a similar way to the effect that PEGylation of an antibody or antibody fragment can have upon dissociation rate. It is well known that PEGylation of Fabs results in slower association rates [220] with PEGylated Fabs derived from trastuzumab [210], ranibizumab and bevacizumab showing slower association rates [161] than the unconjugated Fabs. A steric shielding effect of the non-binding arm may not be out of the question.

The dissociation rate of the anti-VEGF/IL-6R BsFpF (K_d 1.00 x 10^{-4}) from VEGF was like the dissociation rate of the anti-VEGF TCO functionalised Fab conjugate **28** (K_d 1.45 x 10^{-4}) from the same ligand. This result indicates that BsFpF and Fab conjugate **28** bind to VEGF with a similar strength. The non-binding moiety, in this case the IL-6R binding arm of the BsFpF does not affect the strength of binding of the BsFpF to VEGF. The affinity of the anti-VEGF/IL-6R BsFpF to VEGF (K_D 13.0 nM) was like the anti-VEGF TCO functionalised Fab conjugate **28** (K_D 10.9 nM).

For the dissociation rates of the anti-VEGF/IL-6R BsFpF and anti-IL-6R Tz functionalised Fab conjugate **29** from IL-6R some differences were measured. The BsFpF dissociates slower (K_d 5.73x10^{-4}) than the anti-IL-6R Tz functionalised Fab conjugate **29** (K_d 1.25x10^{-3}) and has greater affinity (K_D 23.3 nM vs K_D 38.1 nM). Quite large standard deviations (presented in Table 18) were seen for the association, dissociation and affinities derived from the IL-6R binding experiments. This may be due to the IL-6R SPR method not being suitably robust. Development of an IL-6R SPR methodology in which the IL-6R is immobilised at a RU level of less than 100 units may lead to more reproducible results.

A caveat when using both SPR and ELISA is that the ligands are either immobilised or captured onto a surface therefore meaning they are not free to move and orientate themselves naturally. MST however is a solution-based method which could mean that *in vivo* conditions are mimicked more accurately. This technique was used to assess the affinities of a range of different antibodies and conjugates to their targets in a solution-based setting, included in the conjugates was an anti-VEGF/IL-

6R BsFpF derived from Fab$_{Beva}$ and Fab$_{Tocili}$ to allow comparison to the ELISA and SPR data generated for the same molecule.

Microscale thermophoresis of antibodies and antibody conjugates

Prior to conducting an affinity measurement using MST either the target or ligand needs to be labelled with a fluorescent dye. For this series of experiments the antibodies or antibody conjugates were chosen to be labelled. This choice was made because ligands such as VEGF, TNF and IL-6R are extremely costly to purchase and because the risk of losing the ligands to waste during the labelling process was deemed too great. The first antibody to be labelled was bevacizumab. The fluorescent dye of choice was a red-NHS labelling kit provided by Nanotemper. A red dye was chosen as this matched the detector on the Monolith Pico MST equipment that was available. An NHS dye was chosen as this dye reacts with amines present on the surface of IgGs to form covalent bonds. Amines such as lysine are found and are available for conjugation on the outside of antibody molecules.

Another option could have been a maleimide based dye. This would have been viable for unmodified antibodies as they contain free disulfide bonds. However, antibody conjugates do not contain free disulfide bonds as they are involved in conjugation to reagents such as PEG *bis*-sulfone TCO **26** and PEG *bis*-sulfone **8**. Because of this it was decided to use an NHS dye for all experimentation to try and ensure consistency.

Firstly, bevacizumab was incubated with the red-NHS dye for 30 minutes at ambient temperature while being protected from light. The bevacizumab / red-NHS dye mixture was then purified using a gravity fed column to allow separation of free red-NHS dye from the bevacizumab/dye conjugate. The eluent was collected in three separate fractions. Figure 95 shows the column purification and then the three collected fractions.
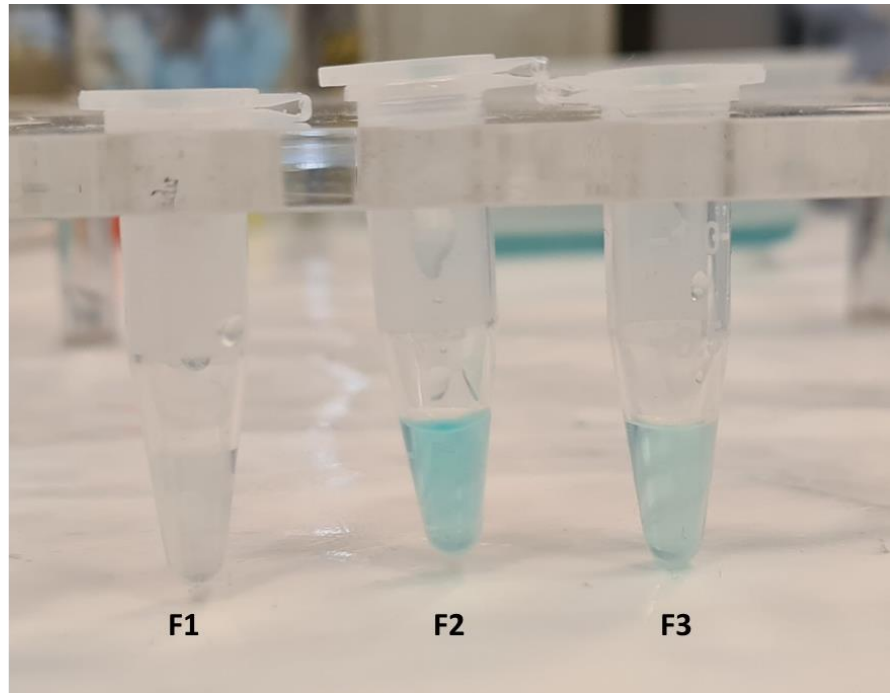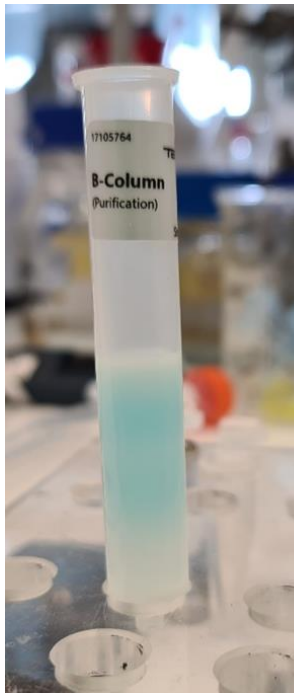
Figure 95: MST purification column loaded with the bevacizumab/dye mixture after 30 minutes of incubation and collected fractions (F1 to F3) eluted from the purification column. The collected fractions contain bevacizumab – red NHS dye conjugates, free red NHS dye was removed during purification

Once the fractions are collected degree of labelling (DOL) needs to be measured. To gain accurate readings during MST the bevacizumab molecule should be conjugated to a single molecule of the red-NHS dye. DOL is calculated by measuring the UV absorbance of each purified fraction at 280 nM (for protein concentration) and 650 nM (dye concentration) to calculate respective concentrations. Using the molar extinction coefficient of the red-NHS dye (195,000 $M^{-1}cm^{-1}$) a degree of labelling was calculated. In this instance the degree of labelling was found to be 0.596, 0.708 and 0.778 for fractions F1, F2 and F3 (Figure 95).

A DOL between 0.5-1.0 indicates that bevacizumab is conjugated to a single molecule of the red-NHS dye. All of the labelled bevacizumab fractions collected were suitable for use in an MST binding assay. However, F3 was chosen over F1 and F2 as the DOL (0.778) for the sample was closest to one. The same labelling process was used for all of the antibodies and antibody conjugates (BsFpFs, functionalised Fab conjugates) that had their binding affinities measured using MST.

Prior to running a binding affinity experiment using MST, a pre-test should be performed. A pre-test can determine whether the labelled molecule, in this case bevacizumab, has agglomerated or has a propensity to stick to any of the test capillary surfaces, agglomeration or sticking will affect the quality and validity of the results generated using MST. The MST equipment performs a pre-test to determine a

capillary shape which should be smooth and reproducible. Splitting of the capillary shape peak indicates agglomeration of the test molecule and poor reproducibility of the capillary shape indicates that the test molecule is sticking to the surfaces of the test capillary.

The labelled bevacizumab was loaded into a standard glass MST capillary at a concentration of 5 nM. 5 nM is the standard recommended concentration recommended by the MST Pico control software. No target ligand was used during the pre-test. The MST trace (Figure 96) for labelled bevacizumab shows that the capillary shape is smooth and uniform, no splitting is observed indicating the labelled bevacizumab is of sufficient quality to be used during an MST kinetic experiment. If splitting or poor reproducibility had occurred, agglomeration or sticking could be reduced by adding a surfactant such as Tween 20 into the experimental buffer or by purchasing capillary tubes with non-adherent coatings.
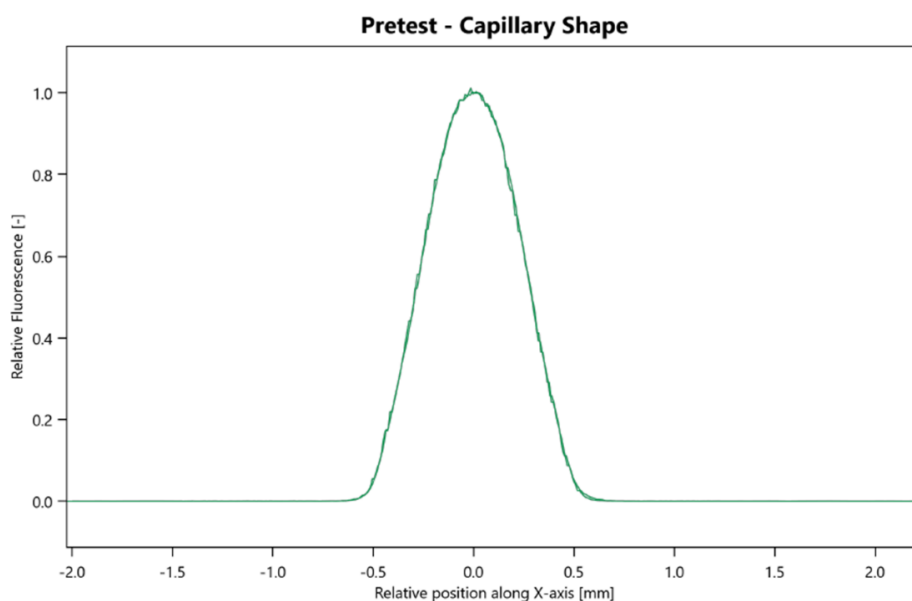
Figure 96: MST trace showing the result of an MST pre-test experiment using bevacizumab labelled with red-NHS dye, 5nM concentration.

The affinity of tagged bevacizumab towards VEGF was measured. To a series of capillary tubes, tagged bevacizumab was added at a concentration of 5 nM. Serially diluted VEGF was added to each of the capillary tubes containing tagged bevacizumab and the loaded tubes placed into the Monolith Pico MST equipment. A binding affinity experiment was performed with the resulting MST trace (Figure 97) having a similar appearance to an ELISA curve. An MST trace derived from a binding affinity experiment plots FNorm against ligand concentration. FNorm is a normalised

fluorescence value calculated by dividing F_1 by F_0. F_1 corresponds to the fluorescence value measured in the heated state, F_0 is the fluorescence value measured in the cold state before the infrared laser is turned on during the binding affinity experiment.

The affinity of bevacizumab to VEGF was found to be 5.7 nM with affinity being calculated using a 1:1 binding model. The affinity of bevacizumab to VEGF generated using MST (K_D 5.7 nM) was found to be lower than the affinity measured using ELISA (K_D 0.02 nM). This is likely due to differences in the methodologies. In ELISA, the ligand is immobile as it is captured to the bottom of a 96 well plate whereas MST is a solution-based method. Values generated using MST and ELISA are not directly comparable as the methodologies are fundamentally different. Despite exact values not being comparable it may be possible to compare trends in affinities measured when using MST, ELISA or SPR.
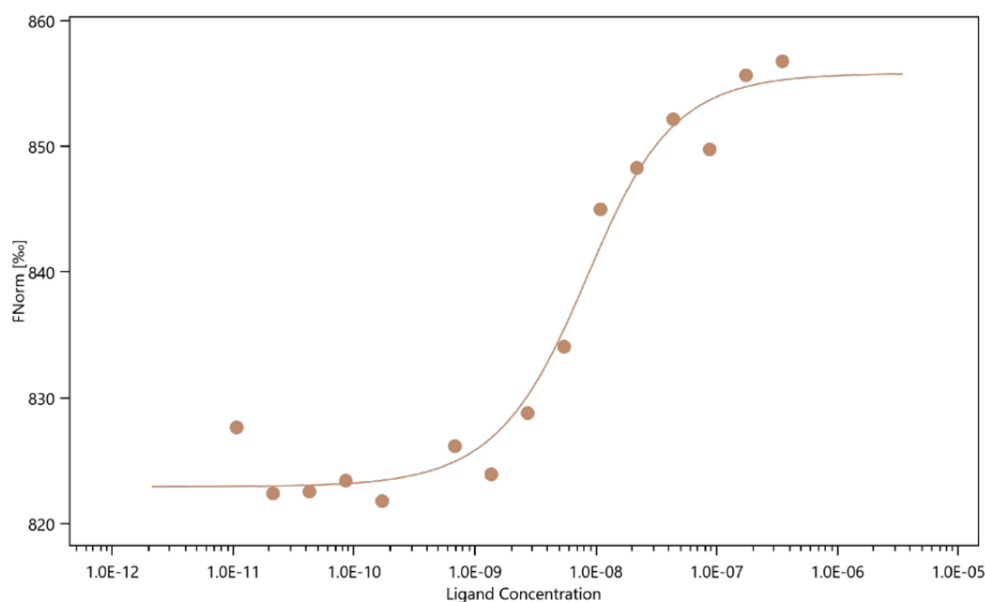
Figure 97: MST dose response curve for the binding of labelled bevacizumab to VEGF. Bevacizumab concentration was 5 nM for all samples. VEGF concentration between 3.50×10^{-7}-1.06×10^{-11} M

A second IgG, tocilizumab was labelled with red-NHS dye and its affinity to IL-6R assessed using MST (Figure 98). An immediate observation is that the dose response curve does not proceed in the same direction (FNorm increasing in tandem with ligand concentration) as the dose response curve for bevacizumab (Figure 97). Nanotemper, the manufacturer of the monolith pico MST equipment say the direction of the curve does not influence further analysis (i.e. deriving affinities) and that the direction of the curve depends on specific properties of the molecules tested, this is confirmed within an application note [221].
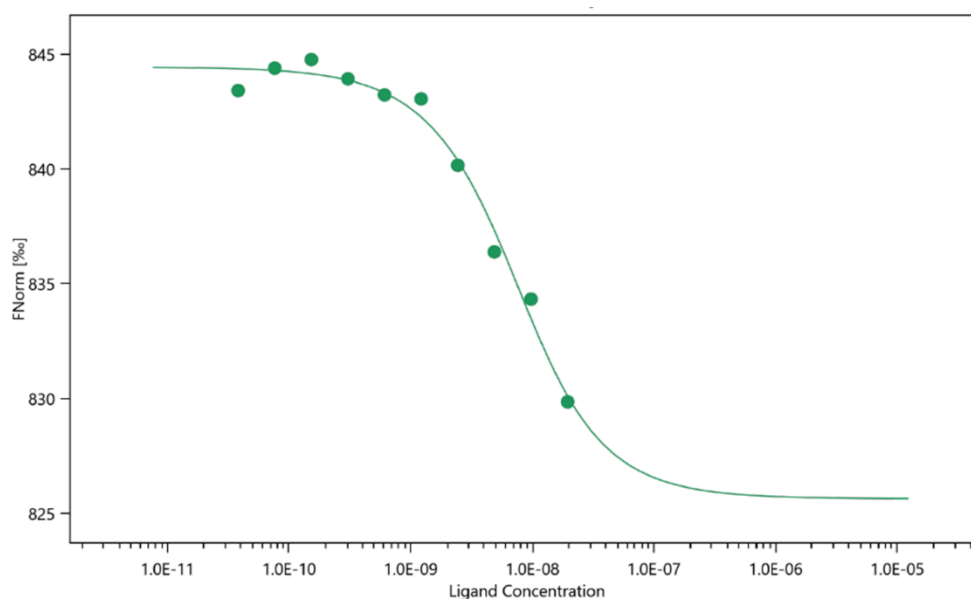
Figure 98: MST dose response curve for the binding of labelled tocilizumab to IL-6R. Tocilizumab concentration was 5 nM for all samples. IL-6R concentration was between 1.95×10^{-7}-3.81×10^{-11}M

The affinity of tocilizumab to IL-6R when measured using MST (K_D 5 nM) was found to be lower than when the affinity was measured during ELISA (K_D 0.13 nM), the same trend seen for measurements using bevacizumab. There are examples in literature of when a solution-based methodology shows that a molecule has a lower affinity towards its target then when a stationary methodology is used. Binding affinities of Fab$_{Beva}$ to VEGF using isothermal calorimetry were found to be lower than binding affinities measured using ELISA and SPR [222], the binding affinity of an omicron COVID-19 variant to the ACE2 receptor was found to be lower when measured using MST compared to ELISA [223].

Next, it was thought to check if MST was sensitive to changes in valency. Fab$_{beva}$ and Fab$_{tocili}$ were labelled and tested in affinity experiments as examples of monovalent molecules. The intention was to compare the affinities of Fab$_{beva}$ and Fab$_{tocili}$ to bivalent bevacizumab and tocilizumab respectively. It was expected that Fab$_{beva}$ and Fab$_{tocili}$ would have lower affinity towards VEGF and IL-6R compared to bevacizumab and tocilizumab. MST dose response curves and affinities for Fab$_{beva}$ and Fab$_{tocili}$ are shown in Figures 99 and 100.
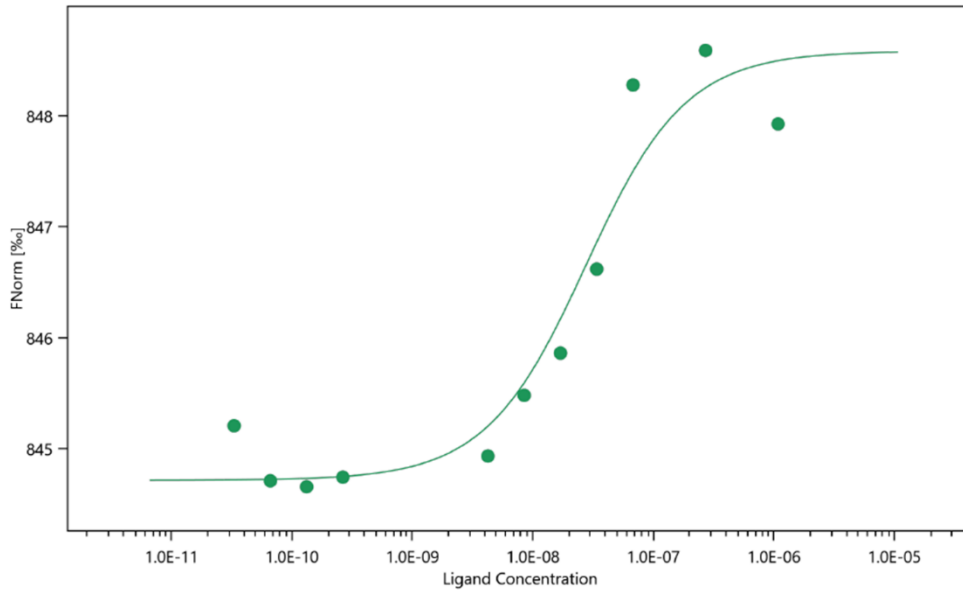
Figure 99: MST dose response curve for the binding of labelled Fab$_{beva}$ to VEGF. Fab$_{beva}$ concentration was 5 nM for all samples. VEGF concentration was between 1.09×10^{-7}-3.31×10^{-11}M
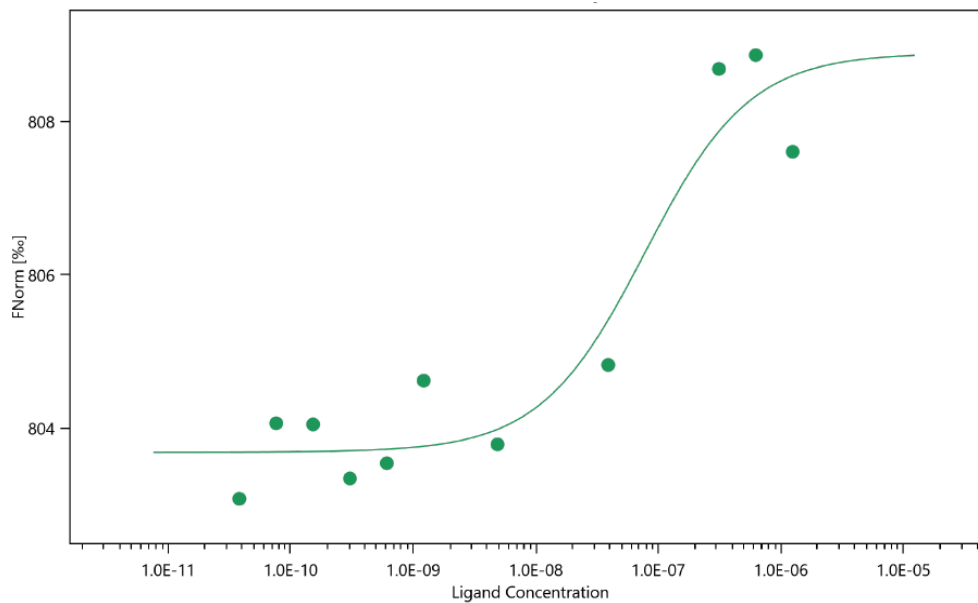
Figure 100: MST dose response curve for the binding of labelled Fab$_{tocili}$ to IL-6R. Fab$_{tocili}$ concentration was 5 nM for all samples. IL-6R concentration was between 1.25×10^{-7}-3.81×10^{-11}M

Both Fab$_{Beva}$ (K$_D$ 25 nM) and Fab$_{Tocili}$ (K$_D$ 75 nM) had lower affinities towards VEGF and IL-6R respectively compared to bevacizumab (K$_D$ 5.7 nM) and tocilizumab (K$_D$ 5 nM). This result is expected as the Fabs are monovalent molecules. The same trend in results was observed for ELISA experiments (Figures 82 and 83) presented earlier in this thesis. Next the affinity of an anti-VEGF/IL-6R BsFpF derived from Fab$_{Beva}$ and Fab$_{Tocili}$ was measured using MST.

MST of an anti-VEGF/IL-6R BsFpF.

The affinity of an anti-VEGF/IL-6R BsFpF derived from Fab$_{Beva}$ and Fab$_{Tocili}$ and prepared via conjugation ligation towards VEGF and IL-6R was measured. Dose response curves were plotted and, from these, binding affinities calculated. An issue to address firstly though is the relevance of IL-6R in a solution-based assay such as MST. IL-6R is present in the human body in two different forms, as a transmembrane receptor but also as a soluble receptor. Increased levels of soluble IL-6R have been found in the vitreous fluid of patients with diabetic retinopathy [224] meaning IL-6R is a suitable choice for use as a ligand in this set of experiments. The same collection of anti-VEGF and anti-IL-6R antibody conjugates used during SPR binding assays (Figure 92) had their affinities measured using MST.

MST dose response curves for the anti-VEGF/IL-6R BsFpF binding to VEGF and IL-6R, the anti-VEGF TCO functionalised Fab conjugate **28** binding to VEGF and the anti-IL-6R Tz functionalised Fab conjugate **29** binding to IL-6R are presented in Figure 101.
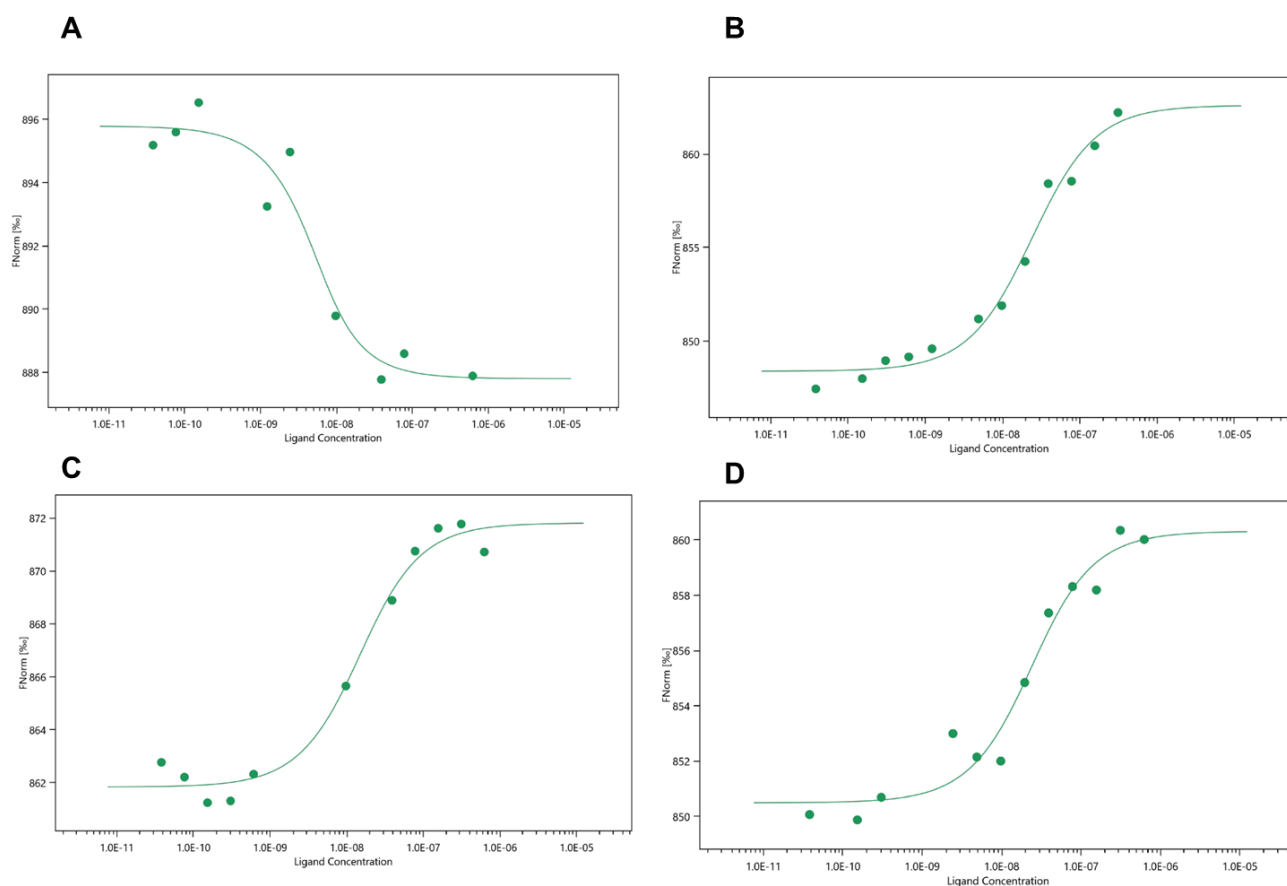
Figure 101: (A) MST dose response curve for the binding of labelled anti-VEGF/IL-6R BsFpF to VEGF. Anti-VEGF/IL-6R BsFpF concentration was 5 nM for all samples, IL-6R concentrations ranging between 6.25×10^{-7} to 3.81×10^{-11}M, **(B)** MST dose response curve for the binding of labelled anti-VEGF/IL-6R BsFpF to IL-6R. Anti-VEGF/IL-6R BsFpF concentration was 5 nM for all samples, IL-6R concentrations ranging between 1.25×10^{-6} to 1.52×10-10M. **(C)** MST dose response curve of an anti-VEGF TCO functionalised Fab conjugate **28** binding to VEGF. Anti-VEGF TCO functionalised Fab conjugate **28** concentration was 5 nM for all samples, IL-6R concentrations ranging between 6.25×10^{-7} to 3.81×10^{-11}M, **(D)** MST dose response curve of an anti-IL-6R Tz functionalised Fab conjugate **29** binding to IL-6R. Anti-IL-6R Tz functionalised Fab conjugate **29** concentration was 5 nM for all samples, IL-6R concentrations ranging between 3.13×10^{-7} to 3.81×10^{-11}M.

From the MST dose response curves affinities were calculated using a 1:1 binding model. It was found that the affinity of the anti-VEGF/IL-6R BsFpF to VEGF (K_D: 2.5 nM) was greater than the affinity of anti-VEGF TCO functionalised Fab conjugate **28** to VEGF (K_D: 12.5 nM). This finding contrasts with the earlier findings during SPR (Table 18) and ELISA (Figure 81) binding experiments in which the affinities of antibody conjugates were shown to be similar. The reverse trend is observed for binding to IL-6R. The affinity of the anti-IL-6R Tz functionalised Fab conjugate **29** to IL-6R is greater (K_D: 20 nM) than the affinity of the anti-VEGF/IL-6R BsFpF to IL-6R (K_D: 73 nM).

There are reasons why this may be the case. Firstly, as MST measures affinity of molecules within solution, the way in which the molecules bind to their targets is

likely to be different as the target ligands are mobile and not immobilised or captured in a set orientation. Secondly, the 2 Fab conjugates **28** and **29** contain free TCO and Tz groups, the impact which these free ligation moieties have upon binding is unknown. Their impact on binding could be assessed by comparing affinities with PEG-Fabs prepared using PEG *bis*-sulfone **8** as they would lack the free TCO and Tz ligating moieties.

The final MST binding experiment performed was the measurement of the affinity of the anti-VEGF/IL-6R BsFpF to both VEGF and IL-6R (Figure 102) in a single experiment. VEGF and IL-6R were added in combination at a 1:1 molar ratio to ensure that neither ligand was in excess of the other. As MST is a solution-based method, ligand mixtures can be used for experimentation quite easily.
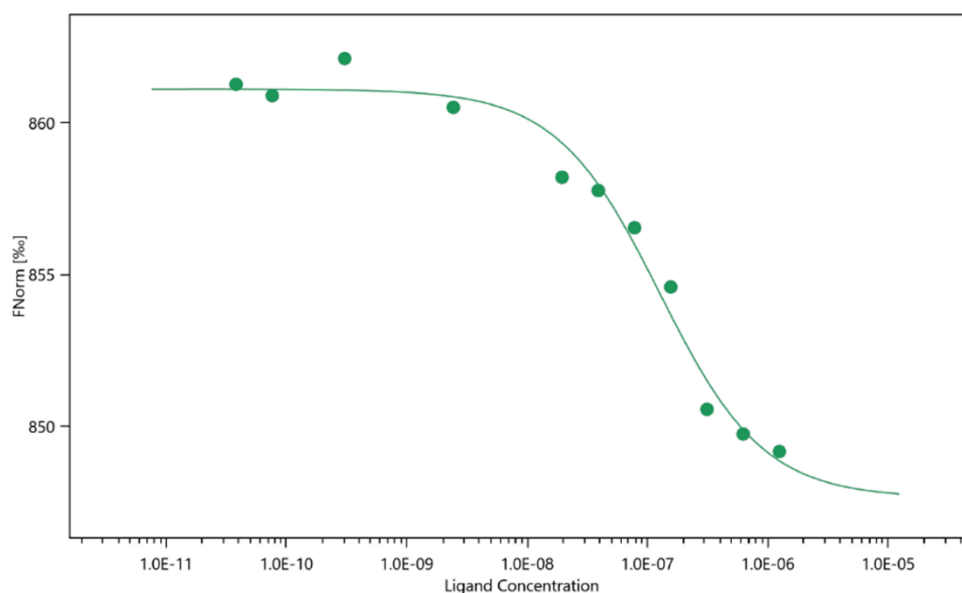
Figure 102: MST dose response curve for the binding of labelled anti-VEGF/IL-6R BsFpF to VEGF and IL-6R simultaneously. Anti-VEGF/IL-6R BsFpF concentration was 5 nM for all samples, Combined ligand concentrations ranging between 1.25x10-6 to 1.52x10-10M with VEGF and IL-6R being combined at a molar ratio of 1:1.

The affinity of the anti-VEGF/IL-6R BsFpF to both VEGF and IL-6R (K_D: 9 nM) was found to be in between the affinities towards VEGF (K_D: 2.5 nM) and IL-6R (K_D: 73 nM). This finding could indicate that the anti-VEGF/IL-6R BsFpF is binding to both of its targets simultaneously.

It is hard to draw definitive conclusions from the binding experiments using MST. More experimental replicates are required to see if results are reproducible. More confidence is also required with the methodology as the technique is quite new within our research group. Despite being potentially expensive it may be worth

185

labelling the target ligands instead of the antibody conjugates to give a different perspective.

Conclusions:

ELISA and SPR were used to compare 2 anti-VEGF monospecific FpFs, one prepared via conjugation to PEG di *bis*-sulfone **5** and the other via conjugation ligation. Both ELISA and SPR found that the anti-VEGF FpF prepared using reagent **5** had greater affinity to VEGF. This finding means that the binding characteristics of an FpF prepared via conjugation ligation should not be assumed to be similar to a FpF prepared using reagent **5**, making comparisons with "legacy" data questionable.

BsFpFs prepared against VEGF/TNF-α, VEGF/IL-6R and TNF-α/IL-6R were found to bind to both of their intended targets in a concentration dependent manner when binding was examined using SPR. However, this set of experiments did not allow conclusions on whether each of the binding arms were able to bind independently. A quantity of an anti-VEGF/IL-6R BsFpF derived from Fab$_{Beva}$ and Fab$_{Tocili}$, an anti-VEGF TCO functionalised Fab conjugate **28** and an anti-IL-6R Tz functionalised Fab conjugate **27** were prepared.

SPR and ELISA binding studies found that the anti-VEGF-IL-6R BsFpF was able to bind with similar affinity to the anti-VEGF TCO functionalised Fab conjugate **28** showing that the VEGF binding arm of the BsFpF can bind independently and without hinderance from the IL-6R binding arm. IL-6R affinities generated using ELISA showed that the IL-6R binding arm of the BsFpF was able to bind to IL-6R without hinderance, however SPR did not show this trend with the affinity of the anti-VEGF/IL-6R BsFpF to IL-6R being greater than the anti-IL-6R Tz functionalised Fab conjugate **27**. Variation in IL-6R concentration from assay to assay may be responsible for this as greater variation of binding constants and affinities were observed during IL-6R binding experiments using SPR. It is also possible that the VEGF binding arm of the BsFpF was binding in a non-specific manner to IL-6R. A control experiment in which the anti-VEGF TCO functionalised Fab conjugate **28** is passed over IL-6R captured onto a NTA chip may help to determine if non-specific binding is occurring.

Chapter 6 – Preliminary *in vitro* functional assays

Treatment of HUVECs with TNF-α and IL-17A

Both TNF-α and IL-17A are found in the aqueous humour of patient with uveitis [225]. For the inflammatory *in vitro* assay the cell model of choice was human umbilical vein endothelial cells (HUVECs) as they express both TNF-α [226] and IL-17 [227] receptors and have precedence of use in experimentation exploring ocular vascular inflammation [228]. Endothelial cells within the eye are implicated in a number of diseases such as dry eye disease, Sjögren's syndrome [229] and inflammatory uveitis [230] making an endothelial cell model a reasonable choice for this set of experiments.

For the inflammatory assay, pro-inflammatory cytokines TNF-α and IL-17A were applied to the HUVECs for a pre-determined period. The cells were tagged with fluorescently labelled antibodies specific for Intercellular adhesion molecule 1 (ICAM-1) or vascular cell adhesion molecule 1 (VCAM-1). Measurement of ICAM-1 and VCAM-1 levels was chosen because both IL-17A [231] and TNF-α [232] upregulate the production of these cell surface markers. The fluorophore of choice for both the ICAM-1 and VCAM-1 antibodies was Allophycocyanin (APC) as endothelial cells can exhibit autofluorescence and interfere with Fluorescein isothiocyanate (FITC) conjugated antibodies [233]. Levels of the cell surface markers were quantified using flow cytometry.

HUVEC cells were grown, sub-cultured and used by passage 5. Figure 103 is a series of images showing the growth of HUVEC cells over a period of 5 days until confluency.
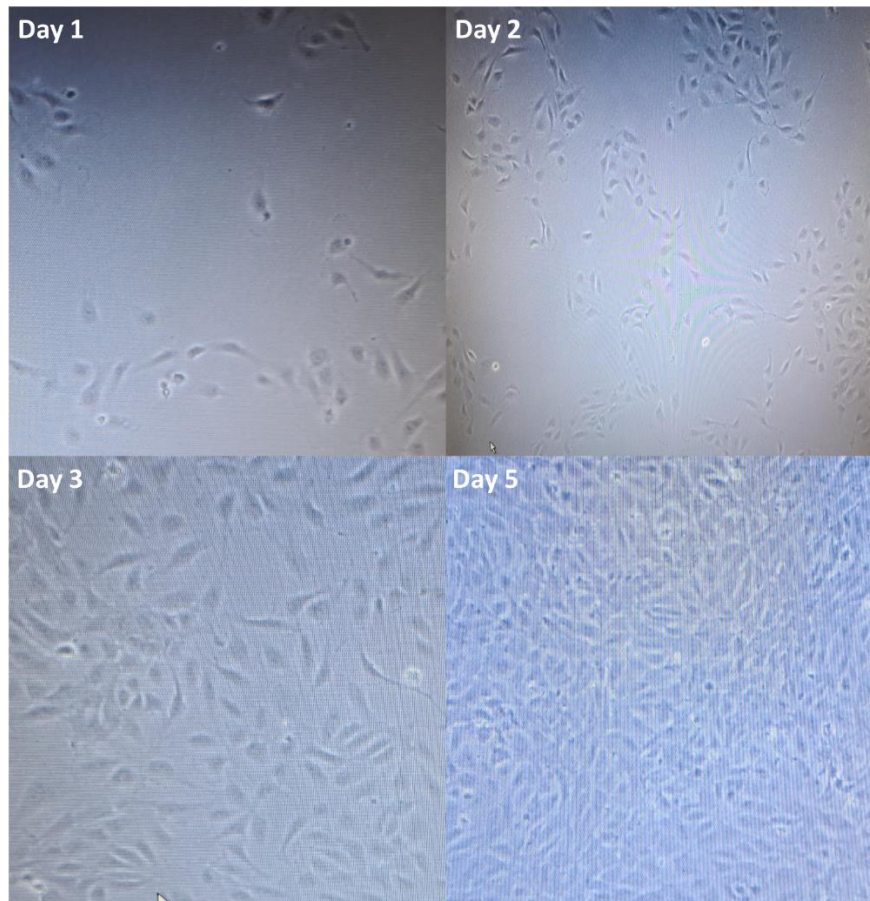
Figure 103: Growth of HUVEC cells using supplemented endothelial cell media. After 5 days the HUVECs were confluent and ready for subculturing. These cells are at passage no. 1. Images were taken at a 10x magnification.

The cells have the typical cobblestone appearance associated with HUVECs, however, further confirmation that the cultured cells were endothelial cells was required. To do this HUVECs were detached from the cell culture flask and tagged with a fluorescently labelled anti-CD31 antibody before checking expression via flow cytometry. CD31 was chosen as it is well known marker for the presence of endothelial cells [234] due to its expression extra-cellularly. Figure 104A is a typical dot plot showing the size (FSC) and granularity (SSC) profile of the HUVECs acquired by flow cytometry. HUVECs are large cells with little internal complexity, as seen under the microscope, the live cells were gated as shown with the dead cells or cell debris, being excluded from further analysis. The histograms depicted in Figure 104B showed that 98.6% of the stained cells in the live gate were CD31 positive (red histogram) compared to the corresponding unstained cells (cells not labelled with antibody, light blue histogram). This indicates the cells stained with the CD31 antibody are endothelial cells.
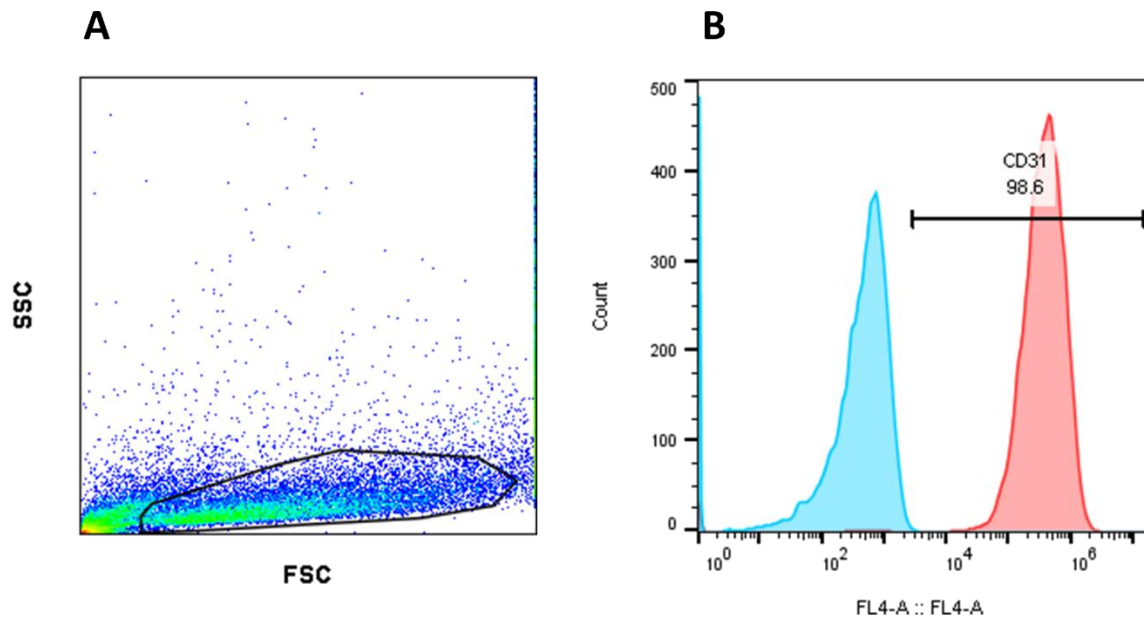
Figure 104: Gated side / forward scatter plot and histograms derived from the flow cytometry of unstained HUVECs and HUVECs stained with an anti-CD31 antibody (APC tagged). **(A)** A dot plot showing the gated live cells based on side and forward scatter plot of unstained HUVEC cells. **(B)** A histogram generated from flow cytometry of unstained live HUVECs (blue histogram) and live HUVECs stained with an anti-CD31 antibody (red histogram).

Next the HUVECs were checked for ICAM-1 and VCAM-1 expression. Obtaining baseline data for the expression of ICAM-1 and VCAM-1 on the surface of HUVECs will allow comparisons to be made when ICAM-1 and VCAM-1 expression is measured following cytokine treatment. As ICAM-1 and VCAM-1 are extracellular markers susceptible to cleavage by trypsin, an enzyme free detachment method was used to detach the cells. If an enzyme-based method such as trypsin was used this could lead to the cell surface markers being removed from the cell surfaces making detection using flow cytometry difficult. Figure 105 shows the live cells gated using forward and side scatter cell properties and histograms with mean fluorescence intensities (MFI) for the unstained and ICAM-1 and VCAM-1 stained live HUVECs.
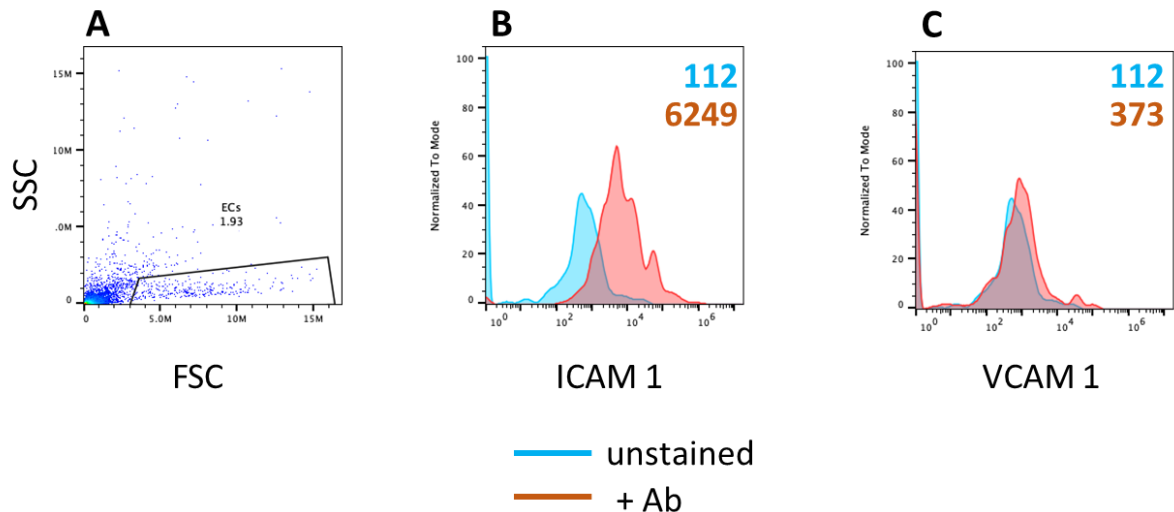
Figure 105: Gated side / forward scatter plot and histograms derived from the flow cytometry of unstained HUVECs and HUVECs stained with anti-ICAM-1 (APC tagged) and anti-VCAM-1 (APC tagged) antibodies. **(A)** A gated side and forward scatter plot of unstained HUVEC cells, same cell gating used for HUVECs stained with anti-ICAM-1 and anti-VCAM-1 antibodies. **(B)** Histogram generated from the flow cytometry of un-stained HUVECs (blue histogram) and HUVECs, ICAM-1 stained (red histogram). The mean fluorescence intensity (MFI) for each histogram is also shown for comparison (blue text unstained MFI, red text ICAM-1 stained MFI) **(C)** Histogram generated from the flow cytometry of unstained HUVECs (blue histogram) and HUVECs, VCAM-1 stained (red histogram), MFI also shown.

An immediate observation from Figure 105A is that not as many healthy cells were present during this experiment as were present during the previous experiment measuring CD31 expression. However, Figures 105B and C show that untreated HUVECs express both ICAM-1 and VCAM-1 on their cell surface compared to the unstained controls. Higher expression of ICAM-1 was observed (MFI of 6,249) than for VCAM-1 (MFI of 373).

Next, HUVECs were seeded with 60,000 cells/well into 12 well plates. Once confluent EC were treated with either TNF-α, IL-17A or a mixture of the two cytokines. TNF-α and IL-17A concentrations were kept constant at 20 ng/mL, with an incubation time of 24hrs. Both the cytokine concentrations and the incubation time were chosen because in the literature ICAM and VCAM are expressed on the surface of HUVECs when using these experimental conditions [231,232]. Microscopy images of each of the wells were taken prior to detachment. It was decided to take microscope images to see if any visible change in cell morphology was visible. Literature has shown that upon exposure of HUVECs to TNF-α the cell morphology does indeed change from the typical cobblestone appearance to more narrow, elongated cells [235]. The pictures shown in Figure 106 are images of HUVECs 24hrs post treatment with TNF-α, IL-17A and the TNF-α/IL-17A mixture.
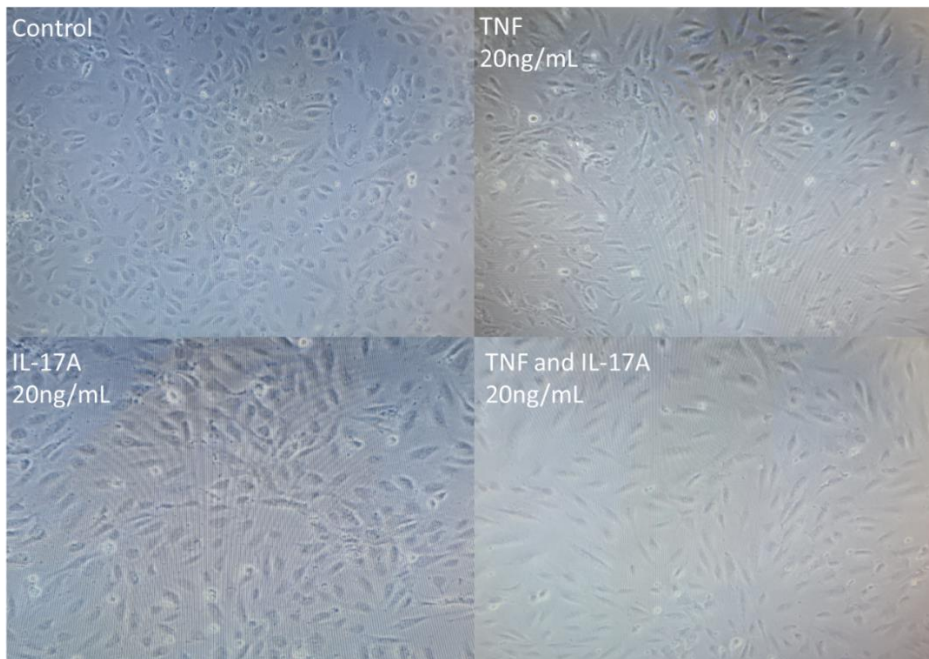
Figure 106: Appearance of HUVEC cells 24 hours post treatment with TNF-α, IL-17A and TNF-α and IL-17A (20 ng/mL each, 40 ng/mL total cytokine concentration) in combination, control is untreated HUVEC cells. These cells are at passage no. 2. Images were taken at a 10x magnification.

Each of the three pictures of cytokine treated HUVEC cells show some differences in morphology compared to control, untreated HUVECs, with longer, more 'swollen' cells being present in each of the cytokine containing samples. This appeared to be the most prevalent HUVECs treated with a mixture of TNF-α and IL-17A. These cells appear to have lengthened and, they are less tightly packed than the control cells. The fact that the cells treated with the cytokine mixture have changed morphology the most, may be because the highest total concentration of cytokine (40 ng/mL) was present within the well. Also, it may be because TNF-α and IL-17A have a synergistic relationship, affecting the inflammatory behaviour of each other. TNF-α and IL-17A have been shown to synergistically drive the expression of proinflammatory molecules in synovial fibroblasts [236] and also have been shown to synergistically regulate the expression of proinflammatory genes in porcine aortic cells [237], meaning that synergy between TNF-α and IL-17A is well known.

In addition, HUVECs were treated with infliximab (100 ng/mL) and secukinumab (anti IL-17A IgG, 150 ng/mL) in combination with TNF-α and IL-17A, to see if they were able to inhibit any potential inflammatory response, the two antibodies were also added as a mixture to the well containing both TNF-α and IL-17A. Figure 107 shows microscopy images of the HUVECs treated with TNF-α, IL-17A and the TNF-α/IL-17A mixture compared to HUVECs treated with the same cytokines but also with the

addition of infliximab and secukinumab. The addition of infliximab appears to have helped maintain the typical cobblestone appearance of the cells. The TNF-α treated control contain some elongated, quite narrow cells whereas this is not seen for cells in which infliximab was added in combination with TNF-α indicating a neutralisation effect. The same observations can be made when infliximab and secukinumab were added in combination to try and attempt to neutralise the effects of the TNF-α/IL-17A cytokine combination. The two neutralising antibodies are again helping to maintain the typical cobblestone appearance of the cells.
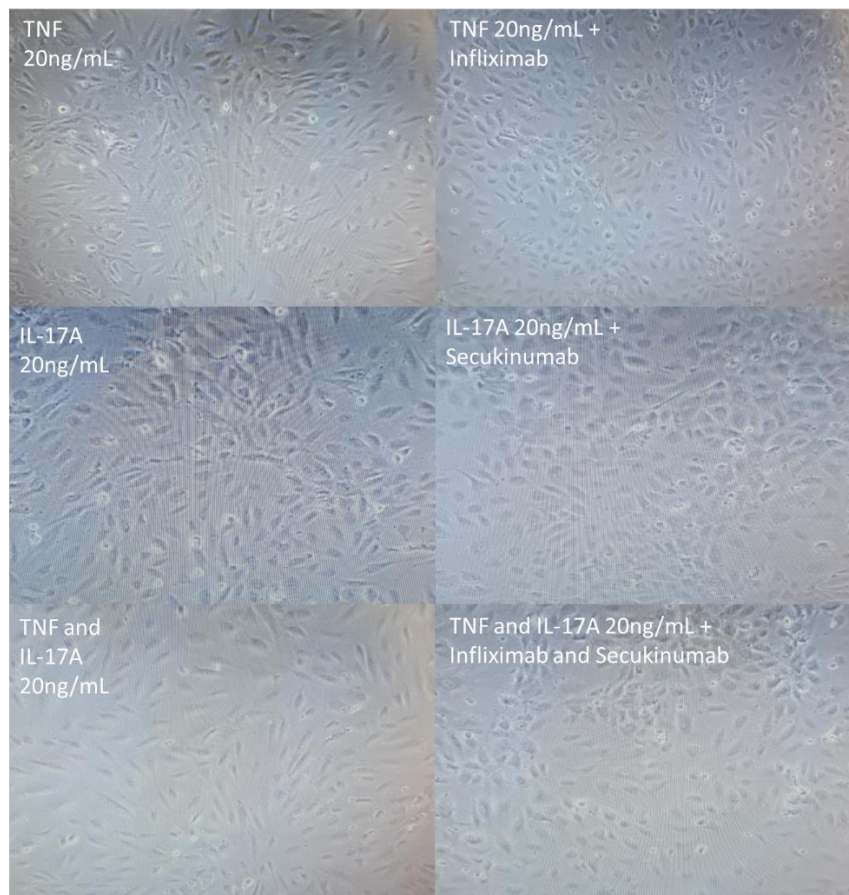
Figure 107: Appearance of HUVEC cell 24 hours post treatment with TNF-α, IL-17A and TNF-α and IL-17A (20 ng/mL each) in combination and HUVEC cells treated with the same cytokines with the addition of either infliximab (100 ng/mL), secukinumab (150 ng/mL) or an infliximab (100 ng/mL) / secukinumab (150 ng/mL) mixture. These cells are at passage no. 2. Images were taken at a 10x magnification.

The HUVEC cells shown in the microscope images in Figures 106 and 107 were then examined for ICAM and VCAM expression using flow cytometry (Figure 108). During this experiment detachment of the cells using the enzyme free buffer proved more challenging, why this was the case is unknown. It was challenging to obtain single cells for flow cytometry analysis, a large quantity of healthy cells may have been excluded from the flow cytometry analysis because it was not possible to

process them in such a way to obtain singlets. However, obtained cells were still examined using flow cytometry and plots generated.

Figure 108: Gated side / forward scatter plot and histograms derived from the flow cytometry of untreated HUVECs stained with anti-ICAM-1 (APC tagged) and anti-VCAM-1 (APC tagged) antibodies and HUVECs treated with TNF-α (20 ng/mL) for 24 hours stained with anti-ICAM-1 and anti-VCAM-1 antibodies. **(A)** A gated side and forward scatter plot of untreated HUVEC cells, same cell gating used for HUVECs treated with TNF-α. **(B)** Histogram generated from the flow cytometry of untreated HUVECs (red histogram) and HUVECs treated with TNF-α (purple histogram), ICAM-1 stained, MFI for each histogram shown **(C)** Histogram generated from the flow cytometry of untreated HUVECs (red histogram) and HUVECs treated with TNF-α (purple histogram), VCAM-1 stained, MFI for each histogram shown. Data represents one experiment.

Figure 108B and C show that treating HUVECs with TNF-α at a concentration of 20 ng/mL upregulated the expression of both ICAM-1 (MFI 6,249 vs 1,050,000) and VCAM-1 (MFI 373 vs 383,056) cell surface markers. Next an identical experiment was performed using IL-17A in place of TNF-α. Figure 109 contains histograms showing ICAM-1 and VCAM-1 expression following treatment with IL-17A.

Figure 109: Gated side / forward scatter plot and histograms derived from the flow cytometry of untreated HUVECs stained with anti-ICAM-1 (APC tagged) and anti-VCAM-1 (APC tagged) antibodies and HUVECs treated with IL-17A (20 ng/mL) for 24 hours stained with anti-ICAM-1 and anti-VCAM-1 antibodies. **(A)** A gated side and forward scatter plot of untreated HUVEC cells, same cell gating used for HUVECs treated with IL-17A. **(B)** Histogram generated from the flow cytometry of untreated HUVECs (red histogram) and HUVECs treated with IL-17A (grey histogram), ICAM-1 stained, MFI for each histogram also shown **(C)** Histogram generated from the flow cytometry of untreated HUVECs (red histogram) and HUVECs treated with IL-17A (grey histogram), VCAM-1 stained, MFI for each histogram also shown. Data represents one experiment.

Addition of IL-17A slightly increased the expression of ICAM-1 (MFI 6,249 vs 7,501) but no increase in VCAM-1 expression was observed (MFI 373 for untreated vs 206 for treated cells). This finding was surprising as the literature suggests that VCAM-1 expression in endothelial cells should increase with IL-17A treatment at concentrations as low as 10 ng/mL [231]. A mixture of TNF-α and IL-17A was then applied to the HUVEC cells. Microscopy images shown previously (Figure 106) indicate that the cytokine combination had the greatest impact upon cell morphology, it was therefore interesting to see if ICAM-1 and VCAM-1 expression increased when a cytokine combination was used. Control HUVECs were treated with a single cytokine. The results of the experiment in which HUVECs were treated with both TNF-α and IL-17A are shown in Figure 110.
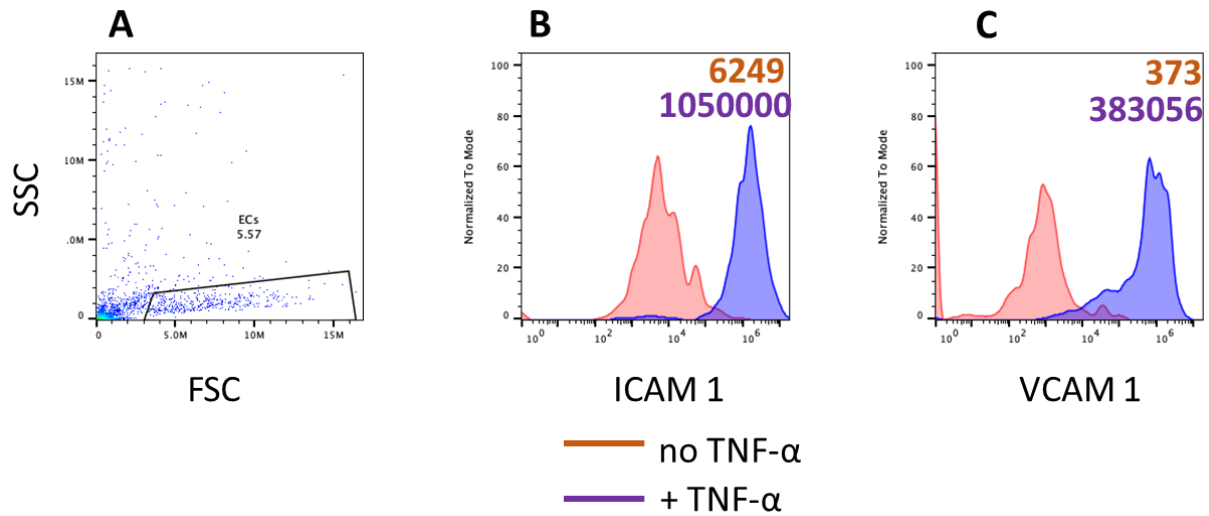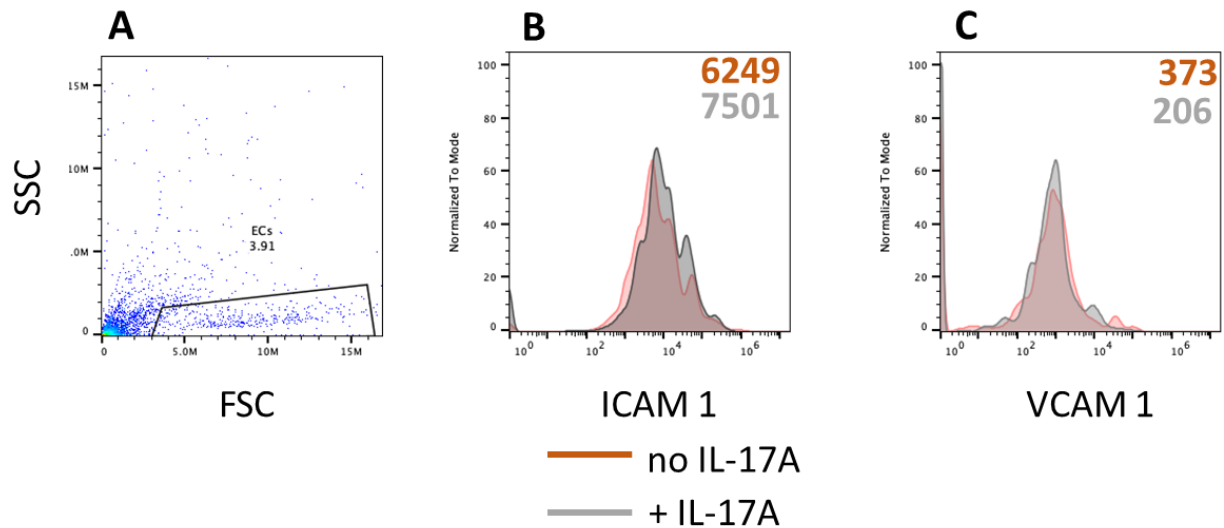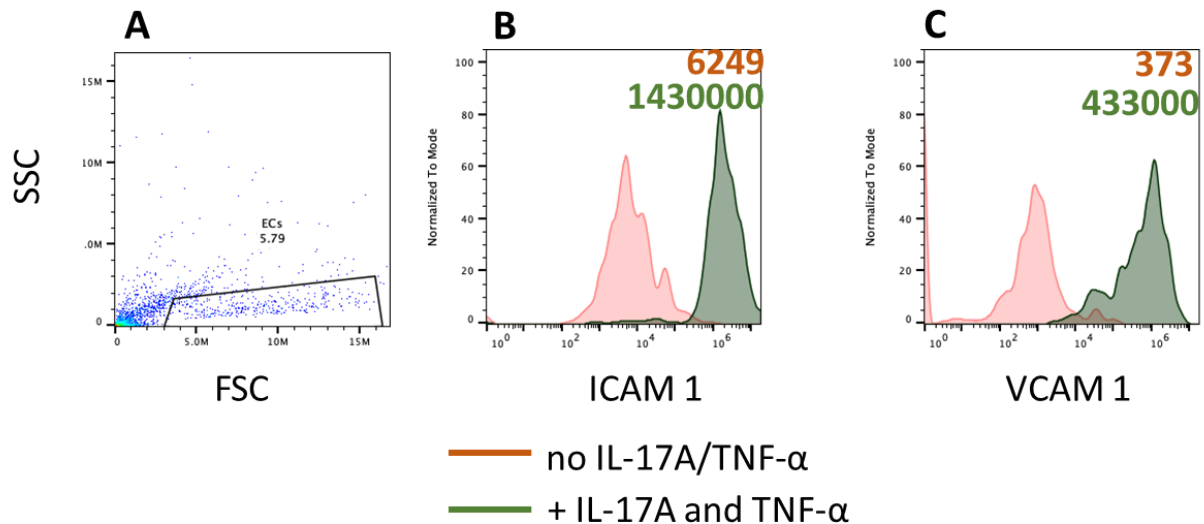
Figure 110: Gated side / forward scatter plot and histograms derived from the flow cytometry of untreated HUVECs stained with anti-ICAM-1 (APC tagged) and anti-VCAM-1 (APC tagged) antibodies and HUVECs treated with TNF-α (20 ng/mL) and IL-17A (20 ng/mL) (40 ng/mL total ligand concentration) stained with anti-ICAM-1 and anti-VCAM-1 antibodies. **(A)** A gated side and forward scatter plot of untreated HUVEC cells, same cell gating used for HUVECs treated with TNF-α and IL-17A. **(B)** Histogram generated from the flow cytometry of untreated HUVECs (red histogram) and HUVECs treated with TNF-α and IL-17A ICAM-1 stained, MFI for each histogram also shown **(C)** Histogram generated from the flow cytometry of untreated HUVECs (red histogram) and HUVECs treated with TNF-α and IL-17A (green histogram) VCAM-1 stained, MFI for each histogram also shown. Data represents one experiment.

Addition of the cytokine mixture increased expression of both ICAM-1 (MFI 6,249 vs 1,430,000) and VCAM-1 (373 vs 433,000) compared to the untreated controls. MFI values the HUVECs treated with the cytokine mixture were also shown to be higher than when HUVECs were treated with just a single cytokine (Figure 108 and 109). This indicated a possible proinflammatory, synergistic relationship between TNF-α and IL-17A when HUVECs are treated with a combination of these two cytokines at the same time. In conjunction with the microscopy images (Figure 106) this gives some confidence that a pro-inflammatory synergistic relationship between the 2 cytokines in this specific model may exist.

Synergy between the two cytokines has been seen previously in hepatocytes [238], a primary epithelial cell found in the liver, in synovial fibroblasts [236] and porcine aortic cells [237] as mentioned earlier in the chapter. The findings in this preliminary experiment also gives confidence that TNF-α and IL-17A are suitable targets for a BsFpF. Both infliximab and secukinumab can be digested to obtain anti-TNF-α and anti-IL-17A Fabs which can be used for the preparation of a BsFpF via conjugation-ligation. To begin to test whether the Fabs obtained from the digestion of these two antibodies can neutralise the effect of TNF-α and IL-17A in this cell model,

HUVECs were treated with TNF-α and IL-17A in the presence of infliximab and secukinumab.

Neutralisation of inflammatory activity with Infliximab and Secukinumab

Having established that TNF-α and a mixture of TNF-α and IL-17A increased expression of ICAM-1 and VCAM-1, the ability of infliximab and secukinumab to inhibit upregulation of ICAM-1 and VCAM-1 was tested. In theory these monoclonal antibodies should reduce both ICAM-1 and VCAM-1 expression as they will bind to the cytokines preventing interaction with TNF-α and IL-17A surface receptors. Histograms derived from the treatment of HUVECS with TNF-α and a mixture of TNF-α and infliximab are shown in Figure 111.

Figure 111: Gated side / forward scatter plot and histograms derived from the flow cytometry of HUVECs treated with TNF-α (20 ng/mL) for 24 hours stained with anti-ICAM-1 (APC tagged) and anti-VCAM-1 (APC tagged) antibodies and HUVECs treated with TNF-α (20 ng/mL) and infliximab (100 ng/mL) for 24 hours stained with anti-ICAM-1 and anti-VCAM-1 antibodies. **(A)** A gated side and forward scatter plot of TNF-α treated HUVEC cells, same cell gating used for HUVECs treated with TNF-α and infliximab. **(B)** Histogram generated from the flow cytometry of HUVECs treated with TNF-α (purple histogram) and HUVECs treated with TNF-α and infliximab (pink histogram) ICAM-1 stained, MFI for each histogram also shown **(C)** Histogram generated from the flow cytometry of HUVECs treated with TNF-α (purple histogram) and HUVECs treated with TNF-α and infliximab (pink histogram) VCAM-1 stained, MFI for each histogram also shown. Data represents one experiment.

Figure 111B and C both show that infliximab neutralises the proinflammatory activity of TNF-α leading to reduced expression of both ICAM-1 (MFI 1,050,000 vs 221,716, without and with antibody, respectively) and VCAM-1 (MFI 383,056 vs 68,233). This result is not surprising as infliximab is a well-known inhibitor of TNF-α [239] and is a marketed therapeutic. Infliximab has also been shown to prevent the

upregulation of ICAM-1 and VCAM-1 in peripheral blood leukocytes and monocytes [240]. Figure 112 contains histograms showing data for when HUVECs have been treated with a mixture of IL17A and secukinumab.

Figure 112: Gated side / forward scatter plot and histograms derived from the flow cytometry of HUVECs treated with IL-17A (20 ng/mL) for 24 hours stained with anti-ICAM-1 (APC tagged) and anti-VCAM-1 (APC tagged) antibodies and HUVECs treated with IL-17A (20 ng/mL) and secukinumab (150 ng/mL) for 24 hours stained with anti-ICAM-1 and anti-VCAM-1 antibodies. **(A)** A gated side and forward scatter plot of IL-17A treated HUVEC cells, same cell gating used for HUVECs treated with IL-17A and secukinumab. **(B)** Histogram generated from the flow cytometry of HUVECs treated with IL-17A (grey histogram) and HUVECs treated with IL-17A and secukinumab (dark green histogram) ICAM-1 stained, MFI for each histogram also shown **(C)** Histogram generated from the flow cytometry of HUVECs treated with IL-17A (grey histogram) and HUVECs treated with IL-17A and secukinumab (dark green histogram) VCAM-1 stained, MFI for each histogram also shown. Data represents one experiment.

Although minimal changes in ICAM-1 and VCAM-1 expression on the surface of HUVECs was observed in the presence of IL-17A (Figure 109), addition of secukinumab reduced the expression of ICAM-1 (MFI 7,501 vs 3,942 without and with antibody, respectively) on the surface of IL-17A treated HUVECs (Figure 112A), secukinumab had no impact on the expression of VCAM-1 (Figure 112B, MFI 597 vs 206 without and with antibody, respectively) and in fact the addition of secukinumab appears to have increased expression of VCAM-1. To really test the neutralising activity of secukinumab in this cell model the applied concentrations of IL-17A and the incubation times need to be optimised. Finding literature showing that ICAM-1 and VCAM-1 expression are down regulated when secukinumab is applied to IL-17A treated cells is challenging. However, it is known that IL-17A upregulates ICAM-1 and VCAM-1 expression [231] and the fact that secukinumab is an approved anti-IL-17A

therapeutic likely means it would be capable of inhibiting the pro inflammatory activity of IL-17A within this HUVEC based model.

Next the ICAM-1 and VCAM-1 expression on HUVECs treated with TNF-α and IL-17A and HUVECs treated with TNF-α, IL-17A, infliximab and secukinumab were compared. The results of this experiment are shown in Figure 113.

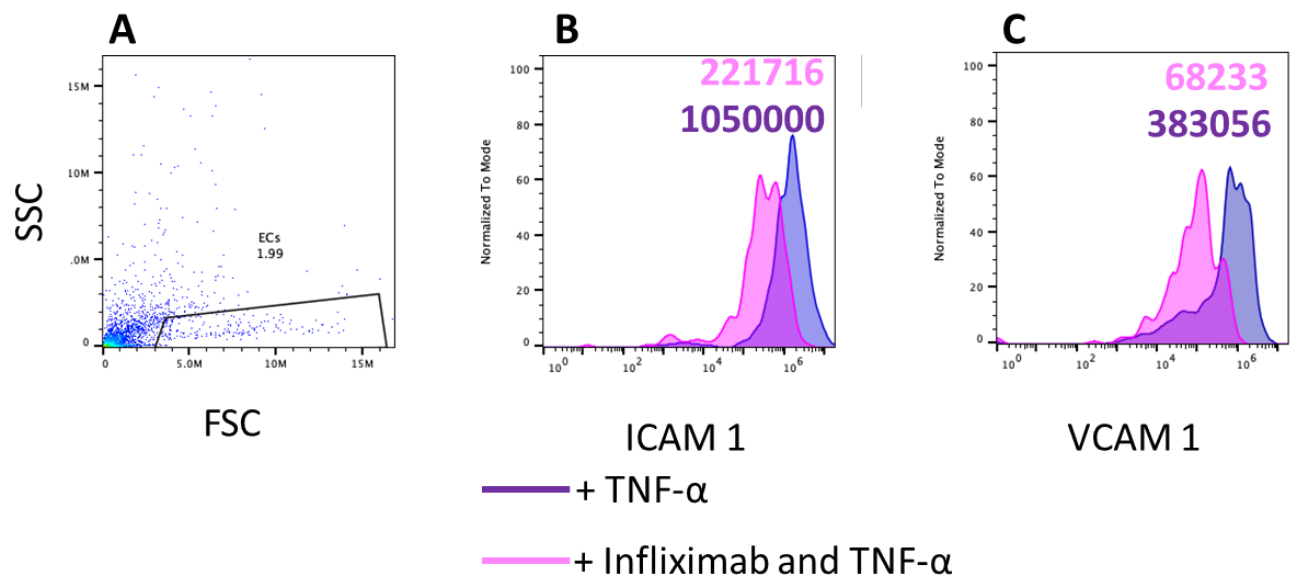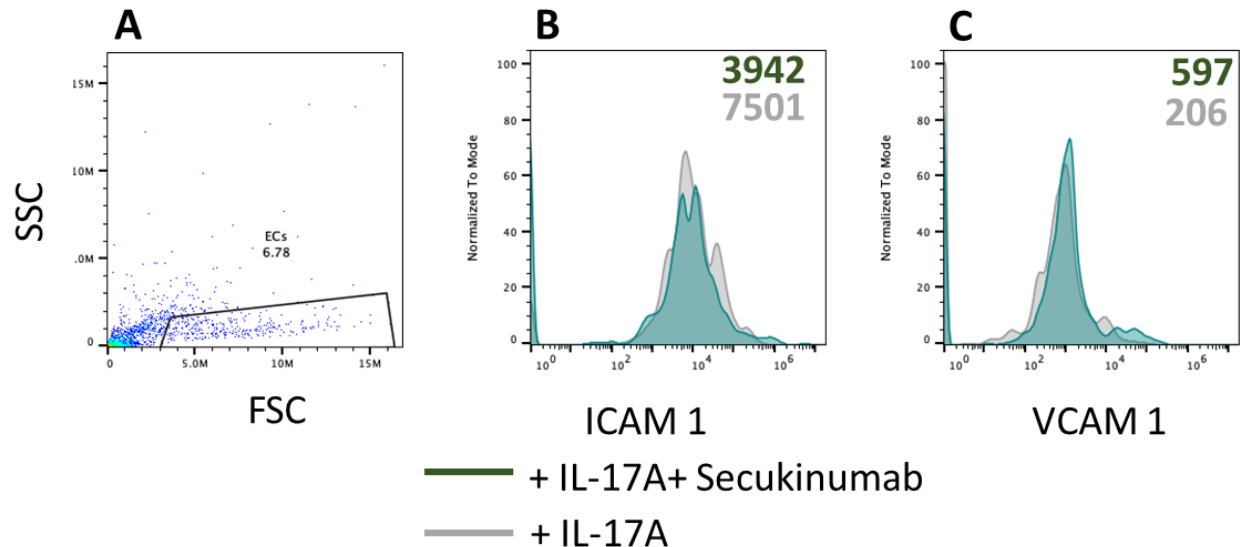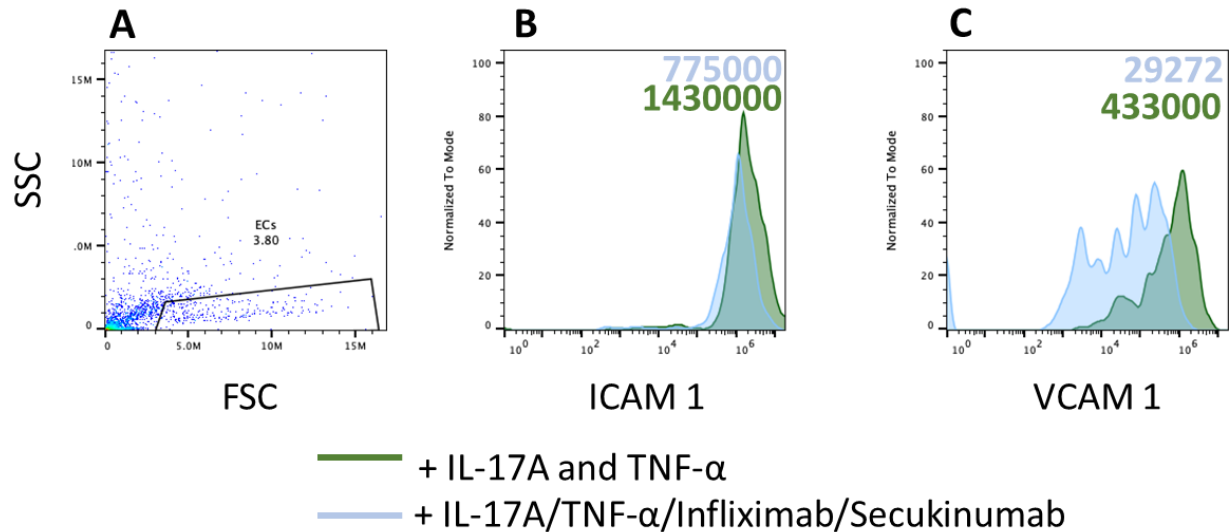**Figure 113:** Gated side / forward scatter plot and histograms derived from the flow cytometry of HUVECs treated with both TNF-α (20 ng/mL) and IL-17A (20 ng/mL) for 24 hours stained with anti-ICAM-1 and anti-VCAM-1 antibodies and HUVECs treated with TNF-α (20 ng/mL) and IL-17A (20 ng/mL) (40 ng/mL total ligand concentration) infliximab (100 ng/mL) and secukinumab (150 ng/mL) for 24 hours stained with anti-ICAM-1 and anti-VCAM-1 antibodies. **(A)** A gated side and forward scatter plot of TNF-α and IL-17A treated HUVEC cells, same cell gating used for HUVECs treated with TNF-α, IL-17A, infliximab and secukinumab. **(B)** Histogram generated from the flow cytometry of HUVECs treated with TNF-α and IL-17A (green histogram) and HUVECs treated with TNF-α, IL-17A, infliximab and secukinumab (light blue histogram) ICAM-1 stained, MFI for each histogram also shown **(C)** Histogram generated from the flow cytometry of HUVECs treated with TNF-α and IL-17A (green histogram) and HUVECs treated with TNF-α, IL-17A, infliximab and secukinumab (light blue histogram) VCAM-1 stained, MFI for each histogram also shown. Data represents one experiment.

The addition of a mixture of infliximab and secukinumab reduced the expression of ICAM-1 (Figure 113B) and VCAM-1 (Figure 113C) upon the surface of TNF-α and IL-17A treated HUVECs. The greatest reduction was seen in the expression of VCAM-1 with a reduction in MFI from 433,000 to 29,272 in the presence of these monoclonal antibodies. ICAM-1 expression was reduced by approximately 50% (MFI 1,430,000 vs 775,000). The result of this experiment gives confidence that using Fabs derived from the digestion of infliximab and secukinumab to prepare a BsFpF targeting TNF-α and IL-17A may have some anti-inflammatory functional activity. TNF-α and IL-17A targeting bispecific molecules have been prepared and tested in the past [241,242] with one molecule, COVA322 progressing to into Phase Ib/IIa clinical studies for the treatment of psoriasis [243].

Conclusions

The pro-inflammatory cytokines, TNF-α and IL-17A were investigated to see if they could induce the expression of ICAM-1 and VCAM-1 upon the surface of HUVEC cells. If expression was induced, it was thought that TNF-α and IL-17A would be a good target pair to prepare a BsFpF against. First preliminary experimentation needed to be performed.

TNF-α was shown to increase expression of both ICAM-1 and VCAM-1 upon the surface of HUVECs, however IL-17A did not have this effect. Increasing IL-17A concentrations and incubation times may induce an IL-17A based inflammatory response on the HUVEC surface. When a mixture of TNF-α and IL-17A was applied to HUVECs greater expression of ICAM-1 and VCAM-1 was measured compared to when TNF-α was solely applied. This is likely due to a synergistic relationship between TNF-α and IL-17A.

Finally anti TNF-α (infliximab) and anti IL-17A (secukinumab) antibodies were applied to HUVECs treated with TNF-α and IL-17A to neutralise the activity of the cytokines. Infliximab was found to neutralise the activity of TNF-α reducing expression of ICAM-1 and VCAM-1 upon the HUVEC surface. Use of secukinumab was found to reduce expression of VCAM-1. When a mixture of infliximab and secukinumab were applied to HUVECs treated with both TNF-α and IL-17A decreases in expression of both ICAM-1 and VCAM-1 were measured.

Unfortunately, no further *in vitro* studies were completed. However, the results presented in this chapter gave some confidence that a anti TNF-α/IL-17A BsFpF would be a suitable molecule to test the functional performance of a BsFpF in the future.

Chapter 7 - Conclusions

The main objective of this PhD was to utilise disulfide bridging *bis*-alkylation conjugation to prepare and characterise bispecific Fab_1-PEG-Fab_2 (BsFpF **7**) antibody mimetics. A BsFpF is a heterogenous dimeric molecule containing two different Fabs conjugated to both ends of a linear PEG linker of moderate molecular weight (i.e. 5-10 kDa). A BsFpF **7** can be designed to interact with two different therapeutic targets. The BsFpFs **7** prepared in this PhD were designed to interact with two therapeutic targets that are relevant for ocular inflammatory and angiogenic conditions. Many of these targets are also relevant for wider immunological conditions such as rheumatoid arthritis and psoriasis. Table 19 summarises the main findings during this PhD and how they relate to the project hypotheses. Findings are discussed in greater detail throughout this chapter.

Findings	Related hypotheses
Soluble papain can digest 100mg of tocilizumab in 30 minutes and a greatly reduced material cost compared to an immobilised papain methodology. Soluble papain can also be used to digest both bevacizumab and infliximab.	1. A soluble form of papain can be used as an alternative to immobilised papain for obtaining Fabs via the digestion of IgGs. Using soluble papain will allow digestion of up to 100 mg of IgG in a single digestion.
The PEG di-*bis*-sulfone reagent **5** was not suitable for preparing BsFpFs **7**. Instead, a conjugation-ligation methodology was developed to prepare BsFpFs 7 using difunctional reagents **26** and **27**. It was possible to isolate BsFpFs **7** using a combination of IEX and SEC. ELISA, SPR and MST confirmed that the prepared BsFpFs **7** were able to bind to their intended therapeutic targets.	2. Using PEG as scaffold and utilising chemical conjugation to combine two Fabs, a BsFpF can be synthesised effectively preserving the antigen binding properties of the individual Fabs. 3. The prepared BsFpF can be isolated from conjugation mixtures to give a final purified product free from impurities.
Monospecific and bispecific FpFs prepared using the conjugation-ligation approach were found to be stable for at least 6 months at 5°C	A BsFpF prepared by chemical conjugation, is stable in the intended storage condition with no deconjugation of Fabs from the PEG scaffold and light/heavy dissociation.

Table 19: Summary of the main findings made during this PhD and how the findings relate to hypotheses set prior to commencing of this research project.

A point concerning the development of a BsFpF **7** is why not prepare a combination therapy containing two or more monospecific FpFs as a single formulated product. There are however several potential advantages bispecific antibodies have over the combination therapy of two monospecific protein therapies.

Development of a bispecific medication reduces costs as only one therapy needs to be developed instead of two and having a molecule capable of binding to two targets simultaneously may improve binding specificity and create synergistic effects [8], something unique to bispecifics.

Combination therapy of IgGs or other protein therapies containing Fc regions may lead to large quantities of Fc regions being present systemically. Certain types of Fc containing therapeutics can recruit proinflammatory effector cells which contain Fc receptors, these cells can contribute to tissue damage [244]. Dosing of bispecific therapies would limit or even eradicate potential Fc related issues depending on the format of the bispecific therapy.

Great effort has been made to develop combination therapies in several areas including oncology [245] , COVID-19 [246] and infection [247] with some progressing to clinical trials and approval. A positive example is the combination of Trastuzumab and Pertuzumab for the treatment of HER-2 (human epidermal growth factor 2) positive breast cancer [248], the combination showed an additive, synergistic anti-tumour effect. In contrast combinations of Bevacizumab with Cetuximab or Panitumumab used for advanced colorectal cancer resulted in shorter progression free survival and increased side effects [248].

In the case of ocular neovascularisation, great efforts have been made to design and formulate drug combinations with multiple targets, with several examples in phase II trials. So far, these have not been translated into successful phase III trials. For example, targeting PDGF and VEGF has been examined with rinucumab (anti-PDGF IgG4 co-formulated with aflibercept) and E10030/pegpleranib (Fovista in combination with ranibizumab) in phase II and III trials for treatment of wet-AMD respectively [110]. Both combinations failed to show a benefit over anti-VEGF monotherapies.

Intravitreal injections are invasive and carry some risk including susceptibility to endophthalmitis post injection [249] and chronic ocular hypertension after repeated injections [250]. To reduce injection burden intraocular combination strategies would probably need to be formulated as fixed dose combinations. The volume of an

intravitreal injection is 50 µL, which is a very small volume for a combination of protein-based drugs at sufficient individual doses while minimising risks of protein misfolding and aggregation.

With careful consideration of target selection bispecific antibodies that are capable of interacting with two target epitopes simultaneously [10,251] have the potential to increase the efficacy of intraocular medicines. Increased efficacy may reduce the frequency of intravitreal injections and improve patient compliance which is known to decrease after the first year of treatment [252–254]. A notable example is Faricimab, a bispecific IgG that targets VEGF and ANG-2.

Faricimab was developed as researchers began to look beyond anti-VEGF monotherapies due to poor response and recurrence of disease [134]. Benest et al. [135] found that a reduction in ANG-2 concentration strongly reduced the effect of vascular leakage upon administration of VEGF as ANG-2 upregulates the neovascularisation effects of VEGF, establishing VEGF and ANG-2 as a suitable target pair. During phase III clinical trials, patients being administered Faricimab had longer intervals between doses compared to ranibizumab indicating a longer duration of action [22]. Also, non-inferior visual acuity outcomes were observed for faricimab dosed every 16 weeks compared to aflibercept given every 8 weeks. Faricimab was approved by the FDA in 2022 for the treatment of w-AMD and DME [255].

Preparing bispecific antibodies in an academic setting is challenging. Previous research has shown that FpFs behave in a similar way to IgGs [161,183] so it was proposed to extend the FpF platform to prepare BsFpFs with the ultimate aim of testing their functional activity within the eye. Firstly, a methodology to prepare purified BsFpFs needed to be developed and once developed the BsFpF needed to be characterised.

To prepare BsFpF molecules purified Fabs were required. There are only three clinically used Fab molecules [256]. Fabs are monovalent in contrast to full IgG molecules and Fabs clear quickly from circulation after administration. While Fabs can be made recombinantly, they can also be obtained by the proteolytic digestion of IgGs using papain, which is a thiol protease. Immobilised forms of papain can be used to digest IgGs in small quantities of no more than 10 mg [183,257]. Within this PhD a methodology to digest IgGs at a scale of up to 100 mg was developed with 100 mg of the anti-IL-6R humanised IgG tocilizumab being digested in a single digestion. Instead

of immobilised papain, a soluble, lyophilised form of papain was used for digestion [170].

Use of soluble papain significantly reduced the material cost (enzyme, purification materials, lab reagents) Digestion time was also reduced from more than 8 hours observed with immobilised papain to approximately 30 minutes. Tocilizumab (100 mg in a single digestion, Figure 29), bevacizumab (37.5 mg in a single digestion, Figure 31) and infliximab (10 mg in a single digestion, Figure 32) were digested using soluble papain. Development of this method allowed large quantities of pure Fabs to be made available quickly, ready for BsFpF preparations. This was key for BsFpF preparation as 2 different Fabs are required in turn meaning 2 IgG digestions need to be carried out. Purification of the IgG digestion mixtures containing soluble papain required considerable effort to optimise.

A protein L resin was determined to be the optimum choice for the purification of the soluble papain digestion mixtures. Use of protein L as opposed to protein A or CH[1] affinity resins was found to be critical to the success of the soluble papain methodology. Use of protein L allowed the efficient and timely purification of the soluble enzyme from the digestion mixture. Protein L also allowed efficient separation of the desired Fabs from the Fc regions as protein L binds to the kappa light chains present on the Fab, whereas the Fc does not bind to the resin. It was found that incubation of the antibody with soluble papain for too long lead to over digestion. Although this was not unexpected, soluble papain was observed to be a non-specific proteolytic enzyme resulting in over-digestion of the IgG and Fab reducing yields and complicating purification.

To further purify the Fabs, SEC was used as a secondary purification step. SEC was used to purify out any remaining undigested IgG or partially digested IgG as protein L was not able to purify these molecules from the Fab solution as they also contain kappa light chains. This two-step purification methodology proved to be successful with silver staining of the purified Fab obtained from the digestion of 100 mg of tocilizumab showing only two bands (Figure 29), one band corresponding to the Fab and another band at a lower molecular weight corresponding to reduced Fab. As mentioned previously one of the key advantages to the soluble papain methodology is the scalability of the method. As the purification columns are connected to an AKTA protein purification system (AKTA prime plus) and sample application is direct to the column, bypassing any sample loop limitations, the method was used to digest IgGs

at a scale of more than 100 mg. Within academic research settings the scale of digestion is likely limited by the quantity of starting IgG that is available, scale is unlikely to be a problem in industry.

Both bevacizumab and tocilizumab were digested using soluble papain (Chapter 3). Purified Fab yields of 50.0% and 57.7% respectively were obtained when 37.5 mg of bevacizumab and 100 mg of tocilizumab were digested. These yields are comparable to what has been obtained using the immobilised papain methodology for the digestion of these two antibodies. Additionally, infliximab was also digested using soluble papain but with a significantly lower isolated Fab yield of 21.0% after a 35-minute digestion time. The lower yield was attributed to the fact that infliximab is a chimeric IgG whereas bevacizumab and tocilizumab are humanised IgGs. Humanised IgGs may exhibit better thermal and physical stability compared to chimeric IgGs [179,180] and therefore be more resistant to papain driven over-digestion. The loss of yield experienced when digesting infliximab is likely a consequence of over-digestion.

Conjugates including PEG-Fabs and FpFs were prepared with Fabs derived from soluble papain digestions (Chapter 4), demonstrating that the accessible interchain disulfide bond was present and able to undergo conjugation. SPR binding assays (Chapter 5) showed that anti-VEGF Fabs and anti-VEGF monospecific FpFs, both prepared using Fabs obtained via the soluble papain digestion of bevacizumab, were able to bind to VEGF. Finally purified Fabs obtained from the digestion of 100 mg tocilizumab were shown to be stable with no aggregation occurring for up to five months at their intended storage condition of -20°C.

The development of this scalable, cheap, and fast IgG digestion method using soluble papain is an important step. This method allows large quantities of purified, functional Fabs to be obtained quickly and with a reasonable cost from therapeutic IgGs. Subsequently it was expected that larger quantities of FpFs or other Fab based conjugates could then be prepared. Other soluble proteolytic enzymes such as GingisKHAN are also used as solutions to digest IgGs and obtain Fabs [169] however the enzyme is extremely expensive. Enzymes such as GingisKHAN have a histidine tag which simplifies purification. For industrial applications the cost of the enzyme may not be of concern however in an academic research setting digesting 100 mg of IgG using GingisKHAN would not be feasible. Therefore the soluble papain digestion methodology should be considered as a valuable research tool with this work being published [170]. Despite the use of papain to digest IgGs not being novel, it was not

possible to find examples of large-scale IgG digestions (approx. 100 mg scale) in literature. Fabs obtained via soluble papain digestions of various IgGs were used for the preparation of monospecific and BsFpFs throughout this PhD.

Monospecific FpFs were successfully prepared and characterised using a previously described PEG di-*bis*-sulfone protein dimerisation reagent **5** [159,161,183]. Initially conjugation of two different Fabs to reagent **5** was performed. Attempts to prepare a BsFpF using reagent **5** were not successful. This was thought to be due to a combination of factors, including, the likely hydrolysis of a free bis-sulfone moiety leading to a loss of reagent reactivity and secondly, a steric shielding effect to hinder the conjugation of a second Fab to the PEG-Fab intermediate **6**. The purity of reagent **5** may also be a factor as the reagent was purified via precipitation. Use of HPLC to purify reagent **5** is likely to be more effective.

A different conjugation moiety *bis*-sulfone glycol **12** was investigated as an alternative to *bis*-sulfone to determine if reagent hydrophobicity might have been a reason to reduce the conjugation of the second Fab. However, there was no evidence of improved performance and in fact the reagents appeared to behave quite similarly during conjugation reactions.

Another thought was that a heterodimeric reagent in which one conjugation moiety is *bis*-sulfone and the other a *bis*-sulfide moiety. The *bis*-sulfide moiety may maintain the stability of the second conjugation moiety. The BsFpF preparation would proceed via conjugation of Fab_1 to the *bis*-sulfone moiety, pH of the conjugation mixture would be increased and Fab_2 introduced to allow conjugation to the free *bis*-sulfide moiety. During conjugations between Fabs and PEG *bis*-sulfide **17** at a pH of 8.2 poor conjugate formation was observed, suggesting the thiol toluene moieties found in PEG *bis*-sulfide **17** are not suitable for this application.

Therefore, a different methodology was proposed to prepare BsFpF molecules. The proposed methodology was based upon copper free bio-orthogonal ligation reactions, in which two functional groups can undergo ligation without undergoing reaction with a Fab. Copper catalysed ligation reactions also known as copper-catalysed azide-alkyne cycloaddition (CuAAC) were examined [182] within our research group to bring two different proteins together. This was found to be unsuccessful as it was thought that the presence of copper was hindering the ligation reaction from proceeding. Another major drawback limiting the use of CuAAC in biological systems is the copper-mediates formation of reactive species, which can

lead to oxidate degradation of proteins [258]. CuAAC has however been successfully used to modify proteins, the developed methodology [259] did require the use of DMSO and triazoles and aminoguanidine acting as protective species, this likely required considerable optimisation to determine the correct concentrations of these protective species. Two examples of copper free reactions are strain-promoted azide-alkyne cycloaddition (SPACC) and inverse-electron-demand Diels-Alder (iEDDA) reactions. Both reaction types do not require any copper to catalyse the reactions [186] and in turn no protective species to protect proteins from reactive species making any reaction mixtures less complex and likely easier to purify.

A set of bi-functional reagents were synthesised by our research group. The pair of reagents, PEG *bis*-sulfone DBCO **23** and PEG *bis*-sulfone azide **22** reagents both contain *bis*-sulfone as the conjugation moiety. The *bis*-sulfone moiety was chosen due to its stability at a range of pHs, its conjugation activity at biorelevant pH, precedence of use [148,159,161] and the fact it performed well during conjugation assessments carried out during this PhD (Figures 35 and 36). DBCO and azide are functional groups that ligate via a SPACC reaction to form a single entity. Initially the ligating functionality of reagents **22** and **23** was evaluated by carrying out reactions without conjugated protein. Results of these experiments indicated that ligation occurred by reaction of the DBCO and azide moieties (Figure 44).

A second pair of reagents, PEG *bis*-sulfone TCO **26** and PEG *bis*-sulfone Tz **27** were also prepared by our research group for comparison to reagents **22** and **23**. The TCO and Tz functional groups present in these reagents ligate via iEDDA reactions. Reagent only reactions between reagents **26** and **27** underwent ligation readily (Figure 45) at a range of different pHs (pH 5-9), although it is known the iEDDA reactions are not sensitive to pH [260] so this result was not unexpected.

Next Fab$_{Rani}$ was conjugated to reagents **26** and **27** to prepare TCO **28** and **29** Tz functionalised Fab conjugates. The functionalised Fab conjugates **28** and **29** were combined using PBS as a reaction medium and left to incubate. SDS PAGE revealed that no cycloaddition had occurred (Figure 46), initial thoughts could be that the presence of protein was hindering the cycloaddition from proceeding. Another possibility was the presence of free PEG *bis*-sulfone TCO **26** or PEG *bis*-sulfone Tz **27** not consumed during the conjugation between reagents **26** and **27** and Fabs hindering the ligation between intermediates **28** and **29**.

It was thought that the TCO **28** functionalised Fab conjugate was ligating to PEG *bis*-sulfone Tz **27** and vice versa for the Tz functionalised Fab conjugate **29** and PEG *bis*-sulfone TCO **26**. Ligation of intermediates **28** and **29** to reagents **26** or **27** respectively would form a PEG-TCO-Tz-PEG-*bis*-sulfone intermediate **31** not the intended FpF. Essentially there was a preference for something large (TCO **28** or Tz **29** functionalised Fab conjugate) to ligate to something small (reagent **26** or **27**). To negate this preference, it was decided to try and remove free reagent **26** and **27** from the conjugation mixtures via centrifugation filtration.

Fab$_{Rani}$ was conjugated to PEG *bis*-sulfone TCO **26** and PEG *bis*-sulfone Tz **27**. Additionally, Fab$_{Rani}$ was conjugated to PEG *bis*-sulfone DBCO **23** and PEG *bis*-sulfone azide **22**. Conjugation of Fab$_{Rani}$ to 4 reagents (**22**, **23**, **26** and **27**) was found to be relatively comparable. Post conjugation, an attempt was made to remove free reagents (**22**, **23**, **26** and **27**) from the respective conjugation mixtures via centrifugation filtration.

The DBCO **25** and azide **24** functionalised Fab conjugates and TCO **28** and Tz **29** functionalised Fab conjugates then combined to see if the cycloaddition reaction would proceed. Cycloaddition reactions between both conjugate pairs (**24** with **25** and **28** with **29**) occurred, indicated by a band appearing at approximately 120 kDa on an SDS PAGE gel (Figure 48). The cycloaddition reaction between the TCO **28** and Tz **29** functionalised Fab conjugates proceeded to the greatest extent, with the greatest concentration of FpF being formed. The ligation reaction mixtures were incubated for approximately 18 hours, ample time for both the DBCO azide and TCO Tz ligations to proceed.

The superior iEDDA ligation speed seen between the TCO **28** and Tz **29** functionalised Fab conjugates is not unexpected or unusual with this finding being consistent with literature [188,261]. Because of experimental performance and superior ligation reaction speed PEG *bis*-sulfone TCO **26** and PEG *bis*-sulfone Tz **27** reagents were used to explore the preparation of BsFpFs **7**.

Further experimentation around the conjugation of Fabs to PEG *bis*-sulfone TCO **26** and PEG *bis*-sulfone Tz **27** reagents found that conjugation proceeded well at a pH of 7.6 and when reagents **26** and **27** were present in molar equivalents (MEQ) of 1.5 (Figure 49). This MEQ is typically higher than what has been used previously for Fab conjugations using the PEG *bis*-sulfone [161] reagent **8**, however di-functional

reagents used previously [182] containing *bis*-sulfone **1** and second reactive moiety had to be used at MEQ of 1.5 or greater for conjugation.

Using MEQs less than 1.5 did not allow enough TCO **28** and Tz **29** functionalised Fab conjugates to form. Not having enough of intermediates **28** and **29** meant that when they were mixed and allowed to ligate only small quantities of FpFs formed.

Other findings from experimentation were that the ligation reaction between the TCO **28** and Tz **29** functionalised Fab conjugates was not sensitive to pH or sensitive to one of the reaction constituents being present more than the other. Non-sensitivity of the ligation reaction to pH is a notable advantage as it gives a wider window in which the reaction can take place.

Several different monospecific FpFs and BsFpFs were prepared using the bifunctional TCO and Tz reagents **26** and **27** (Table 10). A combination of IEX and SEC was able to successfully purify the molecules with silver staining confirming the purity of the monospecific FpFs and BsFpFs (e.g. Figure 53). Typical isolated yields of monospecific and BsFpFs ranged from 10-15%.

To try and improve the final purified FpF yields, an alternative FpF preparation methodology (Figure 60) in which an intermediate molecule, Fab-PEG-TCO-Tz-PEG-*bis*-sulfone **31** was first prepared, and subsequently conjugated to a second reduced Fab(Figure 60). Despite the alternative methodology having little impact upon yield, conducting the experiments did show that the purity of the PEG *bis*-sulfone TCO **26** and PEG *bis*-sulfone Tz **27** reagents is a key aspect to obtaining high, reproducible yields. It was evident that reagents **26** and **27** would benefit from further purification by UPLC to remove impurities that contain dead chain ends (i.e. no bis-sulfone or ligation moiety). These impurities may undergo conjugation or ligation, but not undergo both required conjugation and ligation functions. Incomplete conversion has been observed during all steps of the FpF preparation process and it is thought that better reagent purity would result in better FpF yields at the small scales that were examined. It should be mentioned however that the reagents used during this PhD were more than suitable for preparing the quantities of BsFpFs required for characterisation.

An anti-VEGF/IL-6R BsFpF was shown to be stable for up to 6 (Figure 67) months at its intended storage temperature of 5°C. No Fab deconjugation or aggregation was observed using SDS PAGE. The same was observed for an anti-VEGF monospecific FpF prepared via ligation of TCO **28** and Tz **29** functionalised Fab

conjugates. The same anti-VEGF monospecific FpF was also stored at 37°C for a period of 4 weeks to simulate conditions close to body temperature. A period of 4 weeks was chosen as this represents the dosing regimen of an injection every 4 weeks for a patient starting a course of ranibizumab for the treatment of wet AMD. At 37°C some deconjugation of Fab from the FpF and FpF agglomeration did occur which was surprising as the molecule was treated with STAB to reduce the vulnerable ketone group to an alcohol group essentially "locking" the conjugation.

The use of STAB has been shown to prevent deconjugation previously [262] so it is likely that the STAB treatment was only partially effective. A significant amount of the parent monospecific FpF remained after 4 weeks which is encouraging. Ideally some sort of binding assay such as ELISA or SPR should have been carried out to measure the affinity of the FpF toward VEGF after 4 weeks storage at 37°C and then compared to an initial timepoint. Finally, the bond formed during the ligation between the TCO and Tz functional moieties remained stable.

To examine whether the Fabs used for BsFpF preparation retained their antigen binding characteristics 3 different techniques (ELISA, SPR and MST) were used to measure the affinity of BsFpFs to their intended targets. BsFpFs against 3 different target pairs, VEGF/TNF-α, VEGF/IL-6R and TNF-α /IL-6R had their binding affinities measured first using SPR. BsFpFs against the 3 target pairs were able to bind to each of these targets in a concentration dependent manner.

A more comprehensive set of binding experiments (Figures 84, 85, 96, 97) and Table 18) were conducted using an anti-VEGF/IL-6R BsFpF. ELISA and SPR of an anti-VEGF/IL-6R BsFpF showed that the affinity (K_D) of the BsFpF to VEGF was comparable to an anti-VEGF TCO functionalised Fab conjugate **28**. ELISA and SPR data were not as conclusive for the IL-6R binding region of the anti-VEGF/IL-6R BsFpF. ELISA did show that an anti-IL-6R Tz functionalised Fab conjugate **29** had similar affinity to the anti-IL-6R binding arm of the BsFpF. Binding data for the same 2 molecules generated using SPR showed that the anti-IL-6R binding half of the BsFpF had greater affinity to IL-6R than the corresponding functionalised Fab conjugate. Standard deviations were also found to be quite large between the replicates measured.

Why this result occurred is unknown. It was expected that this result would be the other way around so that the anti-IL-6R functionalised Fab conjugate had greater affinity toward IL-6R. Then arguments could be made that a factor was impeding the

binding of the anti-VEGF/IL-6R BsFpF to IL-6R. This could be a steric shielding type of hinderance or possible non-specific binding of the BsFpF to the immobilised IL-6R chip. Non-specific binding of the anti-IL-6R conjugates to the immobilised IL-6R chip may occur due to the amount of IL-6R immobilised on the surface of the NTA chip. In this case, ligand capture of IL-6R led to a far greater concentration of IL-6R being present on the chip compared to the immobilisation levels attained during the functionalisation of a CM3 chip with VEGF. The greater concentration may lead to non-specific binding which could lead to greater variation in results. Capturing of ligands may also have the disadvantage in that the bonds created are not as strong as when a ligand is covalently immobilised [263]. This may mean that captured ligand dissociates from the chip surface during measurement which could lead to variability of results.

Results from MST affinity experiments involving an anti-VEGF/IL-6R BsFpF were inconclusive and did not reflect any of the trends observed during ELISA and SPR binding experiments. MST is a relatively new technique compared to ELISA and SPR especially within our research group. Greater understanding of the technique may lead to better optimised MST methodologies, which in turn may generate better, more meaningful data.

Results presented in this thesis have demonstrated it was possible to reproducibly prepare and purify BsFpFs against several different intraocular target combinations. During my PhD a bispecific IgG faricimab targeting VEGF and ANG-2 was approved for intraocular use [114], the first bispecific IgG approved for use in the eye. With the ability to prepare BsFpFs and now precedence of use of bispecifics within the eye there are opportunities in the future to further characterise BsFpFs.

Future areas of focus:

In vitro and *in vivo* experimentation assessing the functional characteristics of BsFpFs to treat a medical condition should most definitely be an area of future focus. During this PhD preliminary *in vitro* assays (Chapter 6) investigating a suitable pair of targets for an anti-inflammatory BsFpF was carried out. TNF-α and IL-17A were investigated to see if they could induce the expression of the inflammatory cell surface markers, ICAM-1 and VCAM-1 upon the surface of HUVEC cells and then in turn be a suitable target pair for synthesis of a BsFpF.

TNF-α was shown to increase expression of both ICAM-1 and VCAM-1, however IL-17A did not have this effect. A quite interesting finding however was when TNF-α and IL-17A were combined and HUVECs treated with the mixture. The TNF-α/IL-17A mixture increased ICAM-1 and VCAM-1 expression compared to TNF-α alone, indicating a likely synergistic effect. It is likely that TNF-α and IL-17A would be suitable targets for a BsFpF in an inflammatory cell-based assay.

Careful consideration would need to be taken when deciding the concentrations of BsFpF to be administered as it is a monovalent molecule for each target. A range of different molar concentrations would likely need to be administered including concentrations more than ligand concentration to account for the monovalency of the BsFpF. It may be possible to overcome monovalency by attempting to modify the amino acids sequences within the CDRs of Fabs to improve binding characteristics e.g. increase association and decrease dissociation rates.

Another interesting preliminary piece of work that was performed during this PhD was the preparation of a bivalent bispecific **39** (Scheme 14). Expansion of this work and preparation and identification of a bispecific bivalent may be another strategy to overcome any monovalency limitations that may be encountered with BsFpFs during both *in vitro* and *in vivo* functional assays. Bivalency has been shown to be superior to monovalency in a number of therapeutic areas including viral inhibition [264,265] and within oncology [266].

It has been shown in this research that preparation of a bivalent bispecific **39** may be possible (Figures, 68, 69) when ligating IgGs conjugated to PEG *bis*-sulfone TCO **26** and PEG *bis*-sulfone Tz **27**. This methodology however is quite complex as IgGs contain 4 reducible disulfide bonds, preferentially reducing certain IgG disulfide bonds may be possible using reducing agents such as tris(2-carboxyethyl)phosphine (TCEP) or 2-mercaptoethylamine (2-MEA) [267]. This would allow the conjugation of a single molecule of reagent **26** or **27** instead of potential 4 if all of the IgG disulfide bonds are reduced. Antibody drug conjugates (ADCs) have been prepared using reagents containing *bis*-sulfone **1** [268] requiring the IgG disulfide bonds to be reduced so this approach may be feasible.

Confirmation of the bivalent bispecific **39** could be confirmed by measuring solution size via DLS, SPR binding assays and via MALDI-TOF to determine an accurate molecular weight. An SPR binding assay may help with confirmation because the affinity parent IgG and arm of the bivalent bispecific containing that parent IgG

could be compared. If these techniques were to show a bivalent bispecific had any value, further work could be carried out to try and optimise a preparation process.

A final area of consideration for bispecifics is affinity drug delivery [269] in which one binding arm is therapeutically active and the other binding arm attempts to increase duration of action. There is a recognised need to increase the duration of action of intravitreally administered medicines [254,270–272]. A strategy to potentially increase the residence time of a therapeutic protein in the vitreous is for the protein to associate or bind to a tissue component within the vitreous cavity. One example of such a component is hyaluronic acid (HA). An HA binding moiety has been shown to extend the ocular half-life of the anti-VEGF Fab to which is was fused for 3-4 fold [273]. There is certainly an opportunity to prepare BsFpFs containing a ligand targeting arm for therapeutic value and an affinity binding arm with the aim of extending the BsFpFs duration of action.

Appendix

Proton NMR spectra of conjugation reagents.

A. PEG$_6$ di *bis*-sulfone protein dimerisation reagent **5**
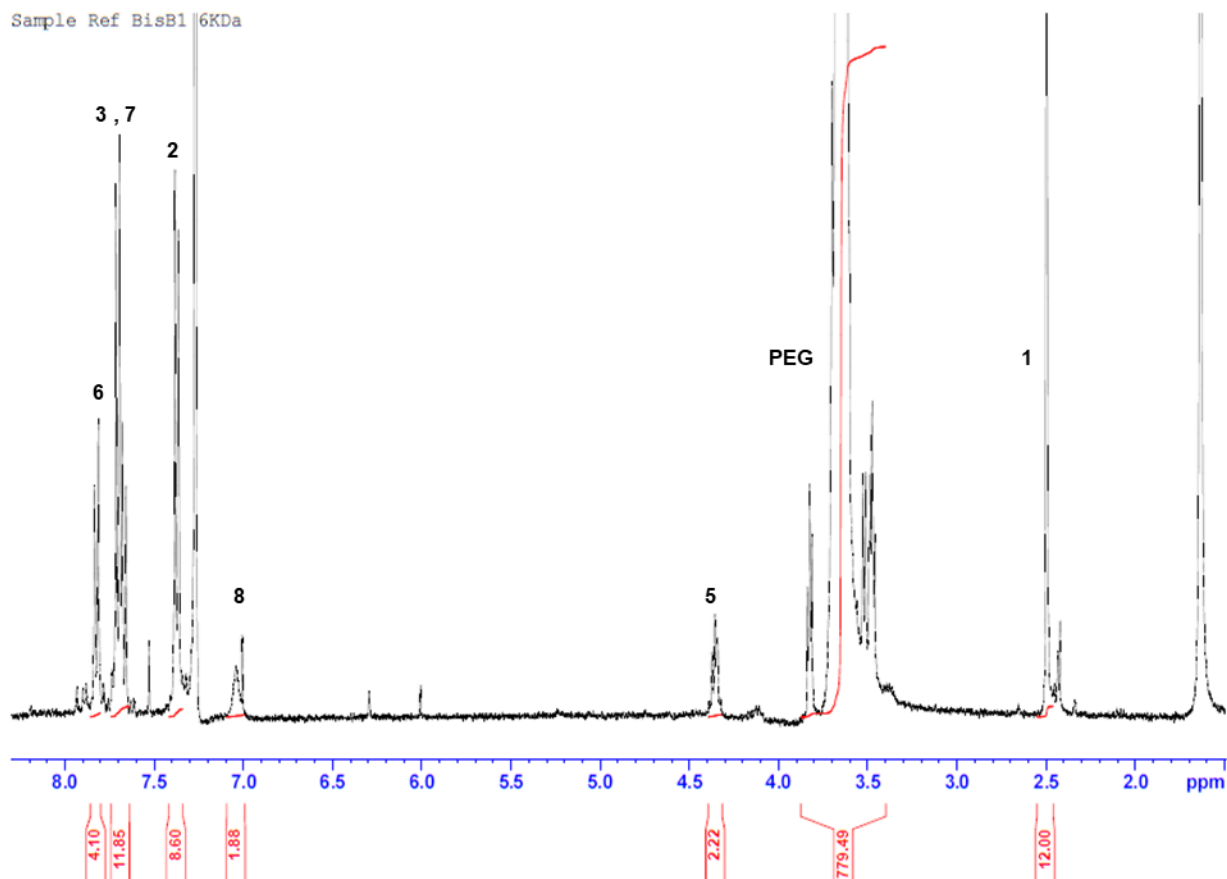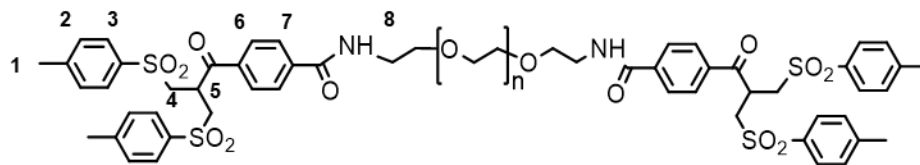
B. PEG$_{20}$ di *bis*-sulfone protein dimerisation reagent **5**
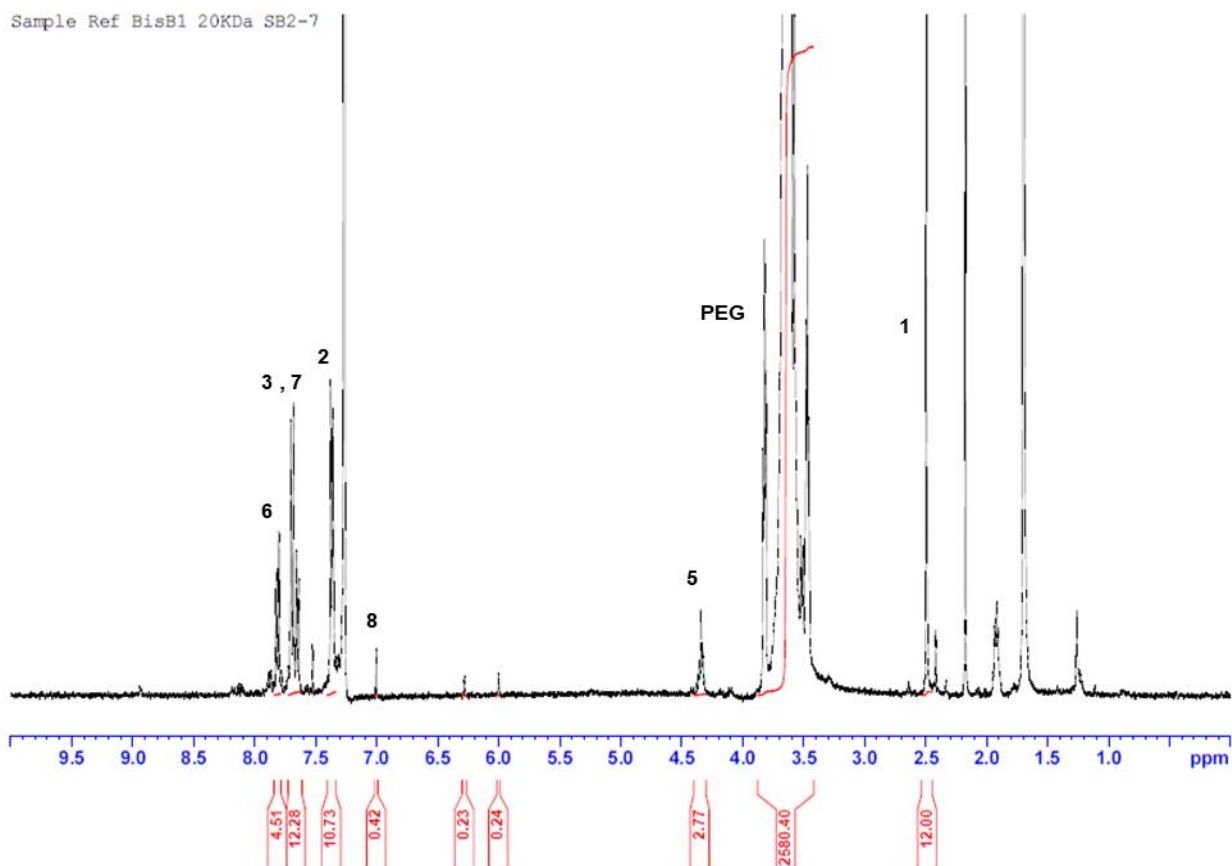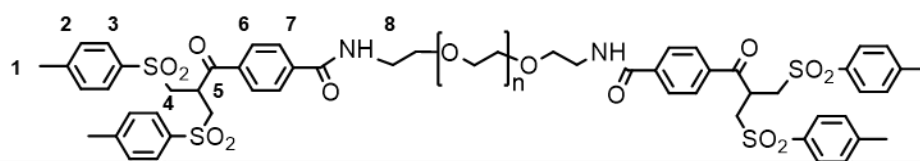
C. PEG₁₀ *bis*-sulfone **8**

D. PEG₂₀ *bis*-sulfone **8**

E. PEG$_{10}$ *bis*-sulfone glycol **12**

Sample Ref #59 Oxidised exchange rxn
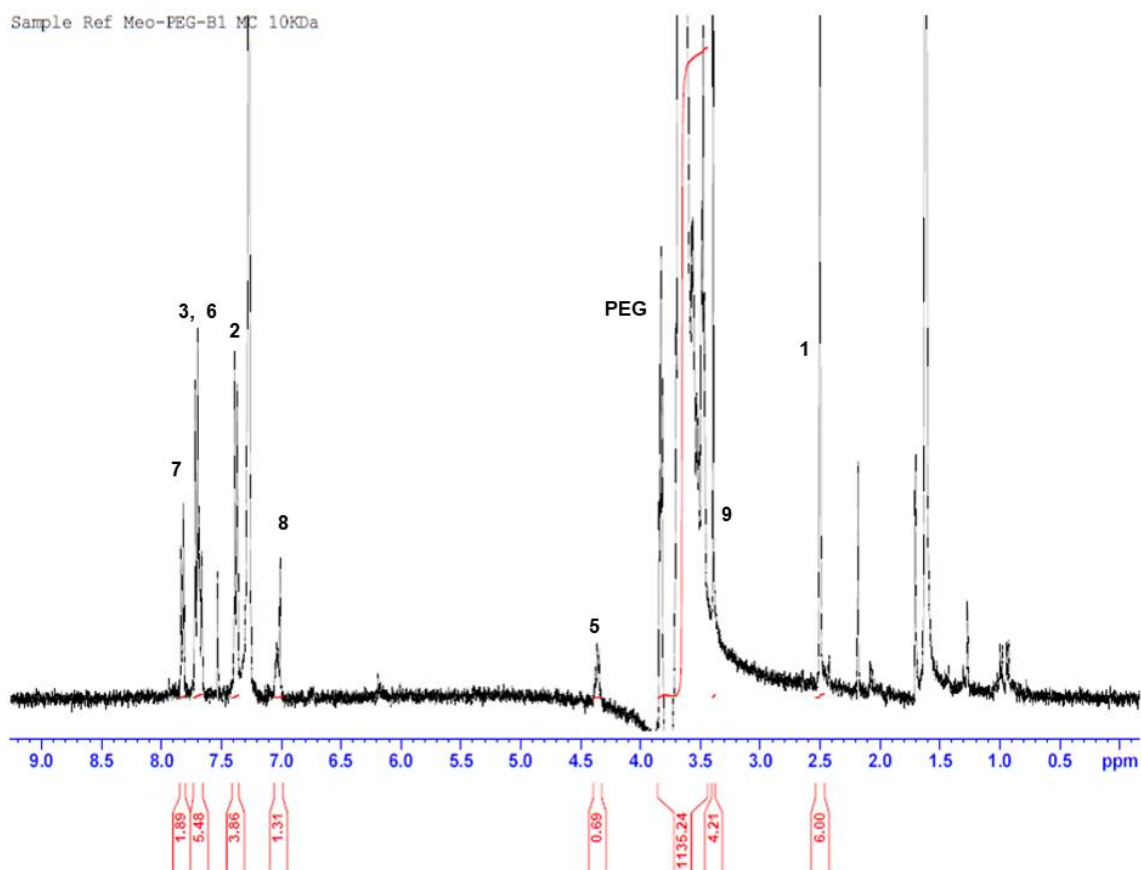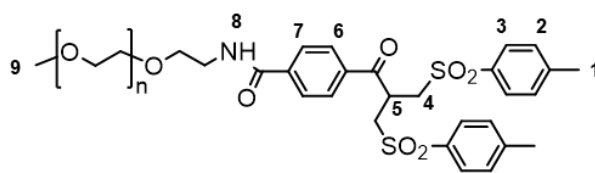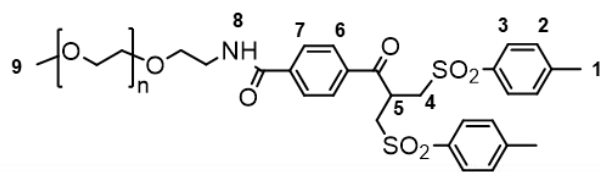
F. PEG$_{10}$ *bis*-sulfide **17**
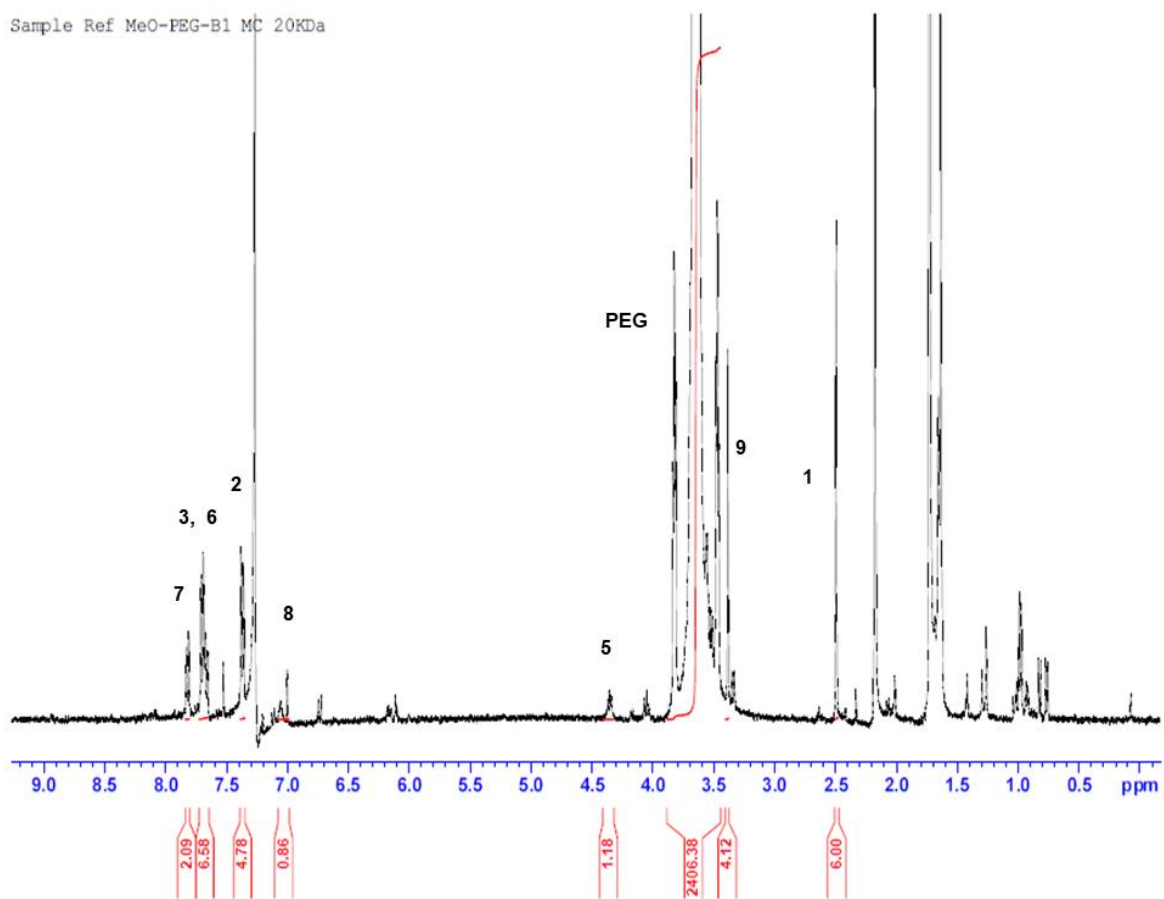
G. PEG$_{10}$ *bis*-sulfone TCO **26**
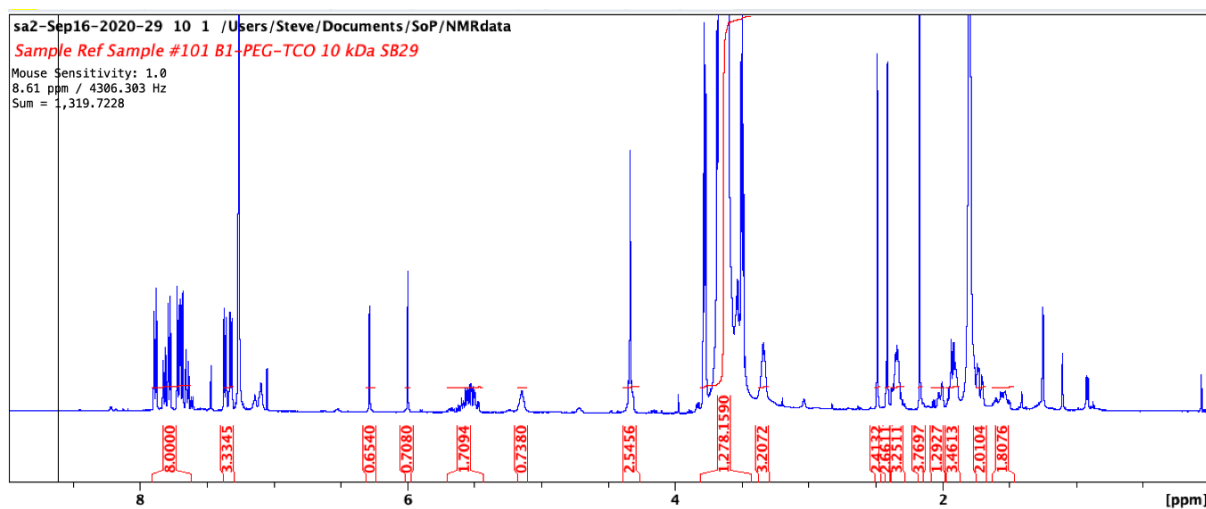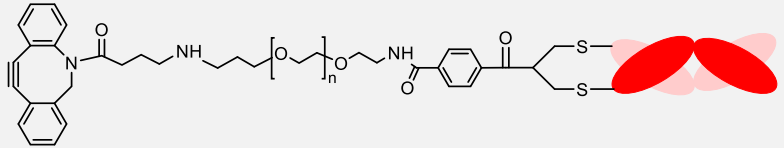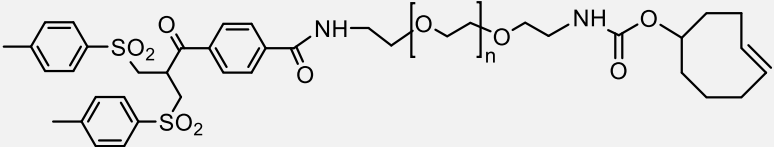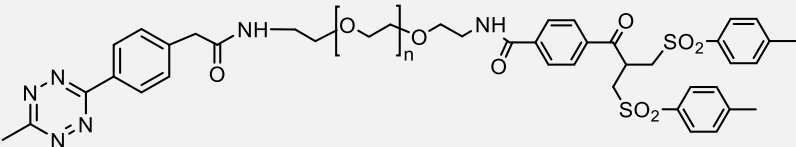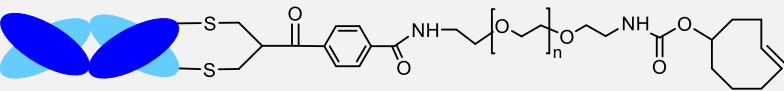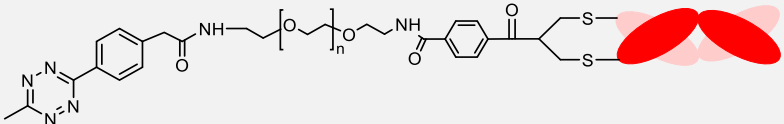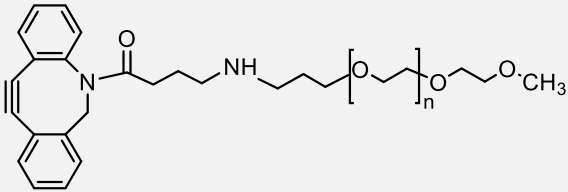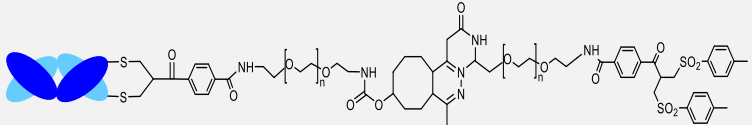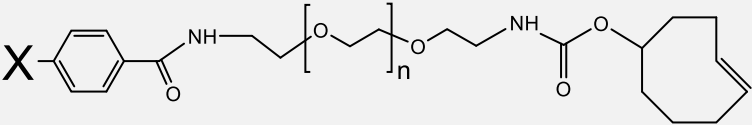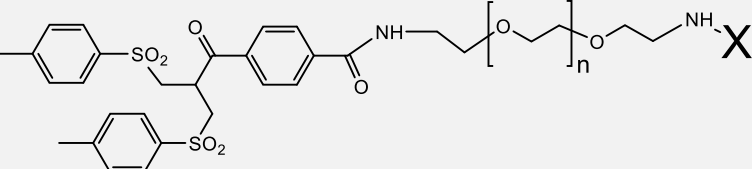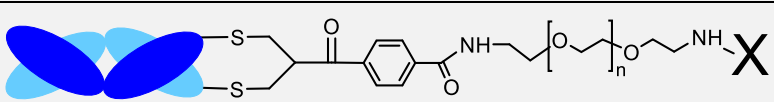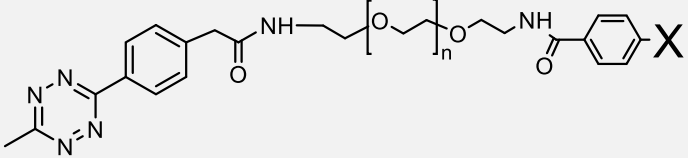
H. PEG$_{10}$ *bis*-sulfone Tz **27**
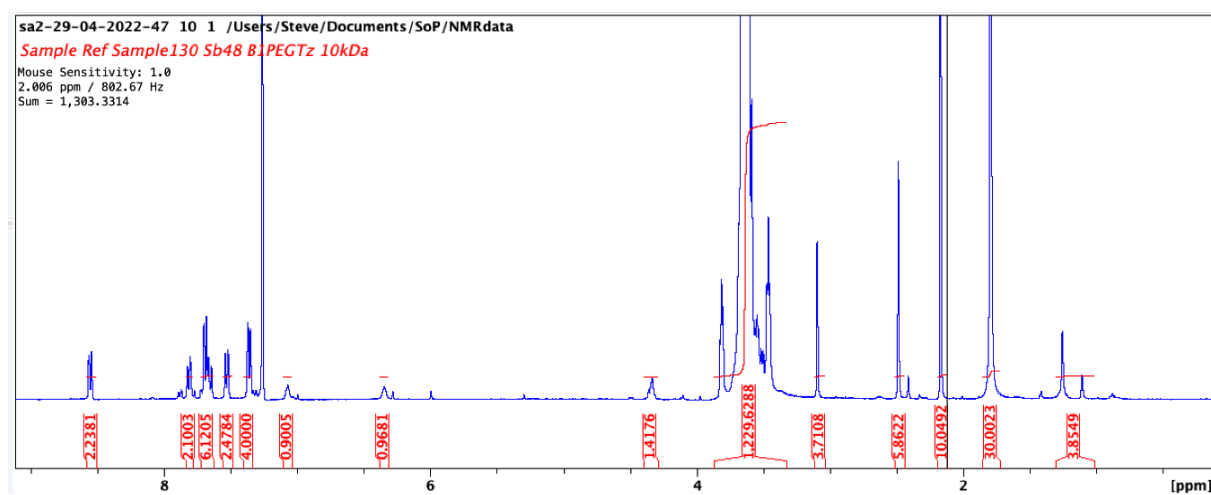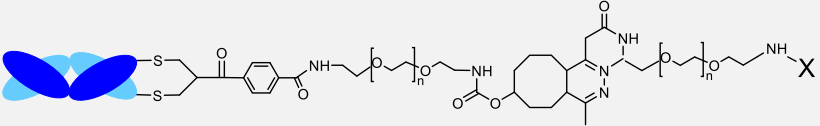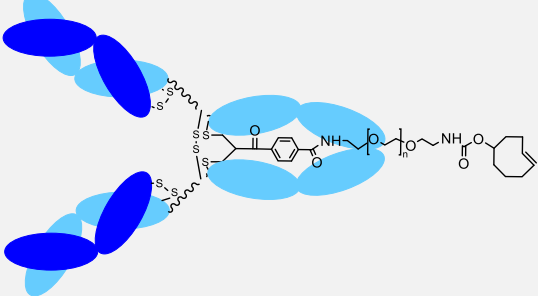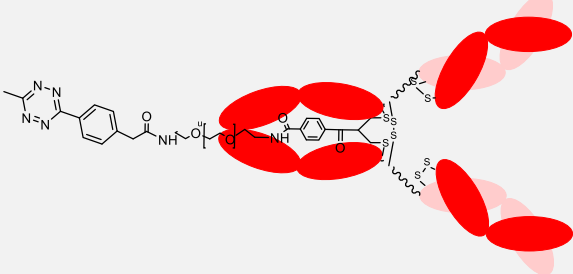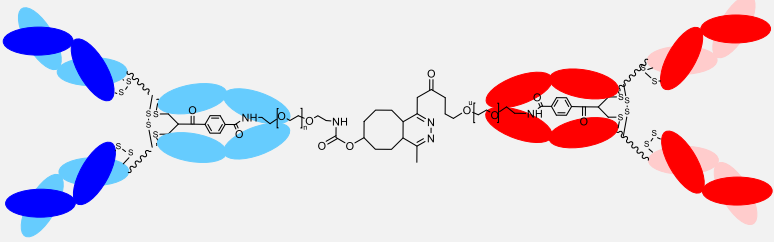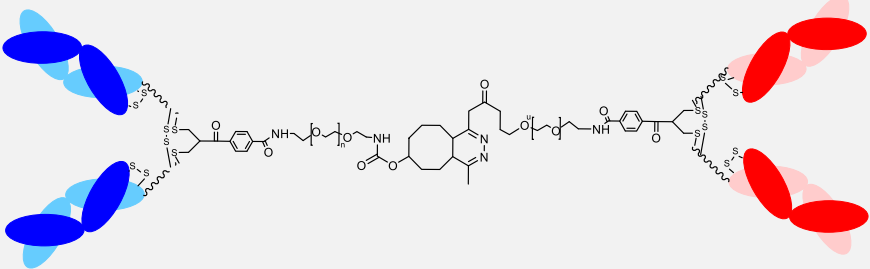
Structures of reagents, intermediates and conjugates referred to within this thesis

No.	Name	Structure
1	*Bis*-sulfone conjugation moiety	
2	Enolate intermediate	
3	*Mono*-sulfone conjugation moiety	
4	Toluene sulfinic acid	
5	PEG di-*bis*-sulfone protein dimerisation reagent	
6	Mono PEG-Fab	
7	Bispecific FpF	
8	PEG *bis*-sulfone	
9	IIDQ	
10	PEG amine	
11	*Bis*-sulfone precursor	

No.	Name	Structure
12	PEG *bis*-sulfone glycol	
13	Monospecific FpF	
14	Mono Fab conjugate	
15	PEG *bis*-sulfone *bis*-sulfide difunctional reagent	
16	Fab PEG *bis*-sulfide intermediate	
17	PEG *bis*-sulfide	
18	Difunctional reagent X	
19	Difunctional reagent Y	
20	Intermediate X	
21	Intermediate Y	
22	PEG *bis*-sulfone azide	
23	PEG *bis*-sulfone DBCO	
24	Azide functionalised Fab conjugate	

No.	Name	Structure
25	DBCO functionalised Fab conjugate	
26	PEG *bis*-sulfone TCO	
27	PEG *bis*-sulfone Tz	
28	TCO functionalised Fab conjugate	
29	Tz functionalised Fab conjugate	
30	Methoxy PEG DBCO	
31	Fab PEG TCO-Tz PEG *bis*-sulfone intermediate	
32	PEG X TCO	
33	PEG *bis*-sulfone X	
34	Fab conjugate lacking a TCO ligating moiety	
35	PEG X Tz	

No.	Name	Structure
36	Fab PEG TCO-Tz PEG X	
37	TCO functionalised IgG	
38	Tz functionalised IgG	
39	Bivalent bispecific molecule	
40	Bispecific Fab2	

References

[1] Ecker DM, Jones SD, Levine HL. The therapeutic monoclonal antibody market. mAbs 2015;7:9–14. https://doi.org/10.4161/19420862.2015.989042.

[2] Mullard A. FDA approves 100th monoclonal antibody product. Nat Rev Drug Discov 2021;20:491–5. https://doi.org/10.1038/d41573-021-00079-7.

[3] PMLiVE. PMLive n.d. http://www.pmlive.com (accessed October 31, 2019).

[4] Inc GMI. Monoclonal Antibodies Market revenue to cross USD 380 Bn by 2027: Global Market Insights Inc. GlobeNewswire News Room 2021. https://www.globenewswire.com/news-release/2021/06/08/2243267/0/en/Monoclonal-Antibodies-Market-revenue-to-cross-USD-380-Bn-by-2027-Global-Market-Insights-Inc.html (accessed February 2, 2022).

[5] Lubberts E, Berg WB van den. Cytokines in the Pathogenesis of Rheumatoid Arthritis and Collagen-Induced Arthritis. Landes Bioscience; 2013.

[6] Mease PJ. Adalimumab in the treatment of arthritis. Ther Clin Risk Manag 2007;3:133–48.

[7] Labrijn AF, Janmaat ML, Reichert JM, Parren PWHI. Bispecific antibodies: a mechanistic review of the pipeline. Nat Rev Drug Discov 2019;18:585–608. https://doi.org/10.1038/s41573-019-0028-1.

[8] Sedykh SE, Prinz VV, Buneva VN, Nevinsky GA. Bispecific antibodies: design, therapy, perspectives. Drug Des Devel Ther 2018;12:195–208. https://doi.org/10.2147/DDDT.S151282.

[9] Jung K, Lee D, Lim HS, Lee S-I, Kim YJ, Lee GM, et al. Double Anti-angiogenic and Anti-inflammatory Protein Valpha Targeting VEGF-A and TNF-α in Retinopathy and Psoriasis. J Biol Chem 2011;286:14410–8. https://doi.org/10.1074/jbc.M111.228130.

[10] Brinkmann U, Kontermann RE. The making of bispecific antibodies. mAbs 2017;9:182–212. https://doi.org/10.1080/19420862.2016.1268307.

[11] Ma J, Mo Y, Tang M, Shen J, Qi Y, Zhao W, et al. Bispecific Antibodies: From Research to Clinical Application. Front Immunol 2021;12:626616. https://doi.org/10.3389/fimmu.2021.626616.

[12] Esfandiari A, Cassidy S, Webster RM. Bispecific antibodies in oncology. Nat Rev Drug Discov 2022;21:411–2. https://doi.org/10.1038/d41573-022-00040-2.

[13] Nagorsen D, Kufer P, Baeuerle PA, Bargou R. Blinatumomab: a historical perspective. Pharmacol Ther 2012;136:334–42. https://doi.org/10.1016/j.pharmthera.2012.07.013.

[14] Burt R, Warcel D, Fielding AK. Blinatumomab, a bispecific B-cell and T-cell engaging antibody, in the treatment of B-cell malignancies. Hum Vaccines Immunother 2019;15:594–602. https://doi.org/10.1080/21645515.2018.1540828.

[15] Dahlén E, Veitonmäki N, Norlén P. Bispecific antibodies in cancer immunotherapy. Ther Adv Vaccines Immunother 2018;6:3–17. https://doi.org/10.1177/2515135518763280.

[16] Feldmann M, Brennan FM, Maini RN. Role of cytokines in rheumatoid arthritis. Annu Rev Immunol 1996;14:397–440. https://doi.org/10.1146/annurev.immunol.14.1.397.

[17] Lyman M, Lieuw V, Richardson R, Timmer A, Stewart C, Granger S, et al. A bispecific antibody that targets IL-6 receptor and IL-17A for the potential therapy of patients with autoimmune and inflammatory diseases. J Biol Chem 2018;293:9326–34. https://doi.org/10.1074/jbc.M117.818559.

[18]   Pipe SW, Shima M, Lehle M, Shapiro A, Chebon S, Fukutake K, et al. Efficacy, safety, and pharmacokinetics of emicizumab prophylaxis given every 4 weeks in people with haemophilia A (HAVEN 4): a multicentre, open-label, non-randomised phase 3 study. Lancet Haematol 2019;6:e295–305. https://doi.org/10.1016/S2352-3026(19)30054-7.

[19]   Yada K, Nogami K. Spotlight on emicizumab in the management of hemophilia A: patient selection and special considerations. J Blood Med 2019;10:171–81. https://doi.org/10.2147/JBM.S175952.

[20]   Knight T, Callaghan MU. The role of emicizumab, a bispecific factor IXa- and factor X-directed antibody, for the prevention of bleeding episodes in patients with hemophilia   A.   Ther   Adv   Hematol   2018;9:319–34. https://doi.org/10.1177/2040620718799997.

[21]   FDA approves Roche's Vabysmo, the first bispecific antibody for the eye, to treat   two   leading   causes   of   vision   loss   n.d. https://www.roche.com/media/releases/med-cor-2022-01-31.htm   (accessed February 1, 2022).

[22]   Hussain RM, Neiweem AE, Kansara V, Harris A, Ciulla TA. Tie-2/Angiopoietin pathway modulation as a therapeutic strategy for retinal disease. Expert Opin Investig Drugs 2019;28:861–9. https://doi.org/10.1080/13543784.2019.1667333.

[23]   DiGiammarino E, Ghayur T, Liu J. Design and Generation of DVD-Ig^{TM} Molecules for Dual-Specific Targeting. In: Voynov V, Caravella JA, editors. Ther. Proteins Methods Protoc., Totowa, NJ: Humana Press; 2012, p. 145–56. https://doi.org/10.1007/978-1-61779-921-1_9.

[24]   Wu C, Ying H, Grinnell C, Bryant S, Miller R, Clabbers A, et al. Simultaneous targeting of multiple disease mediators by a dual-variable-domain immunoglobulin. Nat Biotechnol 2007;25:1290–7. https://doi.org/10.1038/nbt1345.

[25]   Wu C, Ying H, Bose S, Miller R, Medina L, Santora L, et al. Molecular construction and optimization of anti-human IL-1α/β dual variable domain immunoglobulin (DVD-Ig^{TM}) molecules. mAbs 2009;1:339–47.

[26]   Mease PJ, Genovese MC, Weinblatt ME, Peloso PM, Chen K, Othman AA, et al. Phase II Study of ABT-122, a Tumor Necrosis Factor– and Interleukin-17A–Targeted Dual Variable Domain Immunoglobulin, in Patients With Psoriatic Arthritis With an Inadequate Response to Methotrexate. Arthritis Rheumatol 2018;70:1778–89. https://doi.org/10.1002/art.40579.

[27]   Fleischmann RM, Bliddal H, Blanco FJ, Schnitzer TJ, Peterfy C, Chen S, et al. A Phase II Trial of Lutikizumab, an Anti–Interleukin-1α/β Dual Variable Domain Immunoglobulin, in Knee Osteoarthritis Patients With Synovitis. Arthritis Rheumatol 2019;71:1056–69. https://doi.org/10.1002/art.40840.

[28]   Bostrom J, Yu S-F, Kan D, Appleton BA, Lee CV, Billeci K, et al. Variants of the Antibody Herceptin That Interact with HER2 and VEGF at the Antigen Binding Site. Science 2009;323:1610. https://doi.org/10.1126/science.1165480.

[29]   Hill AG, Findlay MP, Burge ME, Jackson C, Alfonso PG, Samuel L, et al. Phase II Study of the Dual EGFR/HER3 Inhibitor Duligotuzumab (MEHD7945A) versus Cetuximab in Combination with FOLFIRI in Second-Line RAS Wild-Type Metastatic Colorectal Cancer. Clin Cancer Res Off J Am Assoc Cancer Res 2018;24:2276–84. https://doi.org/10.1158/1078-0432.CCR-17-0646.

[30]   Bujak E, Matasci M, Neri D, Wulhfard S. Reformatting of scFv Antibodies into the scFv-Fc Format and Their Downstream Purification. In: Ossipow V, Fischer N, editors. Monoclon. Antibodies Methods Protoc., Totowa, NJ: Humana Press; 2014, p. 315–34. https://doi.org/10.1007/978-1-62703-992-5_20.

[31]   Xenaki KT, Oliveira S, van Bergen en Henegouwen PMP. Antibody or Antibody Fragments: Implications for Molecular Imaging and Targeted Therapy of Solid Tumors. Front Immunol 2017;8:1287. https://doi.org/10.3389/fimmu.2017.01287.

[32]   Tapia-Galisteo A, Compte M, Álvarez-Vallina L, Sanz L. When three is not a crowd: trispecific antibodies for enhanced cancer immunotherapy. Theranostics 2023;13:1028–41. https://doi.org/10.7150/thno.81494.

[33]   Holliger P, Prospero T, Winter G. "Diabodies": small bivalent and bispecific antibody fragments. Proc Natl Acad Sci 1993;90:6444–8. https://doi.org/10.1073/pnas.90.14.6444.

[34]   Takemura S, Asano R, Tsumoto K, Ebara S, Sakurai N, Katayose Y, et al. Construction of a diabody (small recombinant bispecific antibody) using a refolding system. Protein Eng Des Sel 2000;13:583–8. https://doi.org/10.1093/protein/13.8.583.

[35]   Wu AM, Chen W, Raubitschek A, Williams LE, Neumaier M, Fischer R, et al. Tumor localization of anti-CEA single-chain Fvs: improved targeting by non-covalent dimers. Immunotechnology 1996;2:21–36. https://doi.org/10.1016/1380-2933(95)00027-5.

[36]   Ahamadi-Fesharaki R, Fateh A, Vaziri F, Solgi G, Siadat SD, Mahboudi F, et al. Single-Chain Variable Fragment-Based Bispecific Antibodies: Hitting Two Targets with One Sophisticated Arrow. Mol Ther Oncolytics 2019;14:38–56. https://doi.org/10.1016/j.omto.2019.02.004.

[37]   Wang Q, Chen Y, Park J, Liu X, Hu Y, Wang T, et al. Design and Production of Bispecific Antibodies. Antibodies 2019;8:43. https://doi.org/10.3390/antib8030043.

[38]   Wolf E, Hofmeister R, Kufer P, Schlereth B, Baeuerle PA. BiTEs: bispecific antibody constructs with unique anti-tumor activity. Drug Discov Today 2005;10:1237–44. https://doi.org/10.1016/S1359-6446(05)03554-3.

[39]   Duell J, Lammers PE, Djuretic I, Chunyk AG, Alekar S, Jacobs I, et al. Bispecific Antibodies in the Treatment of Hematologic Malignancies. Clin Pharmacol Ther 2019;106:781–91. https://doi.org/10.1002/cpt.1396.

[40]   Moore PA, Zhang W, Rainey GJ, Burke S, Li H, Huang L, et al. Application of dual affinity retargeting molecules to achieve optimal redirected T-cell killing of B-cell lymphoma. Blood 2011;117:4542–51. https://doi.org/10.1182/blood-2010-09-306449.

[41]   Campagne O, Delmas A, Fouliard S, Chenel M, Chichili GR, Li H, et al. Integrated Pharmacokinetic/Pharmacodynamic Model of a Bispecific CD3xCD123 DART Molecule in Nonhuman Primates: Evaluation of Activity and Impact of Immunogenicity. Clin Cancer Res 2018;24:2631. https://doi.org/10.1158/1078-0432.CCR-17-2265.

[42]   Patel M, Luke J, Hamilton E, Chmielowski B, Blumenschein G, Kindler H, et al. 313 A phase 1 evaluation of tebotelimab, a bispecific PD-1 x LAG-3 DART® molecule, in combination with margetuximab in patients with advanced HER2+ neoplasms. J Immunother Cancer 2020;8. https://doi.org/10.1136/jitc-2020-SITC2020.0313.

[43]   Fisher TS, Hooper AT, Lucas J, Clark TH, Rohner AK, Peano B, et al. A CD3-bispecific molecule targeting P-cadherin demonstrates T cell-mediated regression of established solid tumors in mice. Cancer Immunol Immunother 2018;67:247–59. https://doi.org/10.1007/s00262-017-2081-0.

[44]   Bannas P, Hambach J, Koch-Nolte F. Nanobodies and Nanobody-Based Human Heavy Chain Antibodies As Antitumor Therapeutics. Front Immunol 2017;8. https://doi.org/10.3389/fimmu.2017.01603.

[45] Van Audenhove I, Gettemans J. Nanobodies as Versatile Tools to Understand, Diagnose, Visualize and Treat Cancer. EBioMedicine 2016;8:40–8. https://doi.org/10.1016/j.ebiom.2016.04.028.

[46] Cortez-Retamozo V, Lauwereys M, Gh GH, Gobert M, Conrath K, Muyldermans S, et al. Efficient tumor targeting by single-domain antibody fragments of camels. Int J Cancer 2002;98:456–62. https://doi.org/10.1002/ijc.10212.

[47] Notification of Approval to Manufacture and Market Nanozora® 30mg Syringes for S.C. Injection, a Therapy for Rheumatoid Arthritis, in Japan Japan's First NANOBODY® Therapeutic | Taisho Pharmaceutical Holdings. Taisho Pharm Hold n.d. https://www.taisho.co.jp/global/news/2022/20220926001109.html (accessed October 25, 2022).

[48] Safarzadeh Kozani P, Naseri A, Mirarefin SMJ, Salem F, Nikbakht M, Evazi Bakhshi S, et al. Nanobody-based CAR-T cells for cancer immunotherapy. Biomark Res 2022;10:24. https://doi.org/10.1186/s40364-022-00371-7.

[49] Yang EY, Shah K. Nanobodies: Next Generation of Cancer Diagnostics and Therapeutics. Front Oncol 2020;10.

[50] Plückthun A. Designed Ankyrin Repeat Proteins (DARPins): Binding Proteins for Research, Diagnostics, and Therapy. Annu Rev Pharmacol Toxicol 2015;55:489–511. https://doi.org/10.1146/annurev-pharmtox-010611-134654.

[51] Stumpp MT, Binz HK, Amstutz P. DARPins: a new generation of protein therapeutics. Drug Discov Today 2008;13:695–701. https://doi.org/10.1016/j.drudis.2008.04.013.

[52] Binz HK, Kohl A, Plückthun A, Grütter MG. Crystal structure of a consensus-designed ankyrin repeat protein: Implications for stability. Proteins Struct Funct Bioinforma 2006;65:280–4. https://doi.org/10.1002/prot.20930.

[53] Fiedler U, Ekawardhani S, Cornelius A, Gilboy P, Bakker TR, Dolado I, et al. MP0250, a VEGF and HGF neutralizing DARPin(®) molecule shows high anti-tumor efficacy in mouse xenograft and patient-derived tumor models. Oncotarget 2017;8:98371–83. https://doi.org/10.18632/oncotarget.21738.

[54] Beckmann R, Jensen K, Fenn S, Speck J, Krause K, Meier A, et al. DutaFabs are engineered therapeutic Fab fragments that can bind two targets simultaneously. Nat Commun 2021;12:708. https://doi.org/10.1038/s41467-021-20949-3.

[55] Genentech: Our Pipeline n.d. https://www.gene.com/medical-professionals/pipeline?phase=1,2,3&category=ophthalmology (accessed October 30, 2022).

[56] Yang O, Qadan M, Ierapetritou M. Economic Analysis of Batch and Continuous Biopharmaceutical Antibody Production: A Review. J Pharm Innov 2019;14:1–19. https://doi.org/10.1007/s12247-018-09370-4.

[57] Moldenhauer G. [PDF] Chapter 2 Bispecific Antibodies from Hybrid Hybridoma | Semantic Scholar 2017. https://www.semanticscholar.org/paper/Chapter-2-Bispecific-Antibodies-from-Hybrid-Moldenhauer/0f07a6ce47fde08686281c4c2d13bf622ed01b6c (accessed January 16, 2020).

[58] Schaefer, W, Volger, HR, Lorenz, S, Imhof-Jung, S, Regula, JT, Klein, C, et al. Heavy and light chain pairing of bivalent quadroma and knobs-into-holes antibodies analyzed by UHR-ESI-QTOF mass spectrometry. - PubMed - NCBI 2016.

[59]   Ridgway, JB, Presta, LG, Carter P. "Knobs-into-holes" engineering of antibody CH3 domains for heavy chain heterodimerization. - PubMed - NCBI. Protein Eng 1996;9:617–21.

[60]   Carter P. Bispecific human IgG by design. J Immunol Methods 2001;248:7–15. https://doi.org/10.1016/S0022-1759(00)00339-2.

[61]   CrossMAb technology for bispecific antibody 2019. https://www.roche.com/research_and_development/what_we_are_working_on/research_technologies/bispecific-antibodies.htm (accessed November 5, 2019).

[62]   Surowka M, Schaefer W, Klein C. Ten years in the making: application of CrossMab technology for the development of therapeutic bispecific antibodies and antibody fusion proteins. mAbs n.d.;13:1967714. https://doi.org/10.1080/19420862.2021.1967714.

[63]   Ackland P, Resnikoff S, Bourne R. World blindness and visual impairment: despite many successes, the problem is growing. Community Eye Health 2017;30:71–3.

[64]   Chen H, Jin Y, Sun L, Li X, Nan K, Liu H, et al. Recent Developments in Ophthalmic Drug Delivery Systems for Therapy of Both Anterior and Posterior Segment Diseases. Colloid Interface Sci Commun 2018;24:54–61. https://doi.org/10.1016/j.colcom.2018.03.008.

[65]   Carmeliet P, Jain RK. Angiogenesis in cancer and other diseases. Nature 2000;407:249–57. https://doi.org/10.1038/35025220.

[66]   Wong WL, Su X, Li X, Cheung CMG, Klein R, Cheng C-Y, et al. Global prevalence of age-related macular degeneration and disease burden projection for 2020 and 2040: a systematic review and meta-analysis. Lancet Glob Health 2014;2:e106-116. https://doi.org/10.1016/S2214-109X(13)70145-1.

[67]   Friedman DS, O'Colmain BJ, Muñoz B, Tomany SC, McCarty C, de Jong PTVM, et al. Prevalence of age-related macular degeneration in the United States. Arch Ophthalmol Chic Ill 1960 2004;122:564–72. https://doi.org/10.1001/archopht.122.4.564.

[68]   Campochiaro PA. Molecular pathogenesis of retinal and choroidal vascular diseases. Prog Retin Eye Res 2015;49:67–81. https://doi.org/10.1016/j.preteyeres.2015.06.002.

[69]   Aiello LP, Avery RL, Arrigg PG, Keyt BA, Jampel HD, Shah ST, et al. Vascular Endothelial Growth Factor in Ocular Fluid of Patients with Diabetic Retinopathy and Other Retinal Disorders. N Engl J Med 1994;331:1480–7. https://doi.org/10.1056/NEJM199412013312203.

[70]   Agrahari V, Mandal A, Agrahari V, Trinh HM, Joseph M, Ray A, et al. A COMPREHENSIVE INSIGHT ON OCULAR PHARMACOKINETICS. Drug Deliv Transl Res 2016;6:735–54. https://doi.org/10.1007/s13346-016-0339-2.

[71]   del Amo EM. Topical ophthalmic administration: Can a drug instilled onto the ocular surface exert an effect at the back of the eye? Front Drug Deliv 2022;2.

[72]   Gadkar K, Pastuskovas CV, Couter JEL, Elliott JM, Zhang J, Lee CV, et al. Design and Pharmacokinetic Characterization of Novel Antibody Formats for Ocular Therapeutics. Invest Ophthalmol Vis Sci 2015;56:5390–400. https://doi.org/10.1167/iovs.15-17108.

[73]   del Amo EM, Rimpelä A-K, Heikkinen E, Kari OK, Ramsay E, Lajunen T, et al. Pharmacokinetic aspects of retinal drug delivery. Prog Retin Eye Res 2017;57:134–85. https://doi.org/10.1016/j.preteyeres.2016.12.001.

[74]   Senger DR, Galli SJ, Dvorak AM, Perruzzi CA, Harvey VS, Dvorak HF. Tumor cells secrete a vascular permeability factor that promotes accumulation of ascites fluid. Science 1983;219:983–5. https://doi.org/10.1126/science.6823562.

[75]   Klettner A, Roider J. Comparison of Bevacizumab, Ranibizumab, and Pegaptanib In Vitro: Efficiency and Possible Additional Pathways. Invest Ophthalmol Vis Sci 2008;49:4523–7. https://doi.org/10.1167/iovs.08-2055.

[76]   de Oliveira Dias JR, de Andrade GC, Novais EA, Farah ME, Rodrigues EB. Fusion proteins for treatment of retinal diseases: aflibercept, ziv-aflibercept, and conbercept. Int J Retina Vitr 2016;2:3. https://doi.org/10.1186/s40942-016-0026-y.

[77]   Nguyen QD, Das A, Do DV, Dugel PU, Gomes A, Holz FG, et al. Brolucizumab: Evolution through Preclinical and Clinical Studies and the Implications for the Management of Neovascular Age-Related Macular Degeneration. Ophthalmology 2020. https://doi.org/10.1016/j.ophtha.2019.12.031.

[78]   Dugel PU, Koh A, Ogura Y, Jaffe GJ, Schmidt-Erfurth U, Brown DM, et al. HAWK and HARRIER: Phase 3, Multicenter, Randomized, Double-Masked Trials of Brolucizumab for Neovascular Age-Related Macular Degeneration. Ophthalmology 2020;127:72–84. https://doi.org/10.1016/j.ophtha.2019.04.017.

[79]   Haug SJ, Hien DL, Uludag G, Ngoc TTT, Lajevardi S, Halim MS, et al. Retinal arterial occlusive vasculitis following intravitreal brolucizumab administration. Am J Ophthalmol Case Rep 2020;18:100680. https://doi.org/10.1016/j.ajoc.2020.100680.

[80]   Jain A, Chea S, Matsumiya W, Halim MS, Yaşar Ç, Kuang G, et al. Severe vision loss secondary to retinal arteriolar occlusions after multiple intravitreal brolucizumab administrations. Am J Ophthalmol Case Rep 2020;18:100687. https://doi.org/10.1016/j.ajoc.2020.100687.

[81]   Baumal CR, Spaide RF, Vajzovic L, Freund KB, Walter SD, John VJ, et al. Retinal vasculitis and intraocular inflammation after intravitreal injection of brolucizumab. Ophthalmology 2020. https://doi.org/10.1016/j.ophtha.2020.04.017.

[82]   Lee J-H, Canny MD, De Erkenez A, Krilleke D, Ng Y-S, Shima DT, et al. A therapeutic aptamer inhibits angiogenesis by specifically targeting the heparin binding domain of VEGF165. Proc Natl Acad Sci U S A 2005;102:18902–7. https://doi.org/10.1073/pnas.0509069102.

[83]   Comparison of Age-related Macular Degeneration Treatments Trials (CATT) Research Group, Martin DF, Maguire MG, Fine SL, Ying G, Jaffe GJ, et al. Ranibizumab and bevacizumab for treatment of neovascular age-related macular degeneration: two-year results. Ophthalmology 2012;119:1388–98. https://doi.org/10.1016/j.ophtha.2012.03.053.

[84]   Chakravarthy U, Harding SP, Rogers CA, Downes SM, Lotery AJ, Culliford LA, et al. Alternative treatments to inhibit VEGF in age-related choroidal neovascularisation: 2-year findings of the IVAN randomised controlled trial. The Lancet 2013;382:1258–67. https://doi.org/10.1016/S0140-6736(13)61501-9.

[85]   Stahl A, Stumpp MT, Schlegel A, Ekawardhani S, Lehrling C, Martin G, et al. Highly potent VEGF-A-antagonistic DARPins as anti-angiogenic agents for topical and intravitreal applications. Angiogenesis 2013;16:101–11. https://doi.org/10.1007/s10456-012-9302-0.

[86]   Callanan D, Kunimoto D, Maturi RK, Patel SS, Staurenghi G, Wolf S, et al. Double-Masked, Randomized, Phase 2 Evaluation of Abicipar Pegol (an Anti-VEGF DARPin Therapeutic) in Neovascular Age-Related Macular Degeneration. J Ocul Pharmacol Ther 2018;34:700–9. https://doi.org/10.1089/jop.2018.0062.

[87]   Kunimoto D, Yoon YH, Wykoff CC, Chang A, Khurana RN, Maturi RK, et al. Efficacy and Safety of Abicipar in Neovascular Age-Related Macular Degeneration: 52-Week Results of Phase 3 Randomized Controlled Study. Ophthalmology 2020. https://doi.org/10.1016/j.ophtha.2020.03.035.

[88]   Moisseiev E, Loewenstein A. Abicipar pegol—a novel anti-VEGF therapy with a long duration of action. Eye 2020;34:605–6. https://doi.org/10.1038/s41433-019-0584-y.

[89]   A Dose-Ranging Study of Intravitreal OPT-302 in Combination With Ranibizumab, Compared With Ranibizumab Alone, in Participants With Neovascular Age-Related Macular Degeneration (Wet AMD) 2020. https://clinicaltrials.gov/ct2/show/NCT03345082 (accessed June 4, 2020).

[90]   Opthea Completes Final Patient Visit in Phase 2b Wet AMD Clinical Trial. GlobeNewswire News Room 2019. http://www.globenewswire.com/news-release/2019/05/15/1824410/0/en/Opthea-Completes-Final-Patient-Visit-in-Phase-2b-Wet-AMD-Clinical-Trial.html (accessed June 8, 2020).

[91]   Dugel PU, Boyer DS, Antoszyk AN, Steinle NC, Varenhorst MP, Pearlman JA, et al. Phase 1 Study of OPT-302 Inhibition of Vascular Endothelial Growth Factors C and D for Neovascular Age-Related Macular Degeneration. Ophthalmol Retina 2020;4:250–63. https://doi.org/10.1016/j.oret.2019.10.008.

[92]   A Phase 2, Prospective, Randomized, Double-masked, Active Comparator-controlled, Multi-center Study to Investigate the Efficacy and Safety of Repeated Intravitreal Administration of KSI-301 in Subjects With Neovascular (Wet) Age-related Macular Degeneration. 2019. https://clinicaltrials.gov/ct2/show/NCT04049266 (accessed June 4, 2020).

[93]   Editor BRMK, Kirkner R. Potential of KSI-301 to extend treatment 2019. http://www.retina-specialist.com/article/potential-of-ksi301-to-extend-treatment (accessed June 10, 2020).

[94]   Rofagha S, Bhisitkul RB, Boyer DS, Sadda SR, Zhang K. Seven-year outcomes in ranibizumab-treated patients in ANCHOR, MARINA, and HORIZON: a multicenter cohort study (SEVEN-UP). Ophthalmology 2013;120:2292–9. https://doi.org/10.1016/j.ophtha.2013.03.046.

[95]   Oliner JD, Bready J, Nguyen L, Estrada J, Hurh E, Ma H, et al. AMG 386, a Selective Angiopoietin 1/2-Neutralizing Peptibody, Inhibits Angiogenesis in Models of Ocular Neovascular Diseases. Invest Ophthalmol Vis Sci 2012;53:2170–80. https://doi.org/10.1167/iovs.11-7381.

[96]   Jo N, Mailhos C, Ju M, Cheung E, Bradley J, Nishijima K, et al. Inhibition of platelet-derived growth factor B signaling enhances the efficacy of anti-vascular endothelial growth factor therapy in multiple models of ocular neovascularization. Am J Pathol 2006;168:2036–53. https://doi.org/10.2353/ajpath.2006.050588.

[97]   Oliner JD, Min H, Leal J, Yu D, Rao S, You E, et al. Suppression of angiogenesis and tumor growth by selective inhibition of Angiopoietin-2. Cancer Res 2005;65:1100.

[98]   Rennel ES, Regula JT, Harper SJ, Thomas M, Klein C, Bates DO. A human neutralizing antibody specific to Ang-2 inhibits ocular angiogenesis. Microcirc N Y N 1994 2011;18:598–607. https://doi.org/10.1111/j.1549-8719.2011.00120.x.

[99]   Gahn GM, Khanani AM. New Therapies of Neovascular AMD beyond Anti-VEGF Injections. Vis Basel Switz 2018;2. https://doi.org/10.3390/vision2010015.

[100] Safety and Efficacy of Abicipar Pegol (AGN-150998) in Patients With Neovascular Age-related Macular Degeneration 2019. https://clinicaltrials.gov/ct2/show/NCT02462486 (accessed June 4, 2020).

[101] Safety and Efficacy of Abicipar Pegol (AGN-150998) in Patients With Neovascular Age-related Macular Degeneration 2019. https://clinicaltrials.gov/ct2/show/NCT02462928 (accessed June 4, 2020).

[102] Safety and Efficacy Study of Conbercept in Diabetic Macular Edema (DME) (Sailing) - Full Text View - ClinicalTrials.gov n.d. https://clinicaltrials.gov/ct2/show/NCT02194634 (accessed June 9, 2020).

[103] Effects of Conbercept in Refractory Uveitic Macular Edema and VEGF - Full Text View - ClinicalTrials.gov n.d. https://clinicaltrials.gov/ct2/show/NCT04296838 (accessed June 9, 2020).

[104] The Safety and Efficacy of Conbercept in the Treatment of Choroidal Neovascularization (CNV) Secondary to High Myopia 2014. https://clinicaltrials.gov/ct2/show/NCT01809223 (accessed June 4, 2020).

[105] An Efficacy and Safety Trial of Intravitreal Injection of Conbercept Ophthalmic Injection in Treatment of Macular Edema Secondary to Central Retinal Vein Occlusion 2018. https://clinicaltrials.gov/ct2/show/NCT03223714 (accessed June 4, 2020).

[106] Multi-center, Randomized, Double-masked, Placebo-controlled Phase III Clinical Study of Conbercept Ophthalmic Injection for Patients With BRVO. 2018. https://clinicaltrials.gov/ct2/show/NCT03108352 (accessed June 4, 2020).

[107] A Multicenter, Double-Masked, Randomized, Dose-Ranging Trial to Evaluate the Efficacy and Safety of Conbercept Intravitreal Injection in Subjects With Neovascular Age-Related Macular Degeneration (AMD) (PANDA-1) 2018. https://clinicaltrials.gov/ct2/show/NCT03577899 (accessed June 4, 2020).

[108] A Multicenter, Double-Masked, Randomized, Dose-Ranging Trial to Evaluate the Efficacy and Safety of Conbercept Intravitreal Injection in Subjects With Neovascular Age-Related Macular Degeneration (AMD) (PANDA-2) 2019. https://clinicaltrials.gov/ct2/show/NCT03630952 (accessed June 4, 2020).

[109] A Randomized, Double-masked, Multicenter,Sham-controlled, Safety and Efficacy Study of KH902 in Patients With Wet AMD - Full Text View - ClinicalTrials.gov n.d. https://clinicaltrials.gov/ct2/show/NCT01436864 (accessed June 9, 2020).

[110] Heier JS, Wykoff CC, Waheed NK, Kitchens JW, Patel SS, Vitti R, et al. Intravitreal Combined Aflibercept + Anti–Platelet-Derived Growth Factor Receptor β for Neovascular Age-Related Macular Degeneration: Results of the Phase 2 CAPELLA Trial. Ophthalmology 2020;127:211–20. https://doi.org/10.1016/j.ophtha.2019.09.021.

[111] Ung C, Agranat J, Yonekawa Y. Ophthalmology Management - The fight against neovascular AMD. Ophthalmol Manag 2019. https://www.ophthalmologymanagement.com/issues/2019/july-2019/the-fight-against-neovascular-amd (accessed June 9, 2020).

[112] Dunn EN, Hariprasad SM, Sheth VS. An Overview of the Fovista and Rinucumab Trials and the Fate of Anti-PDGF Medications. Ophthalmic Surg Lasers Imaging Retina 2017;48:100–4. https://doi.org/10.3928/23258160-20170130-02.

[113] Regeneron suffers research pipeline setback with disappointing Eylea combination therapy. STAT 2017. https://www.statnews.com/2017/11/27/regeneron-eylea-nevascumab-negative-results/ (accessed June 9, 2020).

[114] European Commission approves faricimab for nAMD, DME. Ophthalmol Times n.d. https://www.ophthalmologytimes.com/view/european-commission-approves-faricimab-for-namd-dme (accessed October 30, 2022).

[115] A Phase 2 Randomized, Open-Label, Multicenter Study Evaluating Administration of Repeated Intravitreal Doses of ICON-1 in Patients With Choroidal Neovascularization Secondary to Age-related Macular Degeneration 2018. https://clinicaltrials.gov/ct2/show/NCT03452527 (accessed June 4, 2020).

[116] A Phase 2 Randomized, Double-masked, Multicenter, Active-controlled Study Evaluating Administration of Repeated Intravitreal Doses of hI-con1™ in Patients With Choroidal Neovascularization Secondary to Age-related Macular Degeneration 2017. https://clinicaltrials.gov/ct2/show/NCT02358889 (accessed June 4, 2020).

[117] A Phase 1 Ascending and Parallel Group Trial to Establish the Safety, Tolerability and Pharmacokinetics Profile of Volociximab (Alpha 5 Beta 1 Integrin Antagonist) in Subjects With Neovascular Age- Related Macular Degeneration - Full Text View - ClinicalTrials.gov n.d. https://clinicaltrials.gov/ct2/show/NCT00782093 (accessed June 8, 2020).

[118] Ming S, Xie K, He H, Li Y, Lei B. Efficacy and safety of adalimumab in the treatment of non-infectious uveitis: a meta-analysis and systematic review. Drug Des Devel Ther 2018;12:2005–16. https://doi.org/10.2147/DDDT.S160431.

[119] Schwartzman S, Schwartzman M. The Use of Biologic Therapies in Uveitis. Clin Rev Allergy Immunol 2015;49:307–16. https://doi.org/10.1007/s12016-014-8455-6.

[120] Efficacy and Safety of Tocilizumab in the Treatment of Refractory Uveitis in Patients With Behcet's Disease 2019. https://clinicaltrials.gov/ct2/show/NCT03554161 (accessed June 4, 2020).

[121] Oshima Y, Deering T, Oshima S, Nambu H, Reddy PS, Kaleko M, et al. Angiopoietin-2 enhances retinal vessel sensitivity to vascular endothelial growth factor. J Cell Physiol 2004;199:412–7. https://doi.org/10.1002/jcp.10442.

[122] Sadiq MA, Hanout M, Sarwar S, Hassan M, Agarwal A, Sepah YJ, et al. Platelet-Derived Growth Factor Inhibitors: A Potential Therapeutic Approach for Ocular Neovascularization. Dev Ophthalmol 2016;55:310–6. https://doi.org/10.1159/000438953.

[123] A Phase 3 Randomized, Double-masked, Controlled Trial to Establish the Safety and Efficacy of Intravitreous Administration of Fovista® (Anti PDGF-B Pegylated Aptamer) Administered in Combination With Lucentis® Compared to Lucentis® Monotherapy in Subjects With Subfoveal Neovascular Age-related Macular Degeneration. 2018. https://clinicaltrials.gov/ct2/show/NCT01944839 (accessed June 4, 2020).

[124] Siedlecki J, Wertheimer C, Wolf A, Liegl R, Priglinger C, Priglinger S, et al. Combined VEGF and PDGF inhibition for neovascular AMD: anti-angiogenic properties of axitinib on human endothelial cells and pericytes in vitro. Graefes Arch Clin Exp Ophthalmol Albrecht Von Graefes Arch Klin Exp Ophthalmol 2017;255:963–72. https://doi.org/10.1007/s00417-017-3595-z.

[125] Miller JW. Treatment of age-related macular degeneration: beyond VEGF. Jpn J Ophthalmol 2010;54:523–8. https://doi.org/10.1007/s10384-010-0863-4.

[126] Cho Y, Cao X, Shen D, Tuo J, Parver LM, Rickles FR, et al. Evidence for enhanced tissue factor expression in age-related macular degeneration. Lab Investig J Tech Methods Pathol 2011;91:519–26. https://doi.org/10.1038/labinvest.2010.184.

[127] Wang G-F, Zou X-L. Tissue factor with age-related macular degeneration. Int J Ophthalmol 2012;5:609–13. https://doi.org/10.3980/j.issn.2222-3959.2012.05.13.

[128] Iconic Therapeutics pipeline overview. IconictherapeuticsCom n.d. http://iconictherapeutics.com/pipeline/overview/ (accessed June 9, 2020).

[129] Tosi GM, Barbarino M, Orlandini M, Galvagni F. New molecular targets for the treatment of neovascular age-related macular degeneration. Transl Med Rep 2017;2. https://doi.org/10.4081/tmr.6819.

[130] Danen EHJ. Integrins: An Overview of Structural and Functional Aspects. Landes Bioscience; 2013.

[131] Wang W, Wang F, Lu F, Xu S, Hu W, Huang J, et al. The Antiangiogenic Effects of Integrin α5β1 Inhibitor (ATN-161) In Vitro and In Vivo. Invest Ophthalmol Vis Sci 2011;52:7213–20. https://doi.org/10.1167/iovs.10-7097.

[132] Caballero S, Swaney J, Moreno K, Afzal A, Kielczewski J, Stoller G, et al. Anti-sphingosine-1-phosphate monoclonal antibodies inhibit angiogenesis and sub-retinal fibrosis in a murine model of laser-induced choroidal neovascularization. Exp Eye Res 2009;88:367–77. https://doi.org/10.1016/j.exer.2008.07.012.

[133] O'Brien N, Jones ST, Williams DG, Cunningham HB, Moreno K, Visentin B, et al. Production and characterization of monoclonal anti-sphingosine-1-phosphate antibodies. J Lipid Res 2009;50:2245–57. https://doi.org/10.1194/jlr.M900048-JLR200.

[134] Sharma A, Kumar N, Kuppermann BD, Bandello F, Loewenstein A. Faricimab: expanding horizon beyond VEGF. Eye 2020;34:802–4. https://doi.org/10.1038/s41433-019-0670-1.

[135] Benest AV, Kruse K, Savant S, Thomas M, Laib AM, Loos EK, et al. Angiopoietin-2 Is Critical for Cytokine-Induced Vascular Leakage. PLOS ONE 2013;8:e70459. https://doi.org/10.1371/journal.pone.0070459.

[136] Heier JS, Khanani AM, Quezada Ruiz C, Basu K, Ferrone PJ, Brittain C, et al. Efficacy, durability, and safety of intravitreal faricimab up to every 16 weeks for neovascular age-related macular degeneration (TENAYA and LUCERNE): two randomised, double-masked, phase 3, non-inferiority trials. Lancet Lond Engl 2022;399:729–40. https://doi.org/10.1016/S0140-6736(22)00010-1.

[137] Turecek PL, Bossard MJ, Schoetens F, Ivens IA. PEGylation of Biopharmaceuticals: A Review of Chemistry and Nonclinical Safety Information of Approved Drugs. J Pharm Sci 2016;105:460–75. https://doi.org/10.1016/j.xphs.2015.11.015.

[138] Inactive Ingredient Search for Approved Drug Products n.d. https://www.accessdata.fda.gov/scripts/cder/iig/index.cfm (accessed December 19, 2023).

[139] Dozier JK, Distefano MD. Site-Specific PEGylation of Therapeutic Proteins. Int J Mol Sci 2015;16:25831–64. https://doi.org/10.3390/ijms161025831.

[140] Abuchowski A, McCoy JR, Palczuk NC, van Es T, Davis FF. Effect of covalent attachment of polyethylene glycol on immunogenicity and circulating life of bovine liver catalase. J Biol Chem 1977;252:3582–6.

[141] Foser S, Schacher A, Weyer KA, Brugger D, Dietel E, Marti S, et al. Isolation, structural characterization, and antiviral activity of positional isomers of monopegylated interferon α-2a (PEGASYS). Protein Expr Purif 2003;30:78–87. https://doi.org/10.1016/S1046-5928(03)00055-X.

[142] Peciak K, Laurine E, Tommasi R, Choi J, Brocchini S. Site-selective protein conjugation at histidine. Chem Sci 2019;10:427–39. https://doi.org/10.1039/C8SC03355B.

[143] Gao M, Tong Y, Gao X, Yao W. Development of a C-Terminal Site-Specific PEGylated Analog of GLP-1 with Improved Anti-Diabetic Effects in Diabetic Mice. Drug Dev Res 2013;74:186–93. https://doi.org/10.1002/ddr.21059.

[144] Alconcel SNS, Baas AS, Maynard HD. FDA-approved poly(ethylene glycol)–protein conjugate drugs. Polym Chem 2011;2:1442–8. https://doi.org/10.1039/C1PY00034A.

[145] Fomenko DE, Marino SM, Gladyshev VN. Functional Diversity of Cysteine Residues in Proteins and Unique Features of Catalytic Redox-active Cysteines in Thiol Oxidoreductases. Mol Cells 2008;26:228–35.

[146] Wedemeyer WJ, Welker E, Narayan M, Scheraga HA. Disulfide Bonds and Protein Folding. Biochemistry 2000;39:4207–16. https://doi.org/10.1021/bi992922o.

[147] Trivedi MV, Laurence JS, Siahaan TJ. The role of thiols and disulfides in protein chemical and physical stability. Curr Protein Pept Sci 2009;10:614–25.

[148] Brocchini S, Godwin A, Balan S, Choi J, Zloh M, Shaunak S. Disulfide bridge based PEGylation of proteins. Adv Drug Deliv Rev 2008;60:3–12. https://doi.org/10.1016/j.addr.2007.06.014.

[149] Ginn C, Choi J-W, Brocchini S. Disulfide-bridging PEGylation during refolding for the more efficient production of modified proteins. Biotechnol J 2016;11:1088–99. https://doi.org/10.1002/biot.201600035.

[150] Balan S, Choi J, Godwin A, Teo I, Laborde CM, Heidelberger S, et al. Site-Specific PEGylation of Protein Disulfide Bonds Using a Three-Carbon Bridge. Bioconjug Chem 2007;18:61–76. https://doi.org/10.1021/bc0601471.

[151] Thornton JM. Disulphide bridges in globular proteins. J Mol Biol 1981;151:261–87. https://doi.org/10.1016/0022-2836(81)90515-5.

[152] Leung HJ, Xu G, Narayan M, Scheraga HA. Impact of an easily reducible disulfide bond on the oxidative folding rate of multi-disulfide-containing proteins. J Pept Res Off J Am Pept Soc 2005;65:47–54. https://doi.org/10.1111/j.1399-3011.2004.00189.x.

[153] Petersen MTN, Jonson PH, Petersen SB. Amino acid neighbours and detailed conformational analysis of cysteines in proteins. Protein Eng Des Sel 1999;12:535–48. https://doi.org/10.1093/protein/12.7.535.

[154] Betz SF. Disulfide bonds and the stability of globular proteins. Protein Sci Publ Protein Soc 1993;2:1551–8.

[155] Saunders AJ, Young GB, Pielak GJ. Polarity of disulfide bonds. Protein Sci Publ Protein Soc 1993;2:1183–4.

[156] Khalili H, Godwin A, Choi J, Lever R, Khaw PT, Brocchini S. Fab-PEG-Fab as a Potential Antibody Mimetic. Bioconjug Chem 2013;24:1870–82. https://doi.org/10.1021/bc400246z.

[157] Khalili H, Brocchini S, Khaw PT, Filippov SK. Comparative thermodynamic analysis in solution of a next generation antibody mimetic to VEGF. RSC Adv 2018;8:35787–93. https://doi.org/10.1039/C8RA07059H.

[158] Vauquelin G, Charlton SJ. Long-lasting target binding and rebinding as mechanisms to prolong in vivo drug action. Br J Pharmacol 2010;161:488–508. https://doi.org/10.1111/j.1476-5381.2010.00936.x.

[159] Khalili H, Lee RW, Khaw PT, Brocchini S, Dick AD, Copland DA. An anti-TNF-α antibody mimetic to treat ocular inflammation. Sci Rep 2016;6. https://doi.org/10.1038/srep36905.

[160] Khalili H, Khaw PT, Brocchini S. Fc-fusion mimetics. Biomater Sci 2016;4:943–7. https://doi.org/10.1039/C6BM00077K.

[161] Khalili H. Disulfide-bridging PEGylation of antibody fragments. Doctoral. UCL (University College London), 2012.

[162] Zhao Y, Gutshall L, Jiang H, Baker A, Beil E, Obmolova G, et al. Two routes for production and purification of Fab fragments in biopharmaceutical discovery research: Papain digestion of mAb and transient expression in mammalian cells. Protein Expr Purif 2009;67:182–9. https://doi.org/10.1016/j.pep.2009.04.012.

[163] Humphreys DP, Carrington B, Bowering LC, Ganesh R, Sehdev M, Smith BJ, et al. A plasmid system for optimization of Fab' production in Escherichia coli: importance of balance of heavy chain and light chain synthesis. Protein Expr Purif 2002;26:309–20. https://doi.org/10.1016/s1046-5928(02)00543-0.

[164] Humphreys DP, Glover DJ. Therapeutic antibody production technologies: molecules, applications, expression and purification. Curr Opin Drug Discov Devel 2001;4:172–85.

[165] High level production of functional antibody Fab fragments in an oxidizing bacterial cytoplasm. | Semantic Scholar n.d. https://www.semanticscholar.org/paper/High-level-production-of-functional-antibody-Fab-in-Venturi-Seifert/c5ea8f3667c2437fc2d6976ed69468bb29c29303 (accessed May 17, 2022).

[166] Kinman AWL, Pompano RR. Optimization of Enzymatic Antibody Fragmentation for Yield, Efficiency, and Binding Affinity. Bioconjug Chem 2019;30:800–7. https://doi.org/10.1021/acs.bioconjchem.8b00912.

[167] Mitchel RE, Chaiken IM, Smith EL. The complete amino acid sequence of papain. Additions and corrections. J Biol Chem 1970;245:3485–92.

[168] Khalili H, Godwin A, Choi J, Lever R, Brocchini S. Comparative Binding of Disulfide-Bridged PEG-Fabs. Bioconjug Chem 2012;23:2262–77. https://doi.org/10.1021/bc300372r.

[169] Moelleken J, Endesfelder M, Gassner C, Lingke S, Tomaschek S, Tyshchuk O, et al. GingisKHAN™ protease cleavage allows a high-throughput antibody to Fab conversion enabling direct functional assessment during lead identification of human monoclonal and bispecific IgG1 antibodies. mAbs 2017;9:1076–87. https://doi.org/10.1080/19420862.2017.1364325.

[170] Collins M, Khalili H. Soluble Papain to Digest Monoclonal Antibodies; Time and Cost-Effective Method to Obtain Fab Fragment. Bioengineering 2022;9:209. https://doi.org/10.3390/bioengineering9050209.

[171] Open universiteit, Thames Polytechnic. 9 - Case Study: Myoscint - A monoclonal antibody preparation used for cardiac imaging. In: Open universiteit, Thames Polytechnic, editors. Biotechnol. Innov. Health Care, Butterworth-Heinemann; 1991, p. 225–47. https://doi.org/10.1016/B978-0-7506-1497-9.50016-7.

[172] Hoover SR, Kokes ELC. EFFECT OF pH UPON PROTEOLYSIS BY PAPAIN. J Biol Chem 1947;167:199–207. https://doi.org/10.1016/S0021-9258(17)35156-6.

[173] Milošević J, Janković B, Prodanović R, Polović N. Comparative stability of ficin and papain in acidic conditions and the presence of ethanol. Amino Acids 2019;51:829–38. https://doi.org/10.1007/s00726-019-02724-3.

[174] Affinity Chromatography Applications with Single-Domain Antibodies. BioProcess Int 2013. https://bioprocessintl.com/2013/affinity-chromatography-applications-with-single-domain-antibodies-345480/ (accessed June 21, 2022).

[175] CaptureSelect™ CH1-XL Affinity Matrix Data sheet n.d.

[176] ÄKTAprime plus Operating Instructions n.d.:104.

[177] Cunningham ET, Adán A, Nguyen QD, Zierhut M. Tocilizumab for the Treatment of Ocular Inflammatory Disease. Ocul Immunol Inflamm 2021;29:2–5. https://doi.org/10.1080/09273948.2020.1859257.

[178] Morelock MM, Rothlein R, Bright SM, Robinson MK, Graham ET, Sabo JP, et al. Isotype choice for chimeric antibodies affects binding properties. J Biol Chem 1994;269:13048–55. https://doi.org/10.1016/S0021-9258(18)99982-5.

[179] Park SS, Kim J, Brandts JF, Hong HJ. Stability of murine, chimeric and humanized antibodies against pre-S2 surface antigen of hepatitis B virus. Biol J Int Assoc Biol Stand 2003;31:295–302. https://doi.org/10.1016/j.biologicals.2003.08.003.

[180] Goulet DR, Chatterjee S, Lee W-P, Waight AB, Zhu Y, Mak AN-S. Engineering an Enhanced EGFR Engager: Humanization of Cetuximab for Improved Developability. Antibodies 2022;11:6. https://doi.org/10.3390/antib11010006.

[181] Brocchini S, Balan S, Godwin A, Choi J-W, Zloh M, Shaunak S. PEGylation of native disulfide bonds in proteins. Nat Protoc 2006;1:2241–52. https://doi.org/10.1038/nprot.2006.346.

[182] Farys M. New strategies for protein-to-protein conjugation. Doctoral. UCL (University College London), 2015.

[183] Khalili H, Godwin A, Choi J, Lever R, Khaw PT, Brocchini S. Fab-PEG-Fab as a Potential Antibody Mimetic. Bioconjug Chem 2013;24:1870–82. https://doi.org/10.1021/bc400246z.

[184] Mohamed HE, Mohamed AA, Al-Ghobashy MA, Fathalla FA, Abbas SS. Stability assessment of antibody-drug conjugate Trastuzumab emtansine in comparison to parent monoclonal antibody using orthogonal testing protocol. J Pharm Biomed Anal 2018;150:268–77. https://doi.org/10.1016/j.jpba.2017.12.022.

[185] Glover ZK, Basa L, Moore B, Laurence JS, Sreedhara A. Metal ion interactions with mAbs: Part 1. mAbs 2015;7:901–11. https://doi.org/10.1080/19420862.2015.1062193.

[186] Kim E, Koo H. Biomedical applications of copper-free click chemistry: in vitro, in vivo, and ex vivo. Chem Sci 2019;10:7835–51. https://doi.org/10.1039/C9SC03368H.

[187] Zuma LK, Gasa NL, Makhoba XH, Pooe OJ. Protein PEGylation: Navigating Recombinant Protein Stability, Aggregation, and Bioactivity. BioMed Res Int 2022;2022:8929715. https://doi.org/10.1155/2022/8929715.

[188] Handula M, Chen K-T, Seimbille Y. IEDDA: An Attractive Bioorthogonal Reaction for Biomedical Applications. Molecules 2021;26:4640. https://doi.org/10.3390/molecules26154640.

[189] Muneeruddin K, Bobst CE, Frenkel R, Houde D, Turyan I, Sosic Z, et al. Characterization of a PEGylated protein therapeutic by ion exchange chromatography with on-line detection by native ESI MS and MS/MS. Analyst 2017;142:336–44. https://doi.org/10.1039/C6AN02041K.

[190] Seely JE, Richey CW. Use of ion-exchange chromatography and hydrophobic interaction chromatography in the preparation and recovery of polyethylene glycol-linked proteins. J Chromatogr A 2001;908:235–41. https://doi.org/10.1016/S0021-9673(00)00739-1.

[191] Johann K, Svatunek D, Seidl C, Rizzelli S, Bauer TA, Braun L, et al. Tetrazine- and trans-cyclooctene-functionalised polypept(o)ides for fast bioorthogonal tetrazine ligation. Polym Chem 2020;11:4396–407. https://doi.org/10.1039/D0PY00375A.

[192] Awwad S, Ginn C, Brocchini S. 2 - The case for protein PEGylation. In: Parambath A, editor. Eng. Biomater. Drug Deliv. Syst., Woodhead Publishing; 2018, p. 27–49. https://doi.org/10.1016/B978-0-08-101750-0.00002-7.

[193] Mu Q, Hu T, Yu J. Molecular Insight into the Steric Shielding Effect of PEG on the Conjugated Staphylokinase: Biochemical Characterization and Molecular Dynamics Simulation. PLoS ONE 2013;8:e68559. https://doi.org/10.1371/journal.pone.0068559.

[194] Thi Nguyen N-T, Yun S, Lim DW, Lee EK. Shielding effect of a PEG molecule of a mono-PEGylated peptide varies with PEG chain length. Prep Biochem Biotechnol 2018;48:522–7. https://doi.org/10.1080/10826068.2018.1466157.

[195] Zhu S, Ji T, Yang B, Yang Z. Preparation and characterization of PEG/surface-modified layered double hydroxides as a new shape-stabilized phase change material. RSC Adv 2019;9:23435–43. https://doi.org/10.1039/C9RA03329G.

[196] Protein Gel Staining Methods - UK n.d. https://www.thermofisher.com/uk/en/home/life-science/protein-biology/protein-biology-learning-center/protein-biology-resource-library/pierce-protein-methods/protein-gel-stains.html (accessed July 28, 2022).

[197] VABYSMO™ (faricimab-svoa) | DME Dosing & Study Design. Vabysmo n.d. https://www.vabysmo-hcp.com/dme-data/dme-dosing-study-design.html (accessed June 17, 2023).

[198] Abedi M, Ahangari Cohan R, Mahboudi F, Shafiee Ardestani M, Davami F. MALDI-MS: a Rapid and Reliable Method for Drug-to-Antibody Ratio Determination of Antibody-Drug Conjugates. Iran Biomed J 2019;23:395–403. https://doi.org/10.29252/ibj.23.6.395.

[199] Li Y, Hewitt D, Lentz YK, Ji JA, Zhang TY, Zhang K. Characterization and Stability Study of Polysorbate 20 in Therapeutic Monoclonal Antibody Formulation by Multidimensional Ultrahigh-Performance Liquid Chromatography–Charged Aerosol Detection–Mass Spectrometry. Anal Chem 2014;86:5150–7. https://doi.org/10.1021/ac5009628.

[200] Li W, Prabakaran P, Chen W, Zhu Z, Feng Y, Dimitrov DS. Antibody Aggregation: Insights from Sequence and Structure. Antibodies 2016;5:19. https://doi.org/10.3390/antib5030019.

[201] Wälchli R, Vermeire P-J, Massant J, Arosio P. Accelerated Aggregation Studies of Monoclonal Antibodies: Considerations for Storage Stability. J Pharm Sci 2020;109:595–602. https://doi.org/10.1016/j.xphs.2019.10.048.

[202] Yan R, Wang R, Ju B, Yu J, Zhang Y, Liu N, et al. Structural basis for bivalent binding and inhibition of SARS-CoV-2 infection by human potent neutralizing antibodies. Cell Res 2021;31:517–25. https://doi.org/10.1038/s41422-021-00487-9.

[203] Wagner K, Kwakkenbos MJ, Claassen YB, Maijoor K, Böhne M, Sluijs KF van der, et al. Bispecific antibody generated with sortase and click chemistry has broad antiinfluenza virus activity. Proc Natl Acad Sci 2014;111:16820–5. https://doi.org/10.1073/pnas.1408605111.

[204] Powner MB, McKenzie JAG, Christianson GJ, Roopenian DC, Fruttiger M. Expression of neonatal Fc receptor in the eye. Invest Ophthalmol Vis Sci 2014;55:1607–15. https://doi.org/10.1167/iovs.13-12574.

[205] Regula JT, Lundh von Leithner P, Foxton R, Barathi VA, Cheung CMG, Bo Tun SB, et al. Targeting key angiogenic pathways with a bispecific CrossMAb optimized for neovascular eye diseases. EMBO Mol Med 2016;8:1265–88. https://doi.org/10.15252/emmm.201505889.

[206] Choy EHS, Hazleman B, Smith M, Moss K, Lisi L, Scott DGI, et al. Efficacy of a novel PEGylated humanized anti-TNF fragment (CDP870) in patients with rheumatoid arthritis: a phase II double-blinded, randomized, dose-escalating trial. Rheumatol Oxf Engl 2002;41:1133–7. https://doi.org/10.1093/rheumatology/41.10.1133.

[207] Karlsson R, Michaelsson A, Mattsson L. Kinetic analysis of monoclonal antibody-antigen interactions with a new biosensor based analytical system. J Immunol Methods 1991;145:229–40. https://doi.org/10.1016/0022-1759(91)90331-9.

[208] Jerabek-Willemsen M, André T, Wanner R, Roth HM, Duhr S, Baaske P, et al. MicroScale Thermophoresis: Interaction analysis and beyond. J Mol Struct 2014;1077:101–13. https://doi.org/10.1016/j.molstruc.2014.03.009.

[209] Application Notes - Site-Specific labeling of antibodies for MicroScale Thermophoresis n.d. https://resources.nanotempertech.com/i/1050596-site-specific-labeling-of-antibodies-for-microscale-thermophoresis/3? (accessed May 16, 2021).

[210] Selis F, Focà G, Sandomenico A, Marra C, Di Mauro C, Saccani Jotti G, et al. Pegylated Trastuzumab Fragments Acquire an Increased in Vivo Stability but Show a Largely Reduced Affinity for the Target Antigen. Int J Mol Sci 2016;17:491. https://doi.org/10.3390/ijms17040491.

[211] Pei M, Wang Y, Tang L, Wu W, Wang C, Chen Y-L. Dual-target Bridging ELISA for Bispecific Antibodies. Bio-Protoc 2022;12:e4522. https://doi.org/10.21769/BioProtoc.4522.

[212] Yang J, Wang X, Fuh G, Yu L, Wakshull E, Khosraviani M, et al. Comparison of binding characteristics and in vitro activities of three inhibitors of vascular endothelial growth factor A. Mol Pharm 2014;11:3421–30. https://doi.org/10.1021/mp500160v.

[213] Erbaş A, Inci F. The Role of Ligand Rebinding and Facilitated Dissociation on the Characterization of Dissociation Rates by Surface Plasmon Resonance (SPR) and Benchmarking Performance Metrics. Methods Mol Biol Clifton NJ 2022;2385:237–53. https://doi.org/10.1007/978-1-0716-1767-0_11.

[214] Erbaş A, Olvera de la Cruz M, Marko JF. Receptor-Ligand Rebinding Kinetics in Confinement. Biophys J 2019;116:1609–24. https://doi.org/10.1016/j.bpj.2019.02.033.

[215] Papadopoulos N, Martin J, Ruan Q, Rafique A, Rosconi MP, Shi E, et al. Binding and neutralization of vascular endothelial growth factor (VEGF) and related ligands by VEGF Trap, ranibizumab and bevacizumab. Angiogenesis 2012;15:171–85. https://doi.org/10.1007/s10456-011-9249-6.

[216] Khan AH, Pierce CO, De Salvo G, Griffiths H, Nelson M, Cree AJ, et al. The effect of systemic levels of TNF-alpha and complement pathway activity on outcomes of VEGF inhibition in neovascular AMD. Eye Lond Engl 2022;36:2192–9. https://doi.org/10.1038/s41433-021-01824-3.

[217] Shahidatul-Adha M, Zunaina E, Aini-Amalina MN. Evaluation of vascular endothelial growth factor (VEGF) level in the tears and serum of age-related macular degeneration patients. Sci Rep 2022;12:4423. https://doi.org/10.1038/s41598-022-08492-7.

[218] Anti-TNF Drugs for Chronic Uveitis in Adults—A Systematic Review and Meta-Analysis of Randomized Controlled Trials - PMC n.d. https://www.ncbi.nlm.nih.gov/pmc/articles/PMC6543521/ (accessed August 28, 2023).

[219] Karkhur S, Hasanreisoglu M, Vigil E, Halim MS, Hassan M, Plaza C, et al. Interleukin-6 inhibition in the management of non-infectious uveitis and beyond. J Ophthalmic Inflamm Infect 2019;9. https://doi.org/10.1186/s12348-019-0182-y.

[220] Kubetzko S, Sarkar CA, Plückthun A. Protein PEGylation decreases observed target association rates via a dual blocking mechanism. Mol Pharmacol 2005;68:1439–54. https://doi.org/10.1124/mol.105.014910.

[221] Why does the binding curve go up or down? n.d. https://nanotemper.my.site.com/explore/s/article/Why-does-the-binding-curve-go-up-or-down (accessed May 26, 2022).

[222] Khalili H, Brocchini S, Khaw PT, Filippov SK. Comparative thermodynamic analysis in solution of a next generation antibody mimetic to VEGF. RSC Adv 2018;8:35787–93. https://doi.org/10.1039/C8RA07059H.

[223] Schubert M, Bertoglio F, Steinke S, Heine PA, Ynga-Durand MA, Maass H, et al. Human serum from SARS-CoV-2-vaccinated and COVID-19 patients shows reduced binding to the RBD of SARS-CoV-2 Omicron variant. BMC Med 2022;20:102. https://doi.org/10.1186/s12916-022-02312-5.

[224] Kawashima M, Shoji J, Nakajima M, Kamura Y, Sato Y. Soluble IL-6 Receptor in Vitreous Fluid of Patients with Proliferative Diabetic Retinopathy. Jpn J Ophthalmol 2007;51:100–4. https://doi.org/10.1007/s10384-006-0411-4.

[225] Weinstein JE, Pepple KL. Cytokines in uveitis. Curr Opin Ophthalmol 2018;29:267–74. https://doi.org/10.1097/ICU.0000000000000466.

[226] Tumor necrosis factor alpha (TNF-alpha)-induced cell adhesion to human endothelial cells is under dominant control of one TNF receptor type, TNF-R55. J Exp Med 1993;177:1277–86.

[227] Erbel C, Chen L, Bea F, Wangler S, Celik S, Lasitschka F, et al. Inhibition of IL-17A Attenuates Atherosclerotic Lesion Development in ApoE-Deficient Mice. J Immunol 2009;183:8167–75. https://doi.org/10.4049/jimmunol.0901126.

[228] Mirando AC, Lima e Silva R, Chu Z, Campochiaro PA, Pandey NB, Popel AS. Suppression of Ocular Vascular Inflammation through Peptide-Mediated Activation of Angiopoietin-Tie2 Signaling. Int J Mol Sci 2020;21:5142. https://doi.org/10.3390/ijms21145142.

[229] Sekhon AS, He B, Iovieno A, Yeung SN. Pathophysiology of Corneal Endothelial Cell Loss in Dry Eye Disease and Other Inflammatory Ocular Disorders. Ocul Immunol Inflamm 2023;31:21–31. https://doi.org/10.1080/09273948.2021.1980808.

[230] Alfawaz AM, Holland GN, Yu F, Margolis MS, Giaconi JA, Aldave AJ. Corneal Endothelium in Patients with Anterior Uveitis. Ophthalmology 2016;123:1637–45. https://doi.org/10.1016/j.ophtha.2016.04.036.

[231] Xing X, Yang J, Yang X, Wei Y, Zhu L, Gao D, et al. IL-17A induces endothelial inflammation in systemic sclerosis via the ERK signaling pathway. PloS One 2013;8:e85032. https://doi.org/10.1371/journal.pone.0085032.

[232] Zhu Y, Shen T, Lin Y, Chen B, Ruan Y, Cao Y, et al. Astragalus polysaccharides suppress ICAM-1 and VCAM-1 expression in TNF-α-treated human vascular endothelial cells by blocking NF-κB activation. Acta Pharmacol Sin 2013;34:1036–42. https://doi.org/10.1038/aps.2013.46.

[233] Runnels JM, Zamiri P, Spencer JA, Veilleux I, Wei X, Bogdanov A, et al. Imaging Molecular Expression on Vascular Endothelial Cells by In Vivo Immunofluorescence Microscopy. Mol Imaging 2006;5:31–40.

[234] Lertkiatmongkol P, Liao D, Mei H, Hu Y, Newman PJ. Endothelial functions of PECAM-1 (CD31). Curr Opin Hematol 2016;23:253–9. https://doi.org/10.1097/MOH.0000000000000239.

[235] Dewi BE, Takasaki T, Kurane I. Peripheral blood mononuclear cells increase the permeability of dengue virus-infected endothelial cells in association with downregulation of vascular endothelial cadherin. J Gen Virol 2008;89:642–52. https://doi.org/10.1099/vir.0.83356-0.

[236] Kouri V-P, Olkkonen J, Nurmi K, Peled N, Ainola M, Mandelin J, et al. IL-17A and TNF synergistically drive expression of proinflammatory mediators in synovial fibroblasts via IκBζ-dependent induction of ELF3. Rheumatol Oxf Engl 2022;62:872–85. https://doi.org/10.1093/rheumatology/keac385.

[237] Li W, Chen P, Zhao Y, Cao M, Hu W, Pan L, et al. Human IL-17 and TNF-α Additively or Synergistically Regulate the Expression of Proinflammatory Genes, Coagulation-Related Genes, and Tight Junction Genes in Porcine Aortic Endothelial Cells. Front Immunol 2022;13.

[238] Beringer A, Thiam N, Molle J, Bartosch B, Miossec P. Synergistic effect of interleukin-17 and tumour necrosis factor-α on inflammatory response in hepatocytes through interleukin-6-dependent and independent pathways. Clin Exp Immunol 2018;193:221–33. https://doi.org/10.1111/cei.13140.

[239] Gerriets V, Goyal A, Khaddour K. Tumor Necrosis Factor Inhibitors. StatPearls, Treasure Island (FL): StatPearls Publishing; 2023.

[240] Moriconi F, Malik IA, Amanzada A, Blaschke M, Raddatz D, Khan S, et al. The anti-TNF-α antibody infliximab indirectly regulates PECAM-1 gene expression in two models of in vitro blood cell activation. Lab Invest 2012;92:166–77. https://doi.org/10.1038/labinvest.2011.160.

[241] Silacci M, Lembke W, Woods R, Attinger-Toller I, Baenziger-Tobler N, Batey S, et al. Discovery and characterization of COVA322, a clinical-stage bispecific TNF/IL-17A inhibitor for the treatment of inflammatory diseases. mAbs 2016;8:141–9. https://doi.org/10.1080/19420862.2015.1093266.

[242] Xu T, Ying T, Wang L, Zhang XD, Wang Y, Kang L, et al. A native-like bispecific antibody suppresses the inflammatory cytokine response by simultaneously neutralizing tumor necrosis factor-alpha and interleukin-17A. Oncotarget 2017;8:81860–72. https://doi.org/10.18632/oncotarget.19899.

[243] Covagen. A Randomised, Double-blind, Sequential, Ascending Single-dose Study to Evaluate Safety, Tolerability, Biological Activity, and Systemic Exposure of COVA322, a Bispecific TNF-α / IL-17A Antibody Fusion Protein, in Patients With Stable Chronic Moderate-to-severe Plaque Psoriasis. clinicaltrials.gov; 2016.

[244] Biermann MHC, Griffante G, Podolska MJ, Boeltz S, Stürmer J, Muñoz LE, et al. Sweet but dangerous – the role of immunoglobulin G glycosylation in autoimmunity and inflammation. Lupus 2016;25:934–42. https://doi.org/10.1177/0961203316640368.

[245] Corraliza-Gorjón I, Somovilla-Crespo B, Santamaria S, Garcia-Sanz JA, Kremer L. New Strategies Using Antibody Combinations to Increase Cancer Treatment Effectiveness. Front Immunol 2017;8:1804. https://doi.org/10.3389/fimmu.2017.01804.

[246] Evusheld long-acting antibody combination approved in the EU for the treatment of COVID-19 n.d. https://www.astrazeneca.com/media-centre/press-releases/2022/evusheld-approved-in-eu-for-covid-19-treatment.html (accessed October 22, 2022).

[247] Harper KN. Combination antibody treatment controls HIV infection in phase 1 trial. AIDS 2019;33:N3. https://doi.org/10.1097/QAD.0000000000002117.

[248] Henricks LM, Schellens JHM, Huitema ADR, Beijnen JH. The use of combinations of monoclonal antibodies in clinical oncology. Cancer Treat Rev 2015;41:859–67. https://doi.org/10.1016/j.ctrv.2015.10.008.

[249] Irigoyen C, Ziahosseini K, Morphis G, Stappler T, Heimann H. Endophthalmitis following intravitreal injections. Graefes Arch Clin Exp Ophthalmol 2012;250:499–505. https://doi.org/10.1007/s00417-011-1851-1.

[250] Bracha P, Moore NA, Ciulla TA, WuDunn D, Cantor LB. The acute and chronic effects of intravitreal anti-vascular endothelial growth factor injections on intraocular pressure: A review. Surv Ophthalmol 2018;63:281–95. https://doi.org/10.1016/j.survophthal.2017.08.008.

[251] Labrijn AF, Janmaat ML, Reichert JM, Parren PWHI. Bispecific antibodies: a mechanistic review of the pipeline. Nat Rev Drug Discov 2019;18:585–608. https://doi.org/10.1038/s41573-019-0028-1.

[252] Holz FG, Tadayoni R, Beatty S, Berger A, Cereda MG, Cortez R, et al. Multi-country real-life experience of anti-vascular endothelial growth factor therapy for wet age-related macular degeneration. Br J Ophthalmol 2015;99:220–6. https://doi.org/10.1136/bjophthalmol-2014-305327.

[253] Talks J, Daien V, Finger RP, Eldem B, Sakamoto T, Cardillo JA, et al. The use of real-world evidence for evaluating anti–vascular endothelial growth factor treatment of neovascular age-related macular degeneration. Surv Ophthalmol 2019;64:707–19. https://doi.org/10.1016/j.survophthal.2019.02.008.

[254] Behar-Cohen F. Recent advances in slow and sustained drug release for retina drug delivery. Expert Opin Drug Deliv 2019;16:679–86. https://doi.org/10.1080/17425247.2019.1618829.

[255] Shirley M. Faricimab: First Approval. Drugs 2022;82:825–30. https://doi.org/10.1007/s40265-022-01713-3.

[256] Strohl WR, Strohl LM, editors. 12 - Antibody fragments as therapeutics. Ther. Antib. Eng., Woodhead Publishing; 2012, p. 265–595. https://doi.org/10.1533/9781908818096.265.

[257] Khalili H. Using different proteolytic enzymes to digest antibody and its impact on stability of antibody mimetics. J Immunol Methods 2021;489:112933. https://doi.org/10.1016/j.jim.2020.112933.

[258] Li S, Cai H, He J, Chen H, Lam S, Cai T, et al. Extent of the Oxidative Side Reactions to Peptides and Proteins During the CuAAC Reaction. Bioconjug Chem 2016;27:2315–22. https://doi.org/10.1021/acs.bioconjchem.6b00267.

[259] Presolski S. Modification of Protein Scaffolds via Copper-Catalyzed Azide-Alkyne Cycloaddition. Methods Mol Biol Clifton NJ 2018;1798:187–93. https://doi.org/10.1007/978-1-4939-7893-9_14.

[260] Karver MR, Weissleder R, Hilderbrand SA. Synthesis and Evaluation of a Series of 1,2,4,5-Tetrazines for Bioorthogonal Conjugation. Bioconjug Chem 2011;22:2263–70. https://doi.org/10.1021/bc200295y.

[261] Sauer J, Heldmann DK, Hetzenegger J, Krauthan J, Sichert H, Schuster J. 1,2,4,5-Tetrazine: Synthesis and Reactivity in [4+2] Cycloadditions. Eur J Org Chem 1998;1998:2885–96. https://doi.org/10.1002/(SICI)1099-0690(199812)1998:12<2885::AID-EJOC2885>3.0.CO;2-L.

[262] Khayrzad FA. Site-specific, efficient and stable PEGylation. Doctoral. UCL (University College London), 2019.

[263] Immobilization Strategies n.d. https://www.reichertspr.com/Insights/Blog-Posts/Immobilization Strategies (accessed August 14, 2023).

[264] Sahin M, Remy MM, Fallet B, Sommerstein R, Florova M, Langner A, et al. Antibody bivalency improves antiviral efficacy by inhibiting virion release independently of Fc gamma receptors. Cell Rep 2022;38:110303. https://doi.org/10.1016/j.celrep.2022.110303.

[265] Edeling MA, Austin SK, Shrestha B, Dowd KA, Mukherjee S, Nelson CA, et al. Potent Dengue Virus Neutralization by a Therapeutic Antibody with Low Monovalent Affinity Requires Bivalent Engagement. PLOS Pathog 2014;10:e1004072. https://doi.org/10.1371/journal.ppat.1004072.

[266] Albert S, Arndt C, Koristka S, Berndt N, Bergmann R, Feldmann A, et al. From mono- to bivalent: improving theranostic properties of target modules for redirection of UniCAR T cells against EGFR-expressing tumor cells in vitro and in vivo. Oncotarget 2018;9:25597–616. https://doi.org/10.18632/oncotarget.25390.

[267] Kirley TL, Greis KD, Norman AB. Selective disulfide reduction for labeling and enhancement of Fab antibody fragments. Biochem Biophys Res Commun 2016;480:752–7. https://doi.org/10.1016/j.bbrc.2016.10.128.

[268] Evans N, Grygorash R, Williams P, Kyle A, Kantner T, Pathak R, et al. Incorporation of Hydrophilic Macrocycles Into Drug-Linker Reagents Produces Antibody-Drug Conjugates With Enhanced in vivo Performance. Front Pharmacol 2022;13:764540. https://doi.org/10.3389/fphar.2022.764540.

[269] Collins M, Awwad S, Ibeanu N, Khaw PT, Guiliano D, Brocchini S, et al. Dual-acting therapeutic proteins for intraocular use. Drug Discov Today 2021;26:44–55. https://doi.org/10.1016/j.drudis.2020.10.025.

[270] Neumann R, Barequet D. The gap between the need for novel retinal drug delivery methods, technologies in R&D phase, and approved ocular drug delivery technologies. Drug Discov Today 2019;24:1433–5. https://doi.org/10.1016/j.drudis.2019.03.018.

[271] Stewart MW. Extended Duration Vascular Endothelial Growth Factor Inhibition in the Eye: Failures, Successes, and Future Possibilities. Pharmaceutics 2018;10:21. https://doi.org/10.3390/pharmaceutics10010021.

[272] del Amo EM, Rimpelä A-K, Heikkinen E, Kari OK, Ramsay E, Lajunen T, et al. Pharmacokinetic aspects of retinal drug delivery. Prog Retin Eye Res 2017;57:134–85. https://doi.org/10.1016/j.preteyeres.2016.12.001.

[273] Ghosh JG, Nguyen AA, Bigelow CE, Poor S, Qiu Y, Rangaswamy N, et al. Long-acting protein drugs for the treatment of ocular diseases. Nat Commun 2017;8. https://doi.org/10.1038/ncomms14837.